SITE RESPONSE OF THE 2001 SOUTHERN PERU EARTHQUAKE

By

ADEL M. CORTEZ-FLORES

A thesis submitted in partial fulfilment of
the requirements for the degree of

MASTER OF SCIENCE IN CIVIL ENGINEERING

WASHINGTON STATE UNIVERSITY
Department of Civil and Environmental Engineering

December 2004

To the Faculty of Washington State University:

The members of the Committee appointed to examine the thesis of ADEL M. CORTEZ-FLORES find it satisfactory and recommend that it be accepted.

_____
Chair

_____

_____

ACKNOWLEDGEMENT

First, I would like to express my gratitude and appreciation to my advisor, Dr. Adrian Rodriguez-Marek. His invaluable knowledge, guidance, patience, continuous support and what is more important his friendship made every phase of the project immensely gratifying.

The material presented in this thesis is based on work supported by the National Science Foundation (NSF) under grants No. CMS-0130617 and CMS-0201574. Any opinions, findings and conclusions or recommendations expressed in this material are those of the author and do not necessary reflect the views of the NSF. Special thanks to this prestigious institution, their support allowed me to be here and be part of this prominent university.

I am also indebted to Prof. Balasingam Muhunthan and Prof. Cole Mc Daniel for their time, patience, and suggestions.

I would like to acknowledge all the persons that made this project possible: Dr. James E. Bay (Utah State University), Dr. Joseph Wartman (Drexel University), Efrain Rondinel (Drexel University), Kwangsoo Park (Utah State University), the employees of the “Universidad Catolica del Peru”, Dr. Boroschek (Universidad de Chile), Ricardo Leon, Ruben, the personnel of the secretary and computational services of the civil engineering department in WSU, and all my friends in Pullman.

I must also thank the immense and unconditional love and support that my wife Luisa has given me. Baby I love you. This work is also yours.

Finally, special thanks to my parents, brother, and sister and all my family who have been accompanying me from home through this experience in the United States. Their words, love and guidance were always my inspiration. I love you.

SITE EFFECT ANALYSIS FOR THE 2001

SOUTHERN PERU EARTHQUAKE

Abstract

By Adel M. Cortez-Flores, M. S.
Washington State University
Dec 2004

Chair: Adrian Rodriguez-Marek

On June 23rd 2001 the region of southern Peru and northern Chile was shaken by a M_w 8.4 earthquake. In terms of seismic moment release, the M_w 8.4 earthquake was arguably the largest worldwide since 1965. The Peruvian states of Arequipa, Ayacucho, Tacna, and Moquegua were severely affected by the earthquake.

The Southern Peru earthquake was the result of thrust faulting on the boundary between the Nazca and South American plates. Seismic gaps capable of producing large earthquakes probably still remain along the plate interface to the northwest and to the south of the 23 June source region. These sections of the plate interface retain the potential to produce great earthquakes in upcoming decades.

Seven strong motion instruments recorded the Southern Peru earthquake. These recordings are highly valuable due to the scarcity of recordings for earthquakes of magnitude larger than M_w 8.0. This research documents the site conditions at the recording stations with a field exploration program that includes Spectral Analysis of Seismic Waves (SASW). One dimensional site response analyses indicated that site

effects at the recording stations contributed significantly to amplification in the high-frequency range, but do not affect the recorded motion at periods longer than about 1.0 s.

Observations of damaged buildings in Tacna, Moquegua, and Ilo indicated spatial damage patterns apparently associated with local amplification of seismic waves. A site response study that included field testing using SASW and Standard Penetration Tests (SPT), as well as one-dimensional site response analyses was conducted in the cities of Moquegua and Tacna. The site response analyses indicated that site effects, as evidenced by high ratios of response spectra computed in site response analyses, contributed to the observed levels of damage in both Moquegua and Tacna.

TABLE OF CONTENTS

LIST OF TABLES

LIST OF FIGURES

Page

LIST OF FIGURES **Page**

LIST OF FIGURES **Page**

LIST OF FIGURES **Page**

LIST OF FIGURES **Page**

LIST OF FIGURES

LIST OF FIGURES **Page**

LIST OF FIGURES **Page**

LIST OF FIGURES **Page**

LIST OF FIGURES **Page**

LIST OF FIGURES **Page**

CHAPTER 1

INTRODUCTION

1.1 Introduction and problem statement

On June 23rd, 2001 at 3:33 pm local time, the region of southern Peru and northern Chile (see Fig. 1.1a and Fig. 1.1b) was shaken by a M_w 8.4 earthquake that was the result of thrust faulting on the boundary between the Nazca and South American plates. In terms of seismic moment release the southern Peru earthquake was, at that time, the largest event since 1965[1] and the largest earthquake to have generated recorded strong ground motions. Seven 3-component ground motion records were obtained in the main shock.

The seismic activity occurred within a 1000-km-long seismic gap that was identified prior to the event as having high potential for large earthquakes (Rodriguez-Marek and Edwards 2003). This section of the plate interface has many similarities with the tectonic conditions of the Pacific Northwest and Alaska in the United States, and still retains the potential to produce great earthquakes in upcoming decades. Therefore, the study of this event is relevant to better understand seismicity and better predict seismic risk in these populated areas.

The earthquake severely damaged the Peruvian departments (states) of Arequipa, Ayacucho, Tacna, and Moquegua, affecting around 200,000 people. A substantial number of the adobe houses in the cities of Moquegua and Tacna were damaged. In addition, around 150 casualties were reported. According to the report by the Peruvian

[1] According to the pacific Earthquake Engineering Database (PEER 2004) and the United States Geological Survey.

Council of Civil Engineers, 55 million dollars were lost in the department of Moquegua alone.

After the event, several reconnaissance teams from various institutions, such as the National Science Foundation (NSF), the U.S. Geological Survey (USGS), and the American Society of Civil Engineering (ASCE), as well as various Peruvian institutions, investigated the effects of the earthquake and the resulting damage throughout the region. The NSF sponsored a U.S.-Peruvian geotechnical reconnaissance team that arrived two weeks after the earthquake. Details of this reconnaissance can be found in Rodriguez-Marek and Edwards (2003). The NSF team observed that damage patterns in the cities of Moquegua and Tacna suggested that site effects affected ground motion intensity and thus had an influence in the resulting damages on structures (Keefer et al. 2003). The NSF team leaders suggested that further and more detailed studies were needed, specifically regarding site response at ground motion stations, site effects, seismic compression of embankments, basin effects, and field documentation of liquefaction and lateral spread case histories.

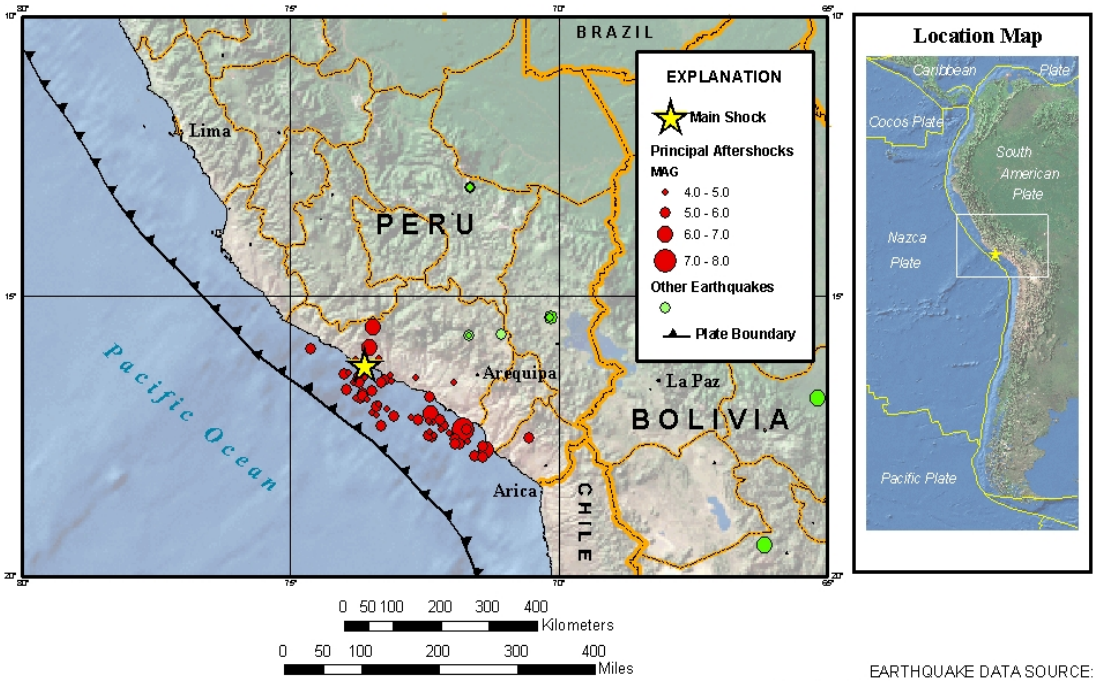

Fig. 1.1a Area of study (maps from the United States Geological Survey website www.USGS.gov)

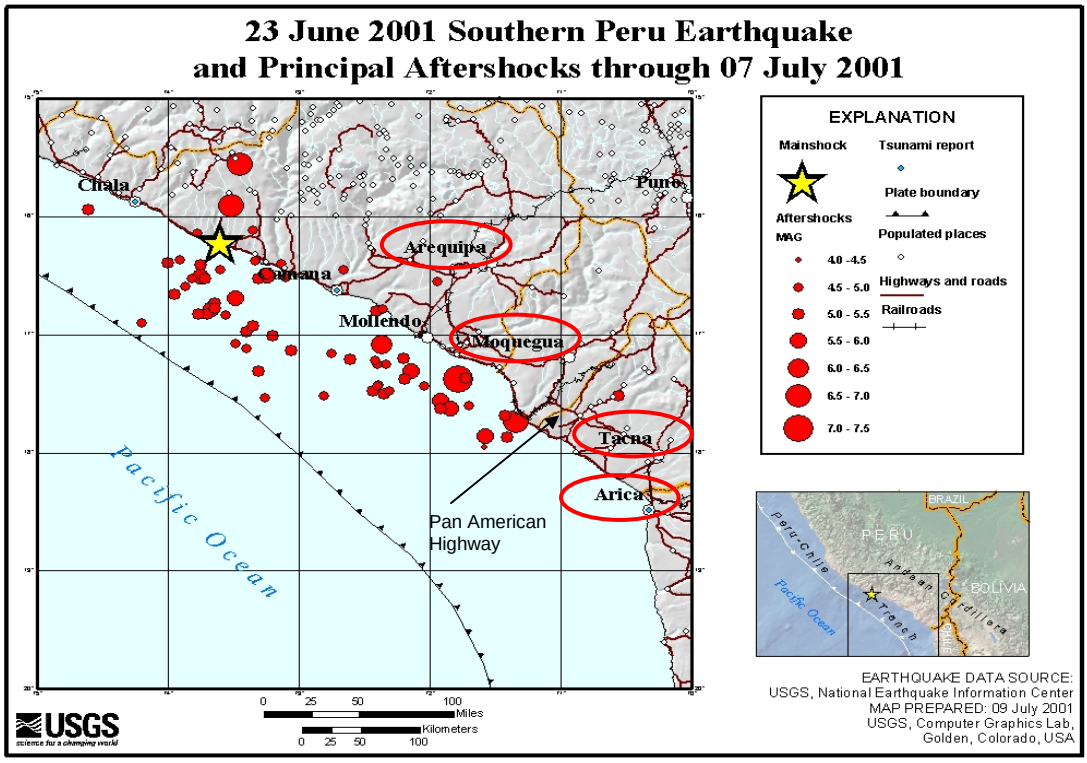

Fig. 1.1b Area of study (maps from the United States Geological Survey website www.USGS.gov)

In the summer of 2003, a joint research team consisting of researchers from Washington State University, Drexel University, and Utah State University performed an extensive geotechnical field investigation, encompassing sites in southern Peru and northern Chile. The objective of the site investigation was to document site conditions at the recording stations and obtain soil properties that would permit an analysis of the previously documented site effects, seismic compression, and liquefaction case histories. This thesis presents the results of the study with an emphasis on the analysis of site response on the recorded ground motions and the correlation between observed damage and site conditions in the cities of Tacna and Moquegua.

1.2 Objectives

The overarching goal of this research is to mitigate damage produced by strong ground motions through a better understanding of soil behavior under seismic loads.

The specific objectives of the present research project are:

(a) To document the results of the geotechnical site investigation performed in the recording stations and the areas affected by the earthquake,

(b) to perform an engineering analysis of the ground motions recorded during the earthquake, including the effects of site response on the recorded ground motion,

(c) to perform site response analyses at different locations in the city of Tacna and Moquegua, and

(d) to study the correlation between observed damage distributions and site amplification in the cities of Tacna and Moquegua.

1.3 Organization of the thesis

The thesis consists of six chapters. A brief description of each of the chapters in the thesis is presented herein. Chapter 1 presents the problem statement, the objectives of the study conducted, and the organization of the entire thesis. An extensive literature review is presented in Chapter 2. Topics include a description of the effects of surface geology and topography on ground motions and the different methodologies available for the estimation of such effects; a brief review of the development of amplification factors in building codes; an explanation of the equivalent linear model used in the present research, and some comments on damage distribution studies following earthquakes. Chapter 3 describes Spectral Analysis of Surface Waves (SASW) tests and the Standard Penetration Tests (SPT) performed during the field investigation. All the data collected from the field is also presented. Chapter 4 presents a detailed analysis of the ground motions recorded during the 2001 Peruvian earthquake, including site response analysis at the ground motion stations. Site response analyses were performed using an equivalent linear approach. Chapter 5 presents the site response analyses for sites located in the cities of Tacna and Moquegua. The chapter also includes the correlation between observed damage distribution and site amplification at various sites. Finally, chapter 6 lists the conclusions obtained from the study and provides recommendations for future research.

CHAPTER 1

INTRODUCTION

1.1 Introduction and problem statement

On June 23rd, 2001 at 3:33 pm local time, the region of southern Peru and northern Chile (see Fig. 1.1a and Fig. 1.1b) was shaken by a M_w 8.4 earthquake that was the result of thrust faulting on the boundary between the Nazca and South American plates. In terms of seismic moment release the southern Peru earthquake was, at that time, the largest event since 1965[1] and the largest earthquake to have generated recorded strong ground motions. Seven 3-component ground motion records were obtained in the main shock.

The seismic activity occurred within a 1000-km-long seismic gap that was identified prior to the event as having high potential for large earthquakes (Rodriguez-Marek and Edwards 2003). This section of the plate interface has many similarities with the tectonic conditions of the Pacific Northwest and Alaska in the United States, and still retains the potential to produce great earthquakes in upcoming decades. Therefore, the study of this event is relevant to better understand seismicity and better predict seismic risk in these populated areas.

The earthquake severely damaged the Peruvian departments (states) of Arequipa, Ayacucho, Tacna, and Moquegua, affecting around 200,000 people. A substantial number of the adobe houses in the cities of Moquegua and Tacna were damaged. In addition, around 150 casualties were reported. According to the report by the Peruvian

[1] According to the pacific Earthquake Engineering Database (PEER 2004) and the United States Geological Survey.

Council of Civil Engineers, 55 million dollars were lost in the department of Moquegua alone.

After the event, several reconnaissance teams from various institutions, such as the National Science Foundation (NSF), the U.S. Geological Survey (USGS), and the American Society of Civil Engineering (ASCE), as well as various Peruvian institutions, investigated the effects of the earthquake and the resulting damage throughout the region. The NSF sponsored a U.S.-Peruvian geotechnical reconnaissance team that arrived two weeks after the earthquake. Details of this reconnaissance can be found in Rodriguez-Marek and Edwards (2003). The NSF team observed that damage patterns in the cities of Moquegua and Tacna suggested that site effects affected ground motion intensity and thus had an influence in the resulting damages on structures (Keefer et al. 2003). The NSF team leaders suggested that further and more detailed studies were needed, specifically regarding site response at ground motion stations, site effects, seismic compression of embankments, basin effects, and field documentation of liquefaction and lateral spread case histories.

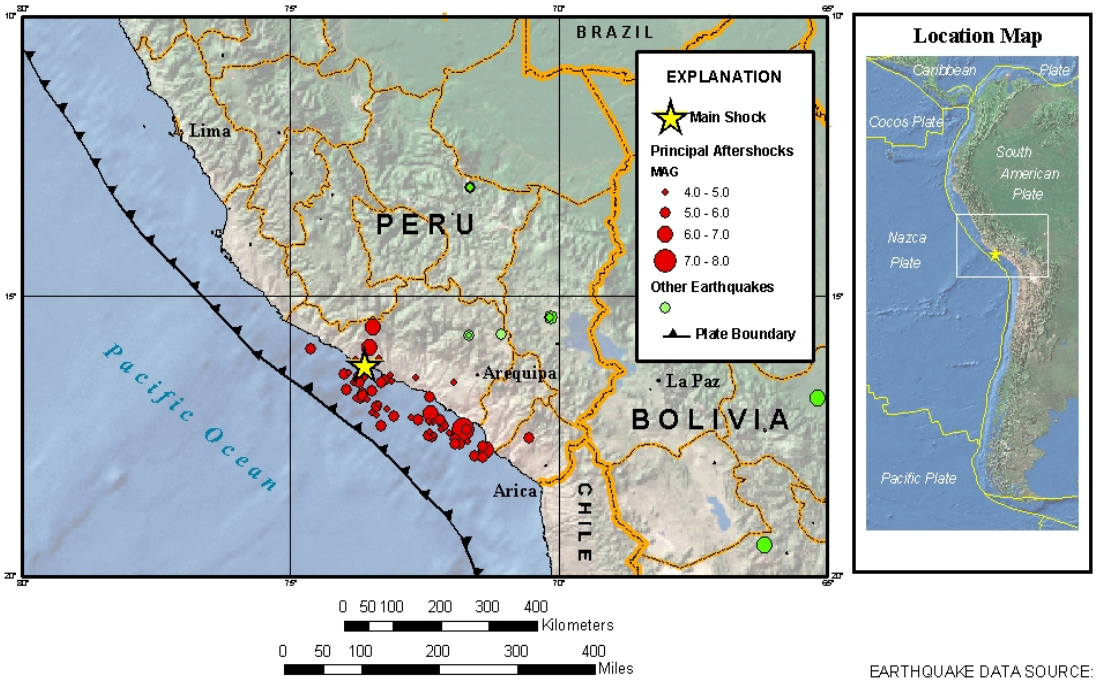

Fig. 1.1a Area of study (maps from the United States Geological Survey website www.USGS.gov)

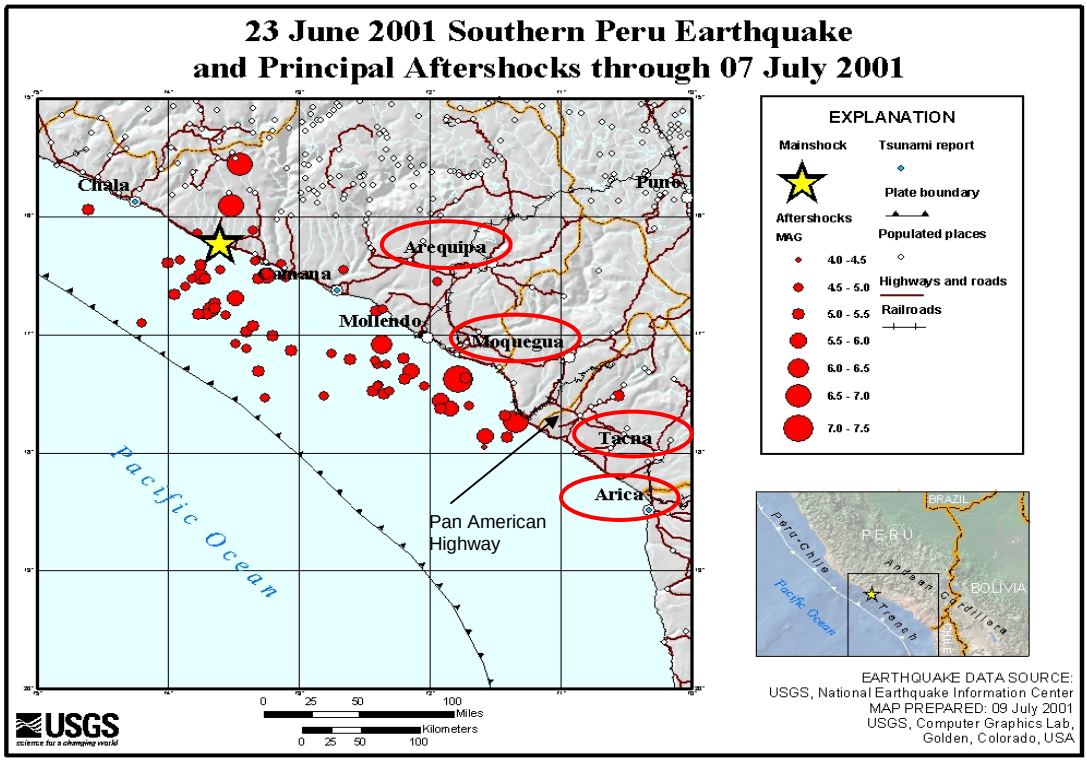

Fig. 1.1b Area of study (maps from the United States Geological Survey website www.USGS.gov)

In the summer of 2003, a joint research team consisting of researchers from Washington State University, Drexel University, and Utah State University performed an extensive geotechnical field investigation, encompassing sites in southern Peru and northern Chile. The objective of the site investigation was to document site conditions at the recording stations and obtain soil properties that would permit an analysis of the previously documented site effects, seismic compression, and liquefaction case histories. This thesis presents the results of the study with an emphasis on the analysis of site response on the recorded ground motions and the correlation between observed damage and site conditions in the cities of Tacna and Moquegua.

1.2 Objectives

The overarching goal of this research is to mitigate damage produced by strong ground motions through a better understanding of soil behavior under seismic loads.

The specific objectives of the present research project are:

(a) To document the results of the geotechnical site investigation performed in the recording stations and the areas affected by the earthquake,

(b) to perform an engineering analysis of the ground motions recorded during the earthquake, including the effects of site response on the recorded ground motion,

(c) to perform site response analyses at different locations in the city of Tacna and Moquegua, and

(d) to study the correlation between observed damage distributions and site amplification in the cities of Tacna and Moquegua.

1.3 Organization of the thesis

The thesis consists of six chapters. A brief description of each of the chapters in the thesis is presented herein. Chapter 1 presents the problem statement, the objectives of the study conducted, and the organization of the entire thesis. An extensive literature review is presented in Chapter 2. Topics include a description of the effects of surface geology and topography on ground motions and the different methodologies available for the estimation of such effects; a brief review of the development of amplification factors in building codes; an explanation of the equivalent linear model used in the present research, and some comments on damage distribution studies following earthquakes. Chapter 3 describes Spectral Analysis of Surface Waves (SASW) tests and the Standard Penetration Tests (SPT) performed during the field investigation. All the data collected from the field is also presented. Chapter 4 presents a detailed analysis of the ground motions recorded during the 2001 Peruvian earthquake, including site response analysis at the ground motion stations. Site response analyses were performed using an equivalent linear approach. Chapter 5 presents the site response analyses for sites located in the cities of Tacna and Moquegua. The chapter also includes the correlation between observed damage distribution and site amplification at various sites. Finally, chapter 6 lists the conclusions obtained from the study and provides recommendations for future research.

CHAPTER 2

LITERATURE REVIEW

2.1 Introduction

The factors that affect a ground motion at a given site are typically grouped into source, path, and site effects. Source effects include both earthquake magnitude as well as the characteristics of the slip distribution within the fault. Path effects include both material and geometrical attenuation and are a function of the travel path geology and the distance from the site to the source. Site effects correspond to the effects of local geology and topography.

Events such as the 1985 Mexico City and 1989 Loma Prieta earthquakes have provided extensive evidence of the effects that the superficial geology and topography have on seismic motions and therefore on resulting damages and damage distribution. Thus, taking site response into account in the design of structures is of considerable importance.

Abundant information on site effects and the tools available to estimate them can be found in the fields of geology, seismology, and other related fields. The two basic methodologies used to quantify site effects are in situ measurements and numerical modeling based on measured soil properties, including the shear wave velocity profile.

The present literature review covers the topics that constitute the theoretical basis for the present study. The subjects include local site effects (such as topographic and basin effects), one dimensional site response analysis, and instrumental methodologies for site response analysis (such as non-reference and reference site techniques). A brief

explanation of the equivalent linear model for soil response analysis, which is extensively used in this study, is also presented.

2.2 Local site effects

Currently, researchers agree that local site conditions can profoundly influence the amplitude, frequency content, and duration of a ground motion, as evidenced by macro seismic observations and instrumental studies. The extent of this influence depends on factors such as the geometry and material properties of the subsurface materials, the site's topography, and the characteristics of the input motion.

2.2.1 Topographic effects

The effect of topography on seismic ground motion has generally not been analyzed in enough detail in the past in spite of evidence that topography has a considerable influence on the amplitude and frequency content of ground motions (Bouckovalas and Papadimitriou 2004) . Topographic effects have been observed in several earthquakes, such as the 1985 Chile, 1985 Mexico 1985, and 1989 Loma Prieta, among others (Bouckovalas and Papadimitriou 2004).

There are selected studies that focus on topographic aspects such as the influence of specific surface geometries on ground motions (Bouckovalas et al. 1999, Gazetas et al. 2002), the wave scattering generated at the vicinity of a slope (Boore et al. 1981), or the effects of soft soils in the area of a slope (Ohtsuki et al. 1983). There are also a few parametric studies such as Ashford et al. (1997) that include factors such as variations in slope inclination, height, wavelength, and angle of incidence in their analysis. Other reports on topographic effects include a study by Bard (1987) on important amplifications

observed in a considerably steep site in the southern Alps, and numerical evaluations of effects of slope topography by Stewart et al. (2001), and Bouckovalas et al (2004).

A synopsis of the most important issues involving topographic effects, based on a review of the publications previously mentioned, is presented below. Three different types of topographic effects have been identified: ridge, canyon, and slope effects (Stewart et al. 2001).

Ridges

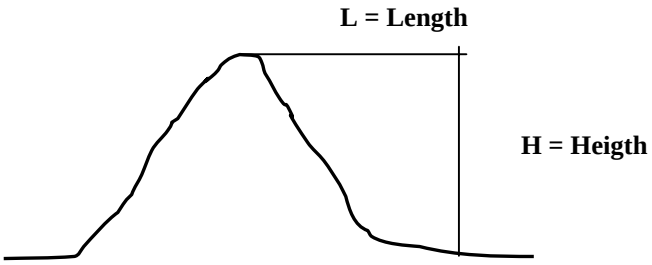

Figure 2.1 Ridge representation.

Just a small number of studies on topographic effects across ridges have been published. In most cases a two-dimensional homogeneous model was assumed, as illustrated in Figure 2.1. A review by Bard (1995) found levels of crest-to-base acceleration ratios and spectral ratios of amplification to be about 1-2 (average height of the ridge used H=1.5) for shape ratios of H/L = 0.3-0.5. Also Stewart et al. (2001) suggested that crest amplification occurs for a wavelength equal to the ridge half-width and that the maximum amplification for spectral accelerations is about 1.6. Pedersen et al. (1994) suggested that amplification was extremely sensitive to the vertical angle of the incident wave field.

Canyons

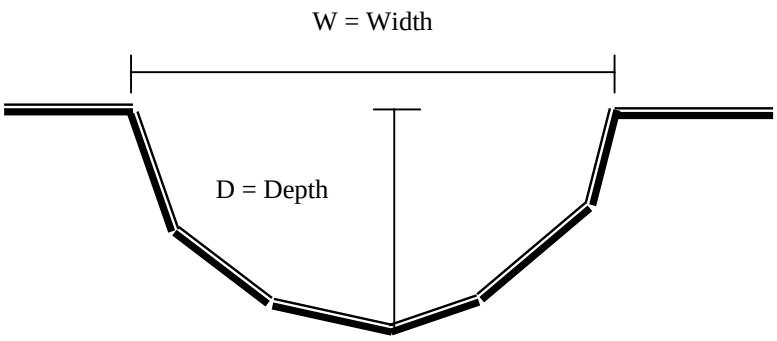

Figure 2.2 Canyon representation.

Important earthquakes such as the 1971 San Fernando or the 1995 Taipei earthquake (Chin-Hsiung Loh et al. 1998) showed the effect of canyon geometries (Figure 2.2) on the amplification of the motions recorded during those events. Stewart et al. (2001) presented a detailed compilation of the results obtained from studies such as Trifunac (1973) and Wong and Trifunac (1974). From the analysis of these studies Stewart et al. (2001) suggested that amplification is particularly frequency dependent and that this dependency becomes more notorious when wavelengths are similar to or smaller than the canyon dimension. Other comments from those studies are that a maximum value of amplification of about 1.4 occurs near the canyon edge and that the maximum base de-amplification is about 0.5 (Stewart 2001). Stewart et al. (2001) also concluded that amplification is usually proportional to the ratio of depth (D) over width (W) (see Figure 2.2).

Slopes

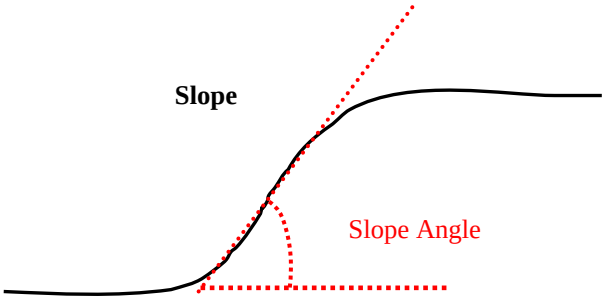

Figure 2.3 Slope representation.

Stewart et al. (2001) also evaluated the current knowledge on the influence of slope geometries (Figure 2.3) on ground motion, concluding that the main factor that influences ground motions on slopes is the slope angle (Figure 2.3). Stewart (2001) also observed that amplification increases with slope angle and becomes even higher with the proximity to crest. Moreover, amplification increases considerably when incident waves travel following the slope. Different values of amplification ratios (crest to toe) were found in different studies. In particular, Stewart and Sholtis (2001) suggests amplification values around 1.2

2.2.2 One dimensional site response

One dimensional ground response is the analysis of the passage of vertically propagating body waves through a horizontally-layered soil profile. The amount of information on ground response is extensive and only a summary is presented herein.

Three different categories of site response models are typically used for the analysis of site amplification, equivalent linear and nonlinear models for one directional shaking, and non linear models for multiple directions of shaking (Stewart 2001). All these models are applied to the solution of equations of motion for vertical propagation of horizontally polarized shear waves. The equivalent linear model, which is explained in section 2.4 is the one used in the present study.

Dynamic soil properties control the response of a site to seismic excitation. These properties are shear wave velocity (V_s), soil density, and the stress-strain behavior of soils. In equivalent linear models, the stress-strain behavior of soils is represented by normalized shear modulus reduction (G/G_{max}) and soil damping (β) versus shear strain (γ) curves. Shear wave velocity is related to shear modulus and density ρ of the soil by:

$$G_{max} = V_s^2 \rho$$

V_s profiles can nowadays be obtained using different in situ methods such as downhole, crosshole, suspension logging and Geophysical techniques such as the spectral analysis of surface waves (SASW). The Geophysical methods, can be particularly effective, useful, and most of times cheap. In particular, SASW testing is a relatively novel technique that provides reliable measurements, while the cross-hole and down-hole methods require the installation of one or more boreholes, which is generally time consuming and costly, in SASW testing both the source and receivers are placed on the ground surface. SASW has other advantages, for instance, while borehole methods are point estimates, SASW testing is a global measurement, which means that a much larger volume of the subsurface is sampled. Moreover, the resulting profile is representative of the subsurface properties averaged over distances of up to several hundred feet. Additionally the resolution obtained with the SASW in the near surface (typically the top 25 ft) is typically greater than with the other methods. The economic cost of testing is low when compared to techniques such as down-hole. Finally the non-invasive and non-destructive characteristic of the SASW method makes relatively easy to obtain the necessary permits for testing. For all these reasons this method was chosen to be used in the present study, a description of the method is presented in Chapter 3. V_s can also be estimated from correlations with other soil properties such as over consolidation ratio and undrained shear strength, penetration resistance and effective stress (Stewart 2001).

Standard modulus reduction and damping are typically used curves for various soil types (e.g. Idriss (1990), Vucetic and Dobry (1991), Seed et al. (1996), and Darendeli (2001)). Two main methods are at this time available to obtain these curves. The first

method is based on laboratory tests, and the second consists in performing a back-analysis of regional ground motion records (Silva et al. 1997). The effective stress dependent curves developed by Darendeli (2001) were obtained from extensive testing and included a measure of uncertainty, which made them advantageous for this study.

2.2.3 Basin effects

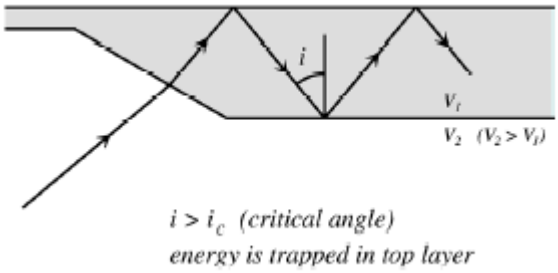

Figure 2.4 Basin Effects (from Stewart et al.2001).

Basin effects on ground motions are the effects caused by sites in which alluvial and sedimentary deposits present notoriously lower shear velocities than the underlying rocks on which they have been deposited. Basins usually have thickness ranging from 100 m to over 10 km (Stewart 2001). It is currently known that 1-D modeling cannot represent the basin effect because 1-D modeling can capture resonance in the layer but cannot model trapped waves within the layer (Stewart 2001). Thus, 2-D and 3-D models are necessary to explain observed amplification levels. Additionally, some post earthquake reports such as the 1994, Northridge (Hall et al. 1995) or the 1994, Taipei (Chin-Hsiung Loh 1998) earthquakes provided some evidence that ground motions may be particularly large at the edges of basins. Subsequent studies on wave propagation modeling using basin structures support this fact (e.g. Graves et al. 1998).

2.3 Instrumental methodologies for estimating site response

It is currently agreed that source and travel path effects typically affect a ground motion. Ground motions also depend on many other aspects, such as earthquake magnitude, characteristics of the slip distribution, material and geometrical attenuation, travel path geology, and distance from the site to the source. When instrumental methodologies are applied to measure site response source and path effects are usually removed. Removing the source and path effects is typically a complicated task, and depending on how this is achieved the instrumental methods available can be divided into reference and non-reference site techniques (Bard 1995).

2.3.1 Reference site techniques

These techniques are based on comparing records of two nearby sites for which differences between source and path effects are assumed to be inexistent (Bard 1995). Spectral ratios are defined as the ratio of response spectra from the site being studied over the response spectra of the reference site. If the site considered as reference has no site effects, the spectral ratios can be considered to represent the site effect with enough reliability.

2.3.2 Non-reference site techniques

Usually, adequate reference sites are not available. There are two main methods that have been developed to overcome this inconvenient. For the first method, source and path effects can be assumed through formulas providing the spectral shape as a function of a few parameters, such as seismic moment and others. This process is known as “parameterized source and path inversion” (Jacob 1994).

The other non-reference site technique, also known as Nakamura's Method, consists in taking the spectral ratio between the horizontal and vertical components of the shear wave and is described in section 2.3.2.1. Reports such as Theodulidis et al. (1994) concluded that the spectral ratios obtained from this method appear to be well correlated with surface geology and are less sensitive to source and path effects. Also Field and Jacob (1994) used Nakamura's method and concluded that site amplification was slightly underestimated. Jacob (1994) also concluded that if the technique is applied to the P-wave part of the recordings, the results were notoriously different, whereas when applied to the S-wave signals the results accurately revealed the overall frequency dependence (Bard 1995).

2.4 Equivalent linear model for site response analysis

The effect of the non-linearity of soils has been reported extensively. Hardin and Drnevitch (1970), Seed and Idriss (1970), Seed et al. (1986), Sun et al. (1988), Vucetic and Dobry (1991), Kramer (1996), Bardet et al. (2000) and Kramer (2000), and Darendeli (2001) reported a decrease of the amplification factors and sometimes a decrease of resonant frequencies at peak accelerations due to non-linearity.

Based on these studies, it is reasonable to expect significant non-linear effects on soft soils when the peak acceleration of rock is greater than 0.1 or 0.2 g. These values vary depending on nature and thickness of the soil deposit, magnitude, duration, and frequency content of the ground motion. This section describes the equivalent linear method for site response analysis.

2.4.1 One dimensional stress-strain relationship

The following description of the equivalent-linear model for one dimensional stress-strain relationships was extracted from Bardet et al. (2000) and Kramer (1996).

The equivalent linear model represents the soil stress-strain response based on a Kelvin-Voigt model as illustrated in Figure 2.5 The shear stress τ depends on the shear strain γ and its rate $\dot{\gamma}$ as follows:

$$\tau = G\gamma + \eta\dot{\gamma} \tag{1}$$

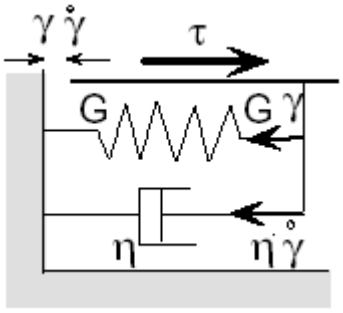

Figure 2.5 Schematic representation of stress-strain model used in equivalent-linear model (Bardet et al. 2000).

where G is the shear modulus and η the viscosity. The shear strain γ and its rate are defined from the horizontal displacement *u(z,t)* at depth *z* and time *t* with the following equation:

$$\gamma = \frac{\partial u(z,t)}{\partial z} \text{ and } \gamma^{\cdot} = \frac{\partial \gamma(z,t)}{\partial t} = \frac{\partial^2 u(z,t)}{\partial z \partial t} \tag{2}$$

For the case of harmonic motion, the displacement, strain, and strain rate can be shown to be:

$$u(z,t) = U(z)e^{i\varpi t}, \gamma(z,t) = \frac{dU}{dz}e^{i\varpi t} = U(z)e^{i\varpi t} \text{ and } \dot{\gamma}(z,t) = i\varpi\gamma(z,t) \tag{3}$$

2.4.2 Equivalent linear approximation of non-linear stress-strain response

The non-linear and hysteretic stress-strain behavior of soils is approximated during cyclic loadings as shown in Figure 2.6. The equivalent linear shear modulus, *G*, is taken as the secant shear modulus G_s. As shown in Figure 2.6a, G_s is defined as:

$$G_s = \frac{\tau_c}{\gamma_c} \qquad (4)$$

Where τ_c and γ_c are the shear stress and strain, respectively. The equivalent linear damping ratio, ξ, is the damping ratio that represents the energy loss in a single cycle.

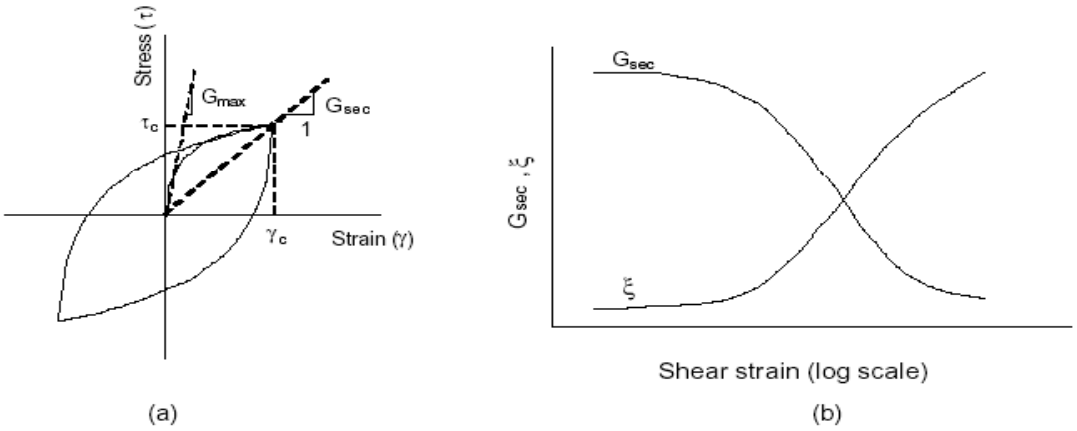

Figure 2.6 Equivalent-linear model: (a) Stress-strain curve; and (b) Modulus degradation and damping ratio increase with sear strain amplitude (Bardet et al. 2000).

Strain softening corresponds to a decrease in stress with an increase in strain. To include this strain softening effect is usually a complicated task. As shown in Fig. 2.8 b, the equivalent linear model consists in the variation of shear modulus and damping ratio with shear strain amplitude. Additional assumptions are required to specify the effects of frequency on stress-strain relations. For this purpose, two basic models have been proposed (Bardet et al. 2000).

Model 1

Model 1 is used in the original version of SHAKE (Schnabel et al. 1972). It assumes that ξ is constant and independent of ω, which implies that the complex shear modulus G^* is also independent of ω. The dissipated energy during a loading cycle is:

$$W_d = 4\pi W_s \xi = 2\pi \xi G \gamma_c^2 = \pi \eta \gamma_c^2 \omega \qquad (5)$$

where: W_d = energy dissipated; W_s = energy; G = shear modulus; γ = strain; ε = damping ratio; and ω = frequency.

The dissipated energy increases linearly with ξ, which implies that the area of stress-strain loops is frequency independent. The amplitudes of the complex (G^*) and the real (G) shear modulus are related by:

$$\left|G^*\right| = G\sqrt{1+4\xi^2} \qquad (6)$$

Model 2

Model 2 is used in SHAKE 91 (Idriss and Sun 1992). It assumes that the complex shear modulus is a function of ξ given by:

$$G^* = G\left\{\left(1-2\xi^2\right)+2\xi i\sqrt{1-\xi^2}\right\} \qquad (7)$$

Equation 7 above is a constitutive assumption that belongs to the description of material behavior. It implies that the complex and the real shear modulus have the same amplitude (Bardet et al. 2000), i.e.:

$$\left|G^*\right| = G\left\{(1-2\xi^2)^2+4\xi^2(1-\xi^2)\right\} = G \qquad (8)$$

The energy dissipated during a loading cycle is:

$$W_d = \frac{1}{2}\omega\gamma_c^2\int_t^{t+2\pi/\omega} 2G\xi\sqrt{1-\xi^2}\,dt = 2\pi G\xi\sqrt{1-\xi^2}\gamma_c^2 \qquad (9)$$

For practical purposes, ξ is usually less than 25% and 5% is the most common value applied. Under these conditions, the energies dissipated by Models 1 and 2 are similar (Bardet et al. 2000).

2.4.3 One dimensional site response Analysis

The present section compiles the explanation given by Kramer (1996) and Bardet et al. (2000). Figure 2.7 shows the one dimensional equivalent linear site response analysis assumption. A vertical harmonic shear wave is assumed to propagate vertically in a one dimensional layered system. The one dimensional equation of motion for vertically propagating shear waves is:

$$\rho \frac{\partial^2 u}{\partial t^2} = \frac{\partial \tau}{\partial z} \qquad (10)$$

Where ρ is the unit mass in any layer. Assuming that the soil behaves as a Kelvin-Voigt solid (as explained in the previous section), equation (10) becomes:

$$\rho \frac{\partial^2 u}{\partial t^2} = G \frac{\partial^2 u}{\partial z^2} + \eta \frac{\partial^3 u}{\partial z^2 \partial t} \qquad (11)$$

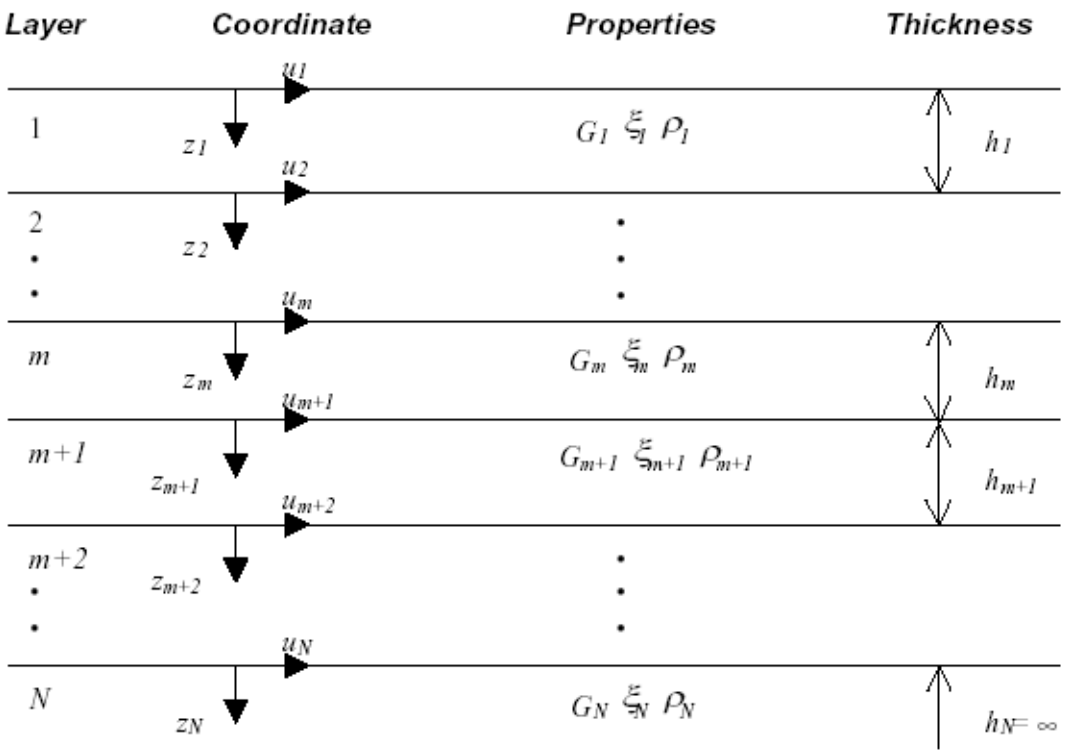

Figure 2.7 One dimensional layered soil deposit system (Kramer 1996).

For harmonic waves, the displacement can be written as a function of frequency:

$$u(z,t) = U(z)e^{i\omega t} \tag{12}$$

Combining equations 11 and 12, this expression becomes:

$$(G + i\omega\eta)\frac{d^2U}{dz^2} = \rho\omega^2 U \tag{13}$$

Which admits the following general solution:

$$U(x) = Ee^{ik^* z} + Fe^{-ik^* z} \tag{14}$$

where:

$$K^{*^2} = \frac{\rho\omega^2}{G + i\omega\eta} = \frac{\rho\omega^2}{G^{\phi}} \tag{15}$$

is the complex wave number. After introducing the critical damping ξ ($\xi = \omega\eta/2G$,) the complex shear modulus G^* becomes:

$$G^* = G + i\omega\eta = G(1 + 2i\xi) \tag{16}$$

The solution for the displacement is:

$$u(z,t) = (Ee^{ik^* z} + Fe^{-ik^* z})e^{i\omega t} \tag{17}$$

and the corresponding stress is:

$$\tau(z,t) = ik^{\phi}G^{\phi}(Ee^{ik^{\phi} z} - Fe^{-ik^{\phi} z})e^{i\omega t} \tag{18}$$

The displacements at the top ($z = 0$) and bottom ($z = hm$) of layer m of thickness hm are:

$$u_m(0,t) = u_m = (E_m + F_m)e^{i\omega t} \text{ and } u_m(h_m,t) = (E_m e^{ik_m^{\phi} h_m} + F_m e^{-ik_m^{\phi} h_m})e^{i\omega t} \tag{19}$$

The shear stresses at the top and bottom of layer m are:

$$\tau_m(0,t) = ik_m^{\phi}G_m^{\phi}(E_m - F_m)e^{i\omega t} \text{ and } \tau_m(h_m,t) = ik_m^{\phi}G_m^{\phi}(E_m e^{ik_m^{\phi} h_m} - F_m e^{-ik_m^{\phi} h_m})e^{i\omega t} \tag{20}$$

At the interface between layers m and $m+1$, displacements and shear stress must be continuous, which implies that:

$$u_m(h_m,t) = u_{m+1}(0,t) \text{ and } \tau_m(h_m,t) = \tau_{m+1}(0,t) \tag{21}$$

The coefficients E_m and F_m can be related through equations (22) and (23):

$$E_{m+1} + F_{m+1} = E_m e^{ik_m^{\phi} h_m} + F_m e^{-k_m^{\phi} h_m} \tag{22}$$

$$E_{m+1} - F_{m+1} = \frac{k_m^{\phi}G_m^{\phi}}{k_{m+1}^{\phi}G_{m+1}^{\phi}}(E_m e^{ik_m^{\phi} h_m} - F_m e^{-ik_m^{\phi} h_m}) \tag{23}$$

These equations give the following formulas for amplitudes E_{m+1} and F_{m+1} in terms of E_m and F_m:

$$E_{m+1} = \frac{1}{2}E_m(1+\alpha_m^{\phi})e^{ik_m^{\phi} h_m} + \frac{1}{2}F_m(1-\alpha_m^{\phi})e^{-ik_m^{\phi} h_m} \tag{24}$$

$$F_{m+1} = \frac{1}{2}E_m(1-\alpha_m^{\phi})e^{ik_m^{\phi} h_m} + \frac{1}{2}F_m(1+\alpha_m^{\phi})e^{-ik_m^{\phi} h_m} \tag{25}$$

where α_m^{ϕ}

is the complex impedance ratio at the interface between layers *m* and *m+1*:

$$\alpha_m^{\phi} = \frac{k_m^{\phi} G_m^{\phi}}{k_{m+1}^{\phi} G_{m+1}^{\phi}} = \sqrt{\frac{\rho_m G_m^{\phi}}{\rho_{m+1} G_{m+1}^{\phi}}} \tag{26}$$

The algorithm is started at the top free surface, for which there is no shear stress:

$$\tau_1(0,t) = ik_1^{\phi} G_1^{\phi} (E_1 - F_1) e^{i\omega t} \quad , \tag{27}$$

which implies:

$$E_1 = F_1$$

The same equations are then applied successively to layers 2 to *m*. The transfer function A_{mn} relating the displacements at the top of layers *m* and *n* is defined by

$$A_{mn}(\omega) = \frac{u_m}{u_n} = \frac{E_m + F_m}{E_n + F_n} \tag{28}$$

The velocity $\dot{u}(z,t)$ and acceleration $\ddot{u}(z,t)$ are related to displacement through:

$$\dot{u}(z,t) = \frac{\partial u}{\partial t} = i\omega u(z,t) \text{ and } \ddot{u}(z,t) = \frac{\partial^2 u}{\partial t^2} = -\omega^2 u(z,t) \tag{29}$$

Therefore, A_{mn} is also the transfer function relating the velocities and displacements at the top of layers *m* and *n*:

$$A_{mn}(\omega) = \frac{U_m}{U_n} = \frac{\dot{U}_m}{\dot{U}_n} = \frac{\ddot{U}_m}{\ddot{U}_n} = \frac{E_m + F_m}{E_n + F_n} \tag{30}$$

The shear strain at depth *z* and time *t* can be derived:

$$\gamma(z,t) = \frac{\partial u}{\partial z} = ik^{\phi}(Ee^{ik^{\phi}z} - Fe^{-ik^{\phi}z})e^{i\omega t} \tag{31}$$

The corresponding shear stress at depth *z* and time *t* is:

$$\tau(z,t) = G^{\phi}\gamma(z,t) \tag{32}$$

2.4.4 Transient motions

The one dimensional soil column response theory presented in the previous section applies to a steady state harmonic motion in the frequency domain. Using Fourier series the theory can be extended to the time histories of transient motions. A real-valued or complex-valued function x (t) can be approximated by a discrete series of N values as follows (Bardet et al. 2000):

$$X_n = \sum_{k=0}^{N-1} X_k e^{i\omega_k t_n} = \sum_{k=0}^{N-1} X_k e^{i\omega_k n\Delta t} = \sum_{k=0}^{N-1} X_k e^{2\pi i k n / N} \quad n = 0,....., N-1 \qquad (33)$$

The values of x_n correspond to times $t_n = n\ \Delta t$, where Δt is a constant time interval (i.e., $x(n\Delta t) = x_n$ for $n = 0, \ldots, N\text{-}1$). The discrete frequencies ω_k are:

$$\omega_k = 2\pi \frac{k}{N\Delta t} \qquad k = 0,....., N-1 \qquad (34)$$

The Fourier components are:

$$X_m = \frac{1}{N} \sum_{k=0}^{N-1} x_n e^{-2\pi i k m / N} \qquad m = 0,....., N+1 \qquad (35)$$

The coefficients X_m are calculated by the Fast Fourier Transform algorithm, which was originally developed by Cooley and Turkey (1965). The number of operations scales as $N\ logN$, which reduces notoriously the total number of operations and processing time, fact that justifies the name of Fast Fourier Transform (FFT).

2.4.5 Iterative approximation of equivalent linear response

This explanation was as well extracted from Bardet et al. (2000). In the equivalent linear program SHAKE 91, the values of shear modulus and damping ratio are determined by iterations and they have to be consistent with the level of strain induced in each layer. Initial values G_o and ξ_o are assumed at small strain values; the maximum

shear strain γ_{max} (the effective shear strain γ_{eff} is assumed to be a percentage of γ_{max}, typically 65%) is then calculated using the equations previously described. The values of G_1 and ξ_1 corresponding to γ_{eff1} are found for the next iteration. The equivalent linear analysis is repeated with new values of G and ξ until the difference between the values of G and ξ of the new iteration and the ones from the previous one have a predetermined permissible difference. The iteration procedure for the equivalent linear approach in each layer is summarized as follows:

a) Assume initial values of G_i and ξ_i at small strain values.

b) Obtain the ground response and the amplitudes at the maximum shear strain (γ_{max}) from the shear strain time histories in each layer.

c) Determine the effective shear strain γ_{eff} from γ_{max}

$$\gamma_{eff}^{i} = R_{\gamma}\gamma_{\max}^{i} \tag{39}$$

where $R\gamma$ is the ratio of the effective shear strain to maximum shear strain; it accounts for the number of cycles during earthquakes. $R\gamma$ is constant for all layers (65 % was assumed for the present study).

d) Calculate the new values G_{i+1} and ξ_{i+1} corresponding to the effective shear strain γ_{eff}.

e) Repeat steps 2 to 4 until the differences between the computed values of shear modulus and damping ratio in two successive iterations have a predetermined permissible difference in all layers. Generally, eight iterations are sufficient to achieve convergence.

2.5 Development of site coefficients or amplification factors in the USA

This section summarizes the review of amplification factors presented by Dobry et al. (2000). Also a comparison between amplification factors for generic site categories and site-specific factors defined from ground response analysis is made. Finally, a brief evaluation of the current code factors is presented.

2.5.1 History of the amplification factors

The Applied Technology Council first introduced the effect of geological soil conditions into the U.S. seismic building codes in 1976 by providing the use of three site coefficients (S1, S2 and S3). These coefficients, which were in use until 1994, took into account the stiffness and soil depth at the site and were based on statistical studies (Seed et al. 1976a,b and Mohraz 1976). After the 1985, Mexico City earthquake a fourth category, with its respective coefficient S4 for deep soft clay deposits, was introduced in the Uniform Building Code (UBC 1994). The S factors were implemented by associating each site category with a different spectral shape (Dobry et al. 2000).

The experience learned from the 1985, Mexico City and the 1989, Loma Prieta earthquakes showed that the level of shaking and the low peak ground accelerations and associated low spectral levels for short periods can be amplified at soft sites. The New York city seismic code (Jacob 1990, 1994) was the first to incorporate two important aspects: 1) Larger values of soil site coefficients, as appropriate for areas of lower shaking, and 2) the addition of a “hard rock” category to better characterize the rock conditions in the eastern U. S (Dobry et al. 2000).

A 9-member committee at the 1991 NCEER Workshop was assigned the development of specific code recommendations. In the 1992 Los Angeles Workshop, the

committee had developed recommendations on new site categories and site coefficients that were incorporated in 1994 and 1997 into the National Earthquake Hazards Reduction Program, and in 1997 into the Uniform Building Code (Dobry et al. 2000).

It was also suggested that average values of Ratios of Response Spectra (RRS_{max}) and Ratios of Fourier Spectra (a_A/a_B) for the same period range be within 30% to each other (Joyner et al. 1994). A distinction of terms was made clarifying that amplification ratios are in the Fourier domain while RRS_{max} are in the Spectral domain, as their concepts state.

Empirical studies show that factors calculated using Ratios of Fourier Spectra between soil sites and nearby rock sites are proportional to the mean shear wave velocity of the top 30 m (Borcherdt 1994b, UBC 1997, and Dobry et al.1999). Joyner et al. (1981) alleged that the value is about $(V_s)^{-0.5}$ whereas Borcherdt (1993,1994a) suggested that the value is $(V_s)^{-0.4}$ for short periods and $(V_s)^{-0.6}$ for periods equal to 1 or longer.

2.5.2 Uniform Building Code prior to 1994

Seed (1976) and Idriss (1990, 1991) studied the relationship between peak acceleration recorded on soil and that obtained on a nearby rock outcrop. Idriss (1990) obtained a curve that compares this relationship for the 1985, Mexico City and the Loma Prieta (1989) earthquakes; the curve shows that for low rock accelerations of the order of 0.05 g to 0.10 g, the corresponding soft soil accelerations are 1.5 to 4 times greater than the rock acceleration. This amplification factor decreases as rock acceleration increases and approaches one for a rock acceleration of 0.4 g., with a tendency for de-amplification to occur at larger rock accelerations (Idriss 1990). This phenomenon is directly related to

the non-linear stress-strain behavior of the soil as rock acceleration increases (Figure 2.6a).

An important step in the study of the amplification factors is the study of the shape of the response spectrum and its correlation with site conditions (Figure 2.8). Simplified Response Spectra shapes were developed by the Applied Technology Council (ATC) and incorporated into the Uniform Building Code (1997) as the soil types S1 (rock or shallow stiff soil), S2 (deep firm soils) and S3 (soft soils 20 to 40 ft thick) were accepted and included. The resulting site factors are summarized in Table 2.1

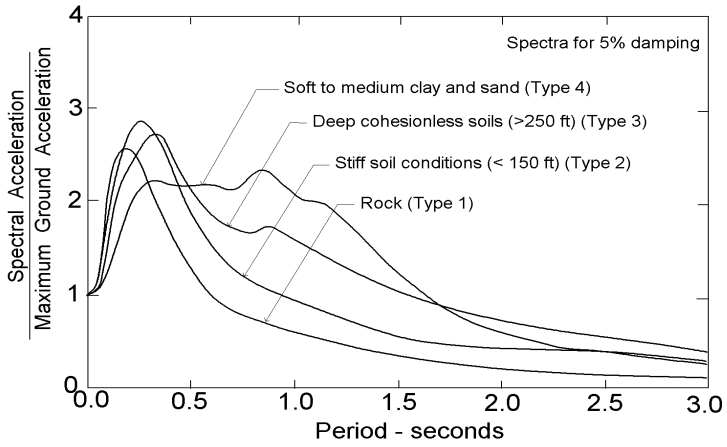

Figure 2.8 Average acceleration spectra for different site conditions (Seed et al. 1976).

Table 2.1 Soil profile types and site factors for calculation of lateral force (Dobry et al. 2000)

Soil Profile Type	Description	Site Coefficient S
S_1	A soil profile with either (1) rock of any characteristic, either shale-like or crystalline in nature, that has a shear wave velocity greater than 2500 ft/s or (2) stiff soil conditions where the soil depth is less than 2000 ft and the soil types overlying the rock are stable deposits of sands, gravels, or stiff clays.	1.0
S_2	A soil profile with deep cohesionless or stiff clay conditions where the soil depth exceeds 200 ft and the soil types overlying rock are stable deposits of sands, gravels, or stiff clays.	1.2
S_3	A soil profile containing 20 to 40 ft in thickness of soft-to medium stiff clays with or without intervening layers of cohesionless soils.	1.5
S_4	A soil profile characterized by a shear wave velocity of less than 500 ft/s containing more than 40 ft of soft clays or silts.	2.0

These S_1 to S_4 factors were removed from the 1994 and 1997 NEHRP and from the 1997 UBC, which means that in the new seismic provisions there is no longer a single multiplication factor for the whole spectrum.

2.5.3 Current site factors and site classifications

A consensus developed during the Site Response Workshop of November 1992 resulted in the incorporation of a new procedure to account for the effects of site conditions on design spectra in the 1994 version of the NEHRP provisions. This procedure has been incorporated into the UBC in 1997 and remains unchanged in the latest International Building Code (IBC 2003).

The new procedure specifies two site coefficients, F_a and F_v, corresponding to the short and long ranges respectively, which replace the single long-period site factor S previously used. Both coefficients depend on site category and intensity of rock motion. In addition, each site category is defined by a representative average V_s of the top 30 m of the profile at the site. The values of F_a and F_v are listed in Table 2.2 and described in Table 2.3.

Table 2.2 Site coefficients for short (F_a) and for long (F_v) periods as a function of site conditions and rock shaking level.

(a) Short period site coefficient F_a

Site Class or Soil Profile Type	Mapped Rock Shaking Level at Short Periods				
	S_s[1] ≤ 0.25	S_s = 0.50	S_s = 0.75	S_s = 1.00	S_s ≥ 1.25
	A_a[2] ≤ 0.10	A_a = 0.20	A_a = 0.30	A_a = 0.40	A_a ≥ 0.50
A	0.8	0.8	0.8	0.8	0.8
B	1.0	1.0	1.0	1.0	1.0
C	1.2	1.2	1.1	1.0	1.0
D	1.6	1.4	1.2	1.1	1.0
E	2.5	1.7	1.2	0.9	*
F	*	*	*	*	*

[1] S_s = Acceleration values for short periods (NEHRP 1997)
[2] A_a = Acceleration values for short periods (NEHRP 1994)

Table 2.2 (Continued)

(b) Long period site coefficient F_v

Site Class or Soil Profile Type	Mapped Rock Shaking Level at Short Periods				
	S_1[1] ≤ 0.10	S_1 = 0.20	S_1 = 0.30	S_1 = 0.40	S_1 ≥ 0.50
	A_v[2] ≤ 0.10	A_v = 0.20	A_v = 0.30	A_v = 0.40	A_v ≥ 0.50
A	0.8	0.8	0.8	0.8	0.8
B	1.0	1.0	1.0	1.0	1.0
C	1.7	1.6	1.5	1.4	1.3
D	2.4	2.0	1.8	1.6	1.5
E	3.5	3.2	2.8	2.4	*
F	*	*	*	*	*

[1]S_1 = Acceleration values for short periods (NEHRP 1997)
[2]A_1 = Acceleration values for short periods (NEHRP 1994)

Table 2.3 Site categories in new seismic codes (from 1994 and 1997 NEHRP).

Site Class or Soil Profile Type	Description	Shear Wave Velocity Top 30 m V_s (m/s)	Standard Penetration Resistance N (blows/ft)	Undrained Shear Strength S_u (kPa)
A	Hard rock	>1500	-	-
B	Rock	760 – 1500	-	-
C	Very dense soil/soft rock	360-760	> 50	> 100
D	Stiff soil	180 – 360	15 – 50	50 – 100
E	Soft soil	< 180	< 15	<50
F	Special soils requiring site-specific evaluation	-	-	-

Site class F is defined for special soils that could not be covered by the new provisions; no values of F_a and F_v are provided for these cases.

The values in Table 2.2 and 2.3 are also based on results derived both from empirical studies of recorded motions and numerical site response analyses (Borcherdt and Glassmoyer 1992, Seed and Idriss 1992, Borcherdt 1993, 1994a-b, Borcherdt 1994, Joyner et al. 1994, Martin and Dobry 1994, Seed et al. 1994, among others).

The values of F_a and F_v obtained directly from recordings, were used to calibrate numerical one dimensional site response analytical techniques, including equivalent

linear programs such as SHAKE (Schnabel et al. 1972), as well as non-linear programs (Dobry et al. 2000). These equivalent linear and non-linear one dimensional site response techniques were used to extrapolate the values of F_a and F_v to larger rock accelerations (up to 0.4 g or 0.5 g) using parametric studies that included equivalent linear and non-linear analyses (Dobry et al. 2000).

Relevant considerations from the analysis of the development of amplification factors used for site characterization are presented below (Dobry et al. 2000).

- Site characterization is now based only on the top 30 m of soil, disregarding the depth of soil to rock if greater than 30 m, the soil properties below 30 m and the properties of the rock underlying the soil. The average shear wave velocity is obtained from the travel time of a vertically propagating shear wave between a depth of 30 m and the ground surface. Penetration resistance and undrained shear strength are also used to characterize the top 30 m of a soil.
- In agreement with the analytical studies and the field evidence, the effect of soil non-linearity is introduced by making both site coefficients F_a and F_v functions of the level of intensity of rock motions given by A_a or A_v. The main consequence of this change is the occurrence of large amplification at both short and long periods on soft soil.

2.5.4 Amplification factors for generic site categories and site-specific factors defined from ground response analysis

Different studies regarding both factors for generic site categories as well as site-specific factors have been presented, for instance Silva (1999), Rodriguez-Marek et al. (2001), Borcherdt (2002) and Stewart and Batusay (2003).

The method for obtaining amplification factors for generic site categories, as explained in Silva (1999), consists in developing amplification factors as a function of surface geology, depth to basement, and control motion amplitude. The amplification factors are derived by developing generic velocity profiles for various geologic units, defining control motions for the reference site condition using a stochastic point-source model, and performing ground response analyses with the equivalent-linear method with the objective of trying to capture variations in ground conditions within geologic categories.

Some conclusions obtained by Silva (1999) explain that high-frequency amplification decreases with control motion amplitude due to non-linearity and low-frequency amplification exhibits significantly less non-linearity. The results also indicate a shifting of the peak amplification to lower frequencies as depth to basement increases, and a reduction of high-frequency amplification due to material damping.

Silva (1999) performed ground response analyses using large sets of control motions that were scaled to match a modified rock attenuation median. Ground motions estimated from these response analyses incorporate the variability in source/path effects for a fixed magnitude and distance to the source. Silva (1999) also concluded that the significance of ground response variability as compared to source/path variability

increased with decreasing site-source distance and increasing site period. Finally, it was shown by Silva (1999) that soil attenuation results presented a positive bias, indicating that the recordings from the sites investigated are unusually large relative to the median attenuation prediction. As this methodology is applied in the present study, the site-specific factors method and its conclusions are especially significant.

For the case of site-specific factors, ground response analyses are performed with the expectation that accounting for nonlinear soil response reduces bias and uncertainty in estimated motions at soil sites.

2.5.5 Evaluation of amplification factors of the Uniform Building Code

The following paragraphs evaluate the amplification factors included in the UBC; the empirical analysis by Borcherdt (2002) was used as a baseline reference. Short period (F_a) and mid-period (F_v) site-specific amplification factors, used in the current U.S. building code are considered to decrease with increasing acceleration at the base of a profile (UBC 1997).

The dependence of amplification on the acceleration at the base is greater for site class D than for the stiffer site class C sites (Borcherdt 2002). By comparing regressions of amplification on shear-wave velocity it was shown that the short-period factors, F_a as well as the mid-period factors F_v, with base accelerations greater than 0.2 g, are significantly less than those with base accelerations smaller than 0.2 g for sites with shear-wave velocity between 200 and 600 m/s and for any shear wave velocity interval, respectively. These results support the fact that the short-period amplification factors show a greater dependency on input acceleration level than the mid-period amplification factors for sites in site classes D and C (Bordcherdt 2002).

For the case of a layered media, non-linear behavior also can be manifest as an increase in amplification for certain period bands due to an increase in the impedance ratio and/or a reduction in the predominant period as suggested by Borcherdt (2002).

2.6 Remarks about Damage Distribution Studies

Earthquake reconnaissance has been the primary tool of earthquake engineers for the advancing the state of the art in geotechnical and structural engineering. In particular, the understanding of site response has evolved form observations from damage observations in past earthquakes. While a description of previous reconnaissance efforts is outside the scope of this work, it was considered appropriate to present certain recommendations extracted from several studies (Hall 1995 for the 1994 Northridge earthquake, Youd et al. 2000 for the 1999 Kocaeli earthquake, Rodriguez-Marek and Edwards 2003 for the Southern Peru earthquake) because of their relevance to the damage data collected in after the 2001 Southern Peru earthquake, which constitutes the basis for the information presented in Chapter 5 of this thesis. The issues that should be accounted for while performing or evaluating damage distribution analyses are:

- The criteria and experience of the reconnaissance team's members is important and determines the methodology to be used in damage distribution assessment.
- The level of development of the cities under study is an important factor that affects the choice of methodology.
- The quality of construction also influences the evaluation process during damage distribution analysis.

- The criteria followed must be consistent during all the data acquisition process.
- Damage distribution is an especially useful tool for site effects analysis and for urban expansion planning.

Generally, the next step after the analysis of damage consists in evaluating site effects from the damage distribution obtained. Usually, correlations between high levels of damage in certain areas and unexpected accelerations due to soil amplification effects can be assessed. This is one of the goals of the present study.

CHAPTER 3

FIELD TESTING AND RESULTS

3.1 Introduction

During June and July 2003, SASW testing was performed at twenty-five selected sites to obtain shear wave velocity profiles; in addition SPT testing was carried out at five of the same sites. These five were chosen because they presented liquefaction effects after the 2001 southern Peru earthquake. General testing procedures for the SASW testing method are addressed in this chapter. Since this is a project shared with Utah Sate University and Drexel University, testing results for twenty-two of twenty-five sites are presented herein, the other three sites as well as other details can be found in Park (2004).

3.2 General testing information

3.2.1 Spectral analysis of surface waves (SASW) method

The SASW test is an in situ geophysical method for determining shear wave velocity (V_s) profiles that is performed on the ground surface. Vs values for a range of frequencies can be obtained by using an impulse source and processing the subsequent records as registered by two or more receivers. The SASW method is based on the analysis of Rayleigh waves and their dispersive characteristic on a layered medium. Rayleigh wave velocity is determined by material properties such as shear wave velocity and material density.

Procedure

The description of the SASW testing method presented herein is obtained mainly from Park (2004) and the following website, http://www.baygeo.com/html/sasw.html. In SASW testing a dynamic source is used to generate surface waves of different

wavelengths (or frequencies) that are monitored by two or more receivers at known offsets. The distance between the source and the first receiver is usually equal to the distance between the two receivers (d_1 and d_2 in Figure 3.1). Data from forward and reverse profiles are averaged together. The geometry is optimized to minimize body wave signal (Stokoe et al. 1995).

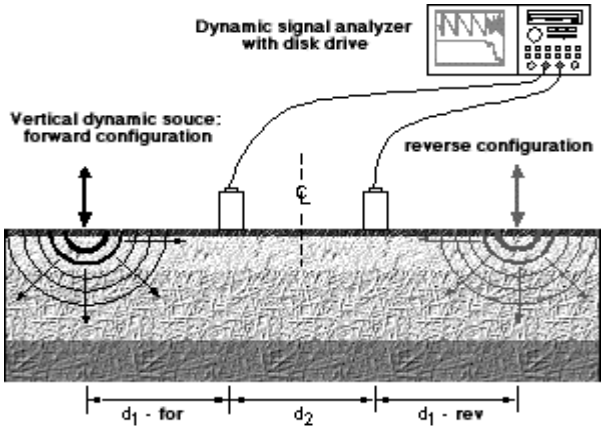

Figure 3.1 Field setup used in SASW testing (http://www.baygeo.com/html/sasw.html)

The testing procedure itself consists of measuring the surface wave dispersion curve at the site and interpreting it to obtain the corresponding shear wave velocity profile. Surface waves are generated by applying a dynamic vertical load to the ground surface. The primary consideration in selecting a source is the required depth of profiling. Deep profiling requires a high-energy, low frequency wave source, whereas for shallow profiling a low-energy, high frequency wave source is required. In the present study sledge hammers, a 100 kg drop weight, and a bulldozer were used for different spacing. Changing the spacing between the receivers and using different sources enables the variation of velocity and a broad range of soil thickness to be explored (Stokoe et al. 1995).

The dispersive characteristic of Rayleigh waves refers to the variation of wave velocity with wavelength. Rayleigh waves of different wavelengths sample different depths in a soil profile, as shown in Figure 3.2. During the test and consequent analysis, all data are manually checked to discard low-quality data.

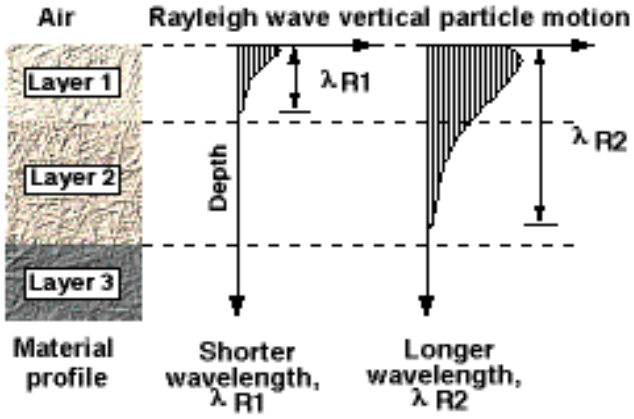

Figure 3.2 Approximate distribution of vertical particle motions with depth of two surface waves of different wavelengths *(*http://www.baygeo.com/html/sasw.html*)*.

The velocity of a wave with a wavelength that is longer than the thickness of the top two soil layers is influenced by the properties of only the upper two layers, where most of the particle motion occurs. Thus, by using surface waves with a range of wavelengths, it is possible to assess material properties over a range of depths (Rathje et al. 2003).

The final step of the analysis consists in obtaining the soil profile and mechanical properties of each layer from the dispersion curve. This process is called inversion. The unknown parameters in each layer are the thickness, density, shear modulus, and Poisson ratio.

Since the solution to the inversion problem is not unique, different inversion techniques have been proposed to obtain V_s profiles and the stiffness parameter *G*. In the inversion technique used in this work, a first tentative profile of the site is obtained and

adjusted by comparing the results of numerical simulation to the dispersion curve obtained from the field test. Different programs have been developed in order to perform this analysis, such as WinSASW (University of Texas at Austin).

Equipment

This section contains the information provided by Dr. James E. Bay and Kwangsoo Park (Utah State University) for the completion of this research. Further details can be found in Park (2004).

A Hewlett-Packard 3562A, two-channel dynamic signal analyzer (Figure 3.3), was used for data acquisition and analysis. Six 4.5-Hz geophones (GeoSpace PAT 3119978) were employed as receivers. One set of receivers consisted of three geophones (Figure 3.4).

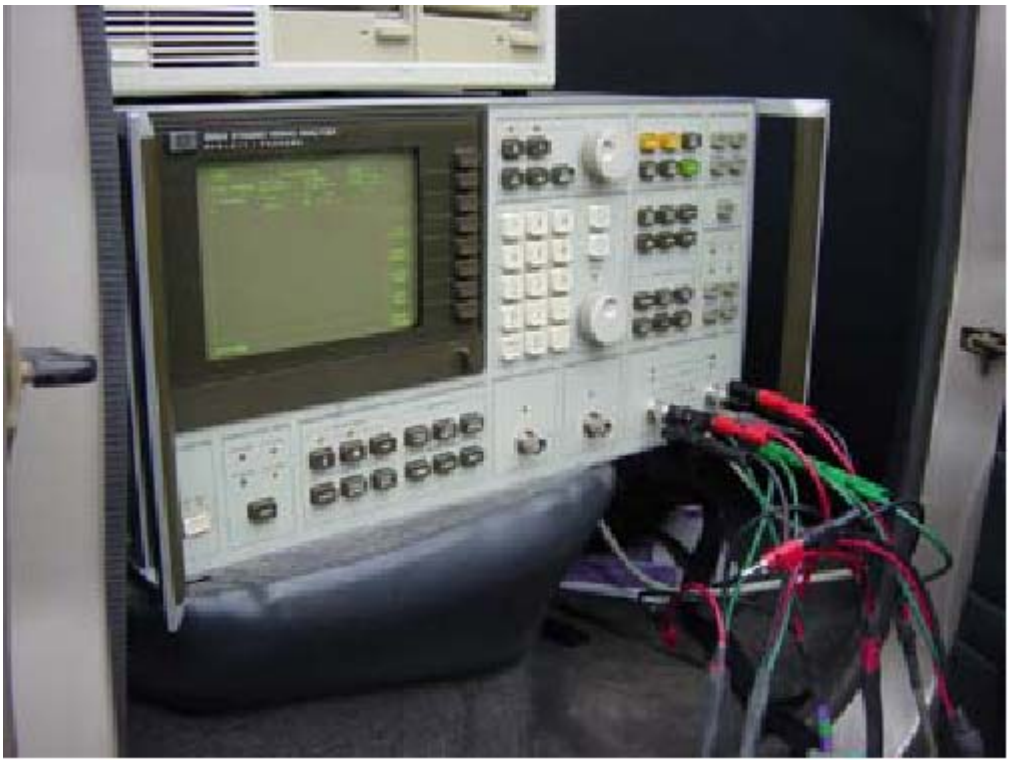

Figure 3.3 HP 3562A dynamic signal analyzer.

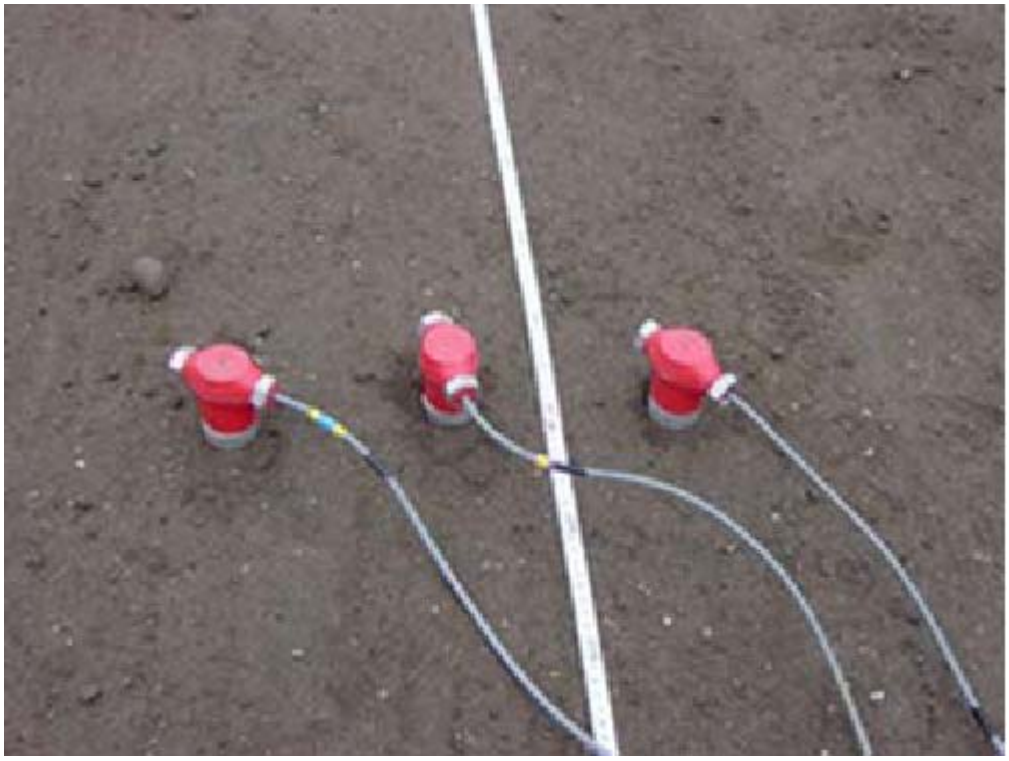

Figure 3.4 One set of receivers consisting of three 4.5-Hz geophones

Typically spacings of 2, 4, 10, and 16 meters were used for shallow profiling. Additionally spacings of 20, 40, 55, or 60 meters were used at sites where deep profiling was needed. Different types of wave sources were employed based on site conditions, such as a small hammer (Figure 3.5a), a sledgehammer (Figure 3.5b), a 100 kg drop weight (Figure A.3c), and a bulldozer (Figure 3.5d).

a) Small hammer

b) Sledge hammer

c) 100 kg drop weight

d) Bulldozer

Figure 3.5 Different sources of energy used in the SASW field testing.

3.2.3 Standard penetration tests

Five standard penetration tests were performed at five of the twenty-five selected sites; the first was located in the city of Tacna, while the remaining four were located on the Pan American Highway, two at landmarks 1234 and 1238 (1234 and 1238 km from Lima, the capital city, respectively), and the remaining two at Locumba Bridge. Details about the sites are presented in appendix A.

The SPT testing was performed by "Michelena & Asociados", a local company hired by the members of the team. The company provided all the necessary means for the testing including the equipment, the crew, and the water supply. The SPT tests followed the ASTM standard, however, the following deficiencies and deviations were observed during testing:

- The Water Jetting method was applied instead of using the Wash Boring method suggested by Seed et al. 1985 to open the initial boring. This factor caused difficulties to create a standard-shaped boring. Thus, the initial diameter of the boring was not standard (diameter of 4-5 inches).
- In some cases the crew forgot to clean the boring after drilling which should be completed before the SPT device is used (Coduto 2001).
- The number of turns of the rope around the cathead was not constant, however, in most cases it was two as suggested in the ASTM standard.
- Since the equipment is not automatic, the drop height was not constant, an error as large as 25% can be assumed (Coduto 2001).

- The test was stopped and after a few seconds re-started when the operator considered necessary some change, factor that may also lead to a variation in results.
- An absence of liners inside the sampler was observed. Tests could be altered by 10 to 30 % because of that reason (Coduto 2001).

Additionally, a Pile Driver Analyzer (PDA) was used to measure the energy provided by the SPT for posterior verifications and corrections. The PDA was a PAL-R model created for use in remote locations. This device is a powerful diagnostic tool that allows their users to assist, control and troubleshoot pile driving and SPT testing. During the test, varied information was obtained including blow count, blow rate, compression stresses, tension stresses, transferred energy (by the STP device), and soil resistances. In order to obtain all this information two sensors were connected to the SPT device. The sensors had a combined function; each of them measured strain and acceleration. Information was stored in a hard disk to preserve signal quality. Then stored signals were retrieved and processed, and the results are shown in Appendix B.

Finally, to correct the blow count values (N) acquired on the field, the following formula was used (Youd and Idriss 2001).

$$(N_1)_{60} = N_m \cdot C_N \cdot C_E \cdot C_B \cdot C_R \cdot C_S \qquad (3.1)$$

where: N_m is the blow count obtained from the field, and C_N, C_E, C_B, C_R, C_S are correction factors given in Table 3.1.

Table 3.1 Correction factors for the SPT test.

Correction Factor	Variable	Value used
C_E	Correction for hammer energy ratio.	A mean value of 0.75 was used based on the results from the PDA analyzer (Appendix B). The standard deviation was 0.05.
C_S	Sampler without liners correction	Youd and Idriss (2001) suggested factors ranging between 1.1 and 1.3 for samplers with no liners, thus a factor a 1.2 was assumed.
C_B	Correction for borehole diameter.	Although the borehole diameter was not standard the diameter had always been between 65-115 mm (Youd and Idriss 2001), thus a factor of 1 was assumed.
C_R	Correction factor for rod length.	This correction factor is a function of depth; the values used were obtained from Youd and Idriss (2001). For 10-13 feet: 0.75. For 13-20 feet: 0.85. For 20-30 feet: 0.95. For > 30 feet: 1.00.

In addition, overburden correction was applied to obtain the $(N_1)_{60}$ values, the criteria used for the overburden correction was:

$$(N_1)_{60} = N_{60}\sqrt{\frac{2000\ lb/\ ft^2}{\sigma_z^{'}}} \quad \text{(Liao and Whitman 1986a))}$$

where: $(N_1)_{60}$ = SPT values corrected for field procedures and overburden stress;

σ_z'= vertical effective stress at the test location, and

N_{60} = SPT values corrected for field procedure.

3.3 Testing results

Table 3.1 presents a summary of the results obtained from testing for all the twenty-five sites; a detailed description of the testing process and results is presented in Appendix A. Problems encountered during the testing process in the sites located in the cities of Arica, Tacna and Moquegua are listed in Table 3.2. This table also includes

specific comments to tests at each of these sites. Appendix A also includes a description of the testing at sites outside these cities. Further detail about other sites is excluded from this chapter because these sites were not an integral part of the work presented in this thesis.

Table 3.1 Summary of results from field work.

Location	Site Name	Coordinates		V_{S30}[1] (m/s)	UBC Class	SPT[3]
		S	W			
Arica Chile	Cerro La Cruz	18.49469°	70.31217°	1132	S_B	N
	Juan Noe Greviani Hospital	18.49469°	70.31417°	*	*	N
	Arica Costanera	18.47382°	70.31342°	389	S_C	N
	Arica Casa[2]	18.48158°	70.30853°	406	S_C	N
	Poconchile	18.45619°	70.06689°	511	S_C	N
	Chacalluta - Immigration office	18.31767°	70.31553°	287	S_D	N
Tacna Peru	Asociacion "San Pedro"	17.99986°	70.25997°	473	S_C	N
	Colegio "Enrique Paillardelle"[2]	18.05993°	70.25031°	670	-	N
	Municipal gas station	17.98100°	70.23183°	419	S_C	Y
	"La Bombonera" stadium	17.98519°	70.23869°	409	S_C	N
	Soccer field - Alto de la Alianza	17.99417°	70.24369°	452	S_C	N
	Colegio "Hermogenes Arenas Yanez"	18.04136°	70.28156°	652	S_C	N
	Colegio "Coronel Bolognesi"	18.00436°	70.25353°	615	S_C	N
Moquegua Peru	Calle Nueva	17.19729°	70.94065°	421	S_C	N
	Ground motion station[2]	17.18913°	70.92921°	542	-	N
	"9 de Octubre" street[2]	17.19834°	70.39993°	567	-	N
	"San Antonio" Hospital[2]	17.21421°	70.94712°	567	-	N
	"474 Lima" street	17.19565°	70.93625°	**	**	N
Pan American Highway - Peru	Shintari	17.79025°	70.67208°	405	***	Y
	Valley Fill	17.28136°	70.71275°	367	***	Y
	Locumba bridge 1	17.68739º	70.84203º	***	***	Y
	Locumba bridge 2	17.68738º	70.84203°	***	***	Y

[1] Average shear wave velocity in the upper 30 meters. (UBC 1997).
[2] Shear wave velocity for this site corresponds to the upper 25 m.
[3] N = SPT was performed. Y = SPT was not performed.
* V_{S30} was not calculated because for this site only resolution down to 8 meters was obtained.
** V_{S30} was not calculated because for this site only resolution down to 12 meters was obtained.
*** For this site only resolution down to 15 meters was obtained.

Table 3.2 Difficulties encountered during SPT and SASW testing

Site	Comment
Arica Sites	
Juan Noe Greviani Hospital	Since testing was performed in very small and busy hospital parking lot, the resolution of this site (around 8 m deep) is not deep enough due to the short wavelength. V_{S30} at this site was not calculated because of the low resolution of the profile.
Arica Costanera	This site apparently presents a thin soft layer close to the surface, stiff materials from the depth of around 36 m, and thick and fairly uniform materials between these two layers.
Arica Casa	Only a good-resolution profile down to 25 meters was obtained due to space problems.
Tacna Sites	
Colegio Enrique Paillardelle	Gravelly soil was found at this site from a shallow test pit of 2.5 m of depth encountered at the site. The soils in this area are considered to be stiff; also cementation was observed, however, this cementation is lost with the presence of water as observed by local engineers.
Municipal gas station	For this site SPT testing was performed, the SPT device was rejected by the soil at about 9.45 meters.
La Bombonera stadium	At this site, a notoriously stiffer layer was detected at around 35 m of depth; however, the precise shear wave velocity could not be determined due to scattered dispersion data measured at this site.
Soccer field – Alto de la Alianza	This site also presented a considerably stiffer layer at 35 m of depth; the shear wave velocity of this layer was not obtained due to scattered dispersion data measured.
Colegio Hermogenes Arenas Yanez	This site presented a very simple profile composed by two or three subsurface layers overlying bedrock.
Colegio Cornel Bolognesi	A very simple profile composed by two or three layers was obtained for this site.
Moquegua Sites	
Ground motion station	Only a 25-meter profile was obtained due to resolution problems.
"9 de Octubre" street	For this site, testing was performed on asphalt paved-narrow road with steep slope. Only a 25-meter profile was obtained.
San Antonio Hospital	An outcrop was exposed next to the SASW line for this site. Also an abrupt velocity increase occurs at around 17 m of depth. However, with this dispersion measurement the SASW can only establish a lower bound for the velocity of the deepest layer. The velocity of this layer is at least 1300 m/s. Note that seismic refraction tests could have been helpful to avoid this limitation of the SASW test.
474 Lima Street	Since testing was conducted at the small parking lot due to difficulties to find a proper site, insufficient wavelength was generated and only a profile of up to 12 m of depth was resolved.

CHAPTER 4

ENGINEERING ANALYSIS OF GROUND MOTION RECORDS

4.1 Introduction

The design of civil engineering infrastructure in areas of the world that are near subduction zones must account for the high seismic potential associated with mega-thrust events. In particular, seismic design in the Pacific Northwest of the United States incorporates magnitude M_w 8.3 and M_w 9.0 Cascadia subduction zone scenarios in the development of current hazard maps (Frankel et al. 2002). The design of non-linear structures typically involves the use of a representative acceleration time history. Such a time history is usually selected to match the design spectra and source characteristics (e.g. magnitude and style of faulting). The effect of site conditions is typically accounted for either by selecting ground motions recorded in similar site conditions to those at a design site, or by modifying rock motions with site response analyses. In addition, the design spectra are typically obtained using empirical relationships (attenuation relationships) derived from recorded data in similar tectonic environments (e.g. Youngs et al. 1997 and Atkinson and Boore 2003). Current strong motion databases, however, do not include recordings for events with magnitudes larger than M_w 8.2.

The strong motions recorded during the M_w 8.4 2001 Southern Peru earthquake constitute the largest strong motions recorded to date within 200 km of the causative fault of an earthquake[1]. However, before these motions can be used in design or can be incorporated into attenuation relationships, the effects the site conditions at the recording stations must be clearly understood. This chapter presents an analysis of the site response

[1] Based on ground motions included in attenuation relationships for subduction zone events (Youngs et al. 1997 and Atkinson and Boore 2003)

effects on the recorded ground motions. The ground motions that were recorded during the 2001 event are located mainly on stiff gravelly soils; hence, the results presented herein will also contribute to the understanding of site response for these particular types of soils.

A total of seven recordings were made during the earthquake, six by the Chilean system of ground motion stations (Boroschek et al. 2001) and one by a ground motion station located in the Peruvian city of Moquegua (CISMID 2001). Rupture distances range from about 75 to 280 km. (Table 4.1). The ground motions are evaluated through a comparison of recorded ground motion parameters with prediction by attenuation relationships.

The study of site response at the ground motion stations is performed using one dimensional site response analyses. The input parameters needed for the site response analyses are the profiles of shear wave velocity and non-linear soil properties, in addition of an input motion. Of these parameters, only the shear wave velocity at selected ground motion stations was recorded (Chapter 3). In order to incorporate the potential effect of uncertainty on the remaining parameters, a stochastic analysis of site response was performed. The contribution of input ground motion uncertainty is accounted for by using a suite of ground motions generated using a finite fault model.

Table 4.1 Ground motion stations

Ground Motion Station	Closest[1] Distance (km)	Hypocentral Distance (km)	Epicentral Distance (km)	PGA[2] (g)	SASW Testing?
Moquegua	76.7	307.3	306.24	0.30	Y
Arica Costanera	141.9	430.3	429.54	0.34	Y
Arica Casa	142.8	431.2	430.46	0.31	Y
Poconchile	160.6	450.9	450.12	0.26	Y
Putre	199.7	490.4	489.74	0.20	N
Cuya	260.6	544.0	543.38	0.16	N
Pisagua	279.5	562.4	561.80	0.04	N

[1] Closest distance to the fault plane (Abrahamson and Shedlock 1997). The fault plane is estimated by the location of earthquake hypocenters (Rodriguez-Marek et al. 2003).
[2] Peak Ground Acceleration. Maximum value of the two horizontal components.

4.2 Ground motion records

The recorded ground motions were obtained from the Chilean "Red Nacional de Acelerografos (RENADIC)" (National Network of Accelerographs) as well as the Peruvian "Instituto Geofisico del Peru" (Peruvian Institute of Geophysics), a description of these networks and the accelerographs can be found at http://ssn.dgf.uchile.cl/ and http://www.igp.gob.pe/cns/ie_main.htm or http://www.cismid.uni.edu.pe/p_acelerograf/index.htm. The recordings were processed by the owner institutions. Figure 4.1 presents the ground motion time histories for the two horizontal ground motion components, while Figure 4.2 presents the time histories of the vertical component of motion.

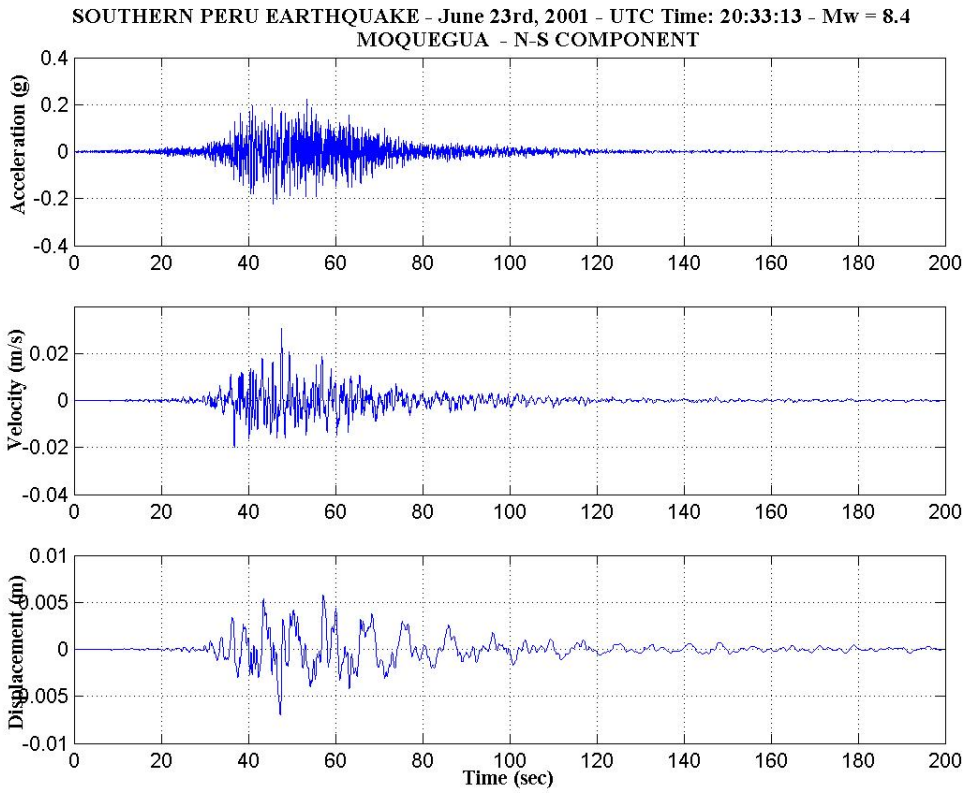
SOUTHERN PERU EARTHQUAKE - June 23rd, 2001 - UTC Time: 20:33:13 - Mw = 8.4
MOQUEGUA - N-S COMPONENT
Acceleration (g)
Velocity (m/s)
Displacement (m)
Time (sec)

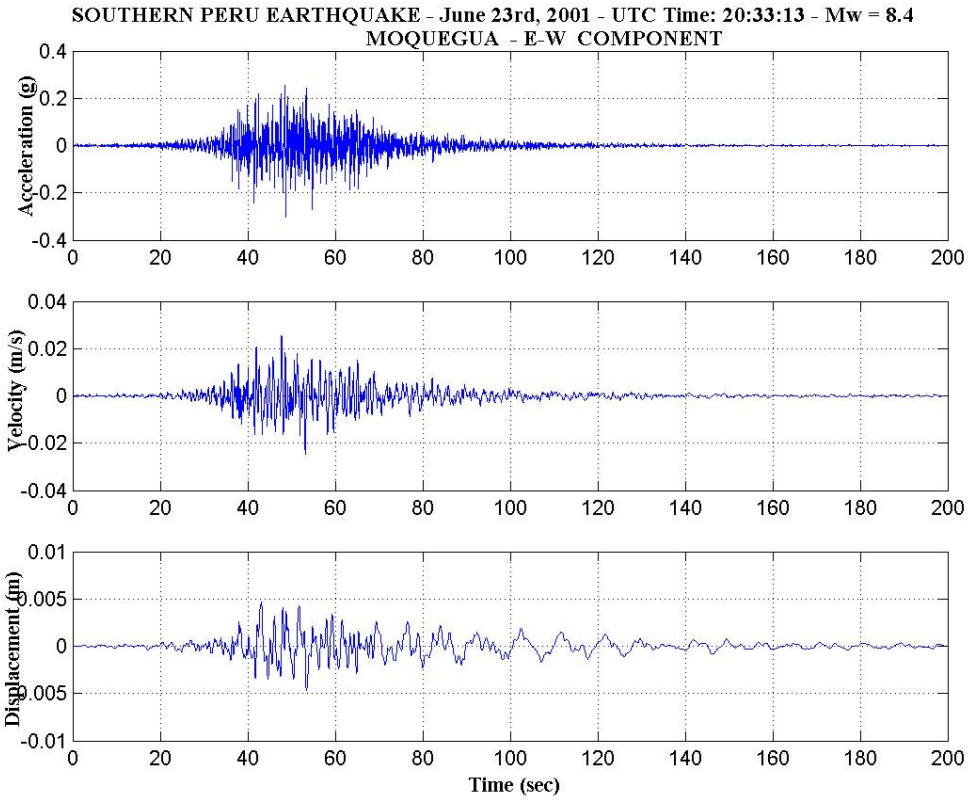
SOUTHERN PERU EARTHQUAKE - June 23rd, 2001 - UTC Time: 20:33:13 - Mw = 8.4
MOQUEGUA - E-W COMPONENT
Acceleration (g)
Velocity (m/s)
Displacement (m)
Time (sec)

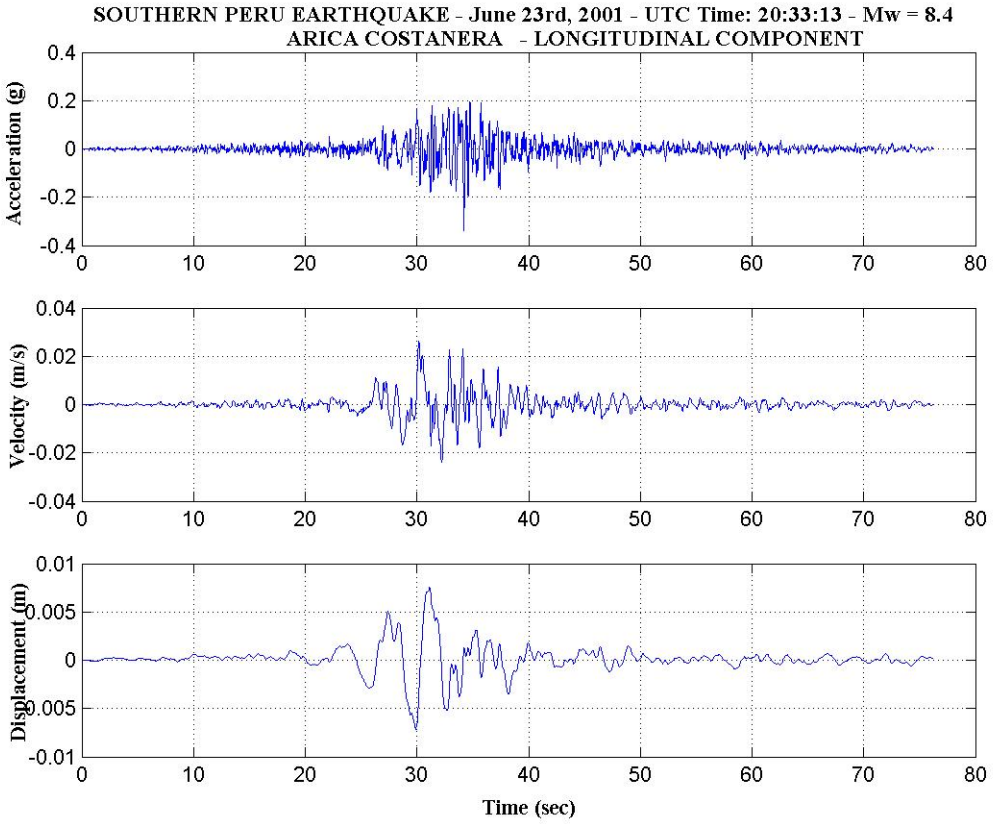
SOUTHERN PERU EARTHQUAKE - June 23rd, 2001 - UTC Time: 20:33:13 - Mw = 8.4
ARICA COSTANERA - LONGITUDINAL COMPONENT
Acceleration (g)
Velocity (m/s)
Displacement (m)
Time (sec)

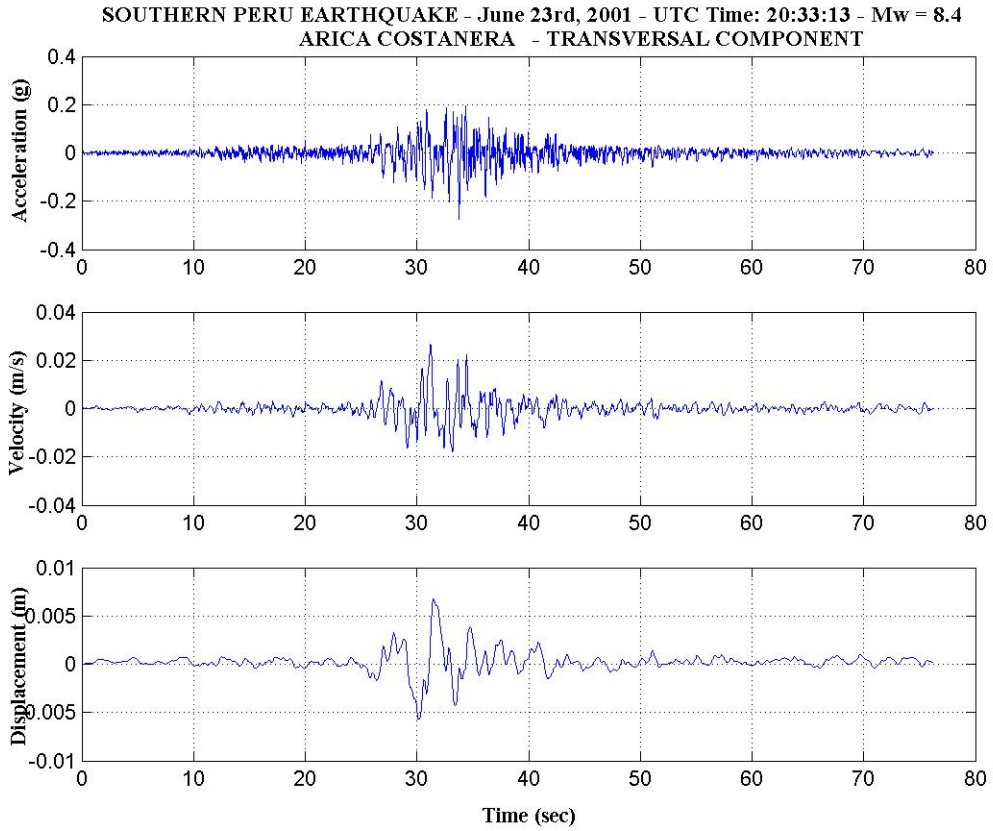
SOUTHERN PERU EARTHQUAKE - June 23rd, 2001 - UTC Time: 20:33:13 - Mw = 8.4
ARICA COSTANERA - TRANSVERSAL COMPONENT
Acceleration (g)
Velocity (m/s)
Displacement (m)
Time (sec)

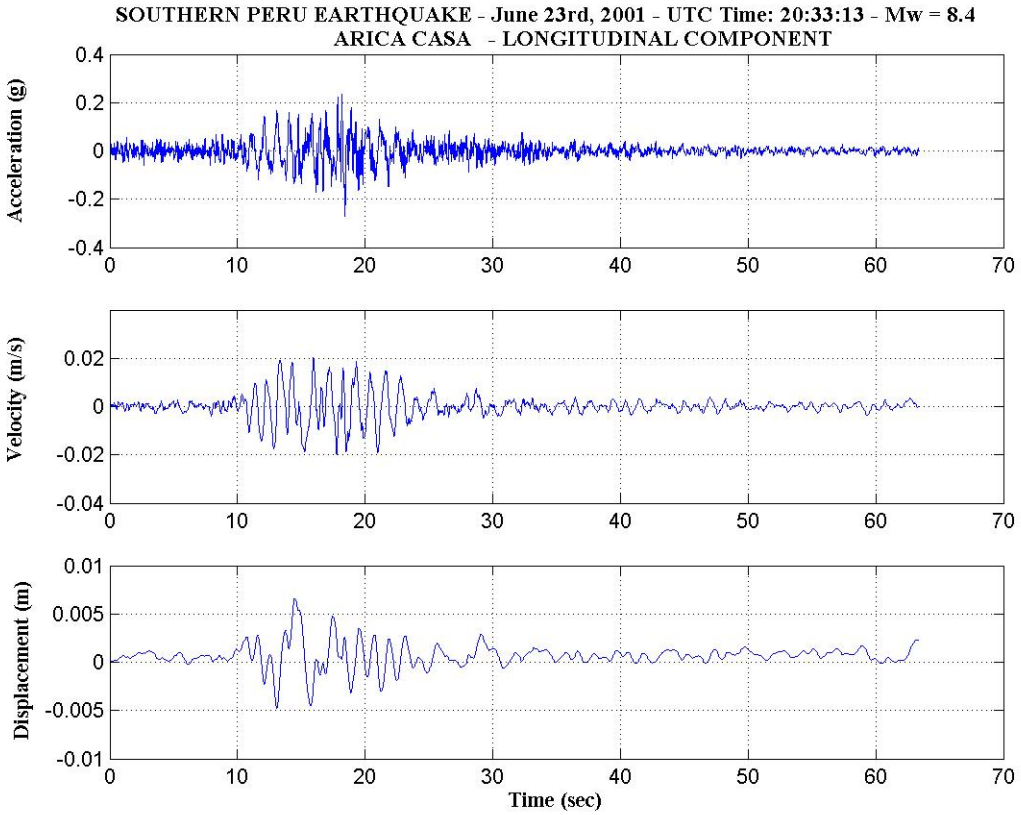
SOUTHERN PERU EARTHQUAKE - June 23rd, 2001 - UTC Time: 20:33:13 - Mw = 8.4
ARICA CASA - LONGITUDINAL COMPONENT
Acceleration (g)
Velocity (m/s)
Displacement (m)
Time (sec)

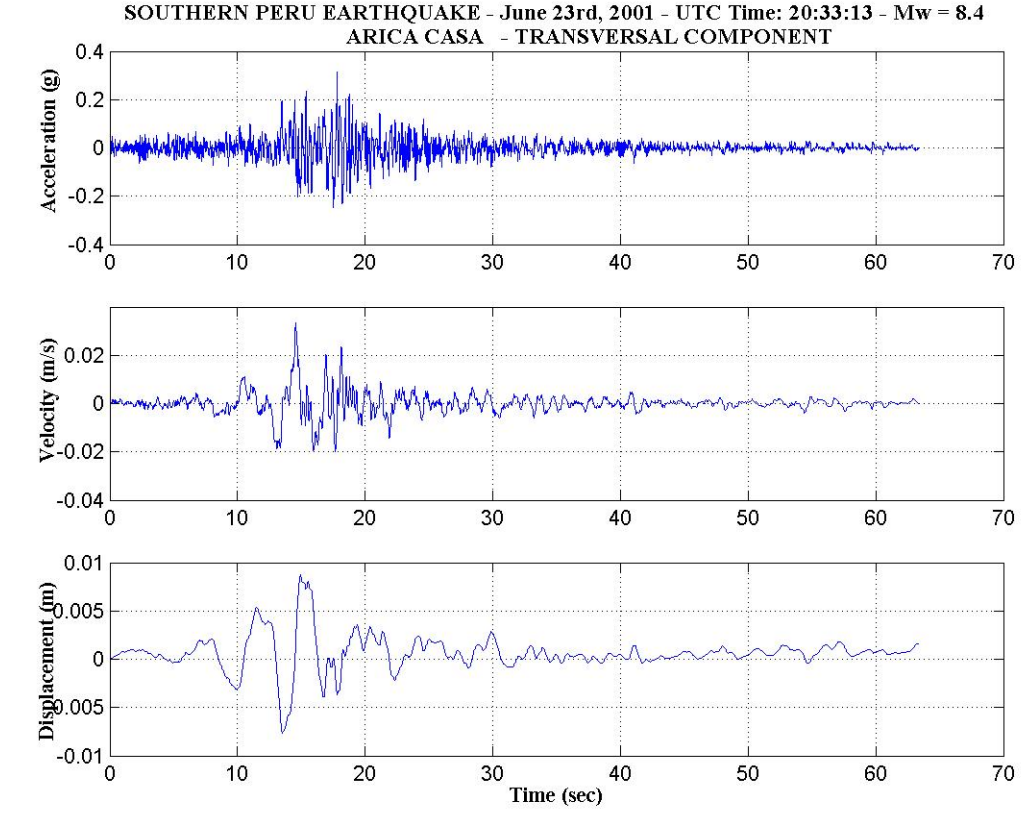
SOUTHERN PERU EARTHQUAKE - June 23rd, 2001 - UTC Time: 20:33:13 - Mw = 8.4
ARICA CASA - TRANSVERSAL COMPONENT
Acceleration (g)
Velocity (m/s)
Displacement (m)
Time (sec)

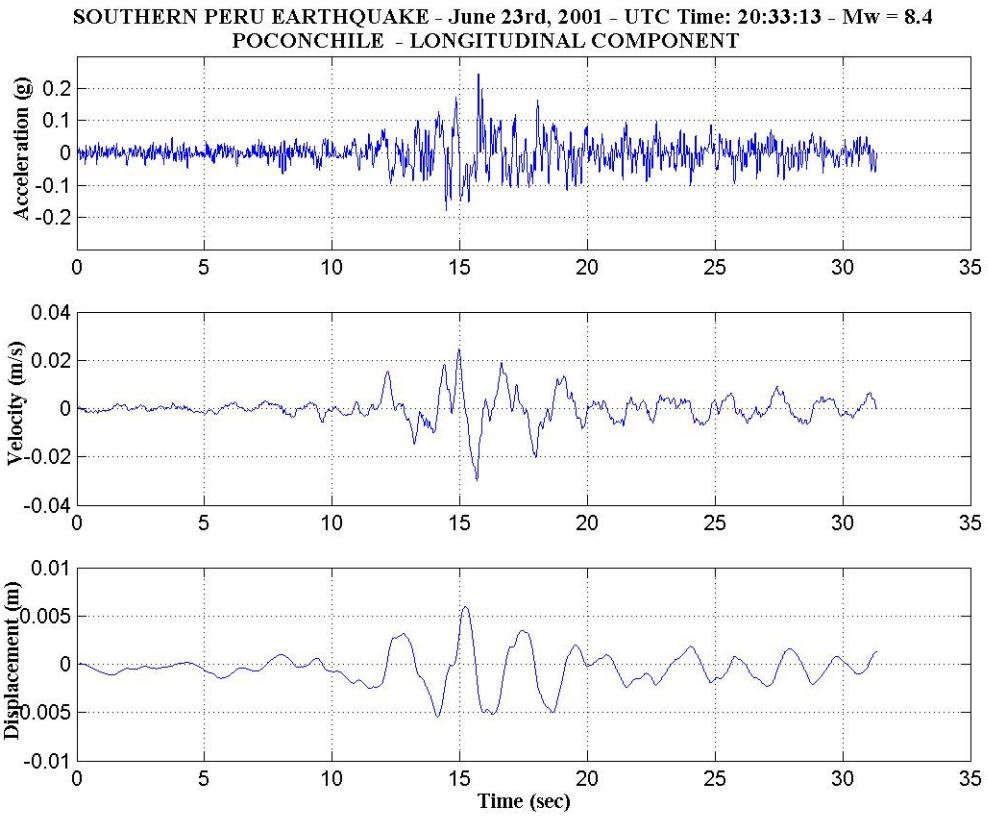
SOUTHERN PERU EARTHQUAKE - June 23rd, 2001 - UTC Time: 20:33:13 - Mw = 8.4
POCONCHILE - LONGITUDINAL COMPONENT
Acceleration (g)
Velocity (m/s)
Displacement (m)
Time (sec)

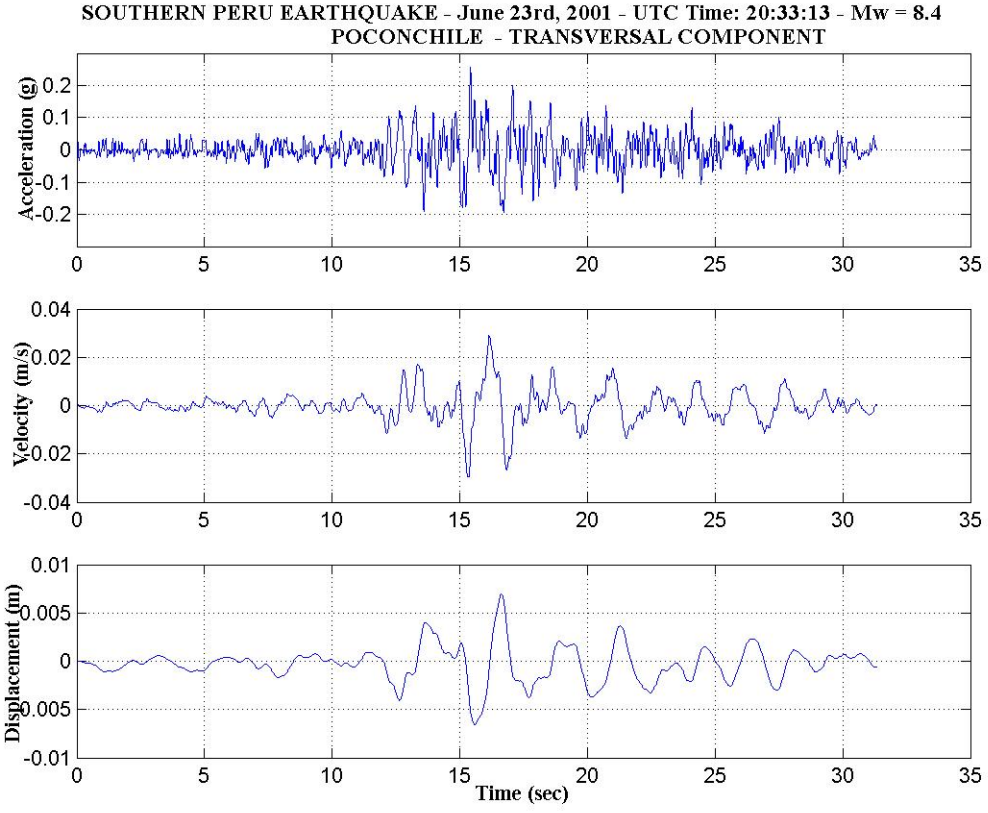
SOUTHERN PERU EARTHQUAKE - June 23rd, 2001 - UTC Time: 20:33:13 - Mw = 8.4
POCONCHILE - TRANSVERSAL COMPONENT
Acceleration (g)
Velocity (m/s)
Displacement (m)
Time (sec)

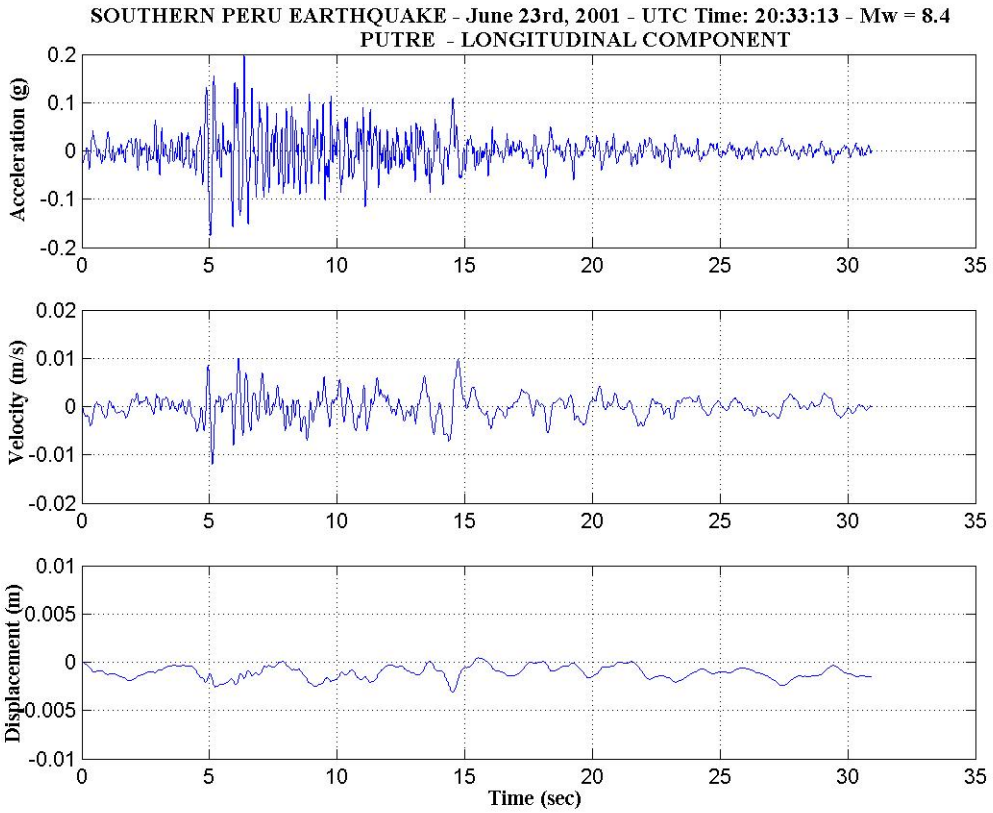
SOUTHERN PERU EARTHQUAKE - June 23rd, 2001 - UTC Time: 20:33:13 - Mw = 8.4
PUTRE - LONGITUDINAL COMPONENT
Acceleration (g)
Velocity (m/s)
Displacement (m)
Time (sec)

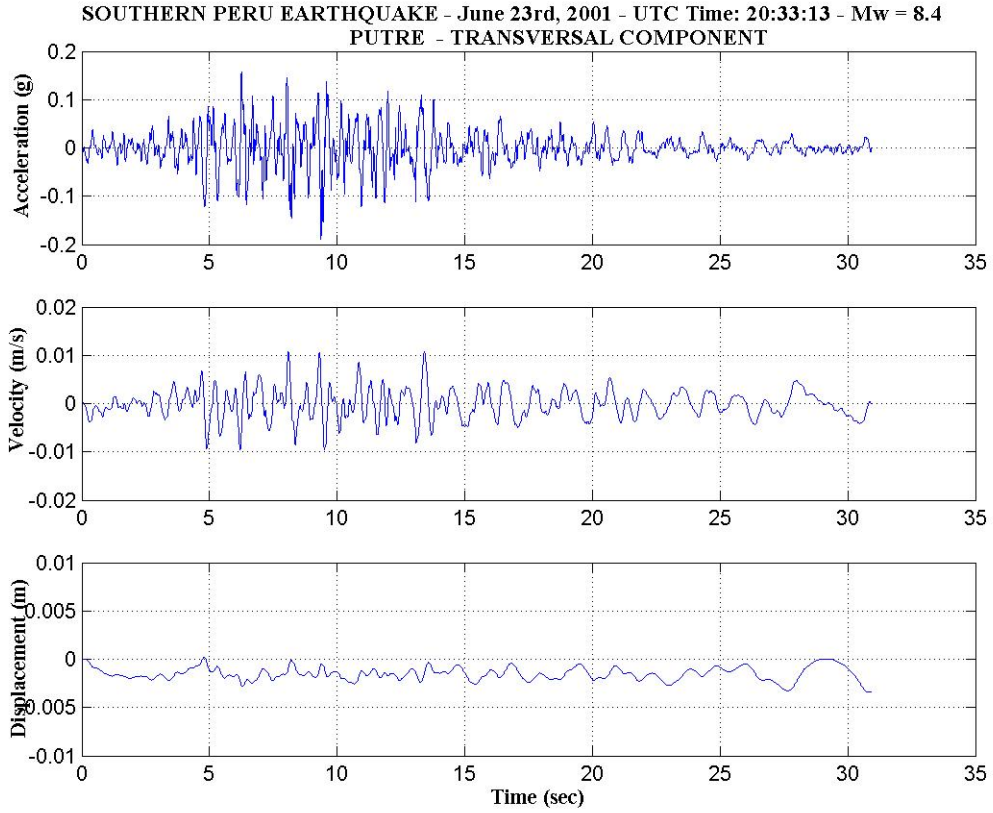
SOUTHERN PERU EARTHQUAKE - June 23rd, 2001 - UTC Time: 20:33:13 - Mw = 8.4
PUTRE - TRANSVERSAL COMPONENT
Acceleration (g)
Velocity (m/s)
Displacement (m)
Time (sec)

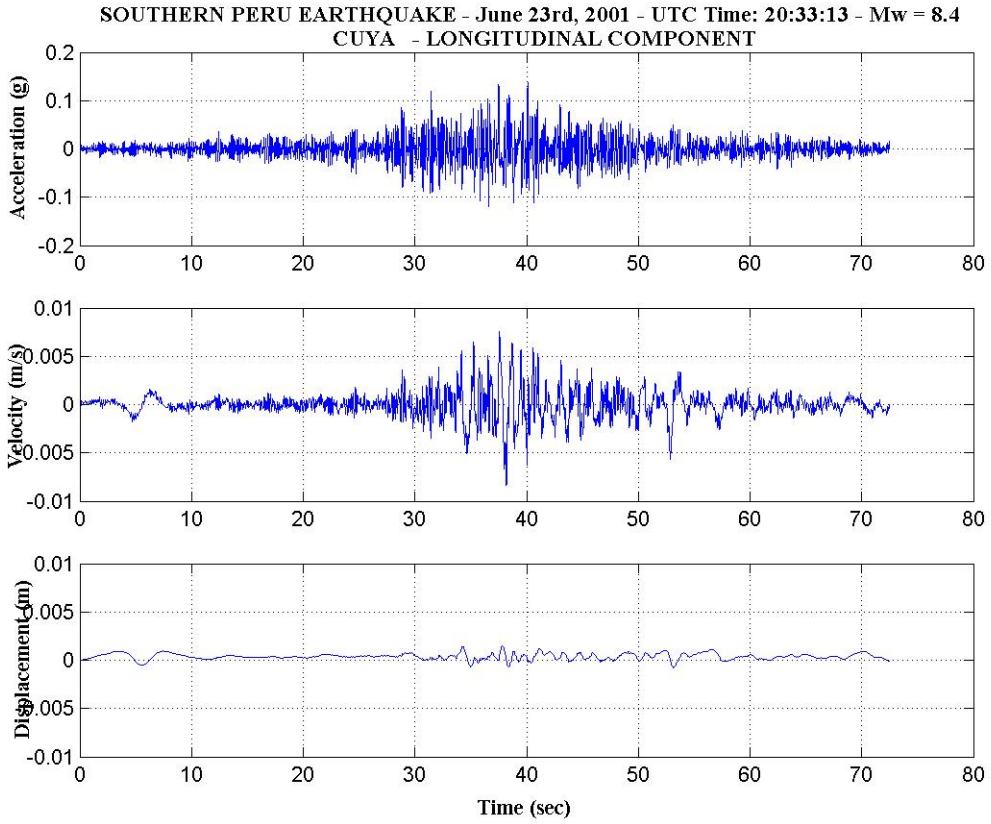
SOUTHERN PERU EARTHQUAKE - June 23rd, 2001 - UTC Time: 20:33:13 - Mw = 8.4
CUYA - LONGITUDINAL COMPONENT
Acceleration (g)
Velocity (m/s)
Displacement (m)
Time (sec)

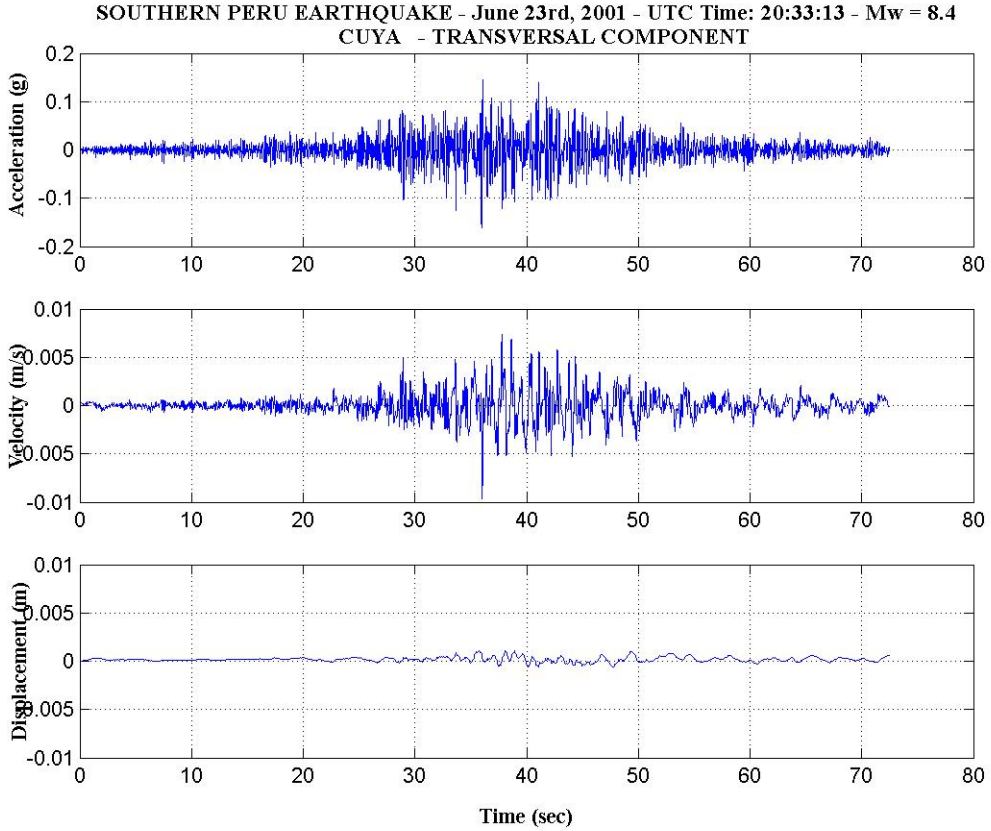
SOUTHERN PERU EARTHQUAKE - June 23rd, 2001 - UTC Time: 20:33:13 - Mw = 8.4
CUYA - TRANSVERSAL COMPONENT
Acceleration (g)
Velocity (m/s)
Displacement (m)
Time (sec)

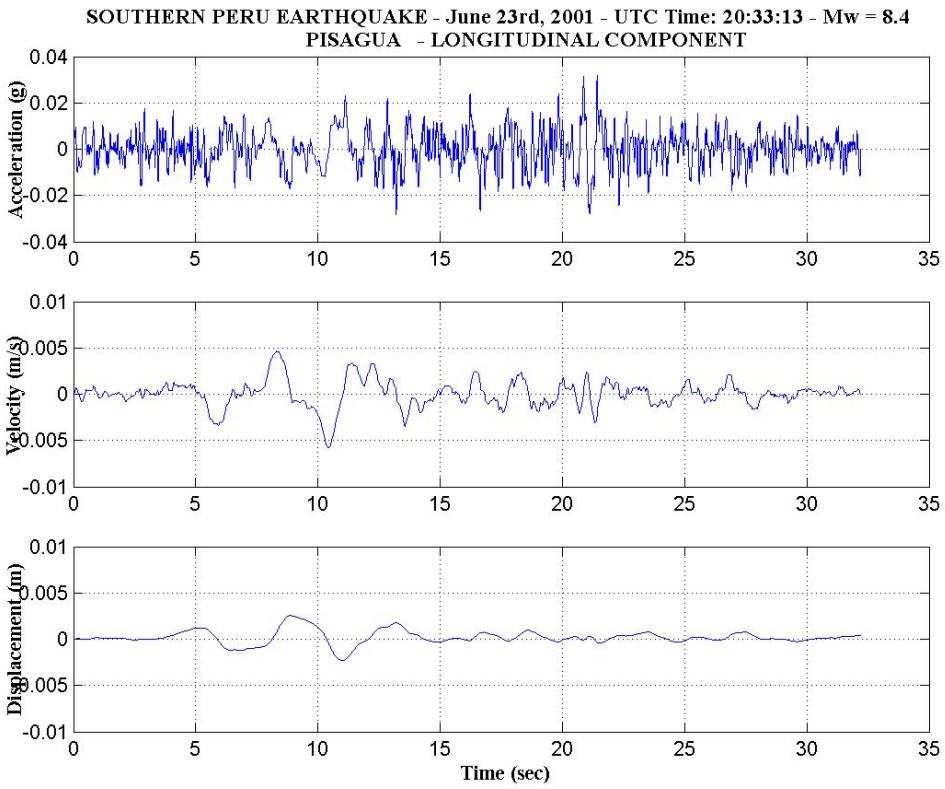

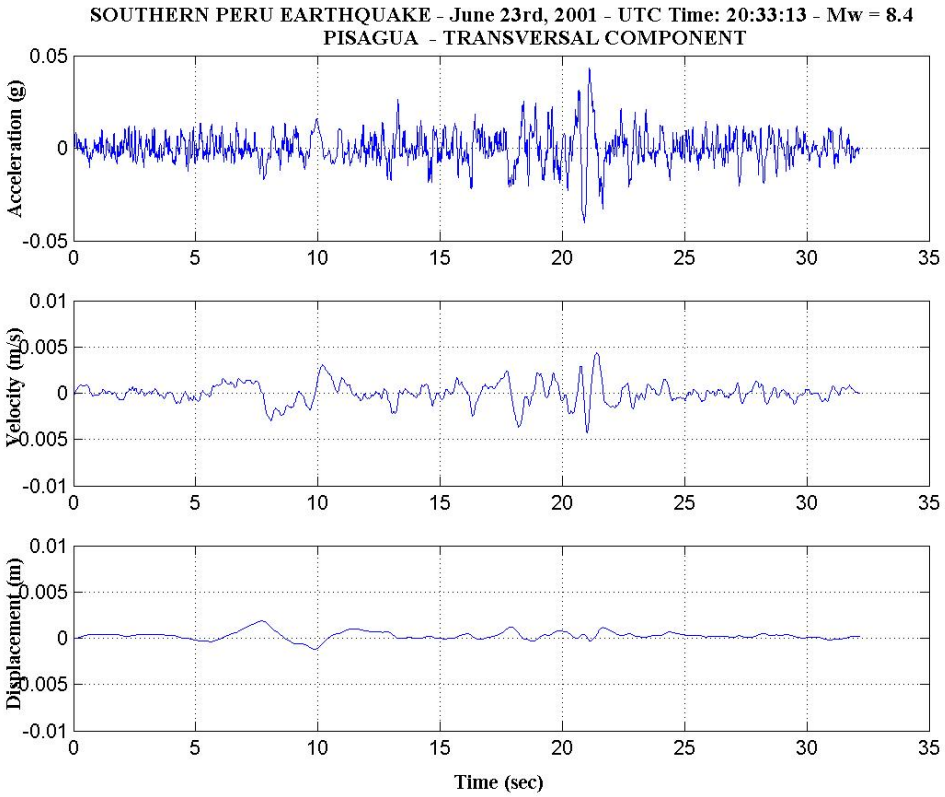

Figure 4.1 Acceleration, velocity, and displacement time histories of recorded ground motions for the longitudinal and transverse ground motion component.

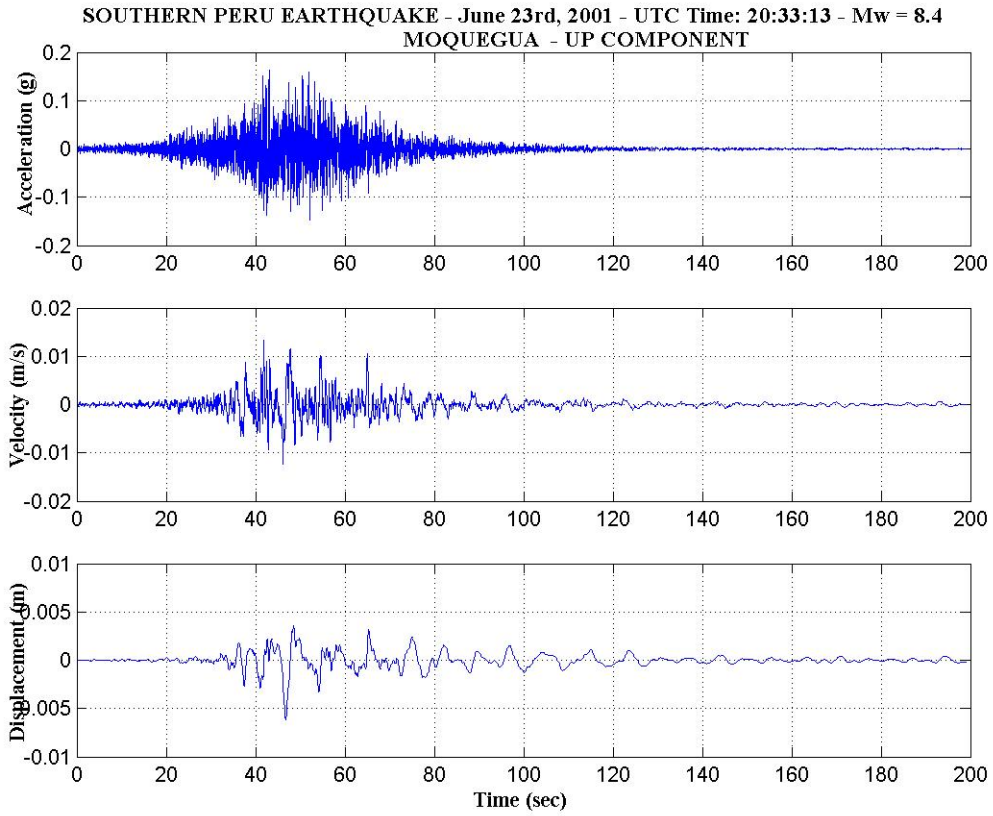
SOUTHERN PERU EARTHQUAKE - June 23rd, 2001 - UTC Time: 20:33:13 - Mw = 8.4
MOQUEGUA - UP COMPONENT
Acceleration (g)
Velocity (m/s)
Displacement (m)
Time (sec)

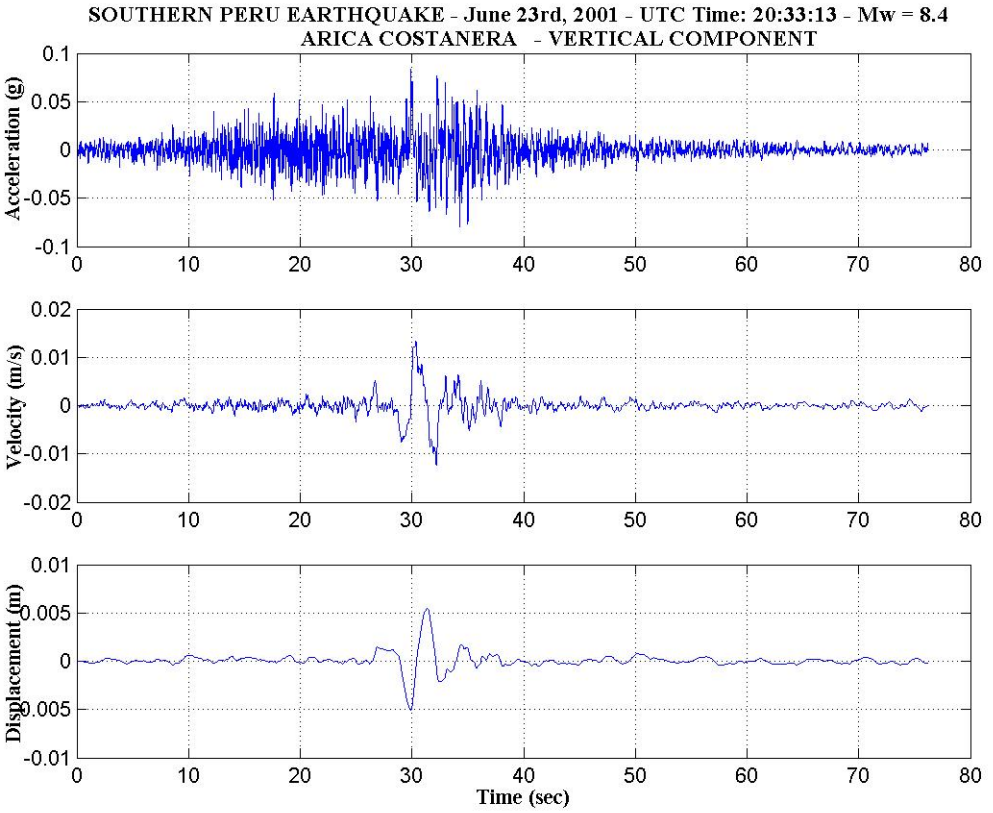
SOUTHERN PERU EARTHQUAKE - June 23rd, 2001 - UTC Time: 20:33:13 - Mw = 8.4
ARICA COSTANERA - VERTICAL COMPONENT
Acceleration (g)
Velocity (m/s)
Displacement (m)
Time (sec)

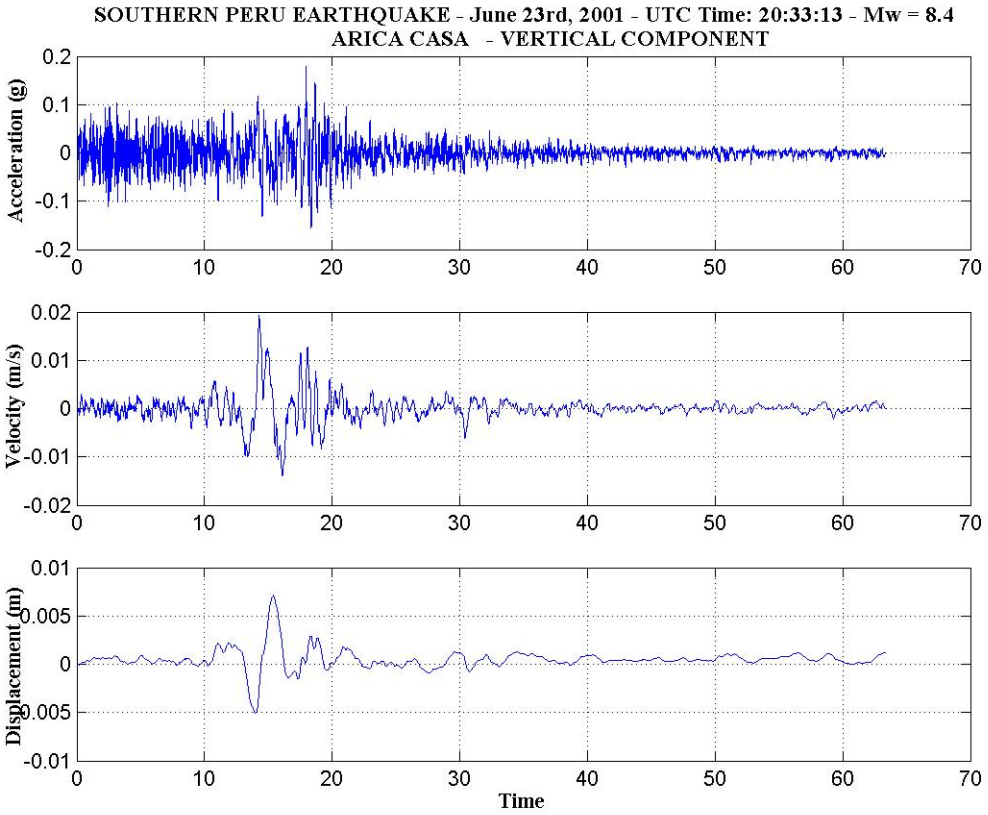
SOUTHERN PERU EARTHQUAKE - June 23rd, 2001 - UTC Time: 20:33:13 - Mw = 8.4
ARICA CASA - VERTICAL COMPONENT
Acceleration (g)
Velocity (m/s)
Displacement (m)
Time

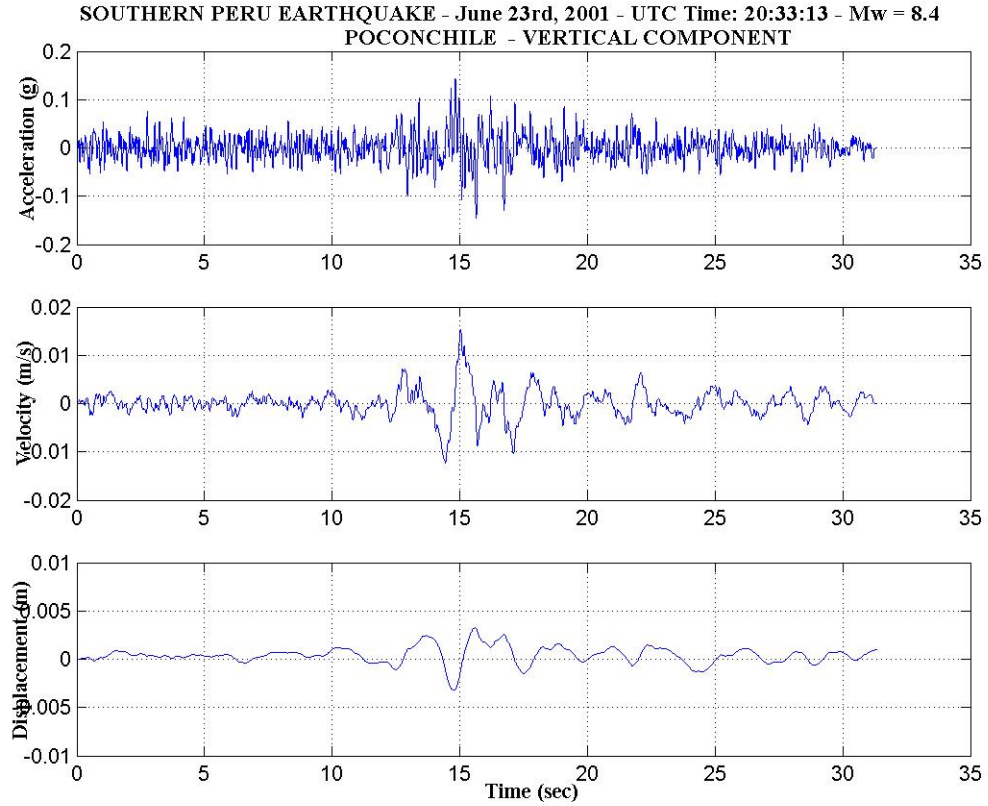
SOUTHERN PERU EARTHQUAKE - June 23rd, 2001 - UTC Time: 20:33:13 - Mw = 8.4
POCONCHILE - VERTICAL COMPONENT
Acceleration (g)
Velocity (m/s)
Displacement (m)
Time (sec)

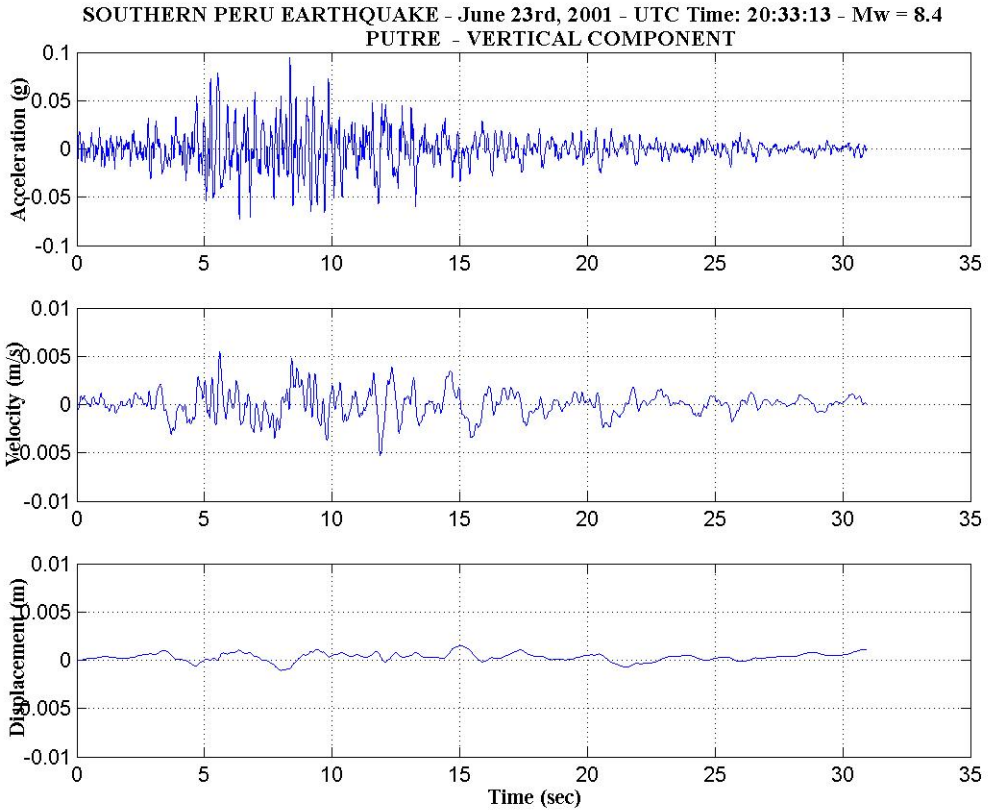
SOUTHERN PERU EARTHQUAKE - June 23rd, 2001 - UTC Time: 20:33:13 - Mw = 8.4
PUTRE - VERTICAL COMPONENT
Acceleration (g)
Velocity (m/s)
Displacement (m)
Time (sec)

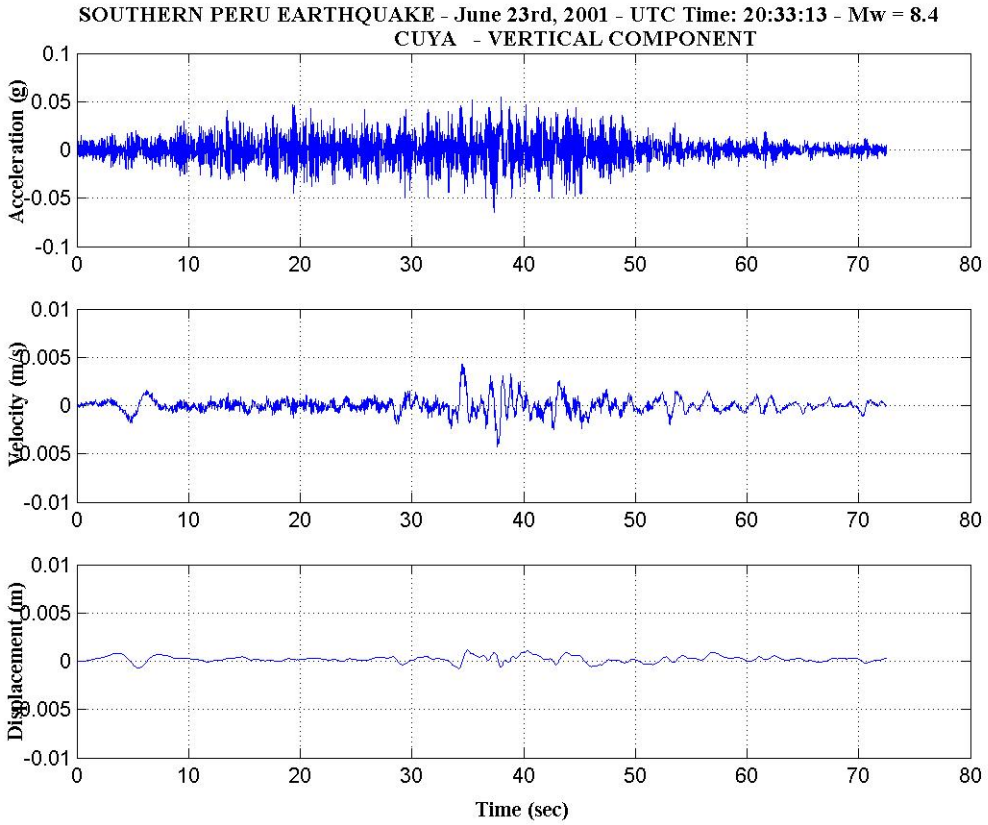
SOUTHERN PERU EARTHQUAKE - June 23rd, 2001 - UTC Time: 20:33:13 - Mw = 8.4
CUYA - VERTICAL COMPONENT
Acceleration (g)
Velocity (m/s)
Displacement (m)
Time (sec)

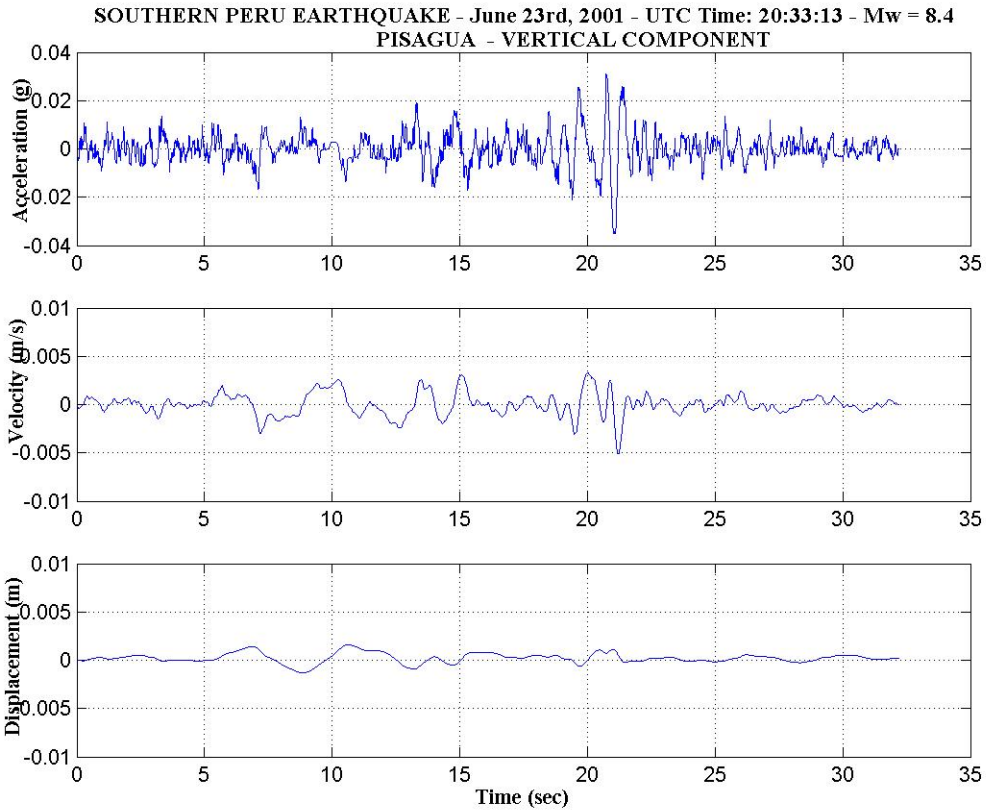

Figure 4.2 Acceleration, velocity, and displacement time histories of recorded ground motions for the vertical ground motion component.

A baseline offset is evident in the displacement time histories of some of the motions (Arica Casa, Cuya, Pisagua, Putre, and to a lesser degree Poconchile). In addition, the horizontal component of the Cuya record shows a displacement pulse at the initiation of the record that is not likely to have been due to the earthquake wave train. It is important to note that the raw ground motions were corrected for baseline and instrument effects by the organization in charge of the instruments, and no additional processing was attempted. The potential errors in baseline correction, however, occur at very low frequencies and have no bearing on the results presented in this chapter.

Time-domain ground motion parameters were calculated for each of the recordings and are summarized in Table 4.2. The maximum absolute values of

acceleration, velocity, and displacement are termed Peak Ground Acceleration (*PGA*), Peak Ground Velocity (*PGV*) and Peak Ground Displacement (*PGD*), respectively. Each of these parameters describes the intensity of the ground motion at a different frequency band. Arias Intensity (I_a) is defined as (Arias 1970):

$$I_a = \frac{\pi}{2g}\int_0^{\infty}[a(t)]^2\,dt \qquad (4.1)$$

where *a(t)* is the acceleration time history. Arias intensity is a measure of the energy of the motion. Duration is quantified either by the Bracketed Duration (Bolt 1969) or by the Significant Duration (Trifunac and Brady 1975b). Bracketed Duration is defined as the time between the first and last exceedances of a threshold acceleration, which is usually 0.05 g as suggested by Kramer (1996). Significant duration represents the time interval between the points at which 5% and 95% of the total energy has been recorded (Kramer 1996).

The ground motion parameters can be compared to those measured in previous earthquakes by means of attenuation relationships, which incorporate previously recorded earthquakes. The PGA recorded in the Southern Peru earthquake range from 0.03g for the most distant sites, to 0.34g for the North-South component of the Arica Costanera station. Figure 4.3 compares recorded PGAs to the predictions of attenuation relationships for subduction zone environments. It is noteworthy that the two ground motion stations of Arica Casa and Arica Costanera have larger PGAs than the Moquegua stations, which is located closer to the fault. These two stations have PGA values significantly higher than those predicted by the attenuation relationships. As it is shown in section 4.2.2, this effect could suggest the presence of site effects.

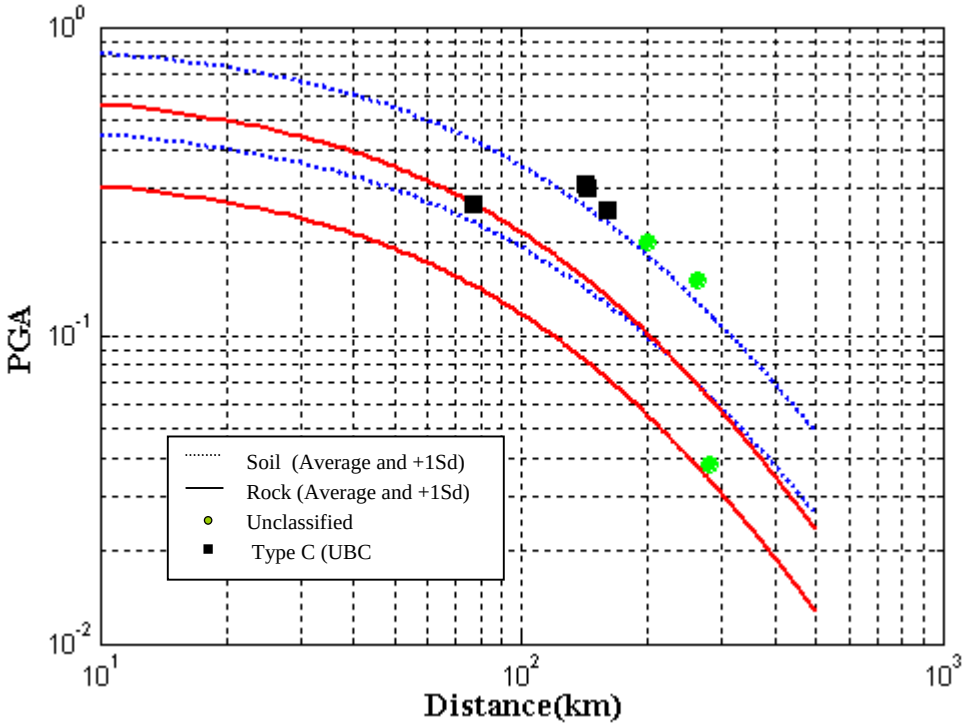

(a)

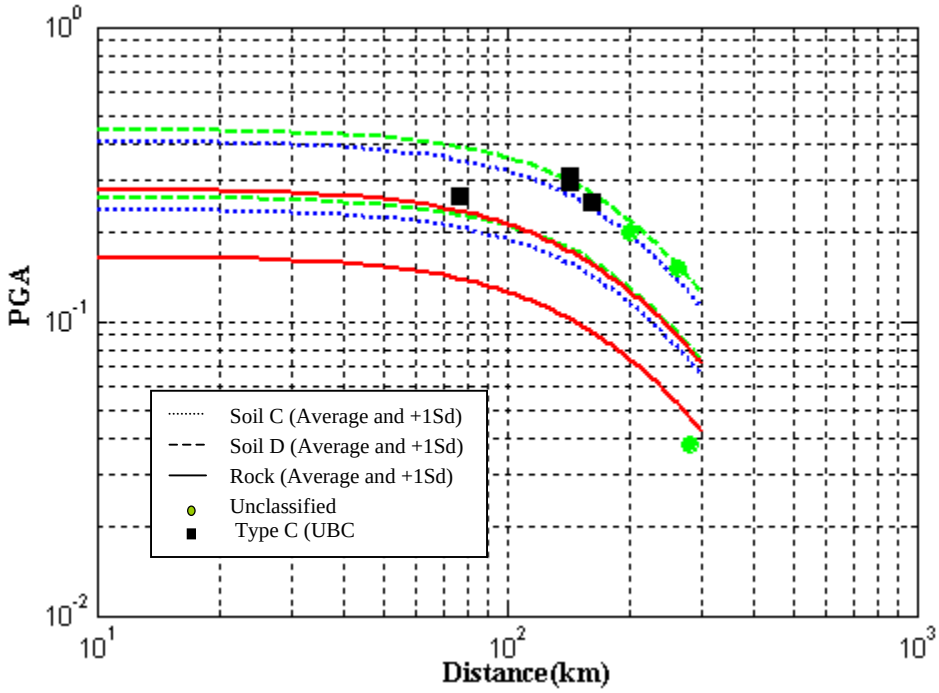

(b)

Figure 4.3 Comparison between recorded PGAs and the predictions of attenuation relationships. (a) Youngs et al. (1997). (b) Atkinson and Boore (2003).

The significant durations estimated for the recorded motions in the Southern Peru earthquake range from 14.5 s for the most distant sites, to 43.2 for the vertical component of Cuya station. Figure 4.4 compares the estimated significant durations to the predictions of the Abrahamson and Silva (1996) attenuation relationship. It is important to note that the Abrahamson and Silva attenuation relationship is only for shallow crustal earthquakes in active tectonic regions. However, it is included in Figure 4.4 to provide a frame of reference to evaluate significant durations. Most of the recorded duration values are around the mean value predicted by the attenuation relationship, however, the duration estimated for Moquegua station was under predicted. Some other duration values are over predicted by the attenuation relationship, as it is the case of Putre and Pisagua stations. For the case of bracketed duration no attenuation relationship was found for comparison purposes.

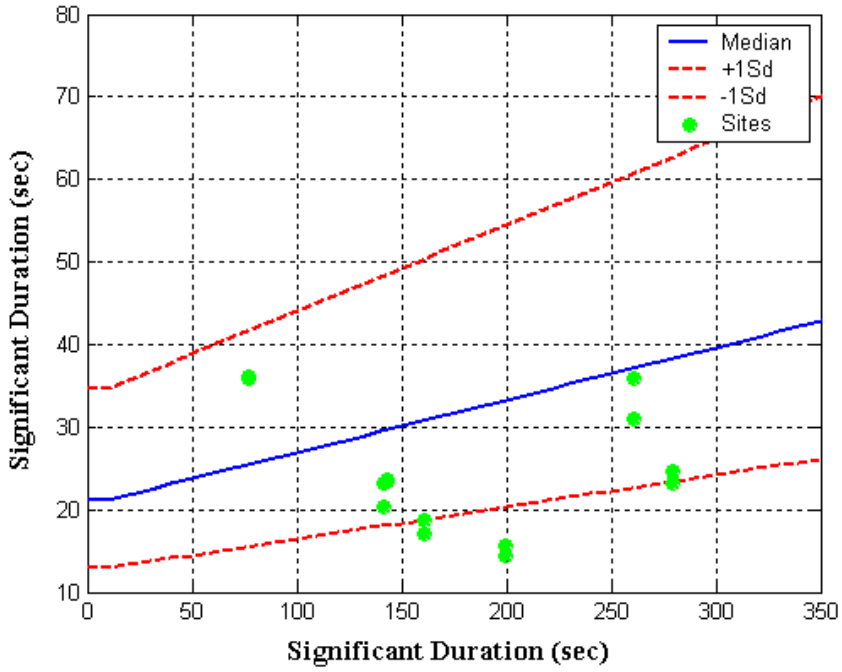

Figure 4.4 Comparison between the recorded significant durations and the predictions of the Abrahamson and Silva (1996) attenuation relationship.

The comparison between the Arias intensity obtained from the records with the predictions of Travasarou et al. (2003) are presented in Figure 4.5. The values calculated for the recorded motions range from 0.02 m/s for the most distant sites, to 2.84 m/s for the E-W component of Moquegua station. It is important to clarify that the figure presented here represents an extrapolation of the attenuation relationship, which has a upper limit of applicability of M_w =7.6. Moreover, this attenuation relationship does not include data from subduction zone events. A general under estimation of the Arias intensity is observed; likely due to the extrapolation used for the present case. However, the author believes that the present comparison is useful and provides a frame of reference evaluating the results.

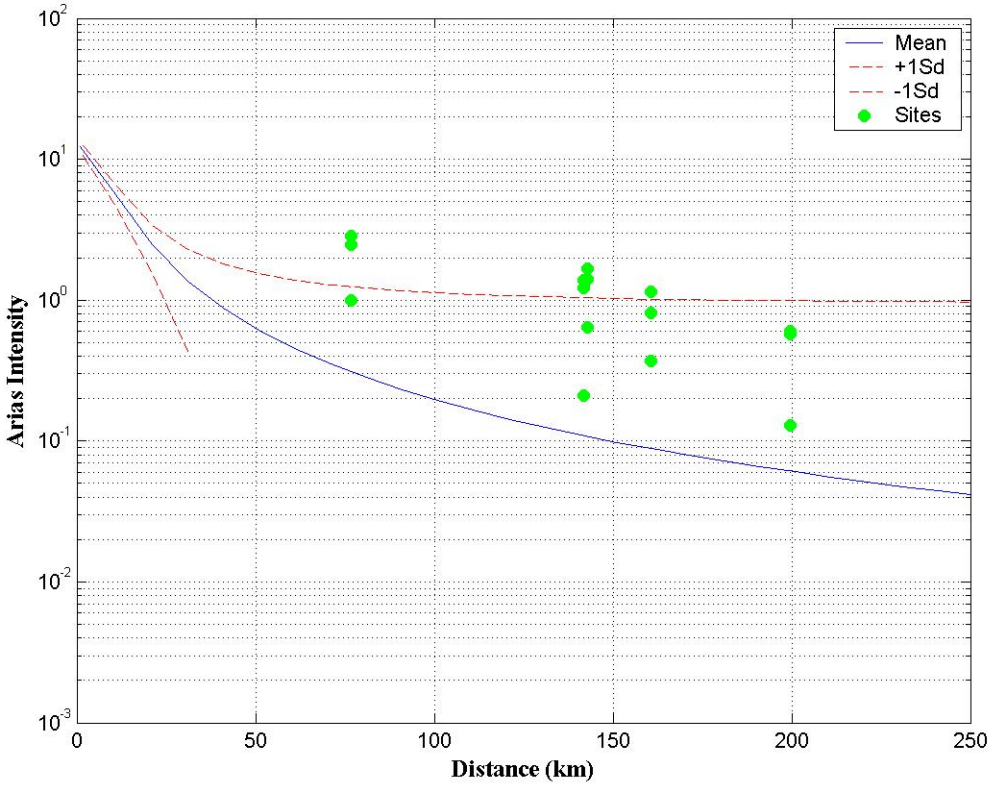

Figure 4.5 Computed values of Arias Intensity vs distance (closest distance to the fault) for recordings in the Southern Peru earthquake. The predictions of the Travasarou et al. (2003) attenuation relationship for an earthquake of M_w 7.6 (the upper limit of applicability of the attenuation relationship) are shown to establish a frame of reference.

Table 4.2 Time domain ground motion parameters.

Ground Motion Station	Closest distance to the fault (km)	Hypocentral Distance (km)	Component	PGA (g)	Peak velocity (cm/s)	Peak displacement (cm)	Bracketed Duration (sec)	Significant Duration (sec)	Arias Intensity (m/s)
Arica Casa	142.8	431.2	N-S	0.27	19.7	6.5	31.7	23.5	1.40
			E-W	0.31	32.6	8.6	38.8	23.7	1.66
			V	0.18	18.8	7.0	24.8	30.0	0.64
Arica Costanera	141.9	430.3	N-S	0.34	25.7	7.4	30.1	20.4	1.39
			E-W	0.28	26.1	6.6	31.2	23.1	1.22
			V	0.08	13.1	5.3	18.7	33.0	0.21
Cuya	260.6	544.0	N-S	0.14	8.2	1.5	28.4	35.8	0.64
			E-W	0.16	9.4	1.1	27.1	30.9	0.71
			V	0.06	4.2	1.2	2.6	43.2	0.19
Pisagua	279.5	562.4	N-S	0.03	5.7	2.5	0.0	24.7	0.03
			E-W	0.04	4.3	1.8	0.0	23.3	0.03
			V	0.04	5.0	1.5	0.0	22.5	0.02
Poconchile	160.6	450.9	N-S	0.25	29.2	5.9	23.2	18.7	0.81
			E-W	0.26	29.2	6.8	23.1	17.1	1.15
			V	0.15	15.1	3.2	24.7	24.5	0.37
Putre	199.7	490.4	N-S	0.20	11.7	3.1	16.4	14.5	0.57
			E-W	0.19	10.6	3.3	16.7	15.6	0.60
			V	0.09	5.4	1.5	8.6	15.9	0.13
Moquegua	76.7	307.3	N-S	0.22	29.9	6.8	43.5	36.0	2.47
			E-W	0.30	24.9	4.6	52.9	35.9	2.84
			V	0.16	13.1	6.1	40.9	38.8	0.99

From the analysis of the previous figures it can be assumed that the different parameters calculated are within a reasonable range when compared to results from attenuation relationships.

The frequency content of ground motions is typically characterized using response spectra. The response spectra (RS) describes the maximum response of a single degree of freedom (SDOF) system to a particular input motion as a function of the natural frequency (or natural period) and damping ratio of the SDOF system. (Kramer 1996). A response spectrum was calculated for all the ground motions and it was compared to the predictions obtained from the Atkinson and Boore (2003) attenuation relationship. Figure 4.6 presents the spectral accelerations of the recorded ground motions. Lines labeled as soil and rock represent the predictions of the Atkinson and Boore (2003) attenuation relationship.

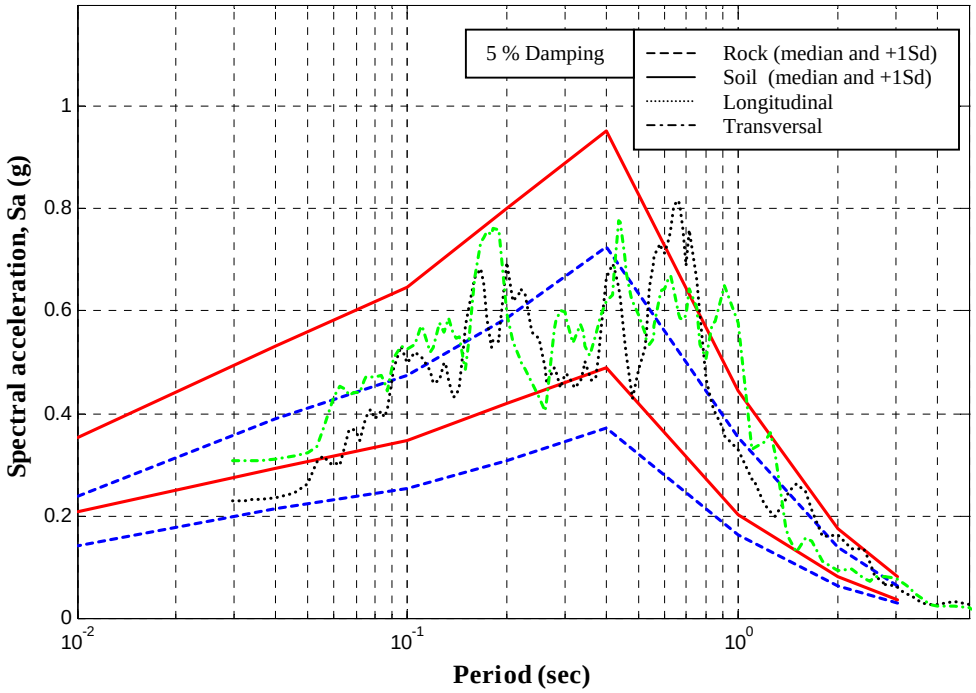

a) Moquegua Station (Closest distance = 76.7 km)

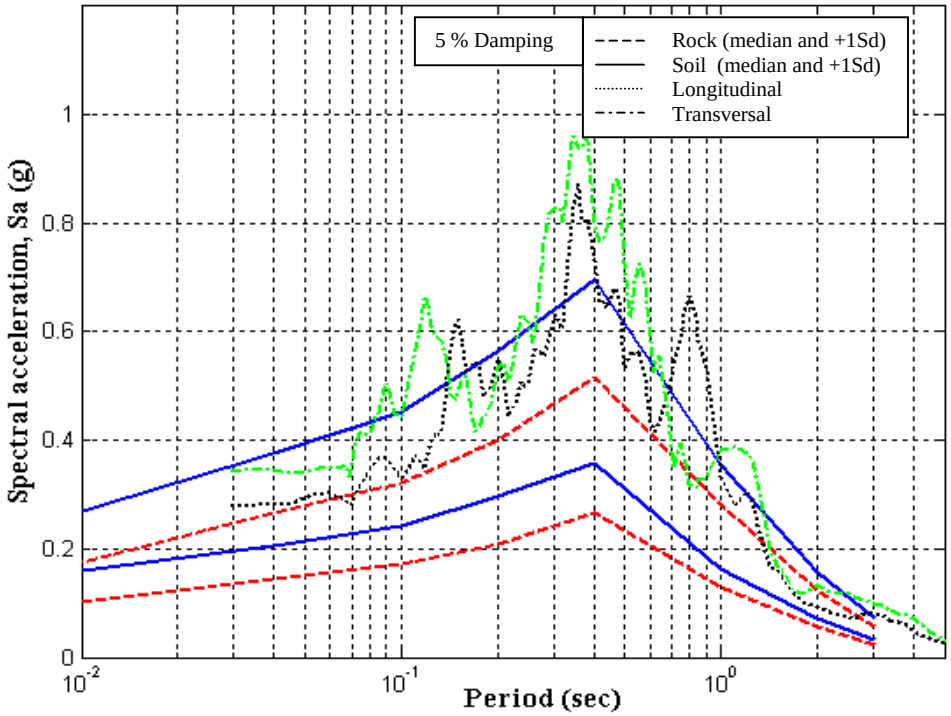

b) Arica Costanera (Closest distance = 141.9 km)

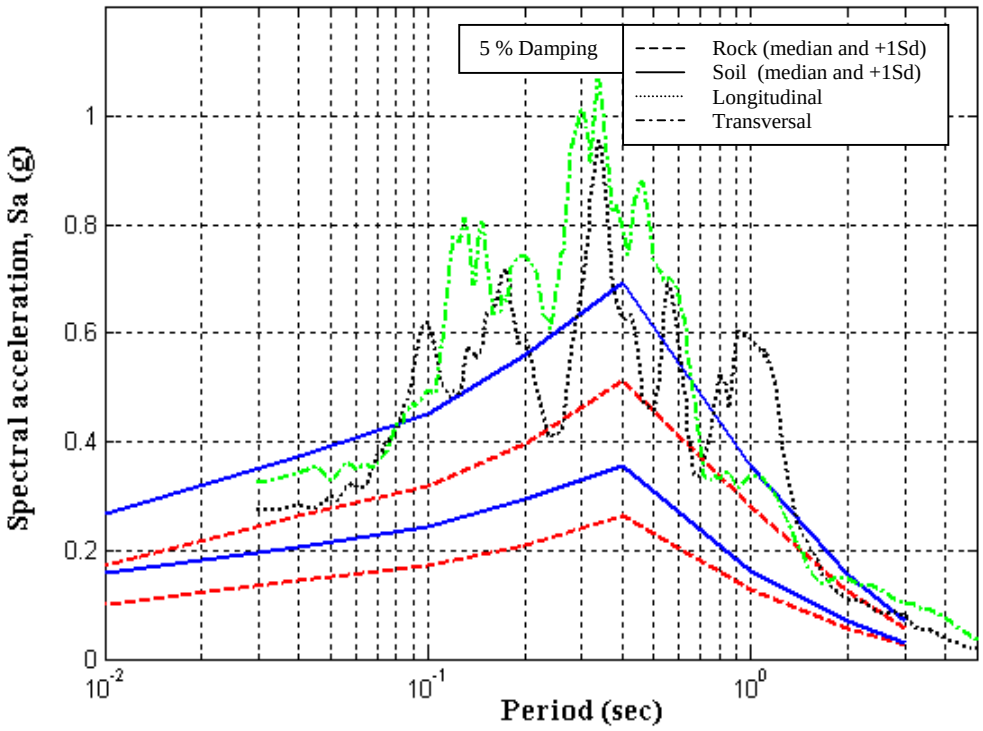

c) Arica Casa (Closest Distance = 142.8 km)

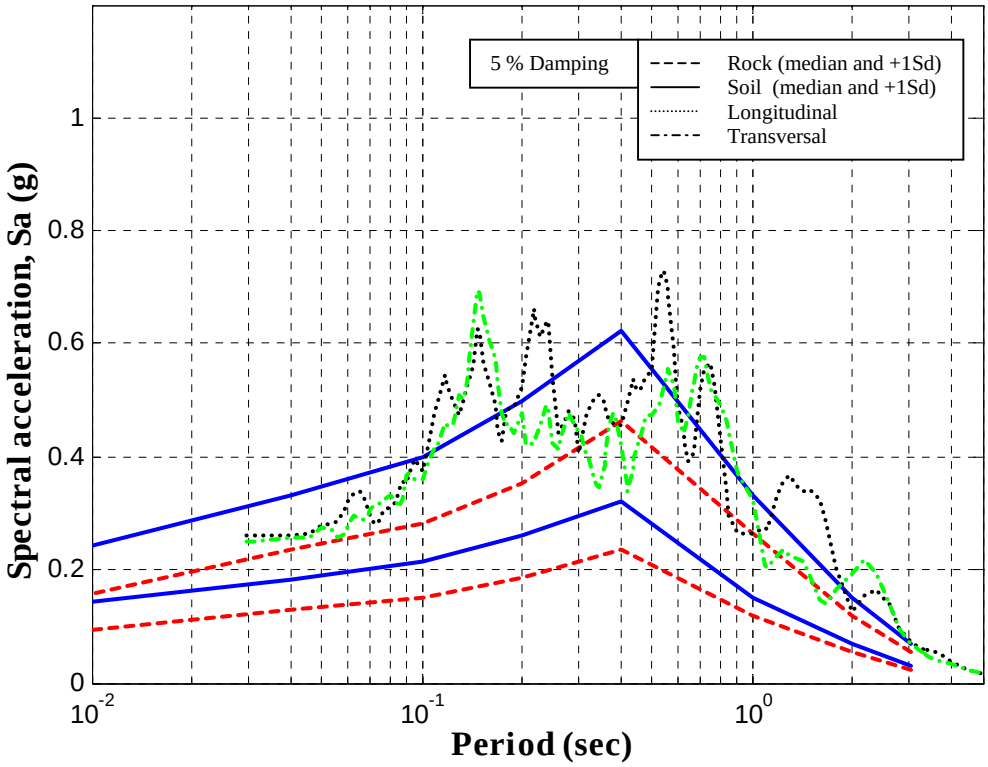

d) Poconchile Station (Closest distance = 160.6 km)

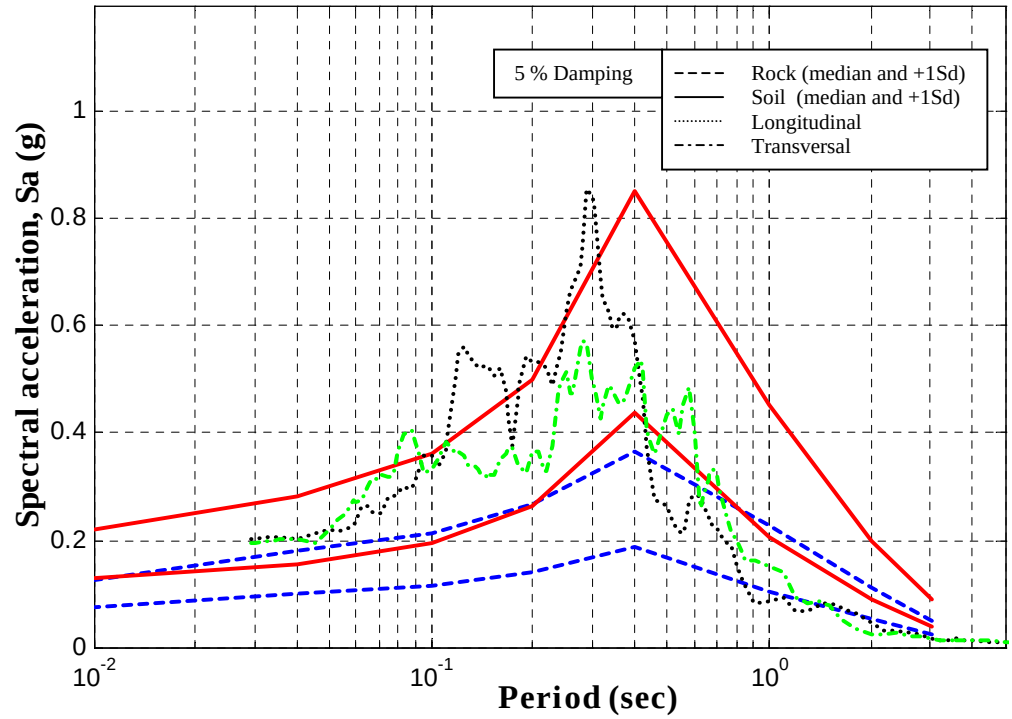

e) Putre Station (Closest distance = 199.7 km)

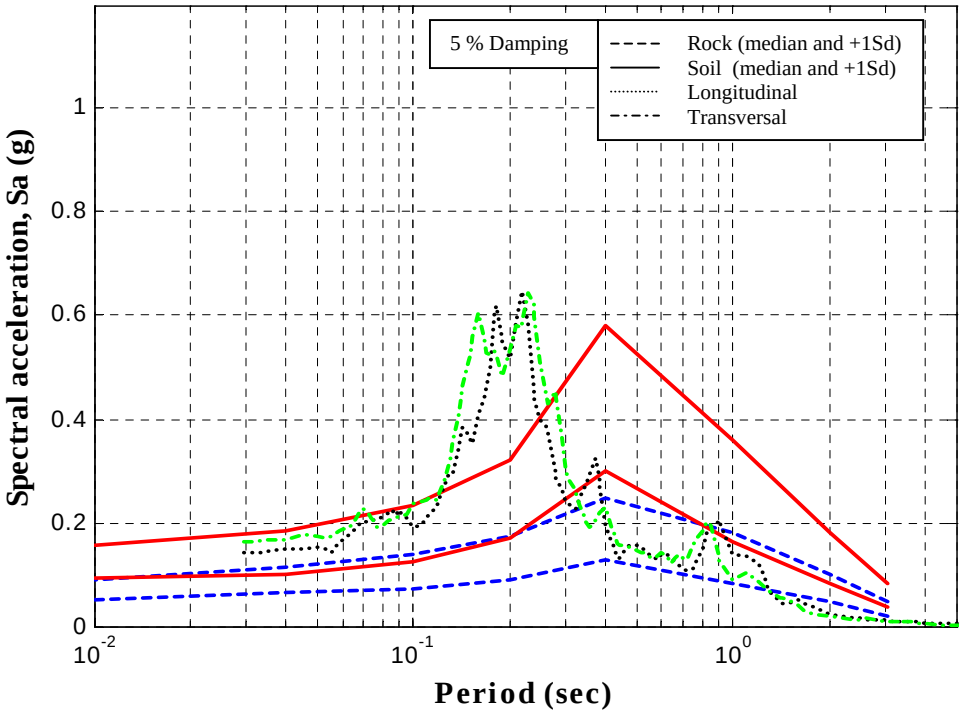

f) Cuya Station (Closest distance = 260.6 km)

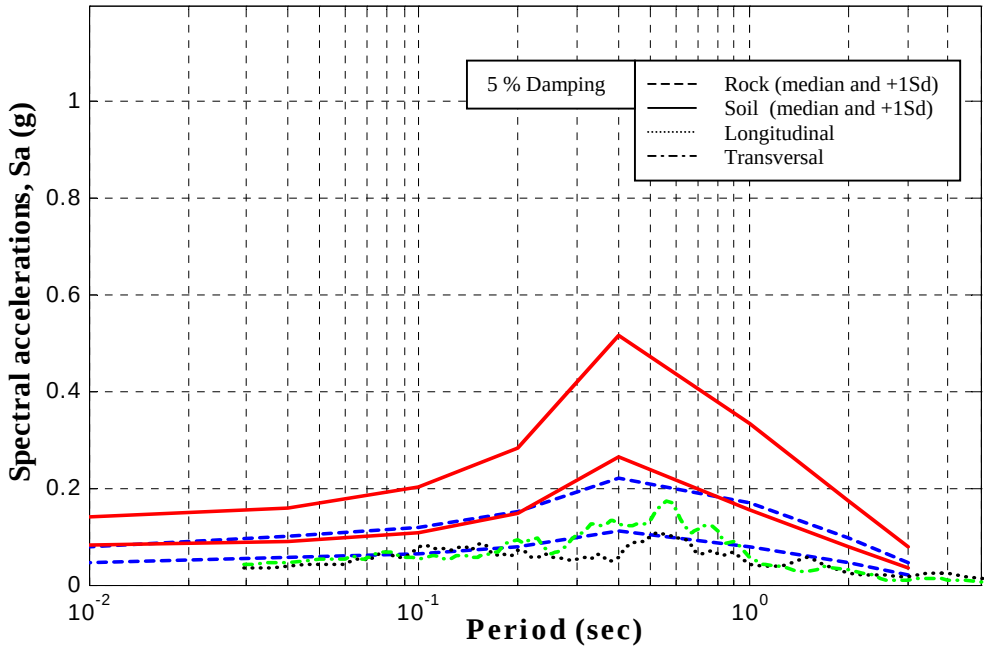

g) Pisagua Station (Closest distance = 279.5 km)

Figure 4.6 Response spectra (5% damping) of recorded ground motions. Predictions of the Atkinson and Boore (2003) attenuation relationships are included for reference (both the median prediction and the 85th percentile (+ 1Sd) lines are included). Distances listed in Table 4.2 are used for the attenuation relationships along with the source parameters discussed in section 4.2.

The Atkinson and Boore (2003) attenuation relationship includes several factors in the analysis. These factors are: closest distance to the fault, moment magnitude, soil type, focal depth (for the present case a value of 30 km was used as suggested by Rodriguez-Marek and Edwards 2003). A differentiation between interface and intra-slab events is also made. The 2001 southern Peru earthquake is an interface event.

Figures 4.6a to 4.6g show that, in most cases, the recorded ground motion matches the predicted median plus one standard deviation line for soil indicating that the attenuation relationships under predicted the recorded accelerations. This phenomenon could be attributed to site effects, as is explored in the next section (Section 4.4). A clear trend cannot be seen in those figures, however, the only tendency that can be observed is that the accelerations for the sites located in Arica are high despite their considerable distance to the source.

Some of the stations (Moquegua, Arica Costanera, Arica Casa, Poconchile, and Cuya) contain a bimodal response spectrum, with one peak at short periods and another at longer periods (Figures 4.6a, 4.6b, 4.6c and 4.6d). There is also a significant dip in spectral accelerations for the three further sites for 2 seconds spectral period (Figures 4.6e, 4.6f and 4.6g).

Although the response spectrum is a full description of a ground motion in the frequency domain, engineers often desire quantification based on single parameter measures. Such parameters are termed frequency-domain ground motion parameters. The three parameters most often used are Predominant Period (T_p), Means Square Period (T_{ms}), and Central Period (or Central Frequency λ_n). The Predominant Period is defined as the vibration period corresponding to the maximum spectral acceleration value. The Central period represents the period at which the power spectral density of a motion is

concentrated (Kramer 1996). Finally the Mean Square period is calculated using the following equation:

$$T_m = \frac{\sum_i C_i^2 . \left(\frac{1}{f_i} \right)}{\sum_i C_i^2} \qquad (4.2)$$

where C_i = Fourier amplitudes of the entire accelerogram; and f_i = discrete Fourier transform. This equation can be applied for frequencies between 0.25 and 20 Hz.

Table 4.3 Frequency content parameters.

Ground Motion Station	Closest distance to the fault (km)	Hypocentral Distance (km)	Component	Predominant Period (sec)	Mean Square Period (sec)	Central Period (sec)
Arica Casa	142.8	431.2	N-S	0.36	0.65	0.80
			E-W	0.25	0.44	0.63
			V	0.18	0.41	0.65
Arica Costanera	141.9	430.3	N-S	0.28	0.56	0.72
			E-W	0.25	0.56	0.70
			V	0.07	0.51	0.84
Cuya	260.6	544.0	N-S	0.18	0.27	0.35
			E-W	0.20	0.26	0.32
			V	0.09	0.21	0.35
Pisagua	279.5	562.4	N-S	0.04	0.69	1.00
			E-W	0.05	0.61	0.77
			V	0.04	0.77	0.94
Poconchile	160.6	450.9	N-S	0.18	0.61	0.87
			E-W	0.24	0.62	0.83
			V	0.10	0.41	0.65
Putre	199.7	490.4	N-S	0.16	0.34	0.43
			E-W	0.15	0.43	0.51
			V	0.06	0.36	0.49
Moquegua	76.7	307.3	N-S	0.44	0.53	0.68
			E-W	0.57	0.54	0.67
			V	0.18	0.34	0.55

The recorded frequency domain parameters were compared to the predictions of the Rathje et al. (1998) attenuation relationship (Figures 4.7 and 4.8), which include relations for Predominant and Mean Square period. In both cases the attenuation relationship over predicts the recorded periods. The reason for the over

prediction could be that an extrapolation for higher magnitudes was applied in order to use the M_w= 8.4 magnitude of the earthquake under study. The upper limit for the attenuation relationship magnitude is M_w 8.0. In addition, the Rathje et al. (1998) attenuation relationship applies for shallow crustal earthquakes in active tectonic regions. It is important to mention that the recorded values present the opposite trend to the predicted by the attenuation relationship, fact that suggests that Predominant Period as well as Mean Square Period are not stable parameters, which suggests that the description of the frequency content of a ground motion using a single parameter is not a suitable practice.

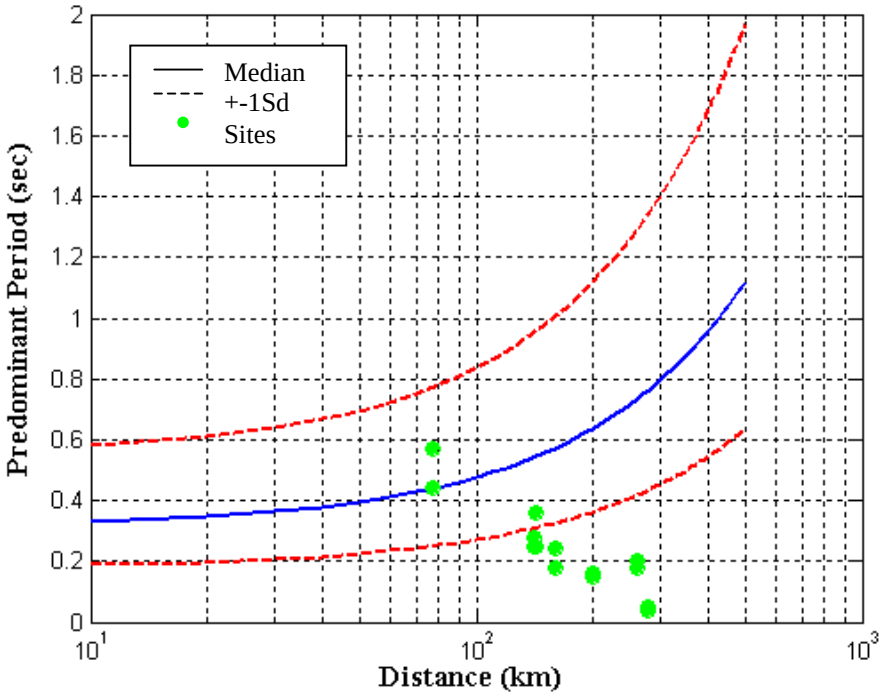

Figure 4.7 Comparison between the recorded Predominant period and the predictions of the Rathje et al. (1998) attenuation relationship.

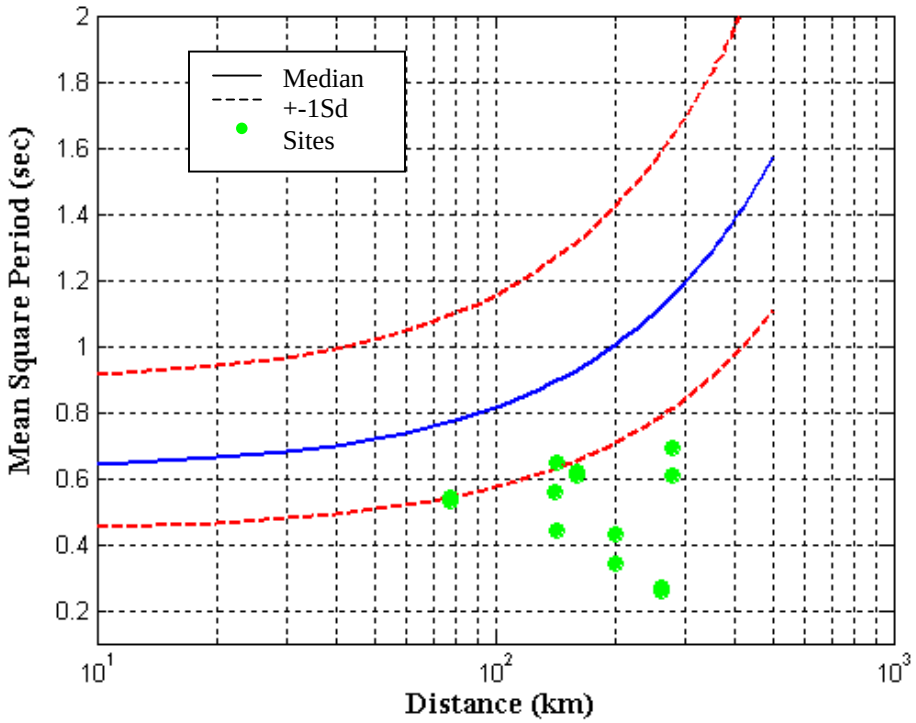

Figure 4.8 Comparison between the recorded Mean Square period and the predictions of the Rathje et al. (1998) attenuation relationship.

4.3 Site properties

The primary factor controlling site response are the properties of the soils underlying the ground motion stations. An understanding of the regional geology is important for an appropriate evaluation of the soil profiles. A very steep relief from the Andes Mountains to the Pacific Ocean characterizes the pacific coast of southern Peru and northern Chile. The elevation change is an average of 3500 m and occurs over a distance of less than 300 kilometers. This high relief implies short drainage basins with a high energy depositional environment. The weather is very arid and rainfall occurs only once every few years. This section presents first an overview of the geology in the two cities where ground motions were recorded; the soil properties used in the subsequent site response analyses are then presented and discussed.

4.3.1 Local Geological Features in Moquegua

The city of Moquegua is located on Quaternary deposits; the majority of which are of alluvial origin and are composed of sandy gravels. A high-energy depositional effect is evident in the large amount of boulders present in the valley. Fluvial deposits in the river margins are mostly loose sands and gravels with the occasional presence of fine-grained sediments such as silts and clays. Densities observed in the Quaternary deposits vary with depositional age. On the other hand, the upper terraces and the surrounding hills are deposits of dense to very dense granular materials. Bedrock outcrops are present in some areas of Moquegua. The bedrock is locally known as the Moquegua formation and is composed mainly of late tertiary sedimentary rocks, including conglomerates, sandstones and tuffs. The Moquegua formation outcrops in the hills surrounding the downtown area, and in the communities surrounding Moquegua (San Antonio and Samegua). (Rodriguez-Marek et al. 2001). The Moquegua formation is underlain by the Toquepala formation. This formation is composed by rhyolite, andesite, dacite and piroclastic flows of early Tertiary - late Cretaceous age. This formation can be observed in the outcropping areas located to the northeast of the city. Weathering effects are variable depending on the area of the city.

4.3.2 Local Geological Features in Arica

The Plateau of Arica is composed mainly of extensive continental sedimentary-volcanic successions of Oligocene – Neocene age rocks, according to radiometric dating (Wörner et al. 2000). These stratigraphic units, highly folded and fractured, lean in angular discordance on rocks of Precambrian to Paleocene age, mainly in the western part of the area of Arica. The segment called Chucal underlies the other areas of the city. Muñoz (1991) defined the Chucal Formation as a sedimentary and volcanic succession of

1,000 m of thickness, assigning it to the Paleocene. According to a tectonic-sedimentary analysis, based on cartography on scale 1:100.000 and radiometric ages, Riquelme (1998) denominated “Estratos Cerro Chucal” to the average-upper part (essentially sedimentary detritus), of the unit defined by Muñoz (1991), and he assigned it to Miocene age. The sediment characteristics of the Chucal Formation indicate an atmosphere of fluvial and initially alluvial lacustrine deposition varying to fluvial and alluvial. (Riquelme, 1998; Chavez, 2001).

4.3.3 Shear Wave Velocity Profiles and soil properties at ground motion stations

The measurement of shear wave velocity *(V_s)* profiles at the ground motion stations is described in detail in Chapter 3. Figure 4.9 presents the measured V_s profiles for these stations. The V_s profile was used to categorize the sites following the classification systems described in Table 4.4. The site classifications are summarized in Table 4.5.

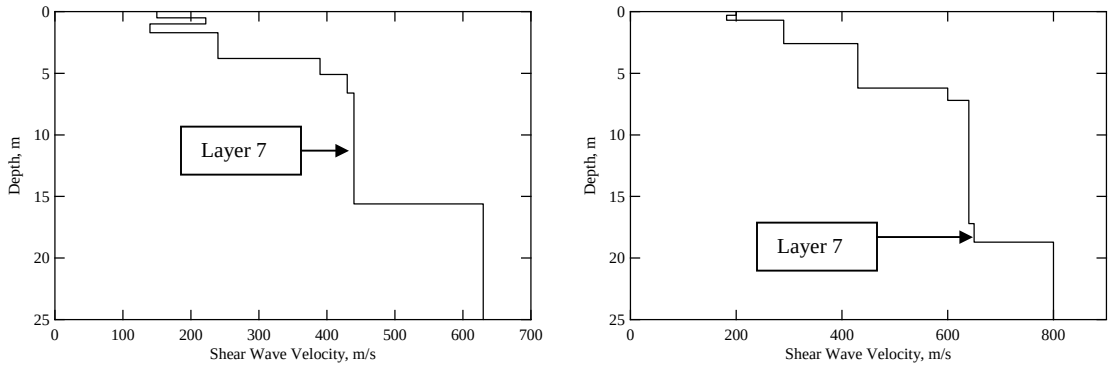

a) Arica Casa **b) Moquegua**

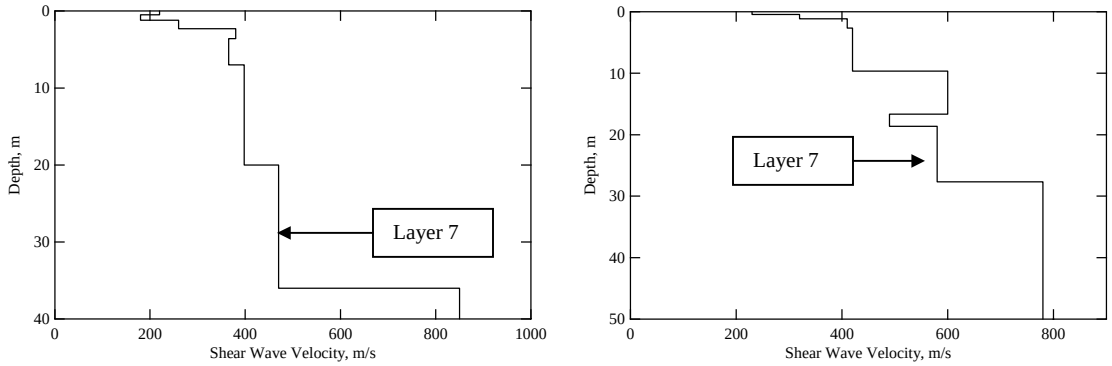

c) Arica Costanera **(d) Poconchile**

Figure 4.9 Shear wave velocity profiles at ground motion stations that recorded the 2001 Southern Peru earthquake. Layers for which different analysis were performed (Table 4.8), are also shown.

Table 4.4 Site Classification Systems

Site Category	Description	Comments
GM – Geomatrix (1993)		
A	Rock	Soil depth < 6 m
B	Shallow Soil	Soil depth < 20 m
C	Deep Soil, Narrow Canyon	Depth>20 m, canyon<2 km wide
D	Deep Soil, Wide Canyon	Depth>20 m, canyon>2 km wide
E	Soft Soil	Vs<150 m/s
BRM – Rodriguez-Marek et al. (2001)		
BRM-A	Hard Rock	Vs≥1500 m/s, Ts≤0.1 s
BRM-B	Rock	Vs≥760 m/s or <6m soil, Ts≤0.2s
BRM-C	Weathered Rock, Shallow Stiff Soil	Soil depth<60 m, Ts≤0.8 s
BRM-D	Deep Stiff Soil	Soil depth>60m, Ts≤2s
BRM-E	Soft Soil	Soft clay thickness>3 m, Ts≤1.4 s
UBC (1997)		
S_A	Hard Rock	Vs > 1500 m/s[1]
S_B	Rock	Vs= 760-1500 m/s
S_C	Very Dense Soil and Soft Rock	Vs=360-760 m/s
S_D	Stiff Soil Profile	Vs=180-360 m/s
S_E	Soft Soil Profile	Vs<180 m/s

[1.] The shear wave velocity is the average of the upper 30 m.

Table 4.5 Site Classifications

Ground Motion Station	$\overline{Vs}$ (m/s)	GM Class	B&RM Class	UBC Class	SASW[1] Quality
Arica Casa	431.85	B*	C2	S_C	1
Arica Costanera	389.26	B*	C2	S_C	1
Cuya	-	-	-	-	-
Pisagua	-	-	-	-	-
Poconchile	510.66	B*	C2	S_C	2
Putre	-	-	-	-	-
Moquegua	573.11	B*	C2	S_C	1

[1] SASW Quality: Level 1 - smooth dispersion data

Level 2 - limited jumps in dispersion data

Level 3 - significant jumps in dispersion data or limited depth achieved

* Vs= 540 m/s was used to define the soil/rock boundary.

Along with the V_s profile, additional soil properties that are needed to perform a one-dimensional site response analysis are the density of the soils and the soil's nonlinear stress-strain behavior that, for equivalent linear analysis, is represented by the modulus reduction and the damping versus cyclic strain curves. The values of density of the soils were provided by Dr. James Bay (Utah State University) as part of the process of obtaining shear wave velocity profiles. Dr. Bay assumed commonly used values for soils with similar characteristics to the ones under study. Information about densities is described in appendix A of the present study. The modulus reduction and damping versus cyclic strain curves were obtained using the model proposed by Darendeli (2001) who suggested the following equations:

$$\frac{G}{G_{\max}} = \frac{1}{1+\left(\frac{\gamma}{\gamma_r}\right)^a} \qquad (4.3)$$

where γ_r = reference strain (described below); γ = strain at which the G/G_{max} value is being calculated; and a = curvature coefficient suggested to be 0.919 by Darendeli (2001). The reference strain is given by:

$$\gamma_r = (0.0352 + 0.001 * PI * OCR^{0.3246}) * SIGo^{0.3483} \qquad (4.4)$$

where γ_r = reference strain; PI = plasticity index; OCR over consolidation ratio, and *SIGo* is the initial effective stress.

For the damping curves, Darendeli (2000) proposed.

$$D_{Masing} = c_1 D_{Masing,a=1.0} + c_2 D_{Masing,a=1.0}{}^2 + c_3 D_{Masing,a=1.0}{}^3 \qquad (4.5)$$

$$\text{where: } D_{Masing,a=1.0}(\%) = \frac{100}{\pi}\left[4\frac{\gamma - \gamma_r \ln\left(\frac{\gamma+\gamma_r}{\gamma_r}\right)}{\frac{\gamma^2}{\gamma+\gamma_r}} - 2\right] \qquad (4.6)$$

and

$$c_1 = -1.1143a^2 + 1.8618a + 0.2523$$
$$c_2 = 0.0805a^2 - 0.0710a - 0.0095$$
$$c_3 = -0.0005a^2 + 0.0002a + 0.0003$$

The standard deviation of the modulus reduction (σ_{NG}) and damping ratio (σ_D) curves are accounted for using the following equations:

$$\sigma_{NG}(\gamma) = \exp(-4.23) + \sqrt{\frac{0.25}{\exp(3.62)} - \frac{(G/G_{max}(\gamma) - 0.5)^2}{\exp(3.62)}} \qquad (4.7)$$

$$\sigma_D(\gamma) = \exp(-5) + \exp(-0.25) * \sqrt{D(\gamma)} \qquad (4.8)$$

where G/G_{max} (γ) is the value of the modulus reduction curve at a strain γ and D(γ) is the damping ratio in percent of a strain γ.

Finally, the value of the maximum strain used to compute effective strain during the equivalent linear analysis was assumed to be 65 % percent.

4.4 Site effects at ground motions stations

The effect of site response at the recording stations is studied using the equivalent linear one-dimensional wave propagation analysis implemented in the program SHAKE91 (Idriss et al. 1991). The objective of the site response analyses is to capture the effect of the surficial soil layers on the recorded motions. However, as is often the case in geotechnical analysis, the input parameters (both soil properties and input ground motions) necessary for the analyses are incomplete and include varying degrees of uncertainty. In order to incorporate these uncertainties into the analyses, a Montecarlo approach was selected. The variability of input parameters is thus incorporated by repeating the site response analyses while varying the input parameters according to pre-specified probability density functions. Site response is quantified in the spectral domain by the Ratios of Response Spectra (RRS). RRS are defined as the ratio of response spectra at the surface over the response spectra of outcrop input motion. In line with the stochastic approach described herein, RRS has an implicit distribution and is described by the mean values and their corresponding standard deviations.

4.4.1 Variability of Input Parameters

Soil parameters

Site response estimation is usually affected by soil parameters such as shear wave velocity of the different layers (which includes the effect of stiffness and density of the soil), depth of the different layers, and the non linear properties of the soil. The SASW tests render a reliable estimate of the shear wave velocity profile down to an impedance contrast at a depth that varies depending on the characteristic of the site. Thus, the soil parameters for which there is a certain uncertainty are: shear wave velocity of the bedrock, depth to the bedrock, and the non-linear properties of the soils. The influence of

variability in these parameters was studied by randomizing an individual variable in each analysis run. Each of these properties was allowed to vary according to a prescribed statistical distribution as described in Table 4.6. The parameterization model proposed by Darendelli (2000) was used to generate families of Modulus Degradation and Damping Ratio curves that are consistent with the uncertainty in such parameters for gravelly soils at different confining stresses. The MATLAB file used to generate these curves is included in Appendix C. Since the model proposed by Darendeli (2000) does not place any constrains on the G/G_{max} and damping values, G/G_{max} was limited to a minimum value of 0.01 while damping was limited to a minimum value of 5%. Moreover to ensure an appropriate correlation of G/G_{max} and damping curves, the same random number was used to generate both sets of curves, that is, for a given strain:

$$\left(\frac{G}{G_{\max}}\right)_{random} = \left(\frac{G}{G_{\max}}\right)_{median} \pm n\sigma_{NG} \qquad (4.9)$$

$$D_{random} = D_{median} \mp n\sigma_{D} \qquad (4.10)$$

where, *n* is a random variable following a standard normal distribution.

It is also important to mention that this model was used only for the randomization of the non-linear properties of the soils, while for all the other randomizations the EPRI (1993c) curves, which are also a function of depth, were applied. Rock shear wave velocity was modified from the recorded values up to 1000 m/s. This range is assumed to represent the range of probable shear wave velocities at all the sites. In the cases in which depth of rock was modified it was varied from the deterministic value (Figure 4.4) to a depth 20 meters larger. Note that the 20 m is an ad hoc selection and further studies would be necessary to properly quantify the uncertainty of depth to bedrock.

Table 4.6 Statistical distributions.

Site	Parameter	Distribution
Arica Casa	V_s of Rock	Uniform distribution with values ranging from the original 630 m/s to 1000 m/s.
	Depth to bedrock	Uniform distribution between 9 m to 29 m.
	Non Linearity	Equations proposed by Darendeli (2001) with standard deviation of one. (Appendix C).
Arica Costanera	V_s of Rock	Uniform distribution with values ranging from the original 850 m/s to 1000 m/s.
	Depth to bedrock	Uniform distribution between 16 m. to 36 m.
	Non Linearity	Equations proposed by Darendeli (2001) with standard deviation of one. (Appendix C).
Moquegua	V_s of Rock	Uniform distribution with values ranging from the original 780 m/s to 1000 m/s.
	Depth to bedrock	Uniform distribution between 1.5 m. to 21.5 m.
	Non Linearity	Equations proposed by Darendeli (2001) with standard deviation of one. (Appendix C).
Poconchile	V_s of Rock	Uniform distribution with values ranging from the original 850 m/s to 1000 m/s.
	Depth to bedrock	Uniform distribution between 9 m. to 29 m.
	Non Linearity	Equations proposed by Darendeli (2001) with standard deviation of one. (Appendix C).

The randomization of the shear wave velocity of bedrock is, in addition, constrained by specifying a lower bound given by the V_s of the overlying soil layer. This restriction is necessary to prevent unreasonable soil profiles. The value of the depth to bedrock computed from the SASW analyses is assumed to be a lower bound. Note that these additional restrictions imply that the randomized profiles are not centered about the deterministic profiles shown in Figure 4.9.

Input Motions

The input motion (e.g. rock outcrop motion) at each of the ground motion stations is not known. There are no available rock recordings in the 2001 Southern Peru earthquake that would allow an estimate of rock motions. The estimates of site response (quantified by RRS) are affected by the choice of input motion. Given that this input

motion is unknown, it is desired to quantify the extent to which the input motion can affect the resulting RRS. The approach taken in this study is to generate a suite of input motions that would represent a "reasonable" estimate of a bedrock input motion for an event of this magnitude, and at the same time would incorporate a reasonable measure of variability. This is accomplished by using ground motions generated from a finite fault model by Dr. Walter Silva (Silva 2004). The finite fault model generates outcrop bedrock motions for a Vs = 800 m/s layer. These motions incorporate variability in source and path effects. The average response spectra of these motions are shown in Figure 4.10.

It is important to note that this approach provides only an ad-hoc measure of the influence of ground motion uncertainty on site response estimates due to the fact that such uncertainty is not quantifiable and outcrop motions were not recorded in the event. Thus the objective of this exercise is only to estimate the relative effect of ground motion uncertainty with respect to the uncertainty due to other input parameters. Figure 4.11 shows the standard deviation of the input and output motions obtained from the site response analysis. Note that in this case, site response increases the uncertainty by a slight amount.

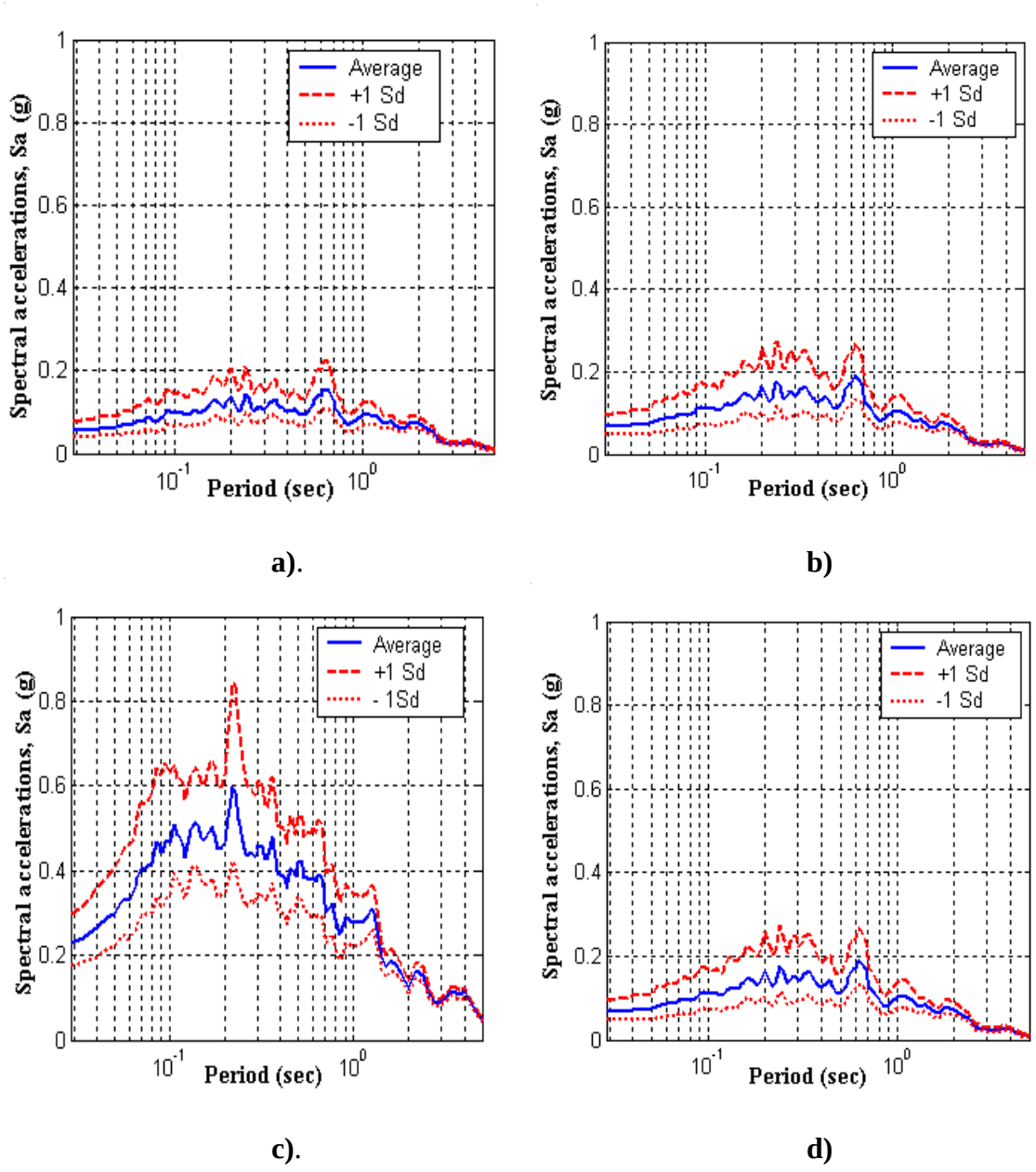

Figure 4.10 Average response spectra of the motions provided by Dr. Silva. +- 1 Standard deviation values included. (a) Arica Casa station, acceleration scaled to 0.1 g. (b) Arica Costanera station, acceleration scaled to 0.1 g. (c) Moquegua station, acceleration scaled to 0.3 g. (d) Poconchile station, acceleration scaled to 0.1 g.

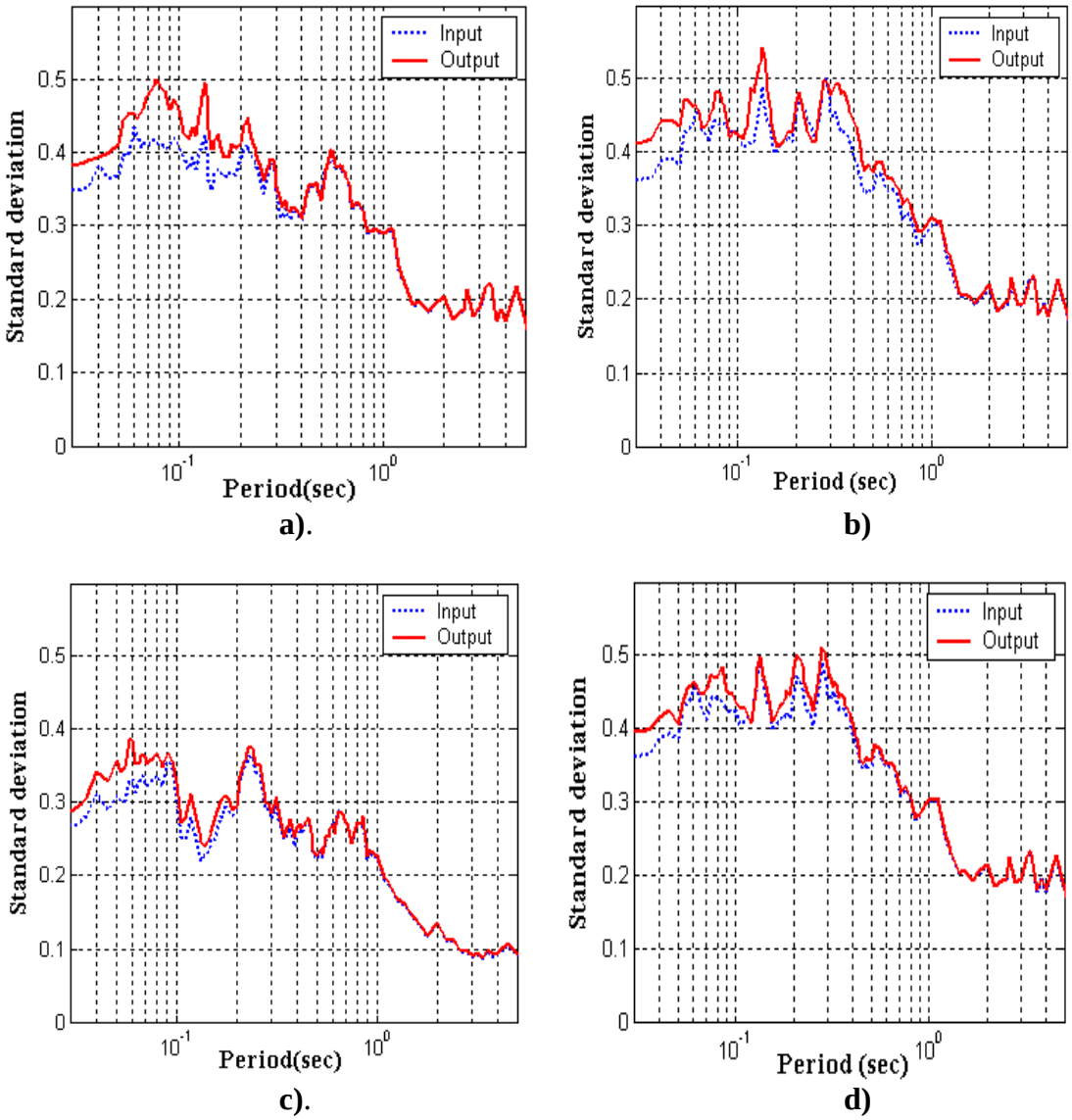

Figure 4.11 Standard deviation of the input motions and the output motions obtained from site response analysis. (a) Arica Casa station. b) Arica Costanera station. (c) Moquegua station. (d) Poconchile station.

An additional check on the effect of ground motion on the estimated RRS is performed by doing analyses for three additional input motions. These motions are selected from the limited number of available recordings from subduction zone events of magnitude larger than M_w 7.9 and a fault distance lower than 100 km. Ground motion properties for these motions are listed in Table 4.8 and their response spectra are shown in Figure 4.12.

Table 4.7 Selected Ground Motions.

	Earthquake Date	Agency	Station Name	Closest Distance to the fault (km)	Ms	Component Azimuth	Location	PGA (cm/s)
Chile	3/3/1985	NOAA	Valparaiso	27	7.9	70	Rock	172.36
Chile	3/3/1985	NOAA	Valparaiso	27	7.9	160	Rock	161.96
Mexico1	9/19/1985	UNAM	Caleta de Campos	19.8*	8.1	090	Rock	-140.7
Mexico1	9/19/1985	UNAM	Caleta de Campos	19.8*	8.1	180	Rock	-139.7
Mexico2	9/19/1985	UNAM	Zihuatanejo	166*	8.1	270	Rock	-154.1
Mexico2	9/19/1985	UNAM	Zihuatanejo	166*	8.1	180	Rock	-98.6

* Epicentral Distance

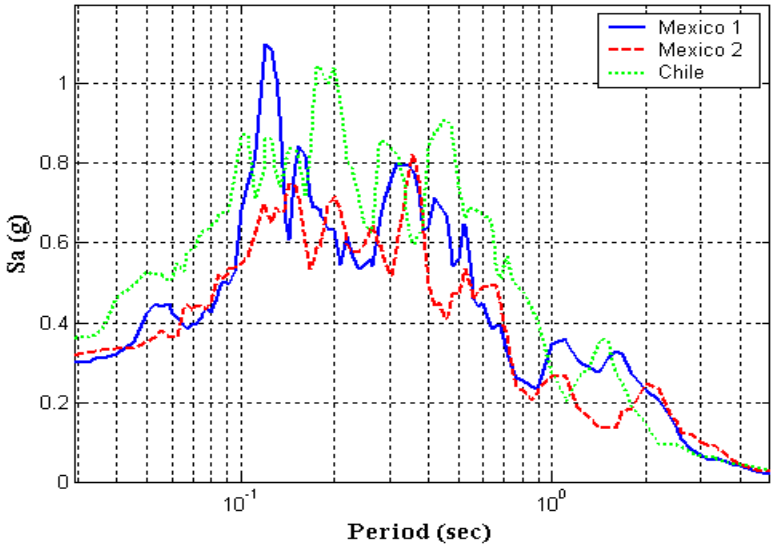

Figure 4.12 Response spectra of the selected motions.

4.4.2 Analyses

The equivalent linear analysis program SHAKE91 described in the literature review was used for all the site response analyses. Table 4.8 presents a summary of the analyses performed including information on the shear wave velocity profile, input motion, and the variable that is randomized. In all of the cases in Table 4.8, the effective strain was selected as 65% of the maximum stress. From all these analyses, acceleration time histories at the ground surface were calculated from which response spectra (RS) were also obtained. Using these RS values, Ratios of Response Spectra (RRS) between the ground surface and bedrock were calculated. In order to facilitate the reproduction of this procedure, a detailed example is shown in Appendix D.

Table 4.8 Summary of the Montecarlo approach.

Case Number	GM Station	Input GM	V_s Profile	Non Linear Soil Properties	V_s Rock
1*	All	Finite source motions (30 per site)	Deterministic[1]	Deterministic[2]	Deterministic - 800 m/s
2*		Recorded GM from previous EQ (3)			
3	Arica Casa	Finite source - Baseline - PGA scaled to 0.1 g.	Vary depth of layer 7[3]	Deterministic[2]	Deterministic - 800 m/s
4			Vary V_s of layer 7		Randomized[5]
5			Deterministic[1]	Randomized[4]	Deterministic - 800 m/s
6	Arica Costanera	Finite source - Baseline - PGA scaled to 0.1 g.	Vary depth of layer 7[3]	Deterministic[2]	Deterministic - 800 m/s
7			Vary V_s of layer 7		Randomized[5]
8			Deterministic[1]	Randomized[4]	Deterministic - 800 m/s
9	Moquegua	Finite source - Baseline - PGA scaled to 0.3 g.	Vary depth of layer 7[3]	Deterministic[2]	Deterministic - 800 m/s
10			Vary V_s of layer 7		Randomized[5]
11			Deterministic[1]	Randomized[4]	Deterministic - 800 m/s
12	Poconchile	Finite source - Baseline - PGA scaled to 0.1 g.	Vary depth of layer 7[3]	Deterministic[2]	Deterministic - 800 m/s
13			Vary V_s of layer 7		Randomized[5]
14			Deterministic[1]	Randomized[4]	Deterministic - 800 m/s

* For these analyses variation of magnitude of ground motion was also performed.

[1] See Figure 4.4.

[2] See equations 4.3 to 4.6.

[3] 150 different values of depth were randomly created. See Table 4.6.

[4] 150 sets of modulus reduction and damping ratio curves were randomly created following the criteria of Darendeli (2001). See Table 4.6.

[5] 150 different values of V_s were randomly created using a uniform distribution. See Table 4.6.

4.4.3 Results

This section discusses the results of the site response analyses. The RRS is used to quantify and evaluate site response at each site. The effects of input motion uncertainty and uncertainty in soil properties are discussed separately.

Input Motion uncertainty

Figure 4.13 shows the median and one standard deviation band of the site response analysis results for varying input motion (Analysis 1 in Table 4.8). The suite of motion generated from finite fault modeling (Silva 2004) was used as input. The PGAs of input motions were selected to loosely match predictions from attenuation relationships for rock corresponding to the distance of each site to the fault; however, as will be shown later, the input motion intensity does not significantly affect the resulting RRS.

The RRS for all of the input motions are shown in Figure 4.14. Observe how the general shape of the RRS is preserved for all of the input motions. Peak amplitudes of RRS (RRS_{max}) also have a relatively small range, with an average coefficient of variation (standard deviation over the mean) of 0.045. This variation is relatively small compared with the potential range of RRS in soils. The period corresponding to the RRS_{max} corresponds to the predominant site period, T_{site}. These periods for each site are listed in Table 4.8. The predominant site periods are consistent with the characteristic site period (Kramer 1996):

$$T_s = \frac{4H}{V_s} \qquad (4.7)$$

where H is the profile depth and V_s is the average shear wave velocity for the whole soil layer obtained from the total travel time of a shear wave velocity (V_s = *H* / *travel time*). Arica Casa and Moquegua have negligible amplification beyond $T = 0.2$ seconds while

Poconchile has negligible amplification beyond about T = 0.4 seconds. On the other hand, Arica Costanera has amplification over a period band of 0.4 to 0.8 seconds, indicating a relatively softer response than the remaining sites. It should also be observed that it is difficult to identify the site period for Arica Costanera and Poconchile due to the presence of three and two periods, respectively, at which amplification is considerable. These periods correspond to the fundamental modes of the upper soil layers (e.g. T = 0.077 is the fundamental period of the upper 3.8 m of soil in Arica Casa, 0.074 is the fundamental period of the upper 6.2 m in Moquegua, and 0.098 s is the fundamental period of the upper 9.65 m in Poconchile).

Table 4.9 Site Period

Site	**Predominant Site Period[1] (sec)**	**Characteristic Site Period[2] (sec)**
Arica Casa	0.077 (0.15)	0.19
Arica Costanera	0.32 (0.14,0.074)	0.36
Moquegua	0.06 (0.11)	0.15
Poconchile	0.24 (0.098)	0.22

[1] Obtained from the average RRS (Figure 4.13). Values in parenthesis correspond to secondary RRS peaks.
[2] Equation 4.7.

With the purpose of understanding the effects of variation in input motion intensity, the finite source motions were scaled to PGA levels ranging from 0.1 to 0.3 g. Resulting median values of Response Spectra are shown in Figure 4.15. While the observed trend (a shift of peak response towards higher periods) follows the expected pattern, the variations in the amplitude and value of RRS are small compared with the variability due to the variation in input motions.

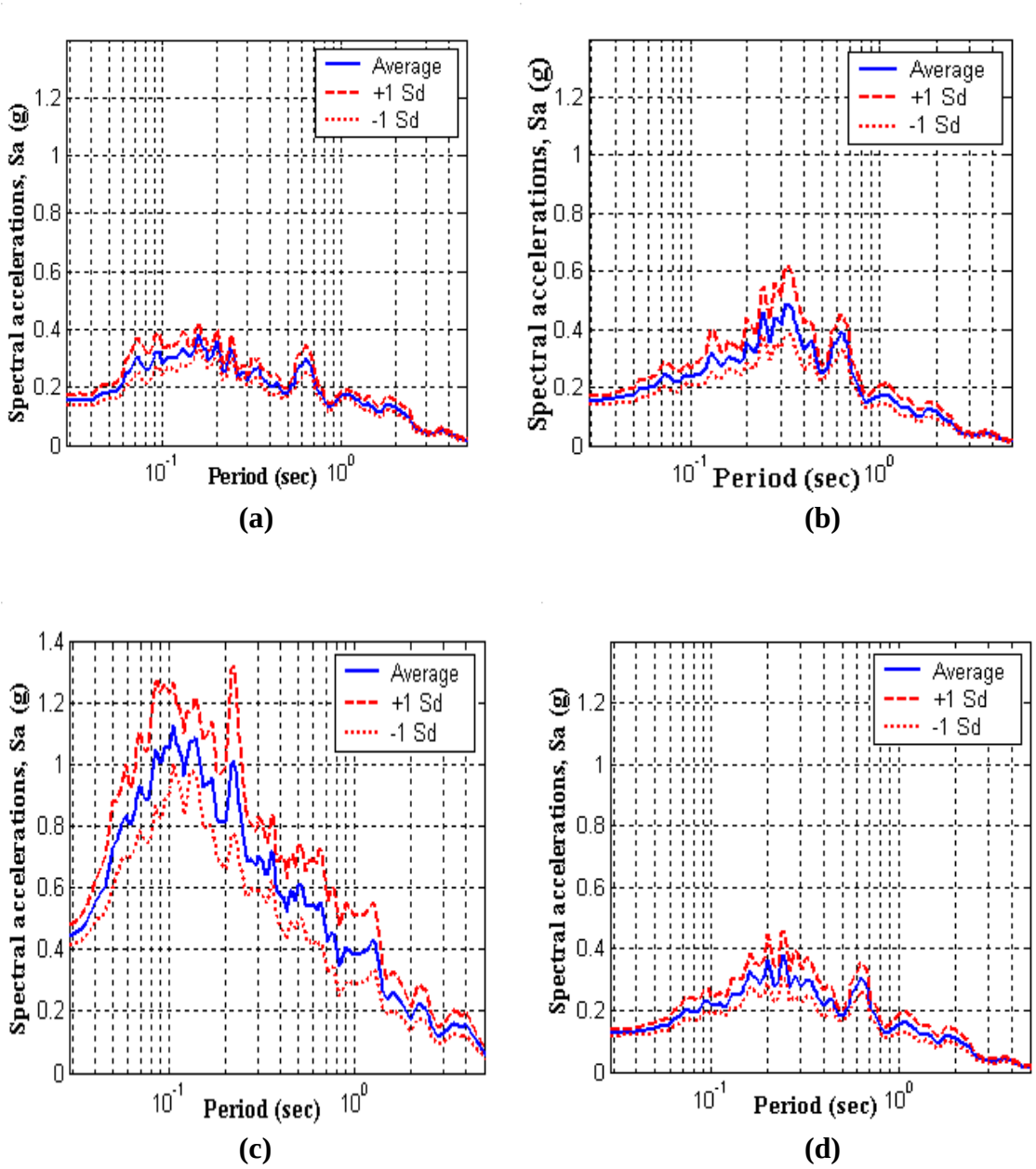

Figure 4.13 Average response spectra (5% damping) for the 150 runs using the scaled records provided by Dr. Silva as input motions; estimated at the ground surface including +-1 standard deviation values. a) Arica Casa station, input acceleration scaled to 0.1 g. (b) Arica Costanera station, input acceleration scaled to 0.1 g. (c) Moquegua station, input acceleration scaled to 0.3 g. (d) Poconchile station, input acceleration scaled to 0.1g.

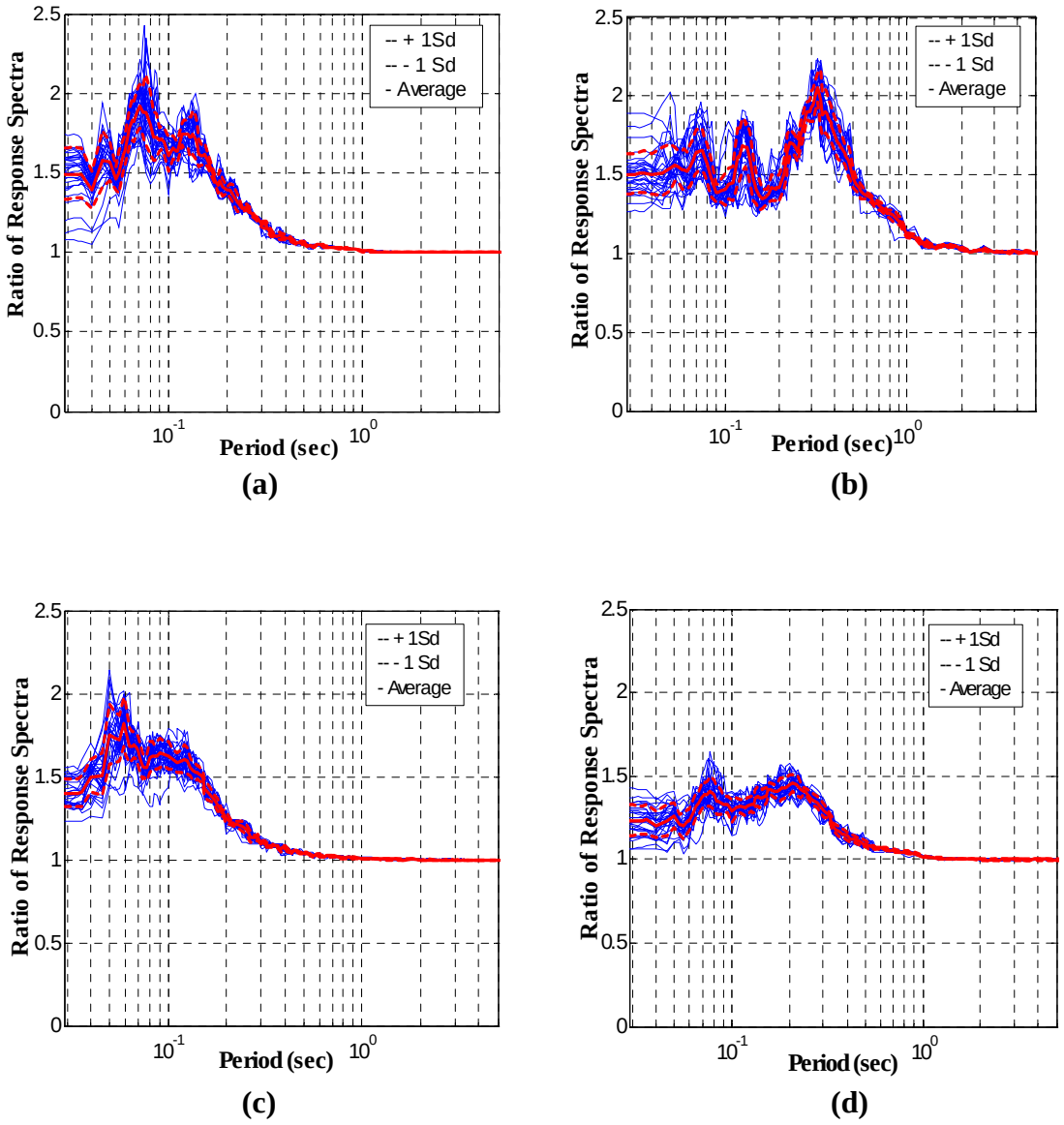

Figure 4.14 Ratio of response spectra obtained for the 150 runs using the scaled records provided by Dr. Silva as input motion, also including mean and +-1 standard deviation values. (a) Arica Casa station, input acceleration scaled to 0.1 g. (b) Arica Costanera station, input acceleration scaled to 0.1 g. (c) Moquegua station, input acceleration scaled to 0.3 g. (d) Poconchile station, input acceleration scaled to 0.1 g.

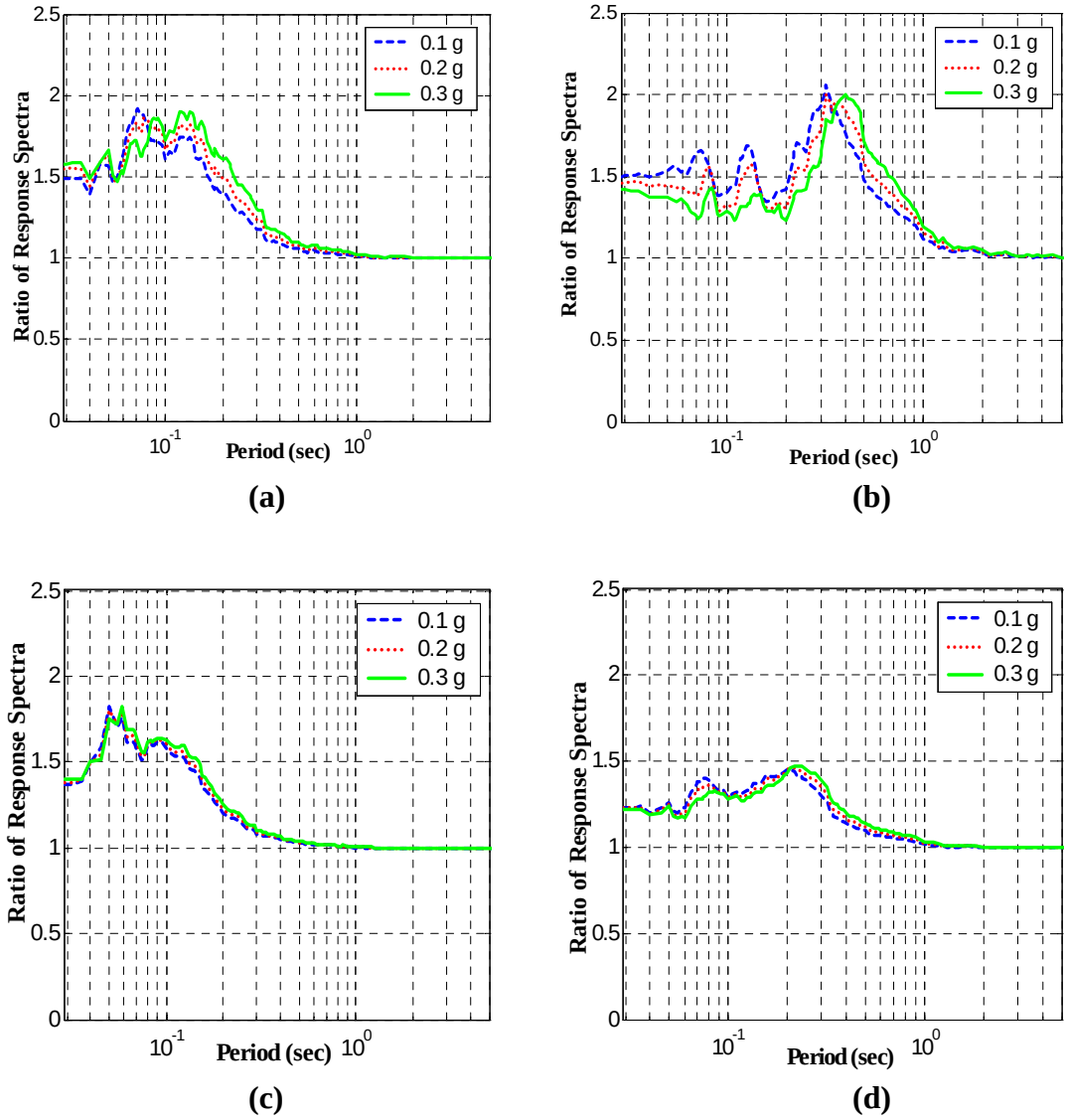

Figure 4.15 RRS (median value) for the 150 runs using the suite of motions generated from the finite fault simulation as input motion (scaled to different PGA levels). (a) Arica Casa. (b) Arica Costanera. (c) Moquegua. (d) Poconchile.

Seismic design of structures is rarely performed solely with simulated earthquake motions such as those generated with finite fault models. In general, actual recorded ground motions (selected to match source and site parameters at the design site) are used in design. To verify the trends that were observed using the finite fault input motions, the analysis of site response was repeated with the motions listed in Table 4.7. The resulting RRS values are shown in Figure 4.16, 4.17, 4.18, and 4.19. A comparison of the results

obtained from the collected ground motions and the ones created by the finite fault motions is presented for the most representative stations in Figure 4.20. Observe that both the frequency content, the amplitudes, and the trends with input motion intensity are the same as those observed for the finite fault motions.

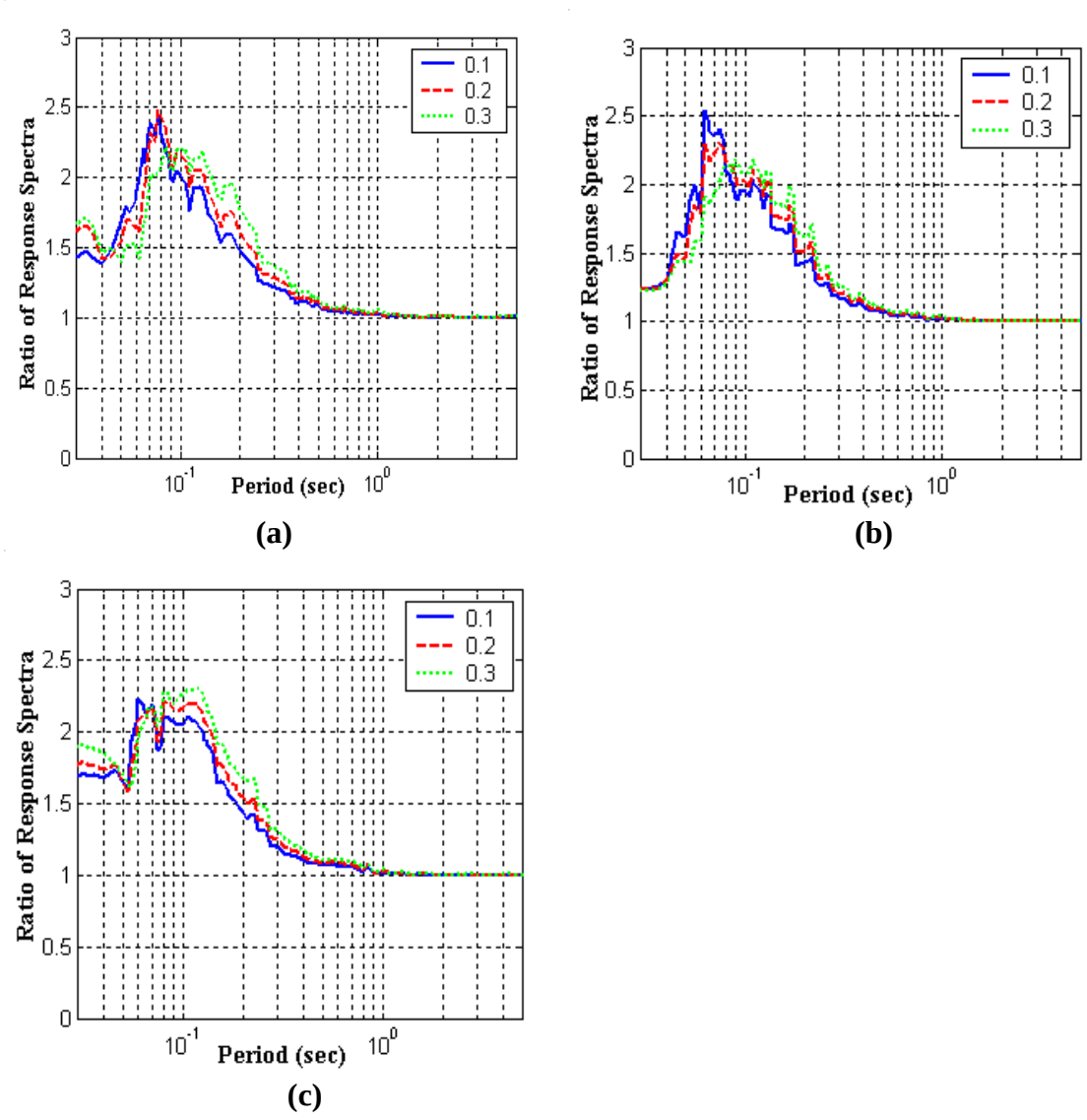

Figure 4.16 Ratio of response spectra obtained for different scaling values, Arica Casa station, using the 3 selected ground motions. (a) Chile; (b) Mexico 1; (c) Mexico 2.

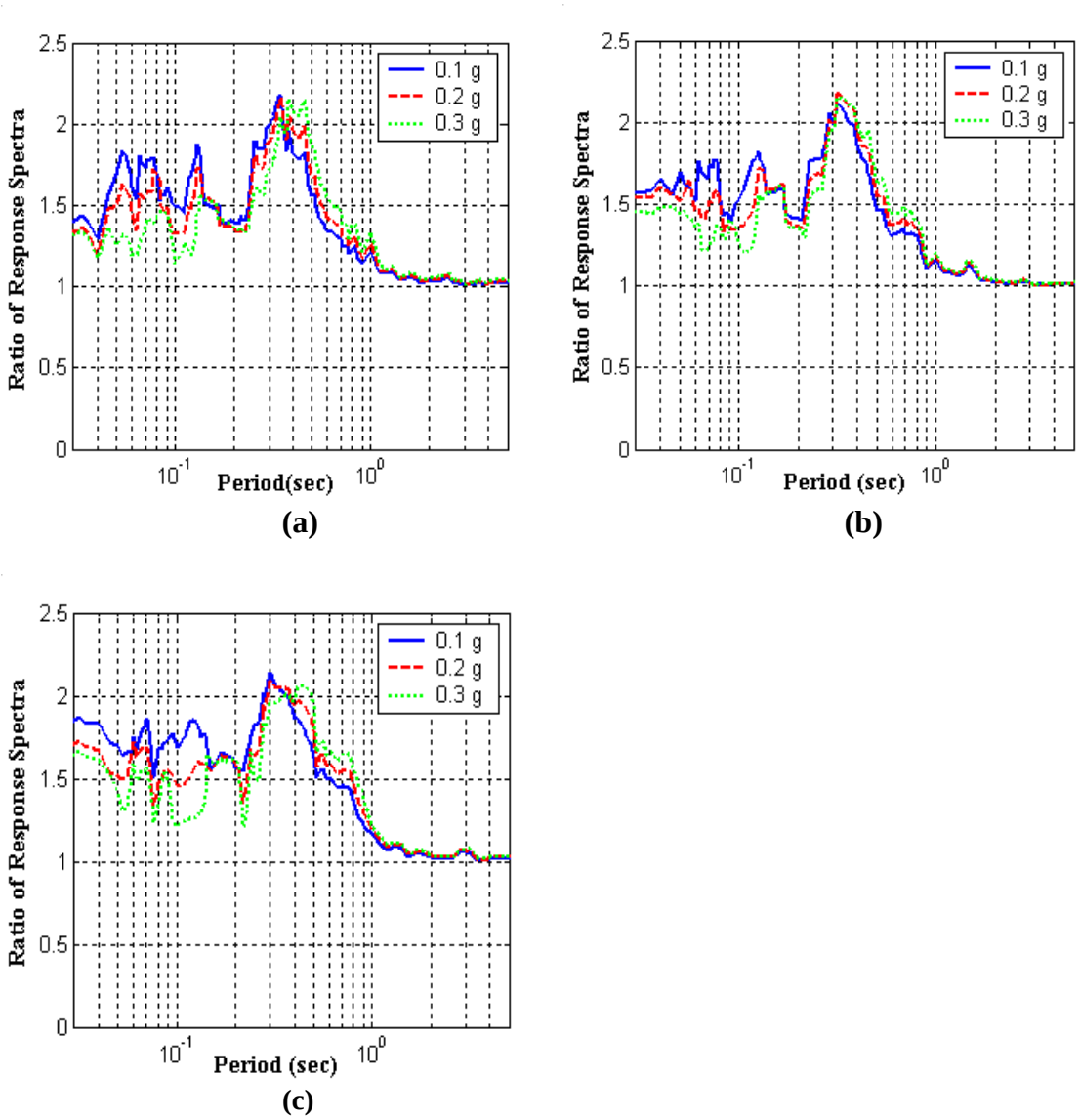

Figure 4.17 Ratio of response spectra obtained for different scaling values, Arica Costanera station, using the 3 selected ground motions. (a) Chile. (b) Mexico 1. (c) Mexico 2.

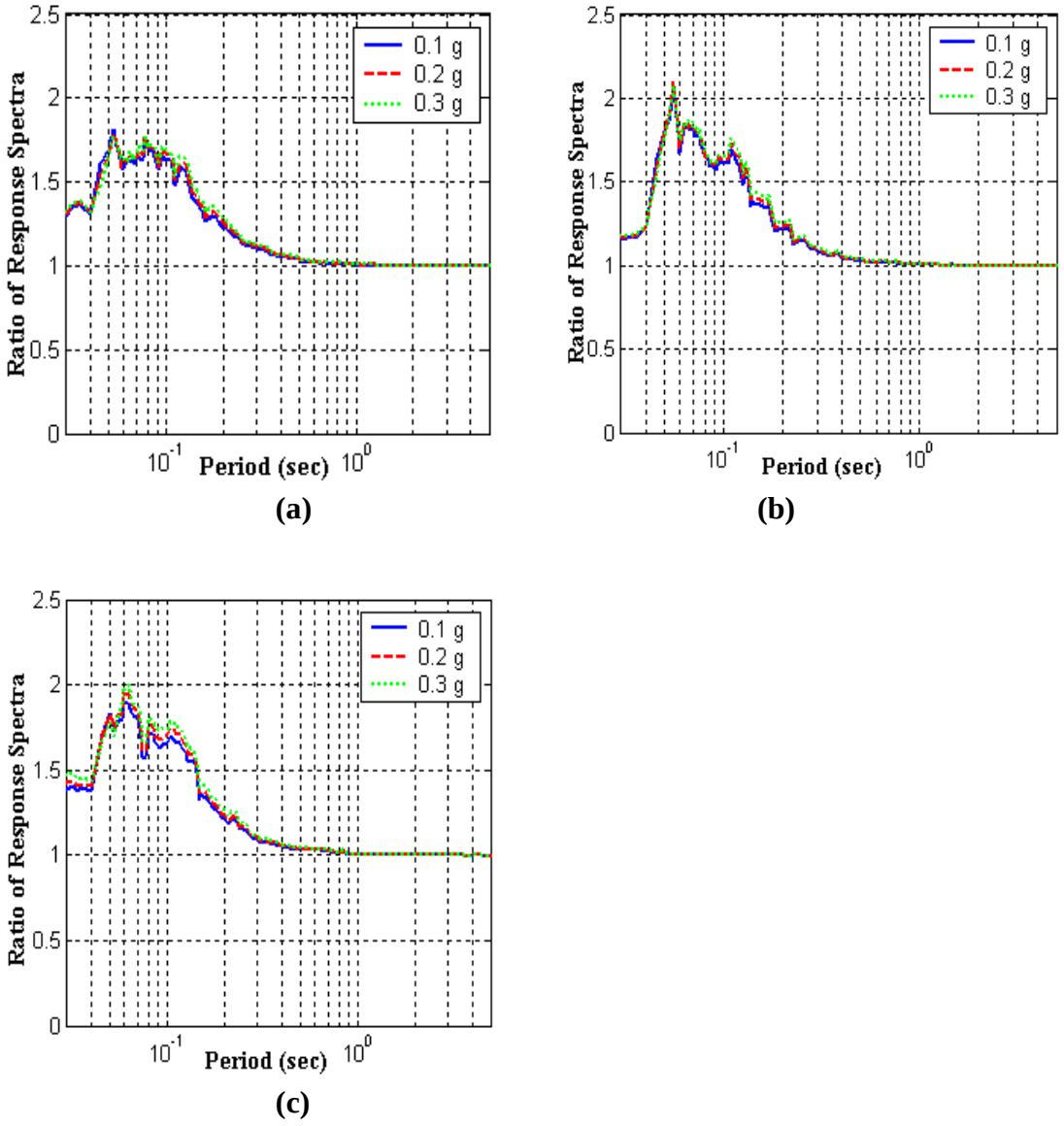

Figure 4.18 Ratio of response spectra obtained for different scaling values, Moquegua station, using the 3 selected ground motions. (a) Chile. (b) Mexico 1. (c) Mexico 2.

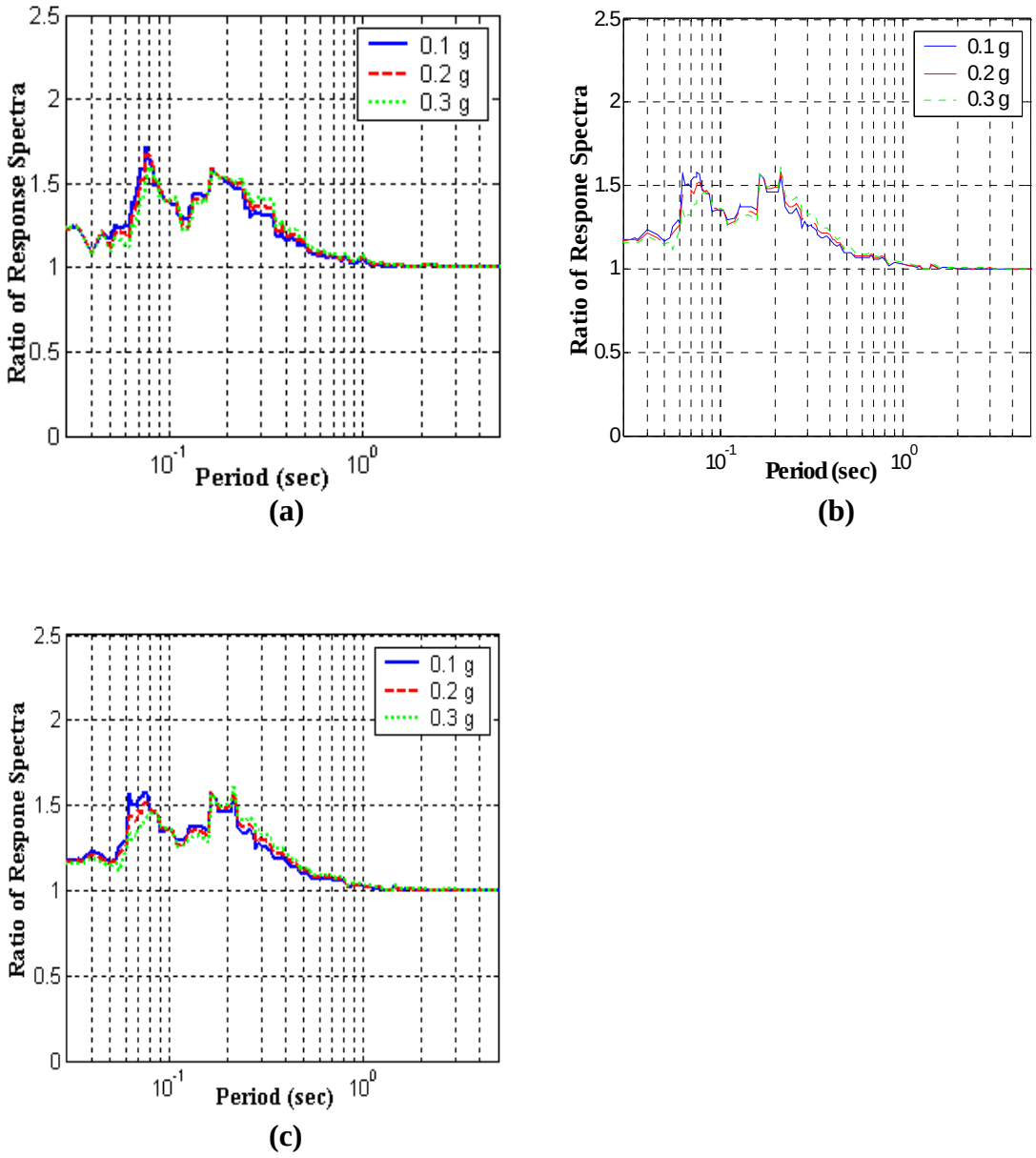

Figure 4.19 Ratio of response spectra obtained for different scaling values, Poconchile station, using the 3 selected ground motions. (a) Chile. (b) Mexico 1. (c) Mexico 2.

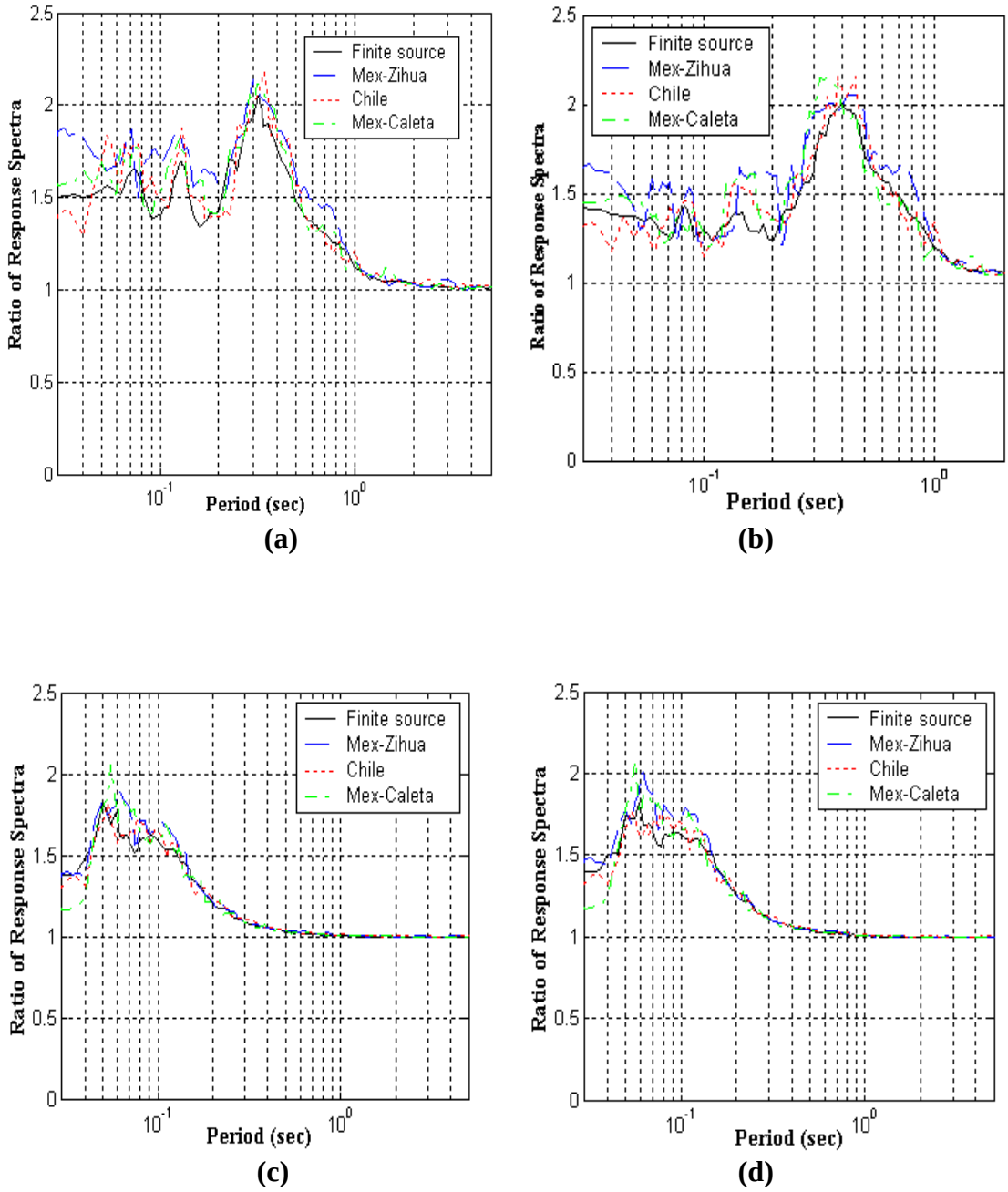

Figure 4.20 Ratio of response spectra comparison between the produced by the selected ground motions and the average produced by the ATH from Dr. Silva. (a) Arica Costanera station, input acceleration scaled to 0.1 g. (b) Arica Costanera station, acceleration scaled to 0.3 g. (c) Moquegua station, acceleration scaled to 0.1 g. (b) Moquegua station, acceleration scaled to 0.3 g.

Uncertainty in Soil Properties

The soil parameters that are randomized are listed in Table 4.8. For each parameter that is randomized, 150 runs were made. This number was selected based on the results of a randomization of shear wave velocity and depth to bedrock parameters for Moquegua station (Analysis 9 and 10 in Table 4.8). For this case, 1000 site response analyses were performed. The resulting median and one standard deviation for the PGA are shown in Figure 4.21a. Observe that after about 150 to 200 runs, the mean as well as the standard deviation was observed to stabilize (Figure4.21a and Figure 4.21b). Consequently, it was decided that 150 runs should capture the statistical distribution of the results. This number was also selected for studying the variation of other soil parameters.

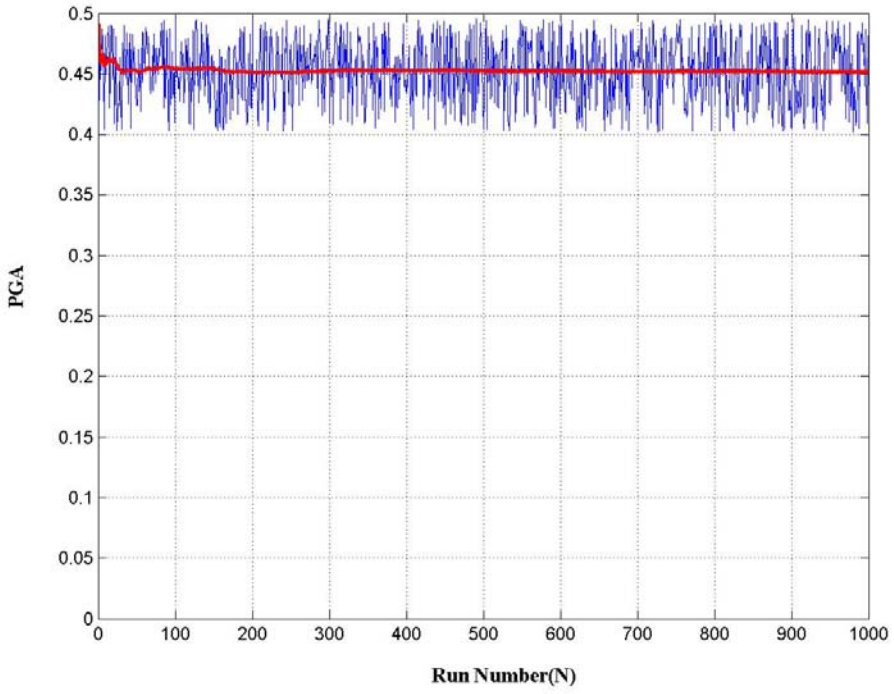

(a)

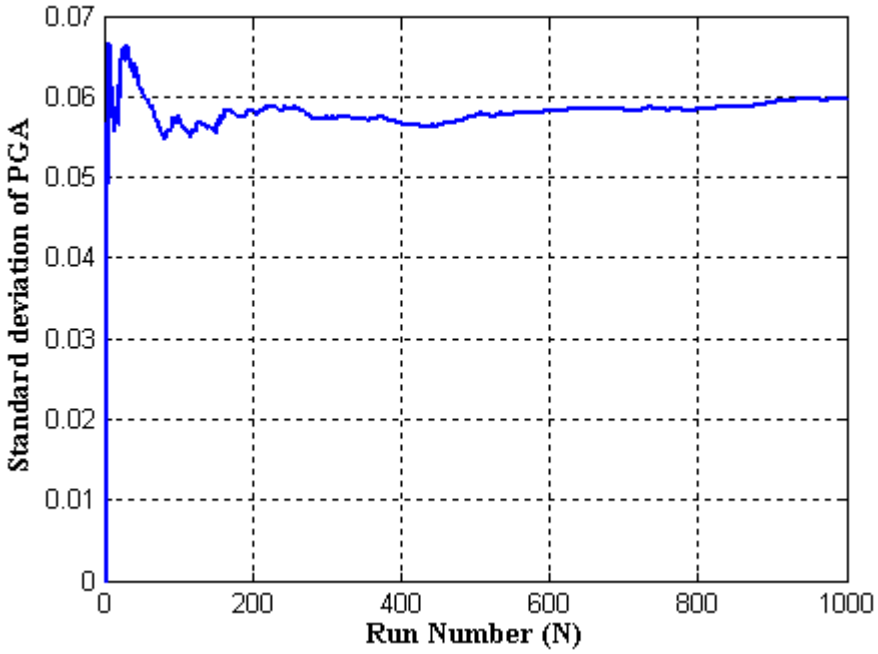

(b)

Figure 4.21 (a) Peak ground acceleration variation. Center line represents mean values. (b) Standard deviation variation.

Figures 4.22, 4.23, 4.24, and 4.25 present the resulting RRS for the Arica Costanera, Arica Casa, Moquegua, and Poconchile sites, respectively. The same patterns are observed in the response spectra at each of the four sites. The RRS values are only affected at periods lower than the characteristic site period. Soil non linearity and the depth to bedrock do not affect much the resulting RRS, while the V_s of bedrock has an influence on the magnitude of the RRS, but does not change its frequency content.

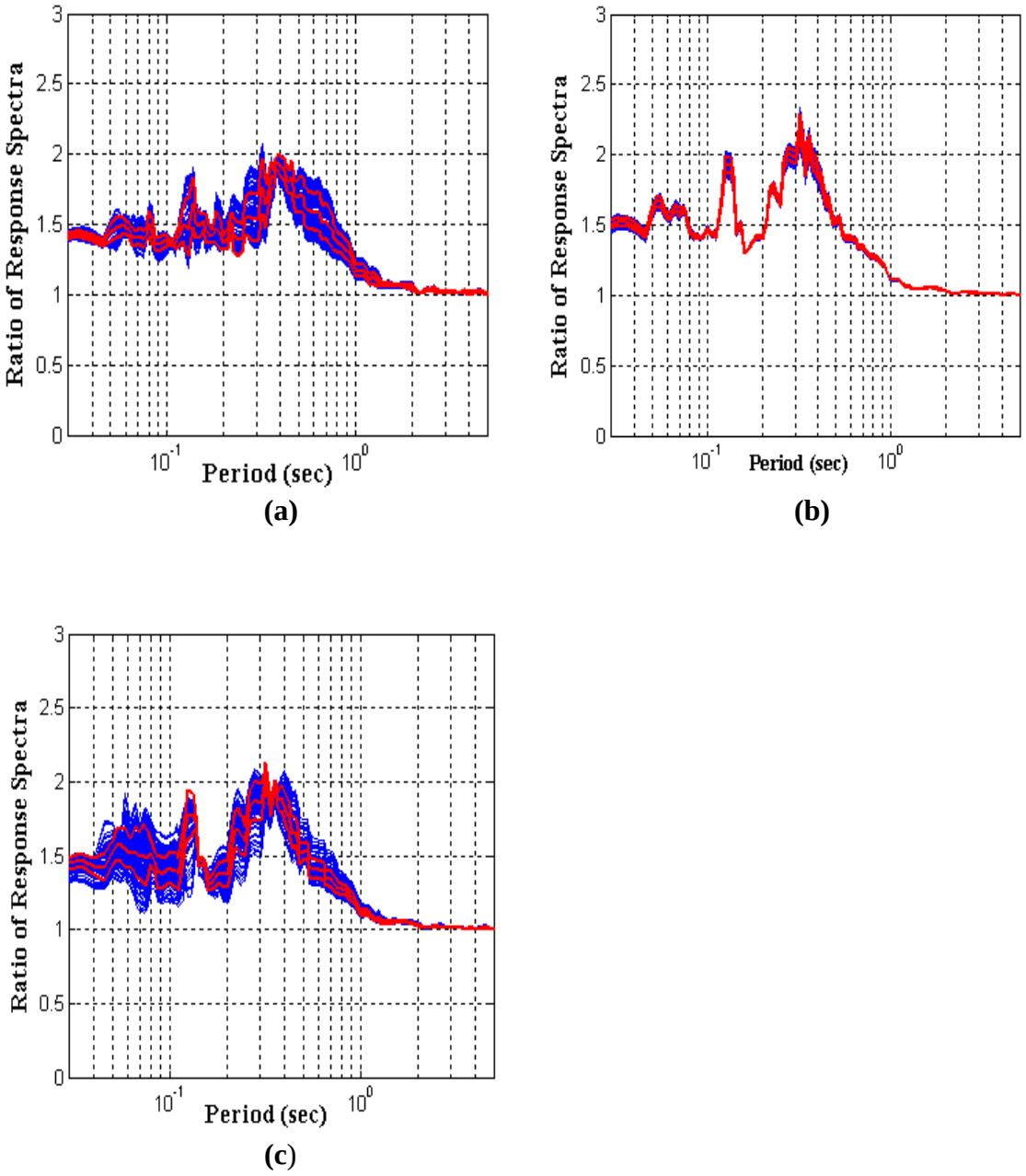

Figure 4.22 Ratio of Response spectra variation for Arica Costanera Station. Parameters used in each of the analyses are given in Table 4.8 for the case number listed below. (a) Randomization of depth to bedrock (Case 6), (b) randomization of V_s of rock (Case 7), and (c) randomization of nonlinear soil properties (Case 8). Average and +-1 standard deviation values included.

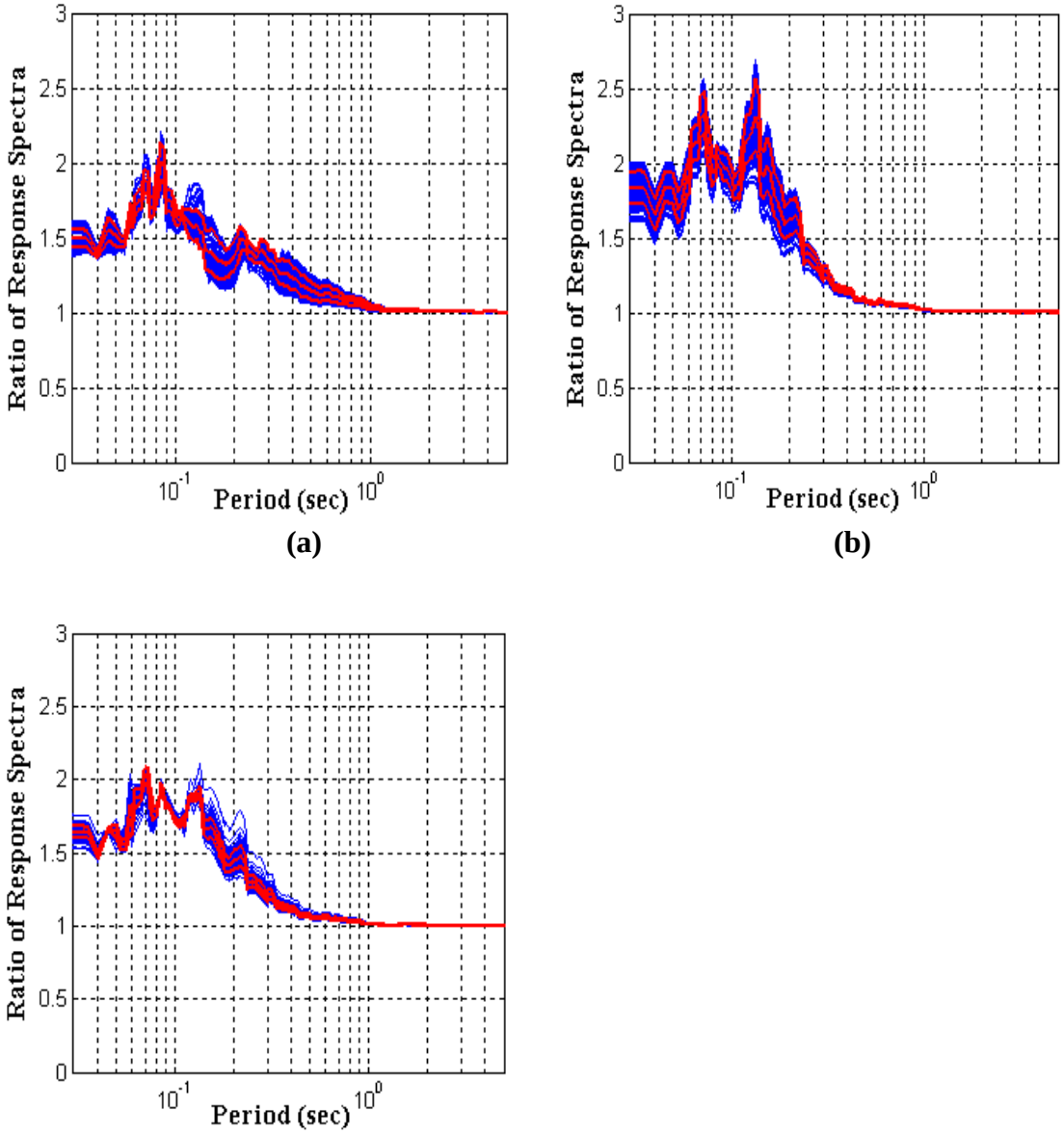

Figure 4.23 Ratio of Response spectra variation for Arica Casa Station. Parameters used in each of the analyses are given in Table 4.8 for the case number listed below. (a) Randomization of depth to bedrock (Case 3), (b) randomization of V_s of rock (Case 4), and (c) randomization of nonlinear soil properties (Case 5). Average and +-1 standard deviation values included.

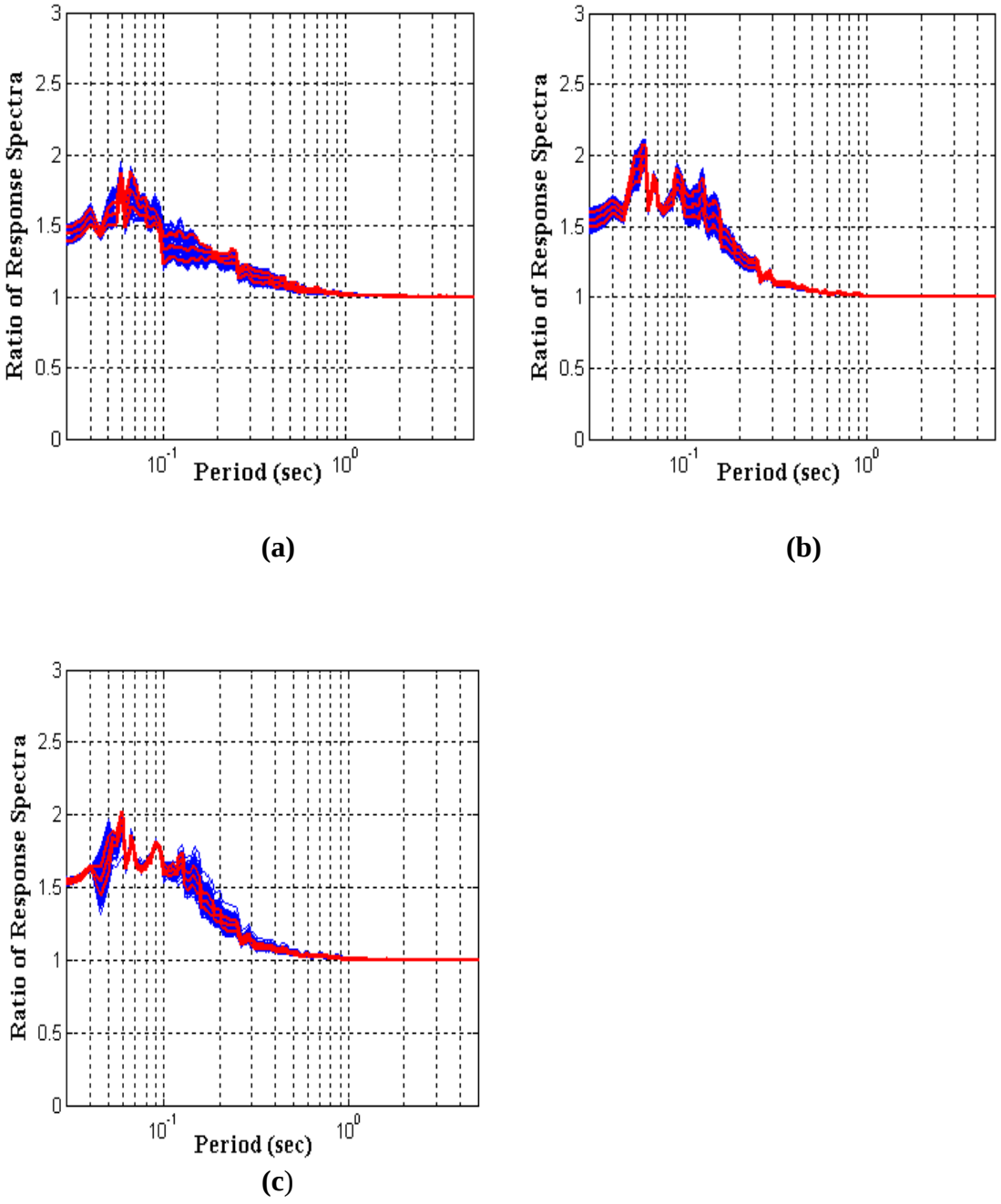

Figure 4.24 Ratio of Response spectra variation for Moquegua Station. Parameters used in each of the analyses are given in Table 4.8 for the case number listed below. (a) Randomization of depth to bedrock (Case 9), (b) randomization of V_s of rock (Case 10), and (c) randomization of nonlinear soil properties (Case 11). Average and +-1 standard deviation values included.

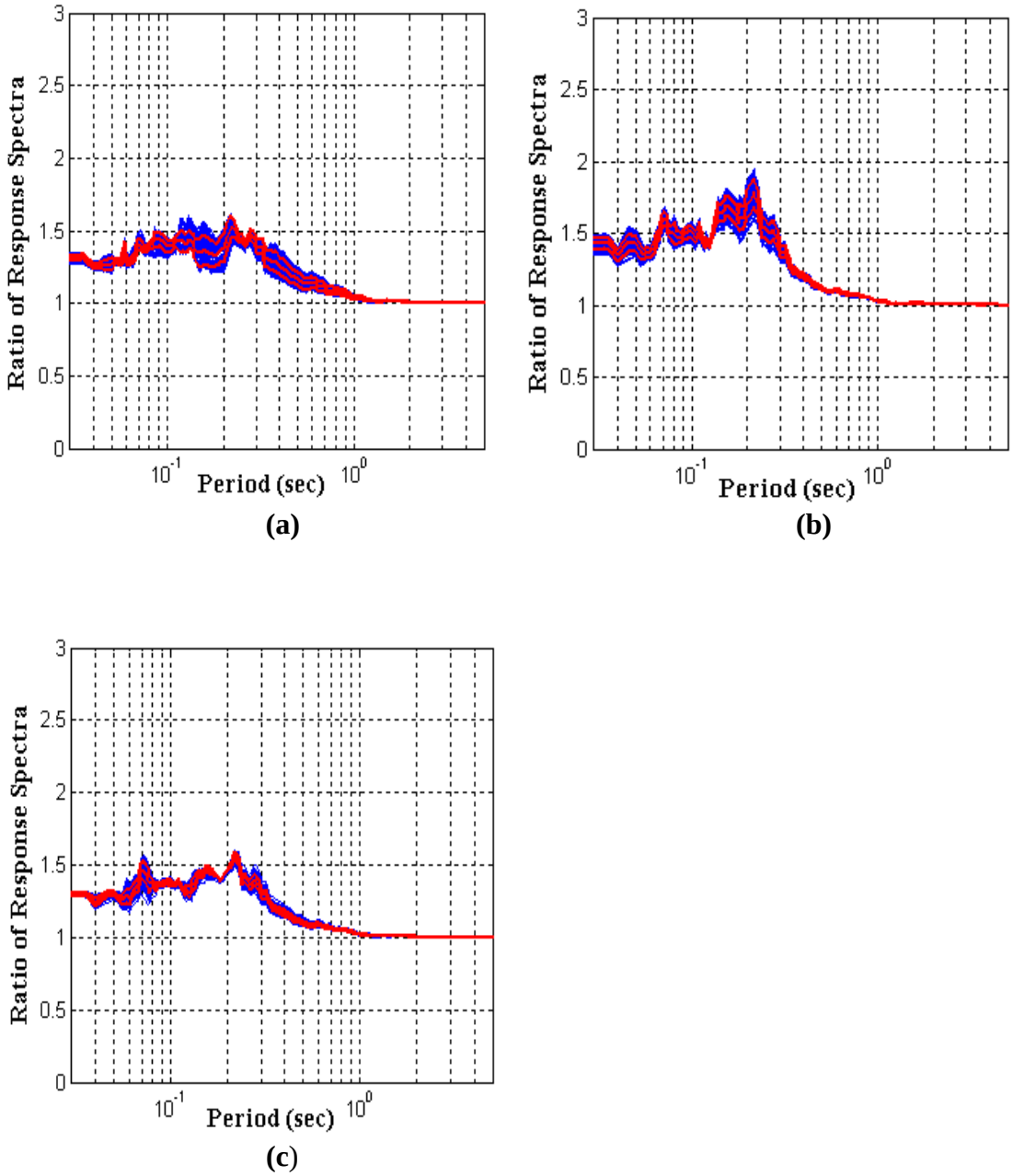

Figure 4.25 Ratio of Response spectra variation for Poconchile Station. Parameters used in each of the analyses are given in Table 4.8 for the case number listed below. (a) Randomization of depth to bedrock (Case 12), (b) randomization of V_s of rock (Case 13), and (c) randomization of nonlinear soil properties (Case 14).

The median values of RRS for each of the analyses are shown in Figure 4.26. This figure permits a comparison of the relative bias introduced by incorporating the randomization of the parameters listed in Table 4.8. The bias is introduced because the randomization is not centered on the deterministic V_s profiles shown in Figure 4.4 (see section 4.4.1). The most significant bias introduced in the analysis results from the randomization of depth to bedrock. The additional depth to bedrock implies lower amplifications at low periods and higher amplifications at long periods. The randomization of the V_s of rock introduces a positive bias at all periods (e.g., higher values of RRS) for all sites but Arica Costanera. Randomization of nonlinear soil properties also introduces a bias towards lower values of RRS.

Analysis of variability in RRS

The standard deviation values of the RRS are plotted in Figure 4.27 for all spectral periods and for all the randomizations described in Table 4.8. Note that the largest standard deviations are due to the uncertainty in input motion. At short periods, the uncertainty due to the variability of bedrock shear wave velocity also has significance, while considerable values of standard deviation are produced for higher periods by the variability of the depth to bedrock. .

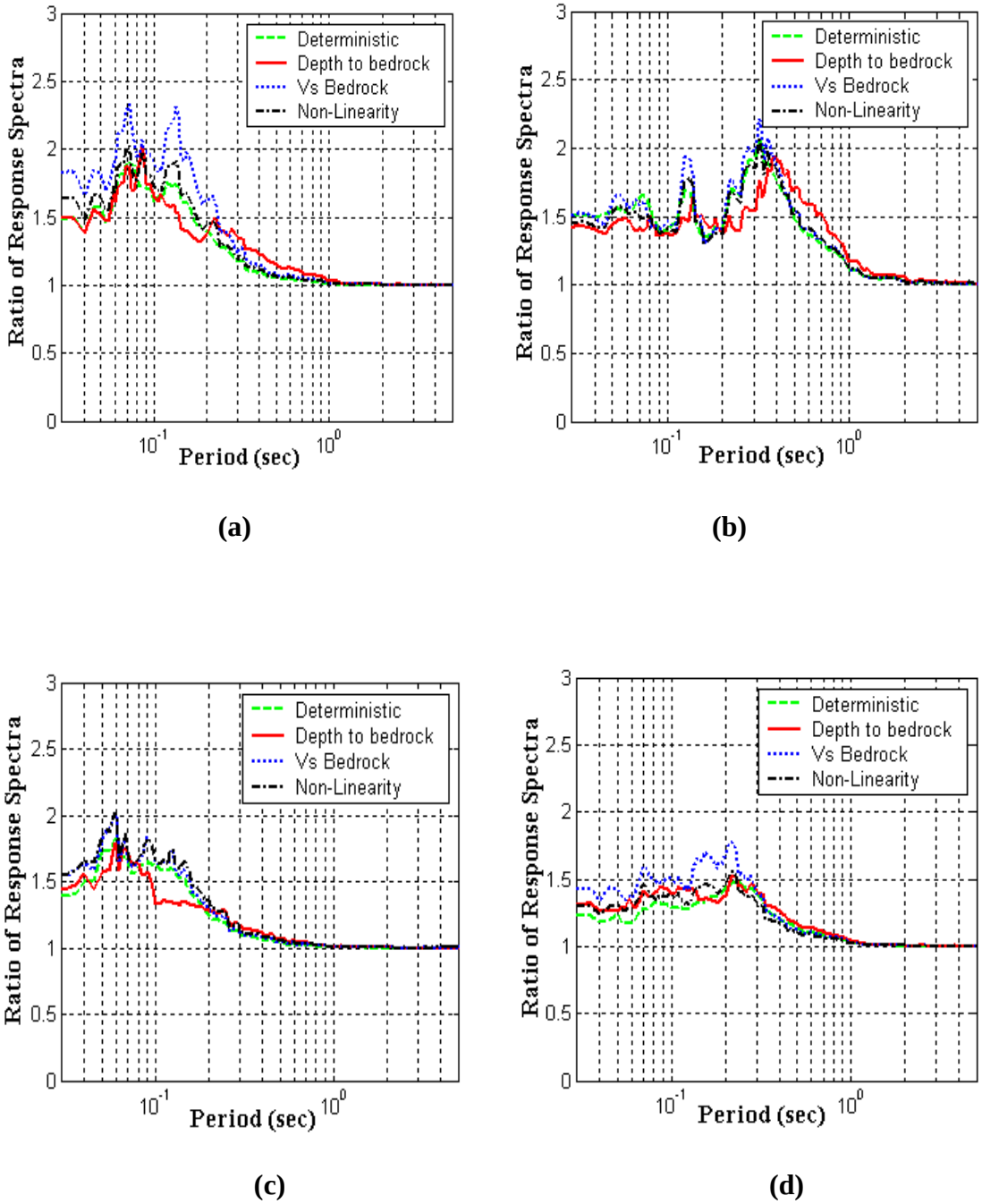

Figure 4.26 Comparison between the average value (of the 150 runs) of the Ratio of Response Spectra for all the different variations proposed. (a) Arica Casa station. (b) Arica Costanera station. (c) Moquegua station. (d) Poconchile station.

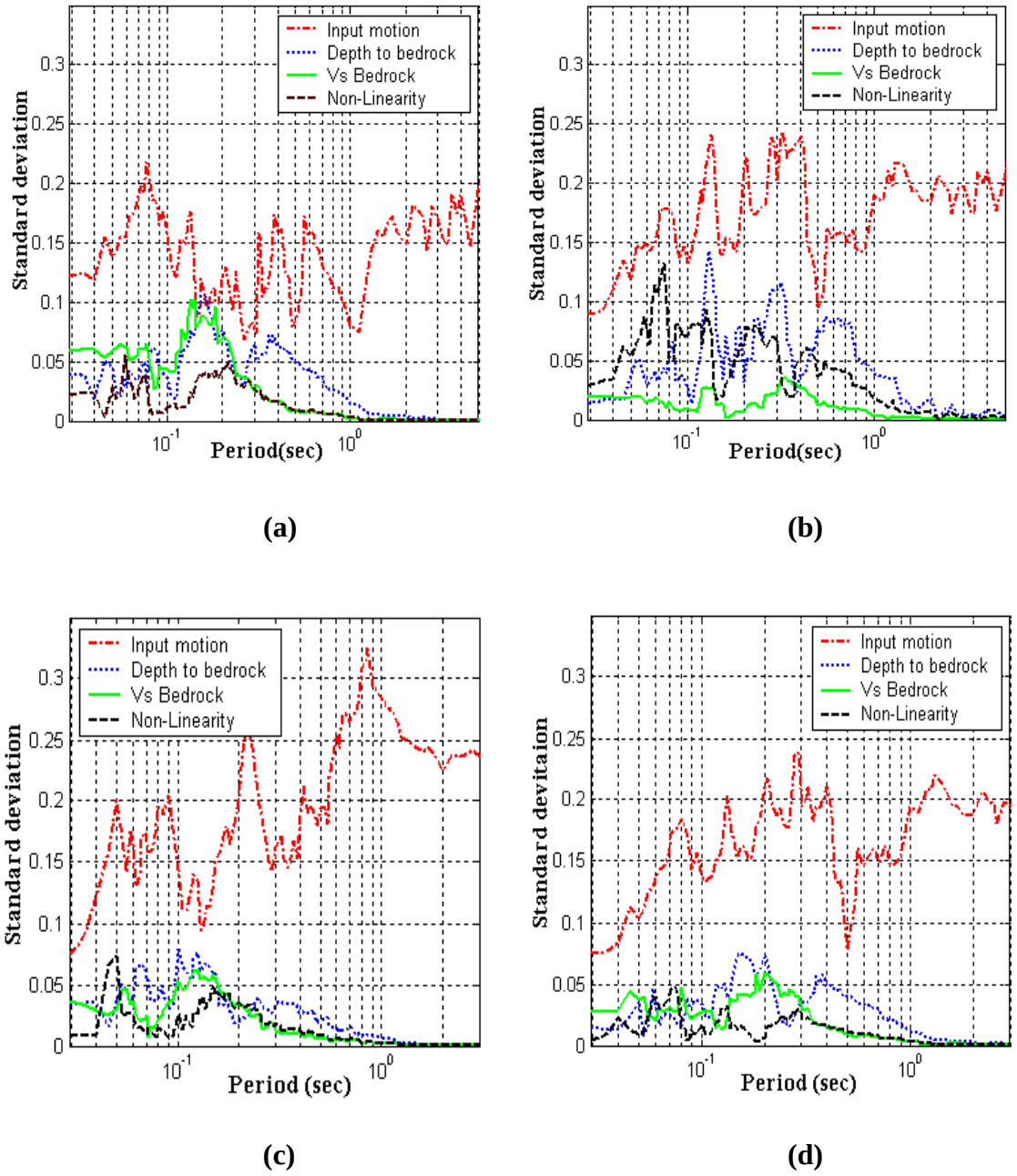

Figure 4.27 Comparison of the discrepancy of the standard deviation (STD) for all periods for all the variations previously described. (a) Standard deviation for Arica Casa station. (b) Standard deviation for Arica Costanera station. (c) Standard deviation for Moquegua station. (d) Standard deviation for Poconchile station.

Additional Observations and Summary of Results

The most relevant conclusions from the site response analyses are summarized as follows:

- In most cases intensity of input motion did not have considerable influence in the resulting response spectra and on site response (i.e., on the RRS values). This implies that soil non-linearity is not a controlling parameter in site response estimates.
- Only structure periods lower than the site period are affected by site response.
- Variation in the shear wave velocity of rock influence the magnitude of RRS. In general, RRS values are larger if V_s is allowed to vary from the values estimated from SASW to a value of 1000 m/s.
- The uncertainty (e.g. standard deviation values) of the site response analyses is relatively small when compared to the uncertainties in input motion parameters.
- The uncertainty in the shear wave velocity of the bedrock and the depth to bedrock may introduce a bias in the estimates of site response.

It is important to note that the site response analyses presented herein have some important limitations. The input motions may have energy at long periods that comes either from surface waves or from site effects due to deeper soil (or rock) layers at each recording station. This should not have a large effect on the results because the analyses are focused on the effect of the surficial layers. Even if the input motion has extra energy at long periods, the RRS at short periods should not be affected much by this energy (as this long periods won't contribute much to strain). However, the presence of impedance contrast at a depth beyond that captured by the SASW analyses may introduce resonances that are not captured by the site response analyses. Thus, the analysis only captures

amplification up to certain periods (usually the site period). Amplification at longer periods is beyond the capability of the analysis. The recorded motions show a secondary peak in response spectra at a period about 1 second (Figure 4.6). This may reflect the influence of a deep impedance contrast, or possibly source effects. Amplification in this period range are not captured by the preceding analysis.

4.5 Implication for seismic hazard analysis

Design ground motions must be compatible (among other things) with the soil conditions at the design site. When ground motion time histories are required for design, ground motions are obtained either from recordings at similar site conditions or by performing site response analyses using bedrock motions as input motions. When design spectra are used, site conditions are incorporated by means of site factors that are applied to rock design spectra. In either case, bedrock motions provide a baseline estimate that can be modified to account for site-specific effects.

The Southern Peru earthquake did not produce any ground motion recordings on rock (the only instrument located on rock did not work during the earthquake). This precludes any empirical estimates of soil amplification factors. However, an estimate of spectral accelerations at bedrock motions can be made from the analytical estimates of site response (i.e. RRS) and the recorded motion.

The preceding site response analyses can be used to obtain values of RRS for each site and for various spectral periods. The inclusion of uncertainty in the analysis is used to obtain a confidence band on the RRS values. These values are obtained as follows:

a) Median RRS values were obtained from the average of the results obtained from the different randomizations in the Montecarlo simulation (Table 4.8).

b) A value of standard deviation for the RRS was selected as the maximum standard deviation produced by each of the randomizations in the Montecarlo simulation for each of the input parameters.

c) The estimate of spectral acceleration for an equivalent bedrock with Vs = 800 m/s was obtained by dividing the recorded spectral acceleration value by the 85 percentile range of RRS values (RRS plus one standard deviation and RRS minus one standard deviation).

The resulting RRS are given in Table 4.10

Table 4.10 Range of uncertainty

Station	Period Band (sec)	RRS[1] Average	Standard deviation[2] (Std)	RRS + 1Std	RRS - 1Std
Arica Casa	0.75	2.211	0.278	2.919	1.675
	0.05 - 0.1125	2.078	0.303	2.812	1.535
	0.1	2.000	0.304	2.710	1.477
	0.075 - 0.1333	2.101	0.294	2.821	1.565
	0.3	1.436	0.337	2.011	1.025
	0.15 - 0.6	1.476	0.328	2.048	1.064
	1	1.184	0.336	1.657	0.846
	0.6 - 1.667	1.193	0.335	1.669	0.854
	2	1.169	0.335	1.634	0.836
	1.5 - 2.6667	1.169	0.335	1.634	0.836
	0.1 - 0.5	1.639	0.319	2.254	1.191
	0.4 -2	1.213	0.335	1.696	0.867
Arica Costanera	0.75	1.694	0.330	2.357	1.217
	0.05 - 0.1125	1.649	0.331	2.296	1.185
	0.1	1.576	0.349	2.233	1.112
	0.075 - 0.1333	1.652	0.324	2.284	1.195
	0.3	2.018	0.330	2.808	1.450
	0.15 - 0.6	1.801	0.345	2.543	1.276
	1	1.252	0.345	1.768	0.886
	0.6 - 1.667	1.299	0.349	1.841	0.916
	2	1.149	0.348	1.628	0.811
	1.5 - 2.6667	1.147	0.352	1.630	0.806
	0.1 - 0.5	1.802	0.336	2.522	1.287
	0.4 -2	1.400	0.349	1.986	0.987

Table 4.10 Range of uncertainty (Continued)

Station	Period Band (sec)	RRS[1] Average	Standard deviation[2] (Std)	RRS + 1Std	RRS - 1Std
Moquegua	0.75	1.736	0.234	2.194	1.373
	0.05 - 0.1125	1.811	0.233	2.285	1.435
	0.1	1.686	0.240	2.143	1.326
	0.075 - 0.1333	1.732	0.236	2.193	1.368
	0.3	1.218	0.249	1.563	0.949
	0.15 - 0.6	1.261	0.246	1.613	0.986
	1	1.092	0.247	1.397	0.853
	0.6 - 1.667	1.097	0.247	1.405	0.857
	2	1.085	0.247	1.390	0.847
	1.5 - 2.6667	1.086	0.248	1.391	0.848
	0.1 - 0.5	1.372	0.244	1.751	1.075
	0.4 -2	1.109	0.247	1.420	0.866
Poconchile	0.75	1.580	0.324	2.186	1.143
	0.05 - 0.1125	1.525	0.336	2.135	1.089
	0.1	1.542	0.351	2.191	1.085
	0.075 - 0.1333	1.551	0.338	2.176	1.106
	0.3	1.501	0.336	2.101	1.072
	0.15 - 0.6	1.452	0.345	2.051	1.028
	1	1.139	0.353	1.621	0.800
	0.6 - 1.667	1.149	0.353	1.635	0.807
	2	1.116	0.354	1.589	0.783
	1.5 - 2.6667	1.116	0.354	1.590	0.783
	0.1 - 0.5	1.514	0.344	2.136	1.073
	0.4 -2	1.174	0.353	1.670	0.825

[1]Average ratio of response spectra from all the randomizations.
[2]Maximum standard deviation from all the randomizations.

The estimates of spectral accelerations on bedrock are shown in Figures 4.28 and 4.29, along with the attenuation relationships of Young's et al. (1997) and Boore and Atkinson (2003), shown here for comparison. The prediction of both attenuation relationships was plotted for periods of 0.1,0.3,1.0 and 2 seconds. It can be seen that the inclusion of the estimated RRS values renders ground motion estimates that are more in line with empirical predictions. This suggests that local site conditions did play a role in amplifying short period motions.

The comparison of the amplification factors obtained for each of the sites with the amplification factors suggested by the UBC is presented in Table 4.11 The values suggested by Rodriguez-Marek et al. (2001) are included.

Table 4.11 Comparison of amplification factors. Values in parenthesis show computed range of RRS values.

	Arica Casa (PGA = 0.1 g)			Arica Costanera (PGA = 0.1 g)		
	UBC*	**B&R-M***	**This work***	**UBC***	**B&R-M***	**This work***
F_a**	1.2	1.5	1.64 (1.19- 2.25)	1.2	1.5	1.80 (1.29 – 2.52)
F_v***	1.7	1.4	1.21 (0.87 – 1.70)	1.7	1.4	1.40 (0.99 – 1.99)

	Moquegua (PGA = 0.3 g)			Poconchile (PGA = 0.1 g)		
	UBC*	**B&R-M***	**This work***	**UBC***	**B&R-M***	**This work***
F_a**	1.2	1.5	1.37 (1.07 - 1.75)	1.2	1.5	1.51 (1.07 – 2.14)
F_v***	1.7	1.4	1.11 (0.87 – 1.42)	1.7	1.4	1.17 (0.82 – 1.67)

* The values represent site condition Type C for the categories proposed in the UBC.
** Amplification factors for the short period range.
*** Amplification factors for the long period range.

It is noteworthy that the amplification factors obtained in the present study are in most cases closer to the values proposed by Rodriguez-Marek et al. (2001). On the other hand, while the amplification factors for the long period range proposed by the UBC are higher than the factors obtained in this study, the amplification factors for the short period range proposed by the UBC are considerably lower than the values obtained in this study.

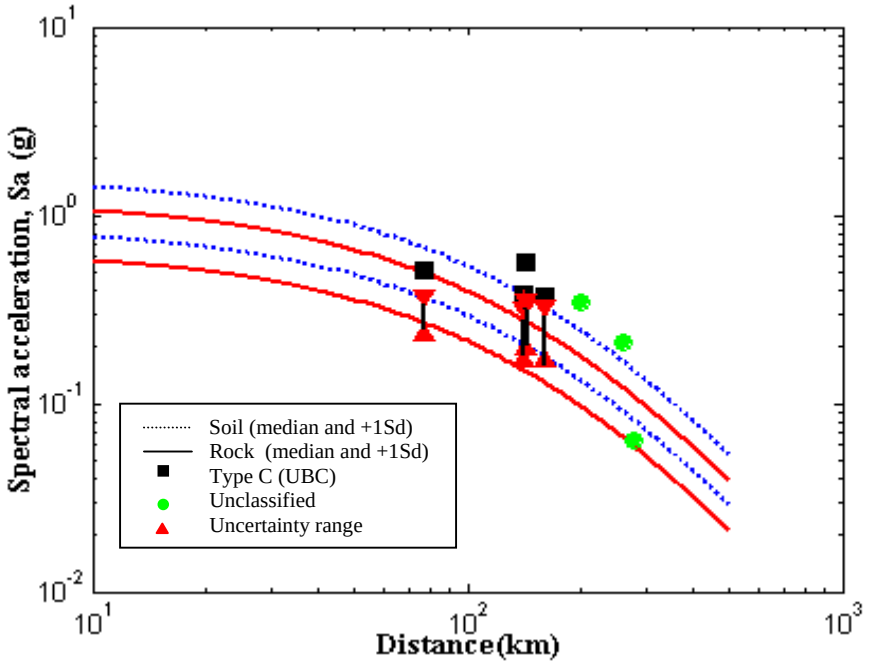
Spectral acceleration, Sa (g)
Distance(km)
Soil (median and +1Sd)
Rock (median and +1Sd)
Type C (UBC)
Unclassified
Uncertainty range

(a)

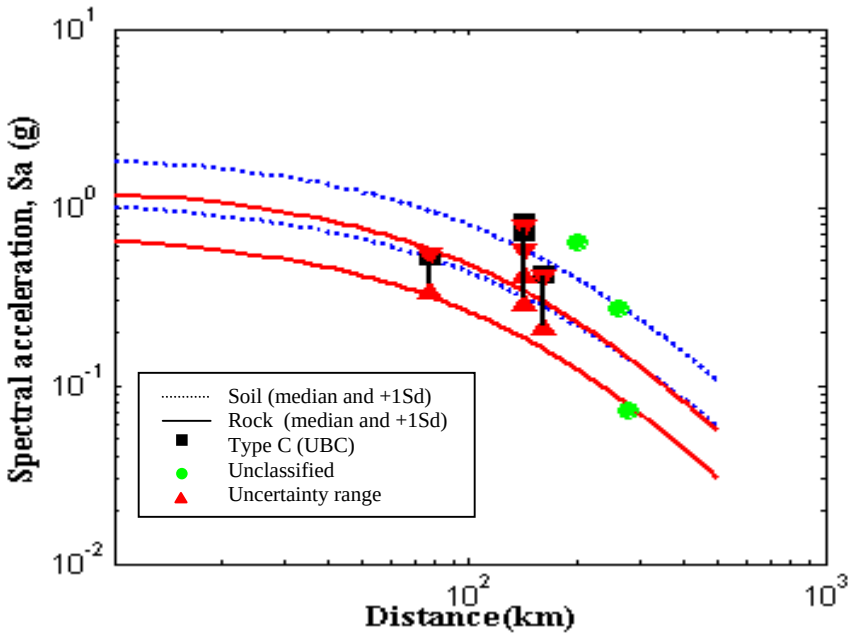
Spectral acceleration, Sa (g)
Distance(km)
Soil (median and +1Sd)
Rock (median and +1Sd)
Type C (UBC)
Unclassified
Uncertainty range

(b)

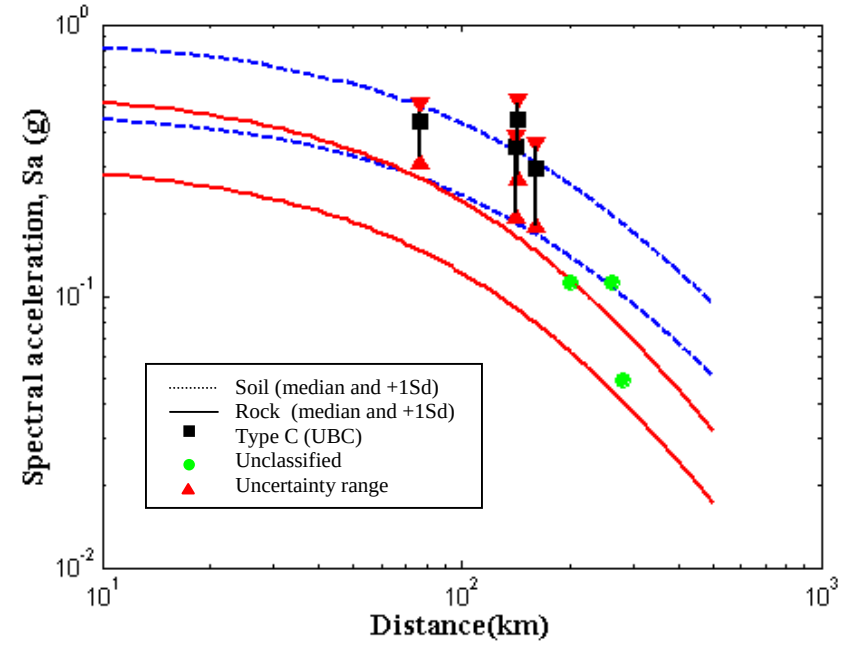

(c)

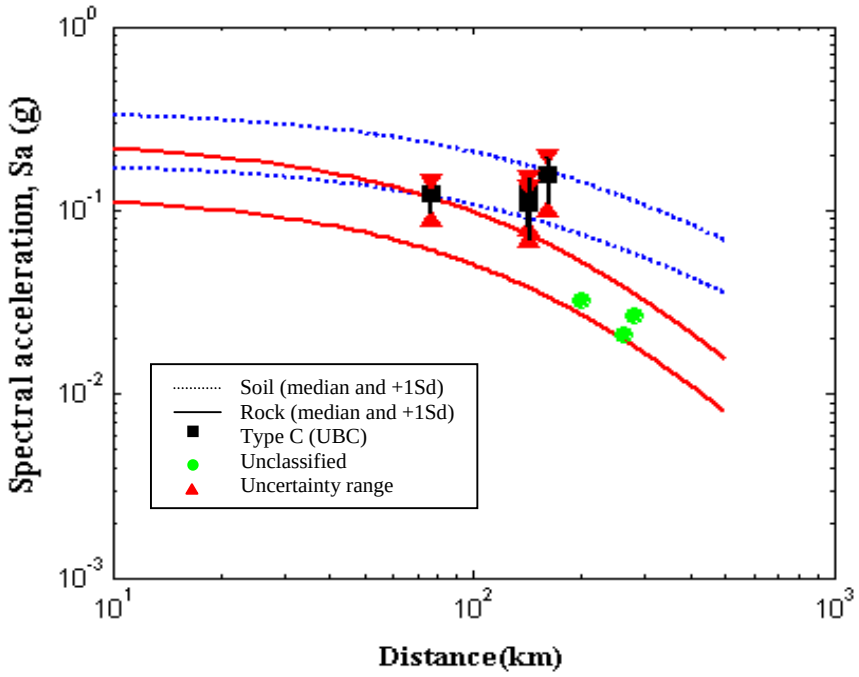

(d)

Figure 4.28 Comparison between the values of acceleration recorded for all the stations and Young's et al. attenuation relationship for certain periods. Also one standard deviation ranges are included. (a) T = 0.1 seconds. (b) T = 0.3 seconds. (c) T = 1 seconds. (d) T = 2 seconds.

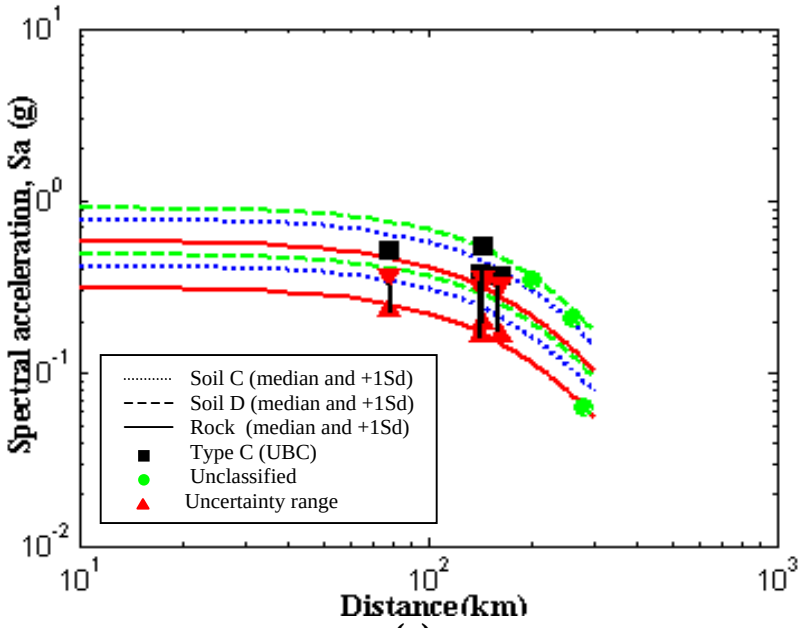
Spectral acceleration, Sa (g)
Distance(km)
Soil C (median and +1Sd)
Soil D (median and +1Sd)
Rock (median and +1Sd)
Type C (UBC)
Unclassified
Uncertainty range

(a)

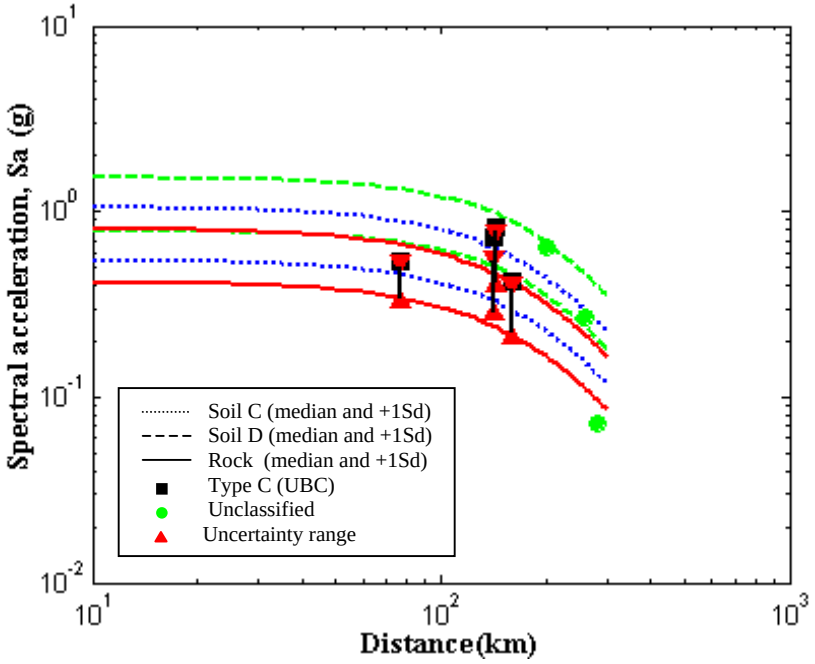
Spectral acceleration, Sa (g)
Distance(km)
Soil C (median and +1Sd)
Soil D (median and +1Sd)
Rock (median and +1Sd)
Type C (UBC)
Unclassified
Uncertainty range

(b)

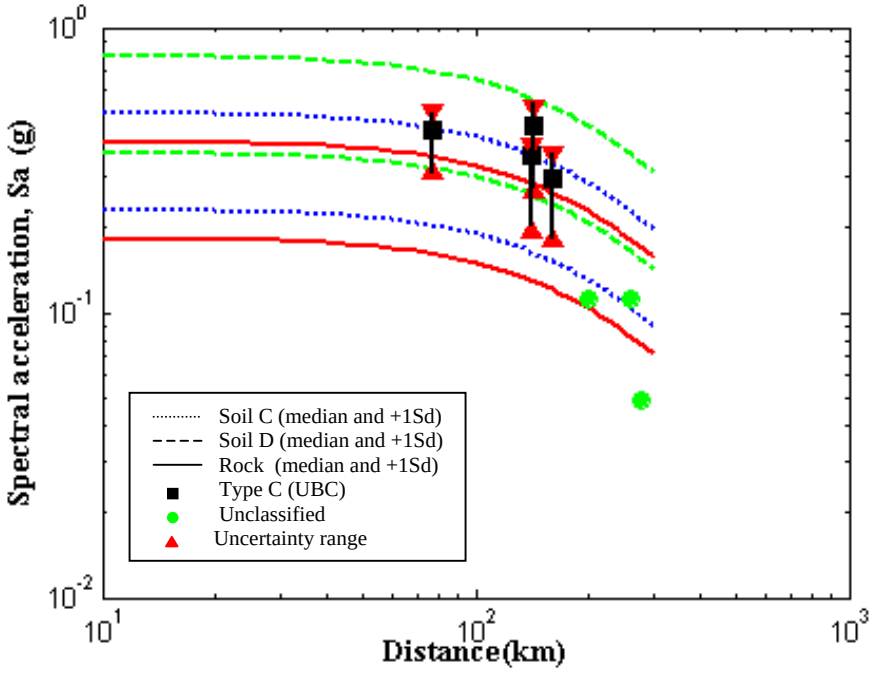

(c)

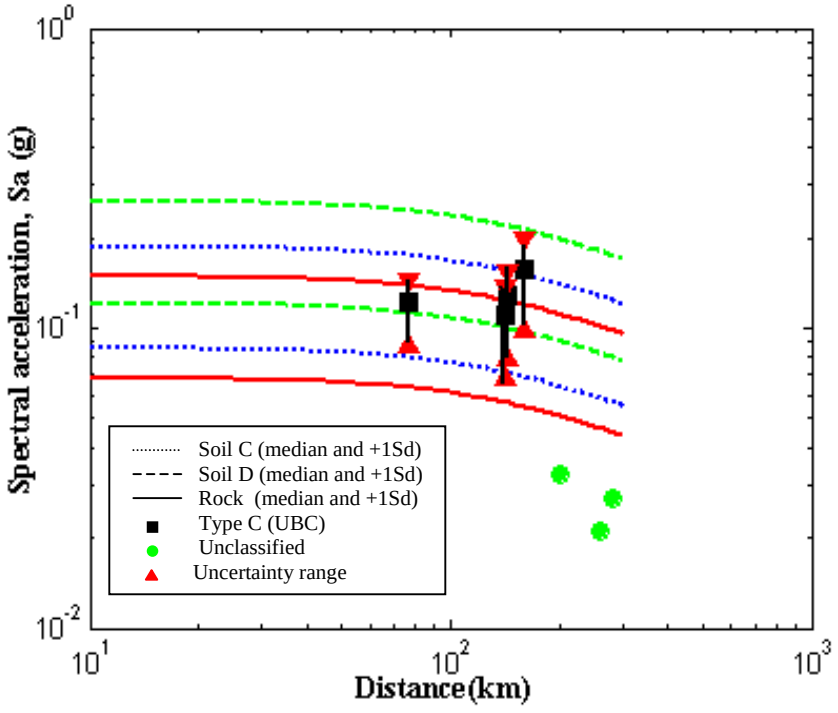

(d)

Figure 4.29 Comparison between the values of acceleration recorded for all the stations and Atkinson and Boore (2003) attenuation relationship for certain periods. Also one standard deviation ranges are included. (a) T = 0.1 seconds. (b) T = 0.3 seconds. (c) T = 1 seconds. (d) T = 2 seconds.

CHAPTER 5

SITE RESPONSE AND DAMAGE DISTRIBUTION IN TACNA AND MOQUEGUA CITIES

5.1 Introduction

The correlation of damage with local site conditions in past earthquakes has led to important conclusions regarding the behavior of soils under seismic conditions. Just to mention a few examples, the 1985 Michoacan, Mexico, earthquake was a stark example of the structural damage that can result when the natural site periods coincide with the structural periods (Kramer 1996); the 1989 Loma Prieta earthquake was a field demonstration on the large amplification that can occur on soft soils; and the 1994 Northridge earthquake proved that site amplification can occur in stiff soils as well as in soft soils. These conclusions came to light during the process of correlating areas with high concentration of building damage to local site conditions.

The typical soil profiles in the region affected by the southern Peru earthquake consist of stiff to very stiff alluvial deposits. These soils would not traditionally be associated with high damage potential in seismic conditions. However, preliminary observations (Rodriguez-Marek et al. 2003) suggested a correlation of damage with site effects. The present chapter elaborates on the original observations by Rodriguez-Marek et al. (2003) regarding potential site and topographic effects in the cities of Moquegua and Tacna, which were most affected by the 2001 Southern Peru earthquake. Additional information on earthquake damage is presented. Observed damage is correlated with estimates of site response obtained from equivalent linear analyses.

5.2 Damage distribution in the city of Moquegua

The information on damage distribution in the city of Moquegua was evaluated by a number of research teams. Rodriguez-Marek et al. (2003) present the observations of an NSF sponsored United States – Peruvian team that performed a comprehensive post-earthquake reconnaissance shortly after the 2001 event. Kosaka-Masuno et al. (2001) evaluated damage distribution in Moquegua city as part of a joint survey made by the Peruvian institutions of “San Agustin de Arequipa University (UNSA)” and the “National Institute of Disaster Prevention (INDECI)" one month after the event. The Peruvian Institute of Geophysics (IGP) developed a very comprehensive report of the 2003 Southern Peru earthquake (IGP 2001). Within this report, Fernandez et al. (2001) present a detailed evaluation of structural damages in Moquegua. This evaluation was made with the goal of defining intensity levels for the earthquake (e.g. Mercalli Intensity). An additional reconnaissance report was prepared by a team from the Japanese Society of Civil Engineers, JSCE (Konagai et al. 2001).

5.2.1 Description of building stock

Low-rise structures in South American cities can be classified into three general categories: adobe, brick bearing wall, and reinforced frame wall with brick infill. Fernandez et al. (2001) surveyed 130 structures in Moquegua and classified the structures in southern Peru into three groups:

- Type A: Usually made of adobe or mud mortar with very shallow stone-mortar unreinforced foundations. Commonly the ceilings have timber beams directly placed on the walls.

- Type B: Commonly present masonry walls with cement-sand mortar. Usually masonry is homogeneous with good quality of materials as well as sound foundations. Ceilings can be flat and leaning on the walls or with a reinforced concrete slab but with no beams or any other reinforcement.
- Type C: Masonry infill with a well-built structure that includes concrete reinforced elements such as beams and columns. Good foundations as well as alleviated slabs in the ceilings.

There is a usually a lack of adequate engineering design incorporated within the majority of the buildings in the area. In addition, construction quality varies widely. Block adobe is the foremost material incorporated in the majority of architectural constructions in the area under study. Construction quality of adobe houses is often poor and highly variable. Moreover, adobe is a material very vulnerable to seismic damage (due to its very low tensile strength). Damage to adobe housing can occur even under relatively low shaking. For these reasons, it is difficult to use adobe housing as an index of ground motion intensity.

5.2.2 Structural Damage Observation

A general understanding of building damage is useful when evaluating spatial damage distributions. The following observations regarding structural damage are summarized from the various aforementioned reconnaissance reports, as well as from additional sources.

Structures made of adobe performed in general poorly and most of them collapsed (CIP 2001, Konagai et al. 2001). Similar levels of damage had been observed in the past in

adobe structures, and can almost exclusively be attributed to structural failures due to the poor performance of adobe under seismic conditions. It is interesting to note that Zegarra et al (2000) had proposed a technique for strengthening the existing adobe houses by providing welded wire reinforcement mesh to the adobe walls. A total of 19 adobe houses were reinforced prior to the event, all of them had a remarkably better performance when compared to the unreinforced ones.

Reinforced concrete structures (Type C) in general performed much better than adobe structures and unreinforced masonry structures (Type B). The latter constructions include construction using hollow bricks with horizontal perforations, which were forbidden by the Masonry design code in Peru (CAPECO 1997). Damage to reinforced concrete structures was categorized as follows:

- Damage to short columns. This type of damage was evident at schools and public buildings; insufficient gaps between columns and non-structural elements caused large shear forces to be induced on the short columns. This effect was worsened by insufficient transverse reinforcement (Konagai et al. 2001, Fierro et al. 2001, CIP 2001).
- Damage to columns for elevated water tanks (Konagai et al. 2001).
- Deficiencies in structural layout. The current code enforces the use of stiff frames in both longitudinal and transversal directions of a building; a common practice in Peru is to provide stiffness only in one direction (Konagai et al. 2001). The insufficient lateral stiffness caused: excessive damage in the infill because it absorbed the seismic loads and failed due to excess shear forces (CIP 2001). Reinforced

concrete structures with appropriate lateral stiffness in both directions performed well (CIP 2001).

Construction quality played a significant role on structural failures. Fernandez et al. (2001) surveyed 130 dwellings with the objective of establishing regional intensity scales. Of the 130 dwellings surveyed, 58 were classified as Type A, 37 as type B, and 35 as type C. Also for type A, 53 % of the dwellings were considered of bad quality, 28% of regular quality and 19% of good quality; for the case of type B, 32% were considered of regular quality and 68 % of good quality; finally for type C, 94% were considered of good quality and only 6% of bad quality. Note that if the percentages assigned are summed the result is not 100%, the percentage missing corresponds to dwellings for which a classification was not given. Figure 5.1 summarizes this information.

Figure 5.1 Damage distribution by quality of construction (Fernandez et al. 2001).

Fernandez et al. (2001) also obtained information about damage using a damage index proposed by Ocola (1979), which categorizes buildings into 6 levels of damage from 0 to 5, being 5 the most severe level of damage. In the case of dwellings of Type A, 14% suffered light damage (level 1), 20% severe damage (level 3) and 48% of the dwellings

suffered partial destruction (level 4); for Type B buildings, 24% presented level 1, 30% showed level 2, and 30 % level 3. For buildings of Type C, 23% didn't suffer damage at all, 57% suffered level 1 of damage, and 14% suffered level 3 of damage. Figure 5.2 summarizes this information. Average and maximum values of damage level were obtained for the different categories of construction quality; Figure 5.3 and Table 5.1 present the results.

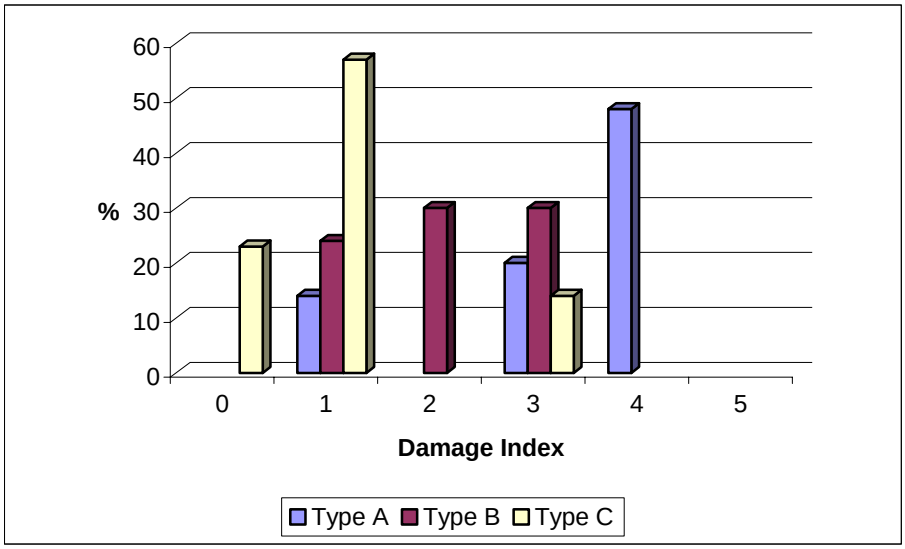

Figure 5.2 Damage distribution by building quality and type (from Fernandez et al. 2001).

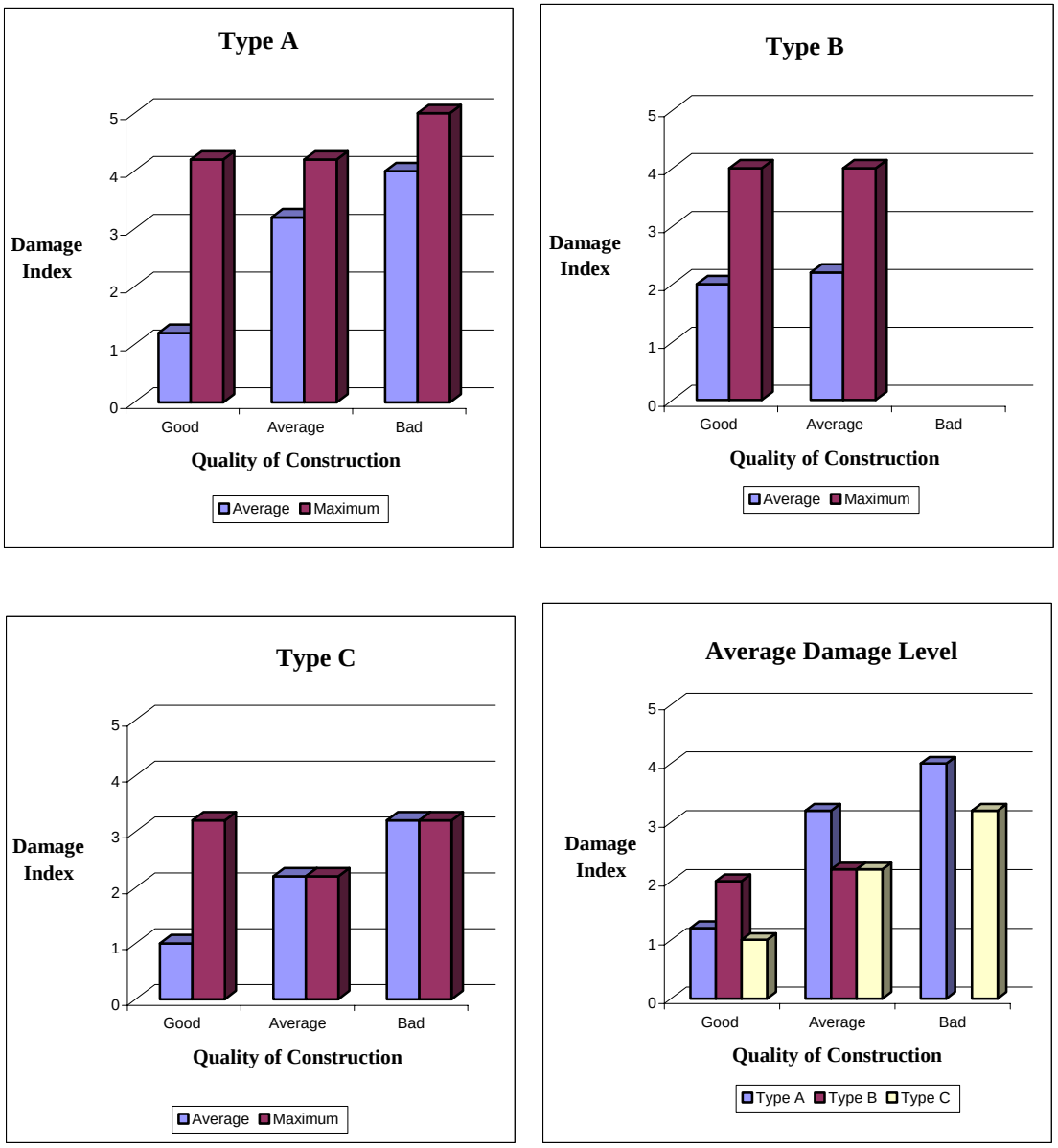

Figure 5.3 Representation of average and maximum level of damage (from Fernandez et al. 2001).

Table 5.1 Average and Maximum level of damage (from Fernandez et al. 2001).

Quality	Type A		Type B		Type C	
	Damage Level		Damage Level		Damage Level	
	Average	Maximum	Average	Maximum	Average	Maximum
Good	1+	4+	2	4	1	3+
Average	3+	4+	2+	4	2+	2+
Bad	4	5			3+	3+

Figures 5.2 and 5.3, as well as Table 5.1, evidence the influence of construction quality in the observed damage levels. Both for adobe and reinforced concrete structures, poorly built structures suffered higher damage levels than well-built structures. While it is obvious that structural and construction factors had an important influence on observed damage levels, the various type of structures were distributed throughout the city hence the spatial distribution of damage is not directly attributable to structural issues.

5.2.3 Spatial distribution of damage

The NSF reconnaissance team (Rodriguez-Marek et al. 2003) and the INDECI team (Kosaka Masuno et al. 2001) performed detailed investigations of the spatial distribution of damage. The observations of these teams are now summarized.

NSF Team (Rodriguez-Marek et al. 2003)

The team inspected the most heavily damaged brick bearing wall and reinforced concrete frame structures, as well as damaged and undamaged public schools and government buildings. Most of the structures that fall under these categories are relatively new buildings, built following two nationwide codes. The older code was used until 1997. The most recent code includes important changes concerning the design of structures under seismic loads. In general, the structures that were built using this code performed remarkably better than their counterparts.

In order to evaluate overall structural damage using a standard method, the reconnaissance team used the rank described by Coburn and Spence (1992) that was adapted to the damages observed in the Southern Peru earthquake (Rodriguez-Marek et al. 2003) to classify structural damage. The rank basically consists in assigning an index of damage to the various structures following the criteria shown in Table 5.1.

Table 5.2 Structural damage index used for mapping damage patterns (Rodriguez-Marek et al. 2003)

Damage Index	Description	Interpretation
D0	No observable damage	No cracking, broken glass, etc.
D1	Light damage	Moderate amounts of cosmetic hairline cracks, no observable distress to load-bearing structural elements, broken glass. Habitable.
D2	Moderate damage	Moderate amounts of thin cracks or a few thick cracks. Cracking in load-bearing elements but no significant displacements across the cracks. Habitable with structural repairs.
D3	Severe damage	Large amount of thick cracks. Walls out of plumb. Cracking in load-bearing elements, with significant deformations across the cracks. Uninhabitable. Major restoration required.
D4	Irreparable damage	Walls fallen, roof distorted, column failure. Uninhabitable. Partial or complete collapse in plan view. Demolition required.

In Moquegua city, most of the buildings that collapsed or suffered high level of damage were adobe-type structures; this was clearly observed in the Cercado and San Francisco Districts, but particularly on the slopes of San Francisco hill. To see a map of the city with the location of the different districts see Figure 5.6.

Some institutional buildings that belong to the other two categories (Type B and C using the classification proposed by Fernandez et al. 2001) were also surveyed. Details about the buildings surveyed, such as, location, possible soil conditions and the damage encountered by the reconnaissance team, are explained in Table 5.3.

Table 5.3 Damaged reinforced concrete buildings (Type C) in Moquegua (Rodriguez-Marek et al. 2001)

No	Building	Damage	Location	Possible soil conditions[1] (Kosaka-Masuno et al. 2001, Salas-Cachay 2001)
1	Simon Bolivar School	D1 to D2	Cercado	Alluvial deposits. Superficial layer (about 1.5 m) or low plasticity clay/clayey sand, relatively soft overlying very stiff alluvial material (possibly the Moquegua formation).
2	Luis Pinto School	D0	Cercado	
3	Sagrado Corazon School	D0 or D1	Cercado	
4	Santa Fortunata School	D1	Cercado contiguous buildings	
5	Angela Barrero School	D3		
6	Private University of Moquegua (two buildings)	D2 and D3	Cercado	Located at higher elevations than other sites in the Cercado district. Possibly in an alluvial terrace deposit.
7	Vitalino Becerra School	D1	Samegua	On Moquegua formation.
8	Modelo School	D2	Samegua	
9	San Antonio Health Center	D1 to D2[3]	San Antonio	Gravels and clayey sands and silts. Clay present only in thin strata (about 30 cm). Local engineers report local areas with expansible soils.
10	San Antonio School (two buildings)	D1 and D2[2]	San Antonio	
11	ESSALUD Hospital	D2	San Francisco	Gravelly silt upper 0.5 to 2 m, overlying the Moquegua formation. Silty clays with expansive properties found at some locations.
12	Peru BIRF (two buildings)	D2 and D3	San Francisco	

[1] Soil conditions obtained from nearby trenches and seismic surveys, as well as observations and inferences.
[2] Cracks were present in the building prior to earthquake. Based on reports from local engineers, no additional cracking was induced by the earthquake.
[3] From Koseki et al.

The level of damage observed in the buildings listed in Table 5.3 is consistent with the levels observed in nearly adobe-type structures. More severe damage was observed in the Cercado and San Francisco districts.

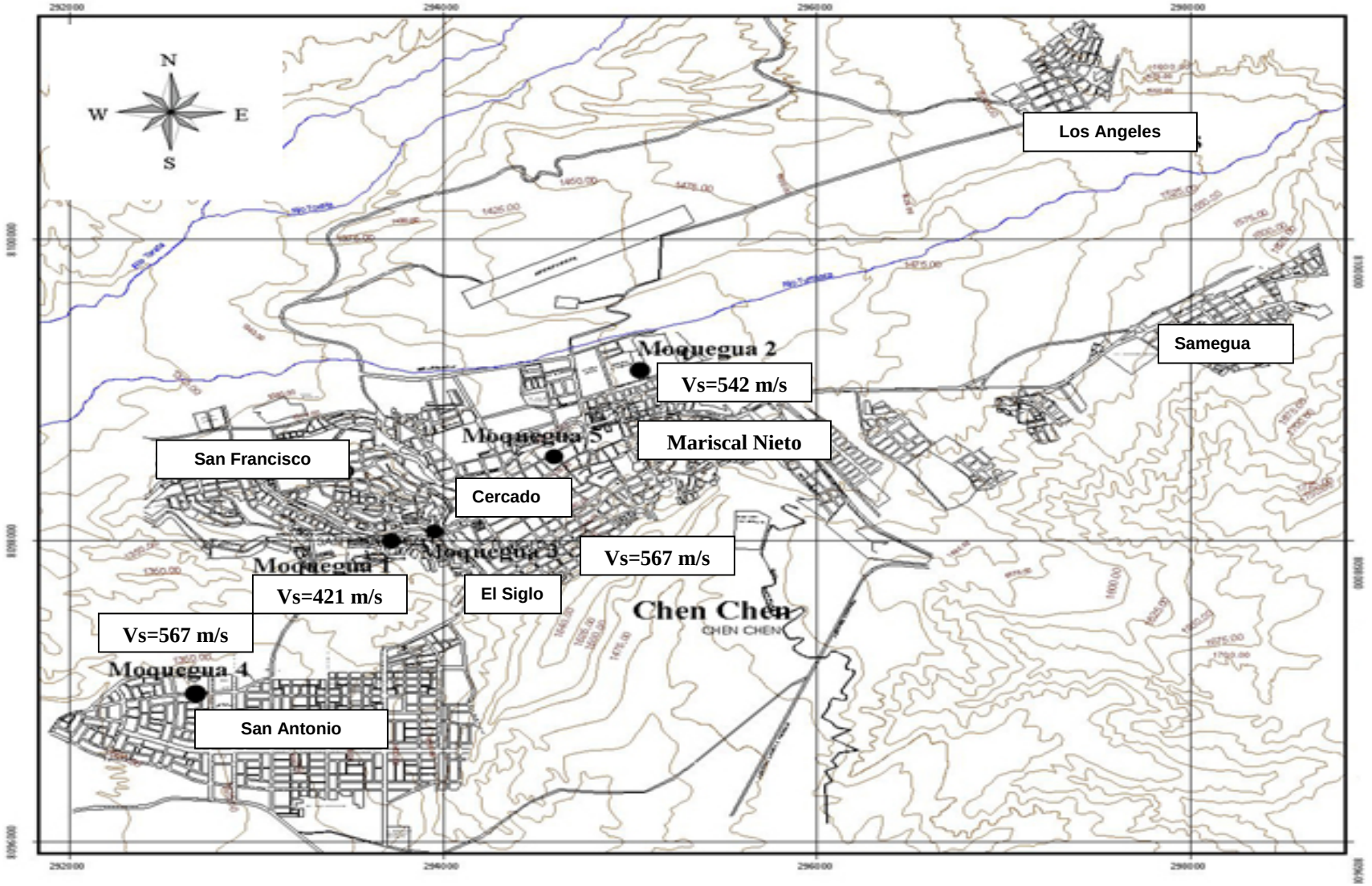

Figure 5.6 Map of the city of Moquegua with the main districts shown. Base map from Kosaka-Masuno et al. (2001).

INDECI Team (Kosaka Masuno et al. 2001)

A total of 2622 dwellings were surveyed in different areas of Moquegua city. The distribution of the dwellings within the city is shown in Figures 5.6 and 5.7. Subsequently those buildings were classified in 4 different groups as it is shown in Table 5.4.

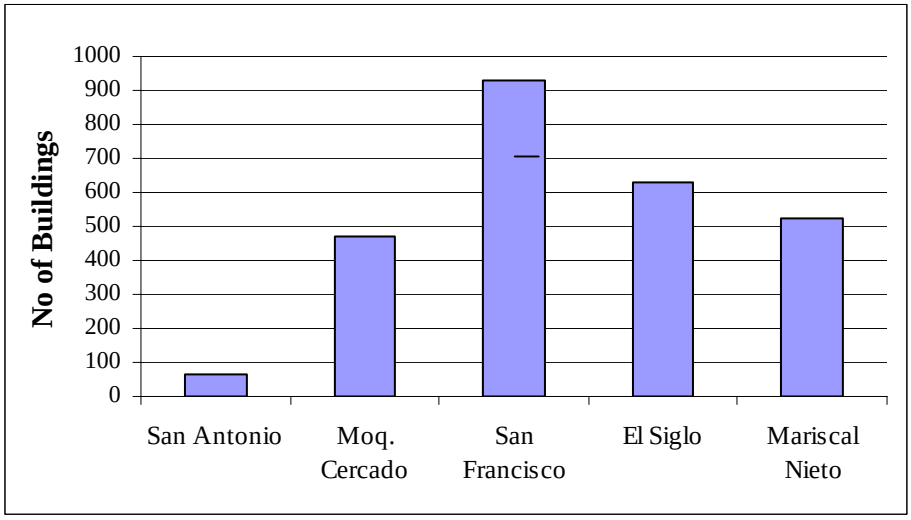

Figure 5.7 Number of buildings evaluated. (Kosaka-Masuno et al. 2001)

Table 5.4 Classified Buildings (Kosaka-Masuno et al. 2001)

	SAN ANTONIO	MOQUEGUA CERCADO	SAN FRANCISCO	EL SIGLO	MARISCAL NIETO
Cracked Concrete	51	103	151	38	34
Collapsed Concrete	1	5	27	6	7
Cracked Adobe	9	143	378	456	353
Collapsed Adobe	5	218	376	131	130
TOTAL	**66**	**469**	**932**	**631**	**524**

It is evident from the information presented in Table 5.3 that reinforced-concrete buildings performed well in comparison with adobe-built structures. It is important to clarify that the age of the evaluated buildings could have influenced damage levels, however, as suggested by Fernandez et al. (2001), quality of construction had considerably

bigger influence than age, fact that led to dismiss the effect of age in damage levels for the present study. On the other hand, on the steep slopes of San Francisco District, the number of reinforced-concrete buildings that collapsed was very high, suggesting the presence of site and topographic-related damage effects (Kosaka-Masuno et al. 2001). Moreover, the largest percentage of adobe-collapsed houses was found in Moquegua Cercado district with 46 %, and then in San Francisco district with 41 %, followed by Mariscal Nieto with 25%, El Siglo with 21 % and finally San Antonio with 8%, as shown in Figure 5.8. (Kosaka-Masuno et al. 2001)

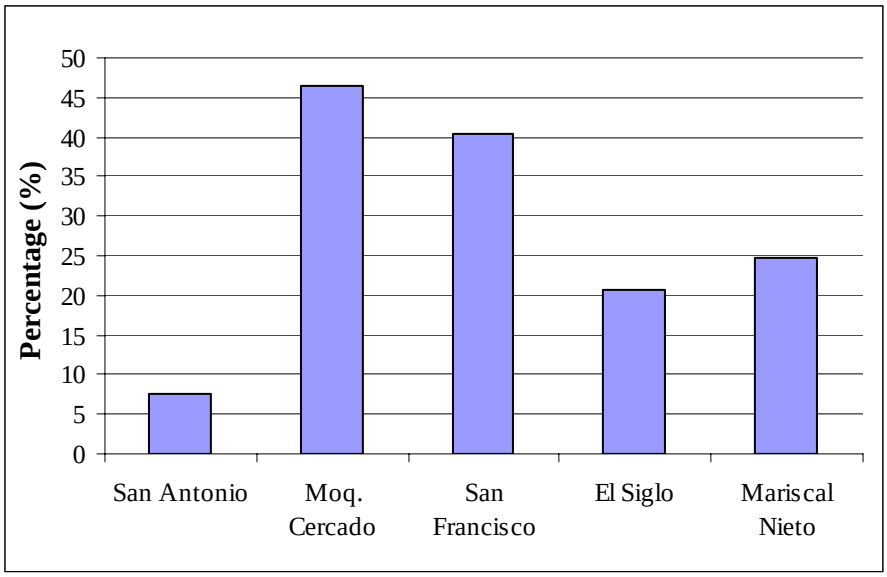

Figure 5.8 Distribution of adobe-collapsed houses in Moquegua city (Kosaka-Masuno et al. 2001).

5.2.3 Correlation with site conditions

The results presented in the previous section point to important concentration of damage in certain locations of the city of Moquegua. Damage in San Francisco Hill was severe, with 70 to 80 % of collapsed buildings. Although poor construction quality in this particular section of the city has been suggested as a culprit for the high damage levels (CIP 2001), site or topographic effects could have lead to higher input motions and hence to

larger damage levels. The San Francisco Hill is an outcrop of the Moquegua formation with 40 to 60 m high and relatively steep slopes (30 to 35 degrees). Other buildings located in different districts at the city, such as San Antonio and El Siglo, performed well during the earthquake. Some cracks were encountered, but local engineers corroborated that this damage was due to expansive soils and had existed before earthquake.

Fernandez et al. (2001) present the spatial distribution of damage (quantified by the scale proposed by Ocola (1979) in Figure 5.9. The following observations are suggested:

- Type A dwellings of regular to bad quality show levels of damage of 4, 4+ and 5 in Cercado, El Siglo, Mariscal Nieto y San Francisco districts. Also levels of 3 and 3+ in dwelling of regular to bad quality were found in Cercado, San Francisco, Samegua, San Antonio y El Siglo districts.
- For type B buildings of average quality, level 4 of damage was found in San Antonio and San Francisco districts; as well as 3+ and 3 levels can be found in San Antonio district.
- For Type C buildings didn't suffer much damage at all, although damage levels of 3+ and 3 were found in Cercado, San Antonio and San Francisco.

The maximum level of damage for type A buildings was 5 in Mariscal Nieto, San Francisco y Cercado districts; for type B the maximum was 4 and was found in San Antonio and San Francisco districts; finally, the maximum for type C was 3 and was found in San Francisco and San Antonio. This may have led to over-estimation of damage levels in San Antonio by Fernandez et al. (2001).

Quantitative correlation of damage with site conditions

In order to correlate possible site effects with damage levels, a few sites with different soil characteristics were selected (Table 5.5). Their shear wave velocity profiles were measured using SASW tests (see Chapter 3 and Appendix A for details). The location of the sites is shown in Figure 5.6, and the shear wave velocity profiles are shown in Figure 5.10.

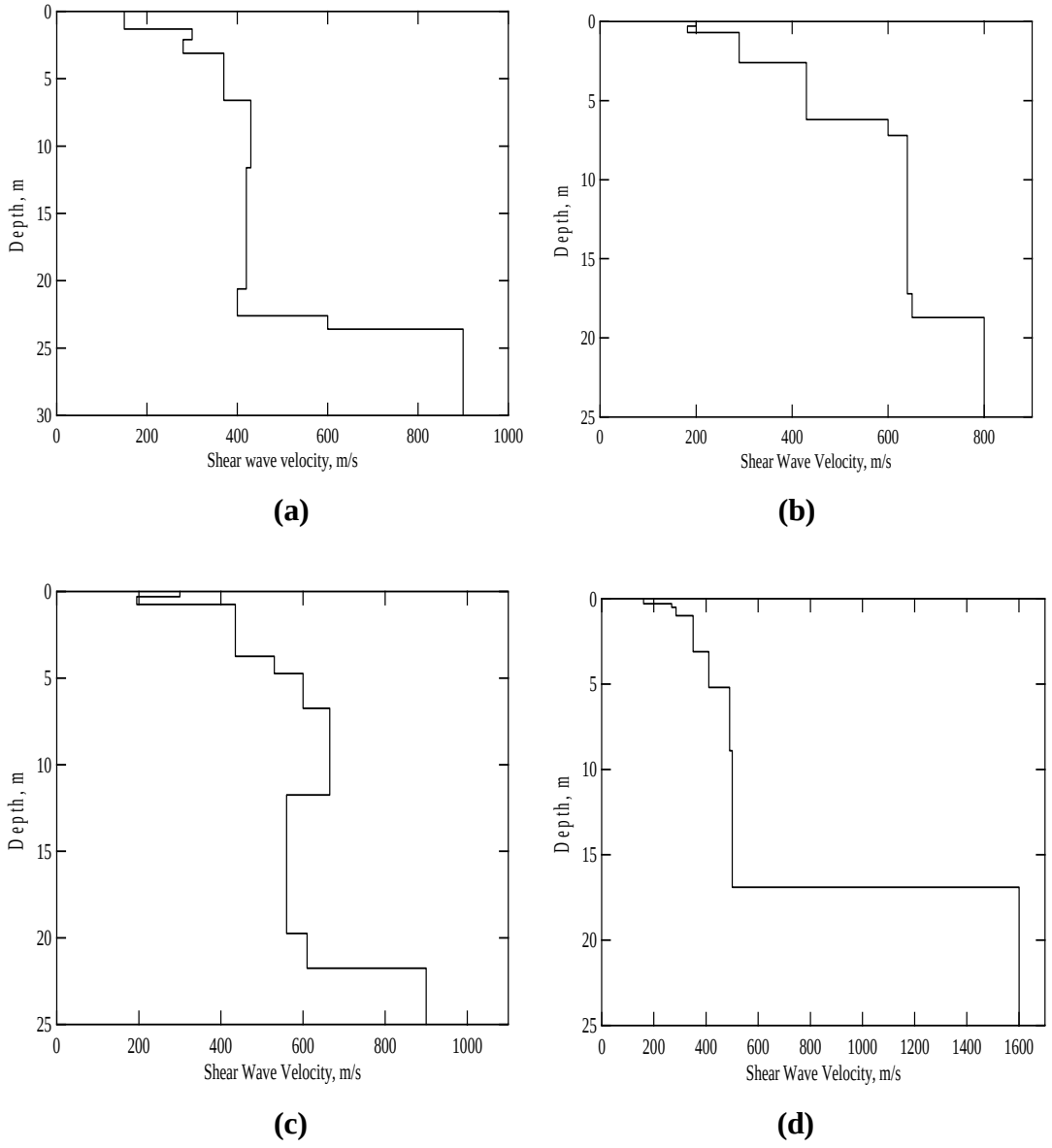

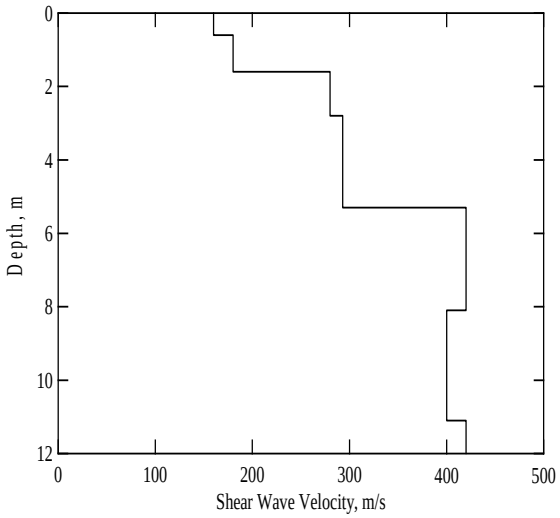

(e)

Figure 5.10 Shear wave velocity profiles. (a) Moquegua 1. (b) Moquegua 2. (c) Moquegua 3. (d) Moquegua 4. (e) Moquegua 5.

Table 5.5 Location of the studied sites.

Station Name	Station Location	Average Damage Index[1]	Site Period (sec)[2]	Average V_s[a] (m/s)
Moquegua 1	Nueva St. on southern part of **San Francisco** hill	D3	0.222	421
Moquegua 2	Strong motion station – **Mariscal Nieto**	D1	0.111	542[b]
Moquegua 3	9 De Octubre St. - northern part of **San Francisco** hill	D3	0.143	567[b]
Moquegua 4	San Antonio Hospital - **San Antonio**	D2	0.133	567[b]
Moquegua 5	Jr. Lima Street (476 Lima) - **Downtown** [c]	D1	0.071	-

[1]Represents the average obtained from the analysis of sites located near the testing sites, which were evaluated by Rodriguez-Marek et al. (2001).
[2] Site Periods were obtained from the first peak of Fourier spectra ratios obtained from the site response analysis.
[a] Average shear wave velocity in the upper 30 m.
[b] This site had average shear wave velocity in the upper 25 m.
[c] V_{S30} was not calculated because this site only had depth resolution of 12 m.

The average damage indices assigned to each of the districts represent the average value obtained by Rodriguez-Marek et al. (2001) for sites classified as Type C (Fernandez et al. 2001) located near the testing sites. However, the information about damage

distribution by Kosaka Masuno et al. (2001) and Fernandez et al. (2001) was also used as reference. The percentages of adobe-collapsed houses presented by Kosaka Masuno et al. (2001) do corroborate what was found by Rodriguez-Marek et al. (2003), except for the case of Cercado district, where a considerable amount of adobe houses collapsed while buildings classified as Type C performed well. On the other hand, the information provided by Fernandez et al. (2001), which includes a significant number of buildings evaluated in the city; supports the average values obtained. It is also worth noting that the average damage indices are regional averages. This presented a particular problem in the San Francisco district, where damage in a hillside appears to be much larger than in nearby areas (Kosaka Masuno et al.(2001), Konagai et al. (2001), Rodriguez-Marek et al. 2003).

Key assumptions must be made to justify using an average damage index for each district: a) construction quality is uniform throughout the city, b) building age, which also may affect performance, is also uniform throughout the city, c) the sample from which building performance was evaluated was representative. It is not easy to verify these assumptions, especially during an earthquake reconnaissance. Hence, there is a degree of subjectivity involved in the selection of average damage indices.

Site response analyses were performed using the equivalent linear program SHAKE91 to estimate the ground motions at the surface. The motions generated from a finite source model (Silva 2004, see Figure 4.10) were used as input motions. The input motions were scaled to 0.3 g, which is the PGA of the only recording made in the city of Moquegua. The response spectrum at the surface of each site is shown in Figure 5.10. The effect of site response on the surface ground motions is then quantified by the Ratio of

Response Spectra (Figure 5.11). Note that the percentages included in this figure were obtained by Kosaka Masuno et al. (2001) for adobe-collapsed.

The spectral acceleration values (for select periods) at the surface of each of the sites listed in Table 5.5 are given in Table 5.6. These spectral acceleration values are compared to the damage measure indices determined by the NSF team in Figure 5.12.

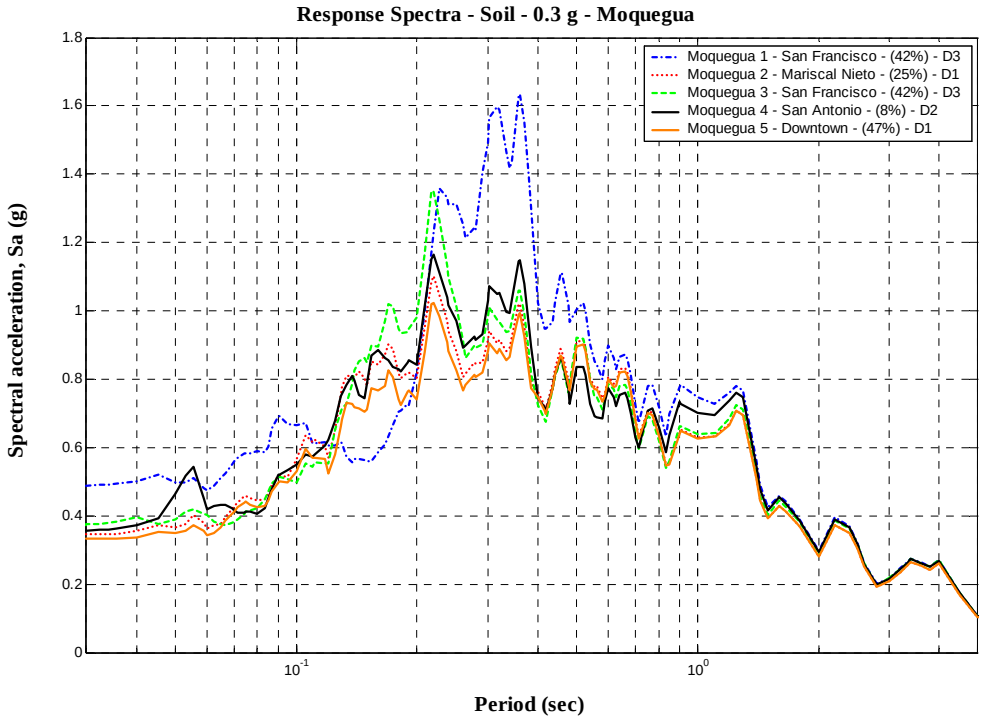

Figure 5.10 Response Spectra – 5% damping obtained from site response analyses for each of the sites listed in Table 5.5. The number in parenthesis indicates the percentage of collapsed adobe houses according to Kosaka Masuno et al. (2001) (Figure 5.8).

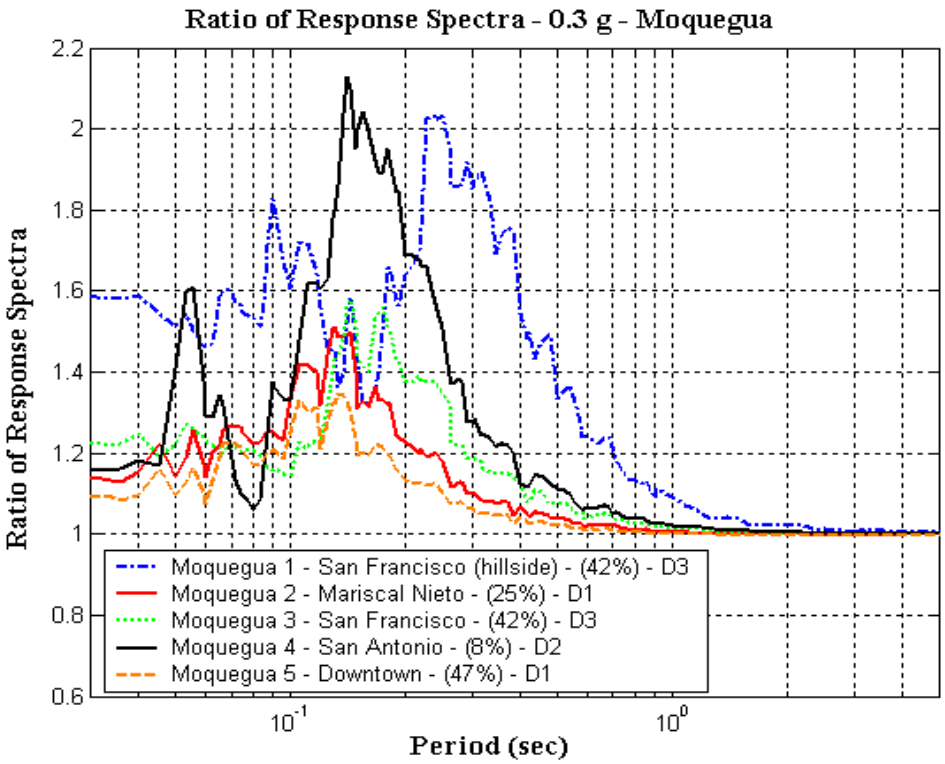

Figure 5.11 Ratio of Response Spectra (input motion scaled to PGA = 0.3 g) obtained from site response analyses for each of the sites listed in Table 5.5. The number in parenthesis indicates the percentage of collapsed adobe houses according to Kosaka Masuno et al. (2001) (Figure 5.8).

Table 5.6 Spectral accelerations at selected periods from site response analyses (PGA of input motion is 0.3 g).

	Spectral Accelerations							
	PGA	**0.05 sec**	**0.1 sec**	**0.2 sec**	**0.3 sec**	**0.5 sec**	**1 sec**	**2 sec**
Moquegua 1: San Francisco	0.49	0.50	0.66	0.82	1.49	1.01	0.75	0.30
Moquegua 2: Mariscal Nieto	0.35	0.37	0.57	0.80	0.91	0.91	0.63	0.28
Moquegua 3: San Francisco	0.37	0.39	0.50	0.98	0.98	0.92	0.64	0.29
Moquegua 4: San Antonio	0.36	0.46	0.55	0.84	1.03	0.84	0.70	0.29
Moquegua 5: Downtown	0.33	0.35	0.53	0.74	0.88	0.89	0.63	0.28

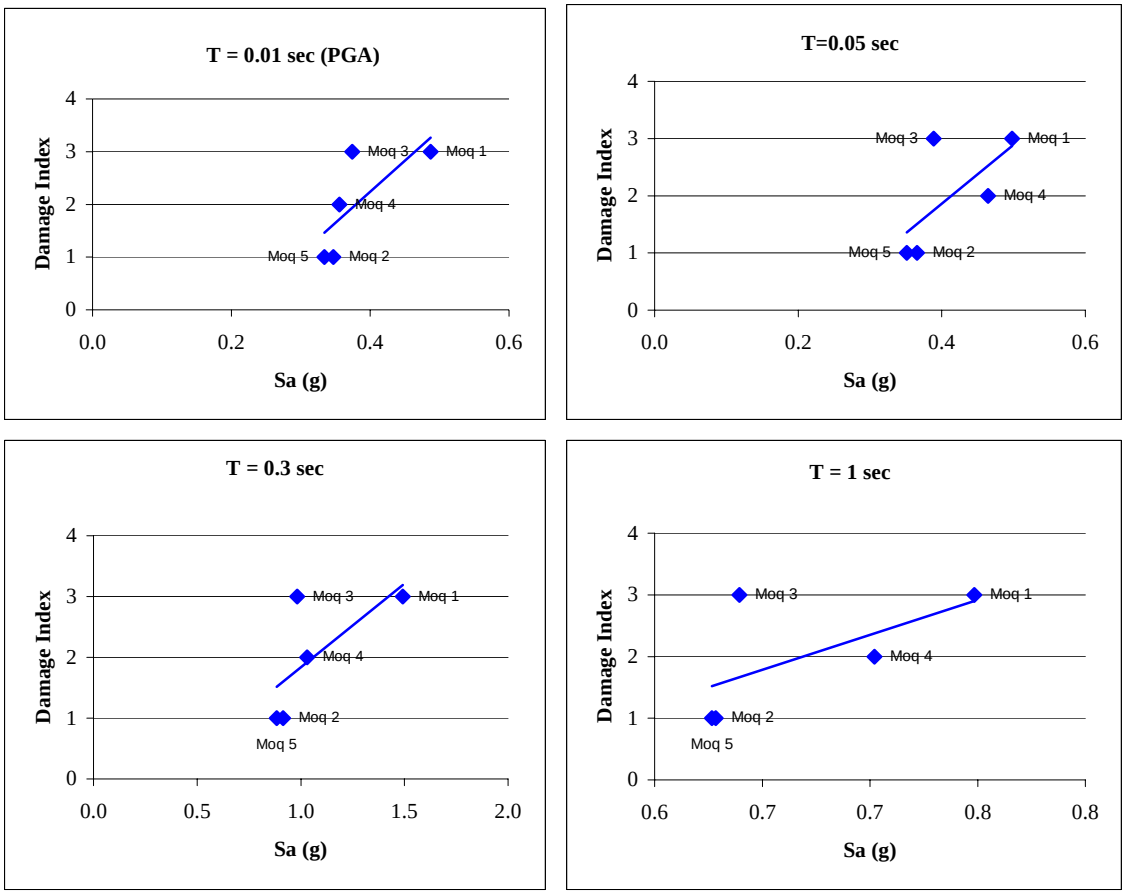

Figure 5.12 Correlation between damage level and spectral accelerations for certain periods.

The results summarized in Figure 5.12 support the hypothesis that site effects played a key role in the observed damage distribution. Larger spectral acceleration values for most periods were obtained for sites located in San Francisco district, which is the district that presented higher damage levels. Also for most periods a pattern shows that the higher the values of spectral acceleration produced the higher the level of damage produced by the earthquake, which is reasonable. This tendency is more evident for T = 1 second. Finally there is an exception with Moquegua 3 site, which presented spectral acceleration values lower than expected. This site is located near the base of San Francisco Hill, in the district of the same name. Note that the average damage indices reflect an

average damage for the whole district; however, while damage in the hillside slopes was very large, reported damage elsewhere was not as significant. This may explain why Moquegua 3 does not follow the trend of other sites in Figure 5.12. In addition, note that one-dimensional site response alone predicts significant difference in amplification from the hillside (Moquegua 1) to the bottom of the hill (Moquegua 3). While this does not negate probable topographic effects, it does indicate that the differences in structural performance between houses in the hillside and the bottom of the hill could be attributed to site effects alone.

The correlations shown in Figure 5.12 do not have much statistical significance. Hence, is difficult to make a general conclusion about the correlation between damage and site effects. Moreover, it is implicitly assumed that soil conditions are uniform throughout each evaluated district. This is partially supported by a previously developed seismic zonation for Moquegua (Bardales et al. 2002). Despite these limitations, site amplification is considered to have affected building performance in the San Francisco district, and may have influenced damages in San Antonio and Cercado. This statement cannot be generalized due to the limitations stated above.

5.2.4 Conclusions regarding damage in Moquegua city

All the evaluated reports coincide with some of the major issues regarding observed damage. For instance, influence of site (and possibly topographic effects) in some areas of city, the effect of low quality of construction and design problems, and with the poor performance of adobe houses.

Analyses showed that site effects influenced the ground motions resulting in high levels of damage in some areas. In particular, the district of San Francisco, at least the

dwellings located on the steep slopes of the hill, had damage that can be related to site and possibly topographic effects. In addition, it is evident that quality of construction should be improved, in addition to the involvement of qualified supervision, which likewise should be enforced. Additionally, quality of materials as well further soils testing, should be performed previous to undergoing any construction projects.

5.3 Damage distribution in the city of Tacna

As in the case of Moquegua city, the information on damage distribution in the city of Tacna was evaluated by a number of research teams, including Rodriguez-Marek et al. (2003), the Japanese Society of Civil Engineers, JSCE (Konagai et al. 2001) and The Peruvian Institute of Geophysics (IGP).

The observations presented in sections 5.2.1 and 5.2.2 regarding building stock and structural damage observations, including the general building categories for south American countries and the three different building types suggested by Fernandez et al. (2001) can also be applied to the city of Tacna.

Fernandez et al. (2001) surveyed a total of 92 dwellings of one and two stories in Tacna city, once again with the objective of establishing regional intensity scales. From the 92 surveyed dwellings, 9 were classified as type A, 44 as type B and 39 as type C. For type A, 67% of the dwellings were considered of bad quality and 33 % of regular quality; for type B, 70% of regular quality and 25% of good quality, finally for type C, 87% were considered of good quality, 7% of regular quality and 6% of bad quality. Figure 5.13 summarizes all these data.

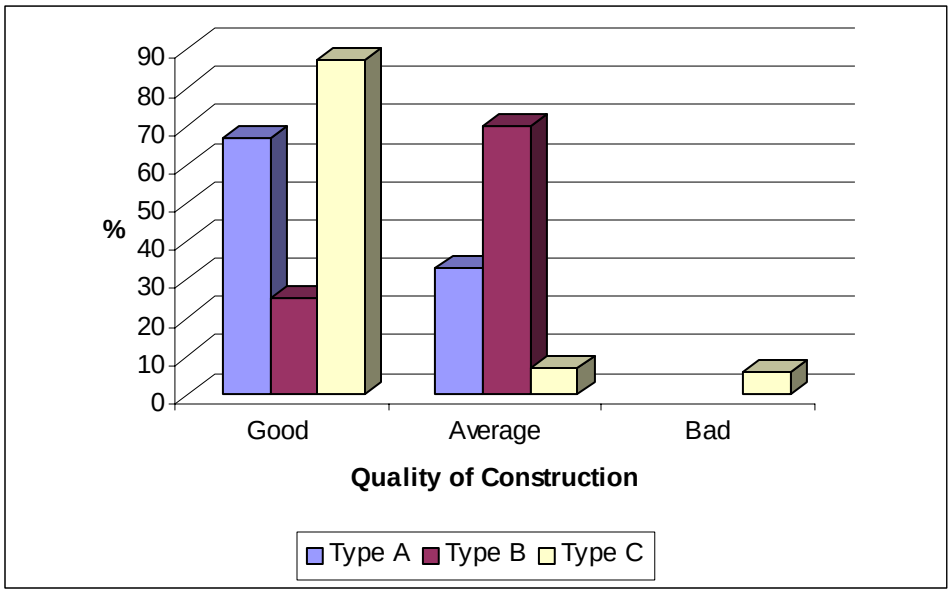

Figure 5.13 Damage distribution by quality of construction.

Fernandez et al. (2001) also obtained information about damage using the ranking previously explained. In the case of dwellings type A, 45% suffered light damage (level 1), 10% severe damage (level 3) and 45% of the dwellings suffered partial destruction (level 4); for type B, 20% presented no damage, 22% showed level 1, 25% level 3 and 29% presented partial destruction (level 4). For type C, 56% had no damage at all, 18% suffered level 1 of damage, 8 % suffered severe damage (level 3) and 14% suffered level 4 of damage. Figure 5.14 shows the summary of these data. Note that Type C buildings suffered higher levels of damage in Tacna than in Moquegua. Average and maximum values were obtained for each of the building types and for the different quality levels; the results are presented in Figure 5.15 and Table 5.7.

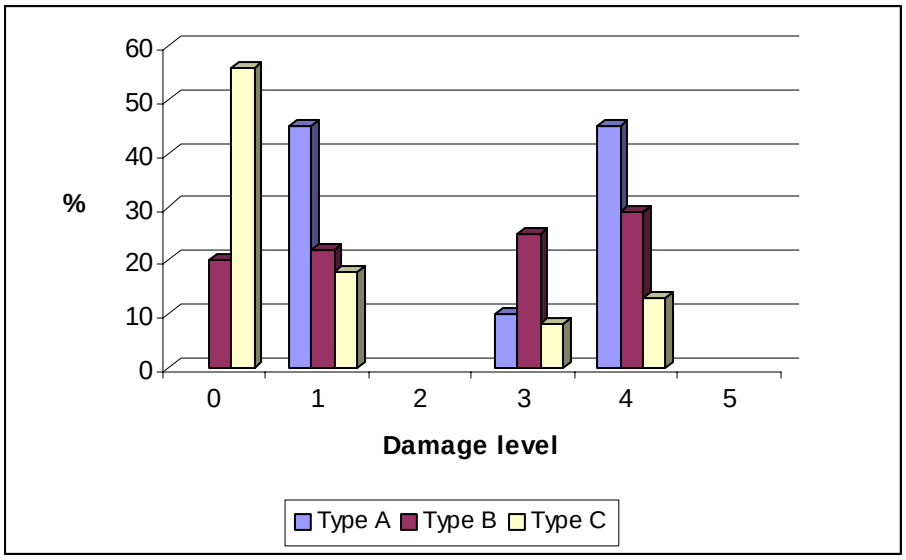

Figure 5.14 Damage distribution by damage level and type of structure.

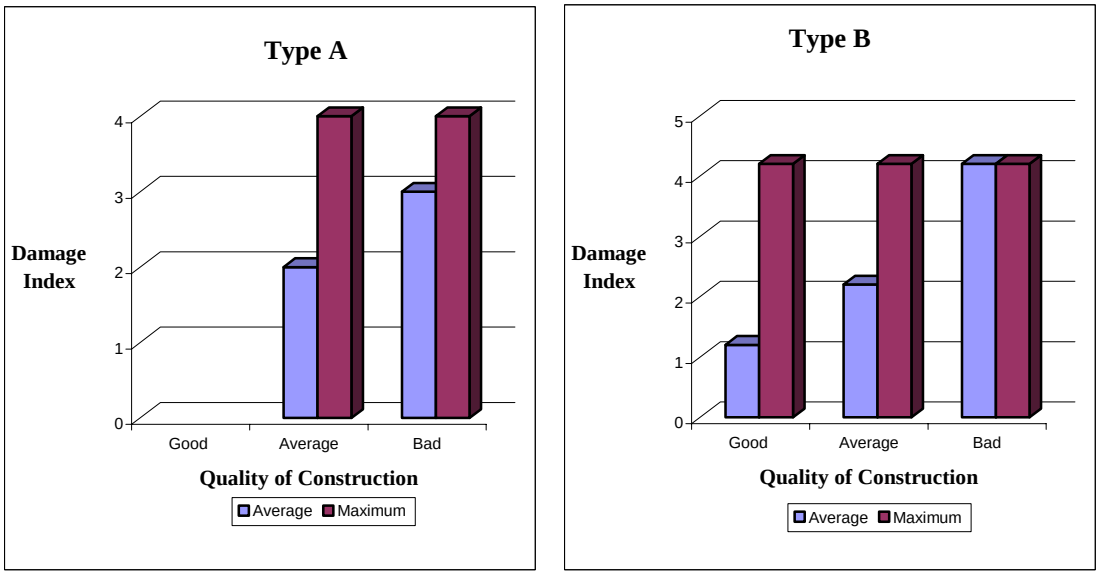

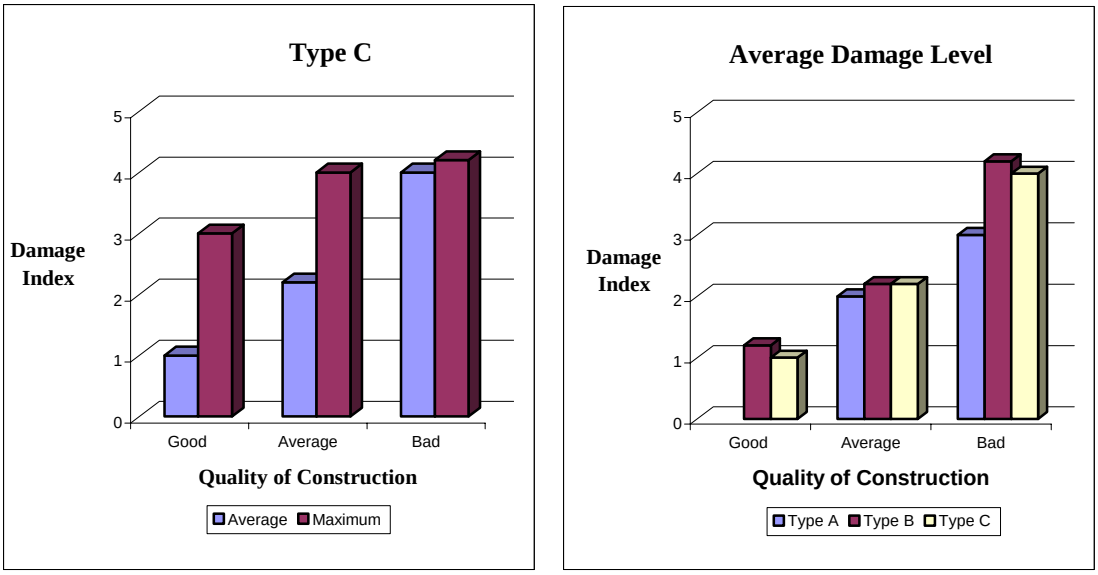

Figure 5.15 Representation of average and maximum level of damage (from Fernandez et al. 2001).

Table 5.7 Average and Maximum level of damage (from Fernandez et al. 2001).

Quality	Type A		Type B		Type C	
	Damage Level		Damage Level		Damage Level	
	Average	Maximum	Average	Maximum	Average	Maximum
Good			1+	4+	1	3
Average	2	4	2+	4+	2+	4
Bad	3	4	4+	4+	4	4+

5.3.1 Spatial distribution of damage

The NSF sponsored reconnaissance team (Rodriguez-Marek et al.2003) also studied damage distribution in the city of Tacna (Figure 5.17). Some important institutional buildings were surveyed, details about those buildings are described in Table 5.8.

Table 5.8 Damage evaluation of surveyed buildings in Tacna (Rodriguez-Marek et al. 2003).

Site No	Site Description	Structure Type	Building Use	Damage Intensity
1	Av. Sol: 2-story house.	Brick (bearing)	House	D4 – Collapse
2	Biblioteca Jose Olaya	Reinforced concrete frame	Library	D2 – Moderate
3	Municipalidad Distrital	Reinforced concrete frame	Municipality	D4 – Irreparable
4	Av. Internacional: Blue house	Brick (bearing)	House	D4 – Irreparable
5	Gray house west of Blue house.	Brick (bearing)	House	D4 – Irreparable
6	Colegio Mariscal Caceres	Reinforced concrete frame	School	D3 – Severe
7	SENATI	Reinforced concrete frame	School	D1 – Light
8	Instituto Vigil	Laminar roof on bearing wall	School	D2 – Moderate
9	CE 42021: Fortunato Zora	Reinforced concrete frame	School	D2 – Moderate
10	Arco de Tacna	Reinforced concrete frame	Monument	D0 – No damage
11	Av. Circunvalacion Sur: House	Brick (bearing)	House	D4 – Irreparable
12	Gran Hotel Tacna	-	Hotel	D1 – Light
13	Complejo de viviendas Jose Rosa Arce (23 de agosto)	Brick (bearing)	Apartment Complex	D1 – Light
14	Colegio Gregorio Albarracin	Reinforced concrete frame	School	D1 – Light
15	Colegio Haya de la Torre	-	School	D0 – No damage
16	Several blocks with intense damage. 3-story building with 4^{th} floor half built	Brick (bearing)	-	D4 – Collapse
17	Agrupamiento 28 de agosto	Reinforced concrete frame	Apartment Complex	D1 – Light
18	CE 42250: Cesar Cohaila	Reinforced concrete frame	School	D0 – No damage (new code) D1 – Light (old code)
19	CE 42088: Jose de San Martin	Reinforced concrete frame	School	D1 - Light

Table 5.8 Damage evaluation of surveyed buildings in Tacna (Rodriguez-Marek et al. 2003). (Continued)

Site No	Site Description	Structure Type	Building Use	Damage Intensity
20	CE 42238: Enrique Pallardelle	Reinforced concrete frame	School	D0 – No damage
21	Instituto formacion artistica Francisco Lazo	Reinforced concrete frame	School	D1 - Light
22	CE Guillermo Auza	Reinforced concrete frame	School	D1 – Light
23	CE 42020: Rosalina Herazo	Reinforced concrete frame	School	D1 – Light
24	CEI 408: Comite 24 y 25	Reinforced concrete frame	School	D1 – Light
25	CE 42237: Jorge Chavez	Reinforced concrete frame	School	D0 – No damage
26	CE 42007: Leoncio Prado	Reinforced concrete frame	School	D1 – Light
27	Conjunto habitacional Alfonso Ugarte	Reinforced concrete frame	Apartment Complex	D0 – No damage
28	Mutual Tacna building	Reinforced concrete frame	Office Building	D0 – No damage
29	Five-story building	Reinforced concrete frame	Office/Apartment Complex	D1 – Light
30	Two-story house	Reinforced concrete frame	House	D1 – Light
31	Four-story building	Reinforced concrete frame	Apartment Complex	D1 – Light
32	School	Reinforced concrete frame	School	D0 – No damage
33	General Attorney's complex.	Reinforced concrete frame	Institutional	D0 – No damage

After the analysis of damage distribution was complete, higher levels of damage were observed in the northern area, which is composed by Alto de la Alianza, Ciudad Nueva and Gregorio Albarracin districts (see Figure 5.14). Note that the northern area presents either fill material or volcanic tuffs that in some cases weathered into loose silty sands (in general finer soils). For this reason it is suggested that important site effects took place on this area, and site effects influenced the observed damage levels. On the

other hand, the structures that are located on alluvial-gravelly deposits (downtown and southern area), performed remarkably better.

The reconnaissance team did not identify foundation failure cases, supporting the fact that building performance was due either to structural performance alone, or a combination of structural performance and amplification of the ground motion due to site effects.

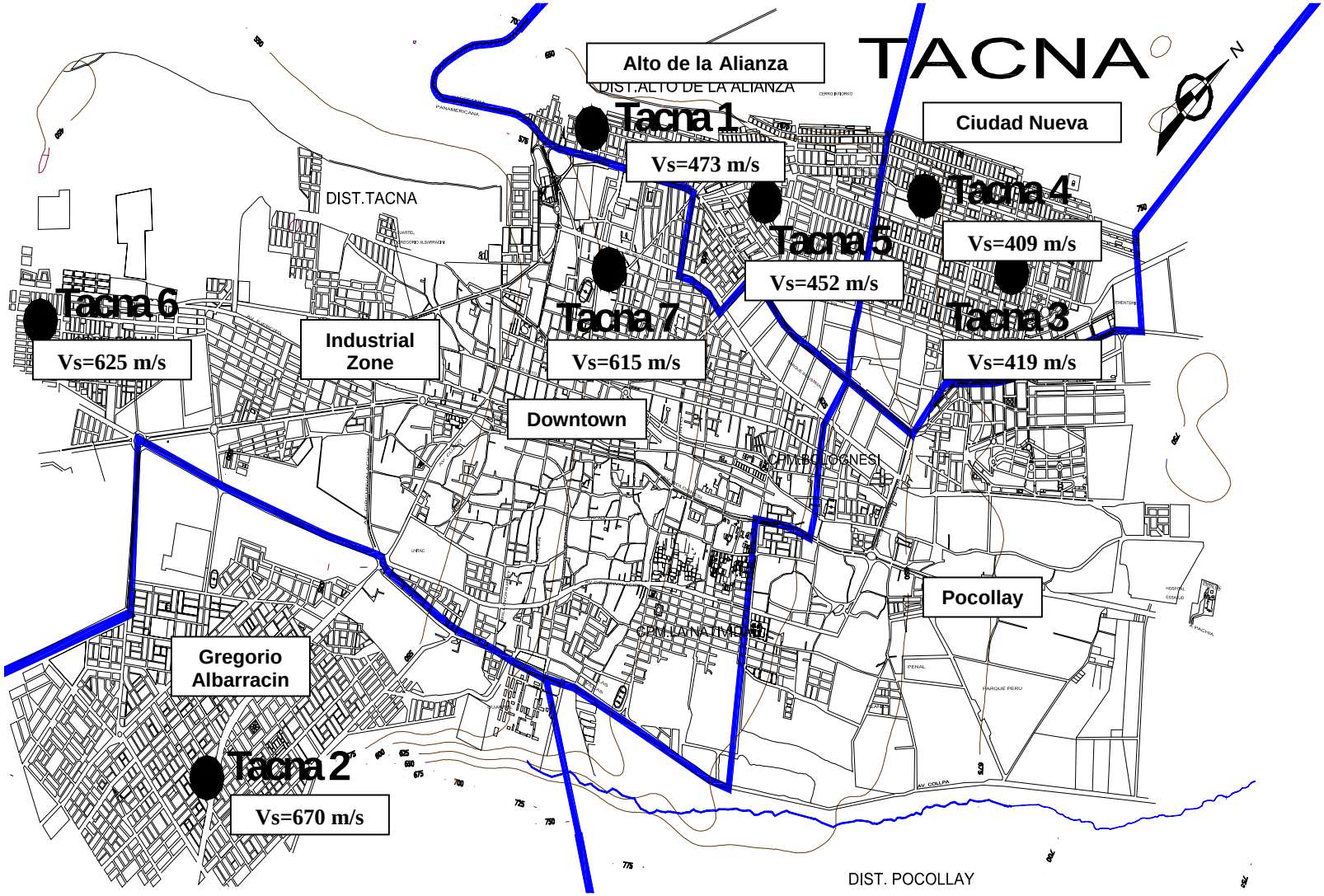

Figure 5.17 Map of the city of Tacna with the main districts shown. Base map from Cotrado-Flores and Sina-Calderon (1994).

5.3.2 Correlation with site conditions

The results presented in the previous section point to important concentration of damage in certain locations of the city of Tacna. Damage in districts located on the northern area of the city (Alto de la Alianza and Ciudad Nueva) was severe, with a considerable amount of collapsed buildings. From the evaluation by Fernandez et al. (2001), it was observed that:

- Type A dwellings were mostly located in the Downtown area, the majority of them suffered level 4 of damage, the others suffered levels 1 and 3, this evaluation considers good, average and bad quality buildings.
- For type B buildings of all qualities, levels 3, 4 and 4+ of damage were found in Alto de la Alianza, Ciudad Nueva and Pocollay districts.
- For Type C buildings, levels 4 and 4+ were found in Ciudad Nueva, Alto de la Alianza for good and average quality buildings, however, 57% of Type C buildings did not suffer damage at all.

The maximum level of damage for type A buildings was 4, mostly located in Cercado district; for type B the maximum damage level was 4 and was found in Alto de la Alianza and Ciudad Nueva districts; finally the maximum level of damage for type C was again 4 and was found in Alto de la Alianza and Ciudad Nueva districts.

While in Tacna district and Pocollay district (southern area of the city) the maximum indexes were D0 and D1, in the northern area indexes up to D3 were identified in some schools. Schools, in general, performed better than housing, mainly because of

better construction quality. A few exceptions were encountered such as Site No 11, where a high level of damage was observed; the apparent reason was a design error.

Quantitative correlation with damage

In order to correlate possible site effects with damage level, a few sites with different soil characteristics were selected (Table 5.9). In addition, their correspondent V_s profiles were obtained using SASW tests (see Chapter 3 and Appendix A for details). Location of the sites can be seen in Figure 5.17, and the shear wave velocity profiles are shown in Figure 5.18.

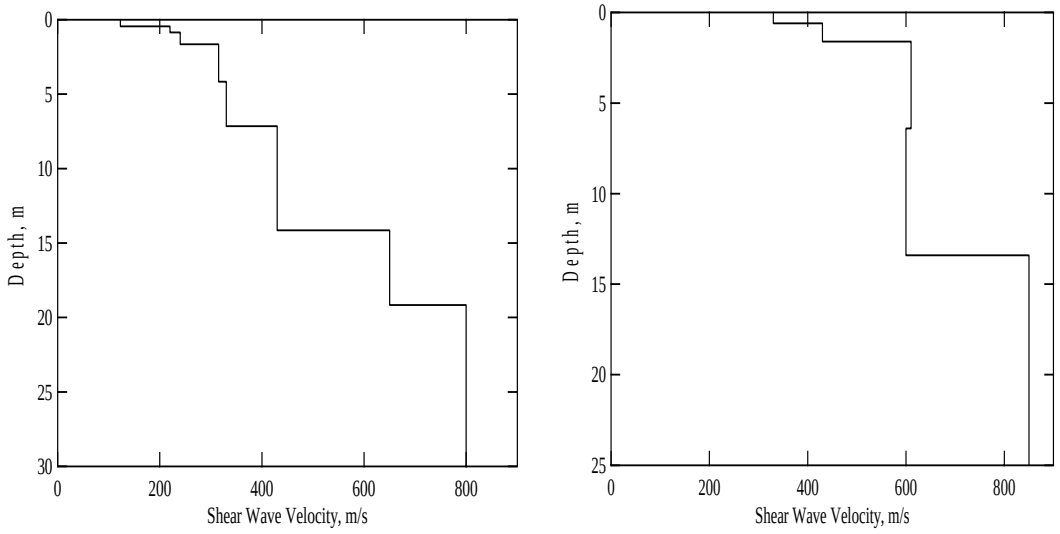

(a) **(b)**

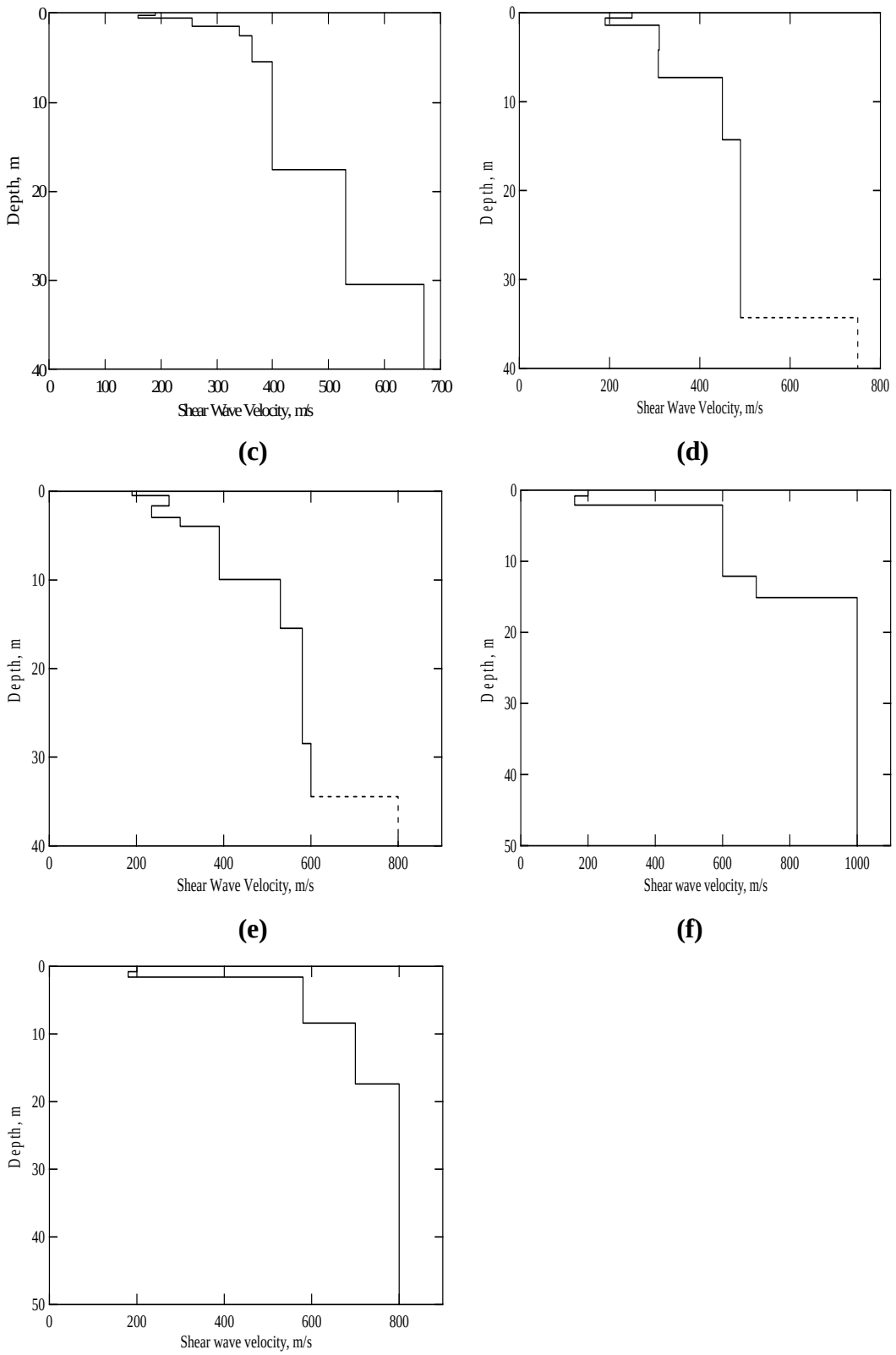

Figure 5.18 Shear wave velocity profiles. (a) Tacna 1. (b) Tacna 2. (c) Tacna 3. (d) Tacna 4. (e) Tacna 5. (f) Tacna 6. (g) Tacna 7.

Table 5.9 Location of the studied sites.

Station Name	Station Location	Average Damage Index[a]	Site Period (sec)[b]	Average V_s[c] (m/s)
Tacna 1	Asociacion 'San Pedro' – **Alto de la Alianza**	D2 ($D2^{9}$)	0.143	473
Tacna 2[d]	Colegio 'Enrique Paillardelle' – **Gregorio Albarracin**	D1 (D0 $D0^{25}$)	0.083	670
Tacna 3	Gas Station – **Ciudad Nueva**	D3 ($D1^{24}$ $D3^{6}$)	0.222	419
Tacna 4	La Bombonera Stadium – **Ciudad Nueva**	D3 ($D1^{24}$ $D3^{6}$)	0.250	409
Tacna 5	Soccer field – **Alto de la Alianza**	D3 ($D1^{7}$ $D2^{8}$ D0 ^{15} $D1^{19}$ $D1^{22}$)	0.222	452
Tacna 6	Colegio 'Hermogenes Arenas Yanez' – **Pocollay**	D1	0.077	625
Tacna 7	Colegio 'Coronel Bolognes' – **Downtown Tacna**	D1 ($D1^{14}$ $D1^{21}$ $D1^{23}$ $D1^{26}$ $D0^{32}$)	0.143	615

[a]Represents the average obtained from sites located near the testing sites, which were evaluated by Rodriguez-Marek et al. (2001). In parentheses are indicated damage indices for school buildings, superscript indicates the building in Table 5.8.
[b] Site Periods were obtained from the first peak of Fourier spectra ratios obtained from the site response analysis.
[c] Average shear wave velocity in the upper 30 m.
[d] This site had average shear wave velocity in the upper 25 m.

The criterion used to assign average damage indices was that used in Moquegua city (Section 5.2.3). The damage indices are based on Rodriguez-Marek et al. (2003) and are corroborated by Fernandez et al. (2001). The information extracted from Fernandez et al. (2001) was used in particular for Pocollay (Tacna 6), where no data was collected by the NSF team. Note that damage in school buildings (shown in parenthesis in Table 5.9) resembles the average damage indices assigned for each district. This is noteworthy because schools are designed and constructed with uniform standards. The exception is Tacna 5, where damage in surrounding buildings was higher than damage in the schools within the district.

The average of the acceleration time histories from the finite fault simulation (Silva 2004, see Figure 4.10), scaled to 0.1 g., was used as input motion in the equivalent linear program SHAKE91. Acceleration time histories at the ground surface were

obtained, and then their correspondent Response Spectra (Figure 5.19) as well as Ratios of Response Spectra (Figure 5.20) were calculated and plotted.

The spectral acceleration values (for select periods) at the surface of each of the sites listed in Table 5.9 are given in Table 5.10. These spectral acceleration values are compared to the damage measure indices determined by the NSF team (Figure 5.21).

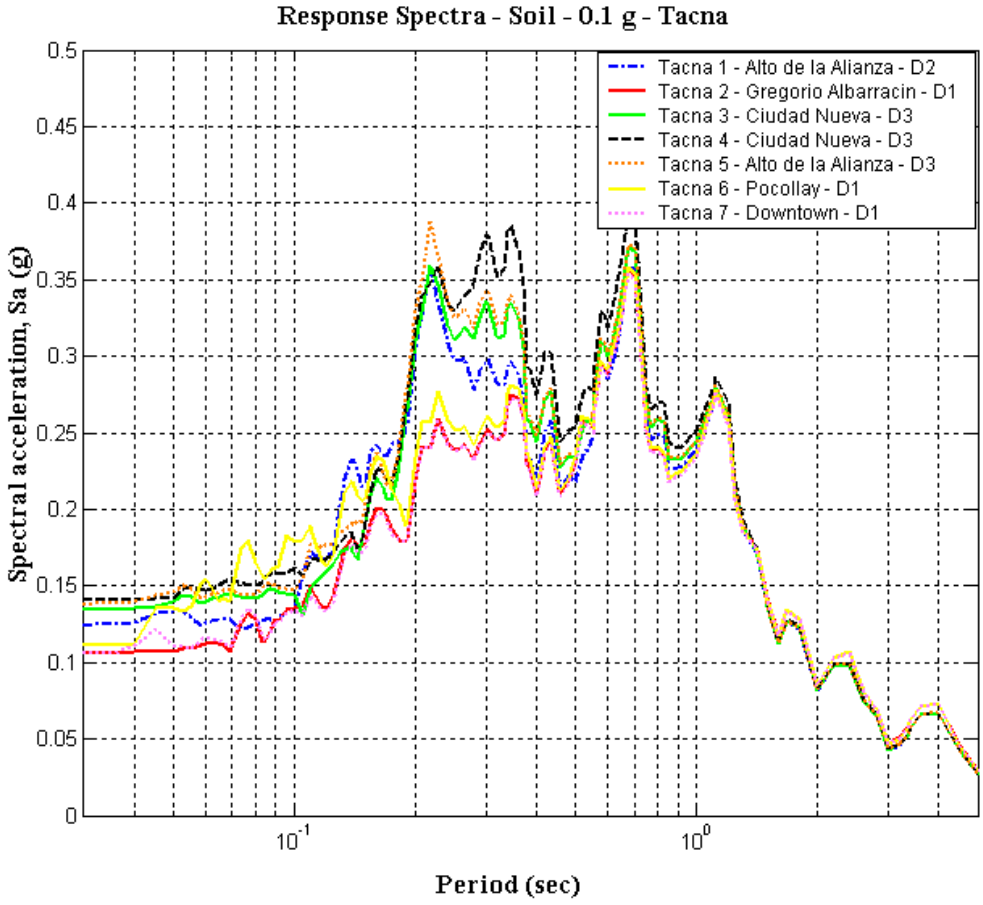

Figure 5.19 Response Spectra – 5% damping – Tacna city.

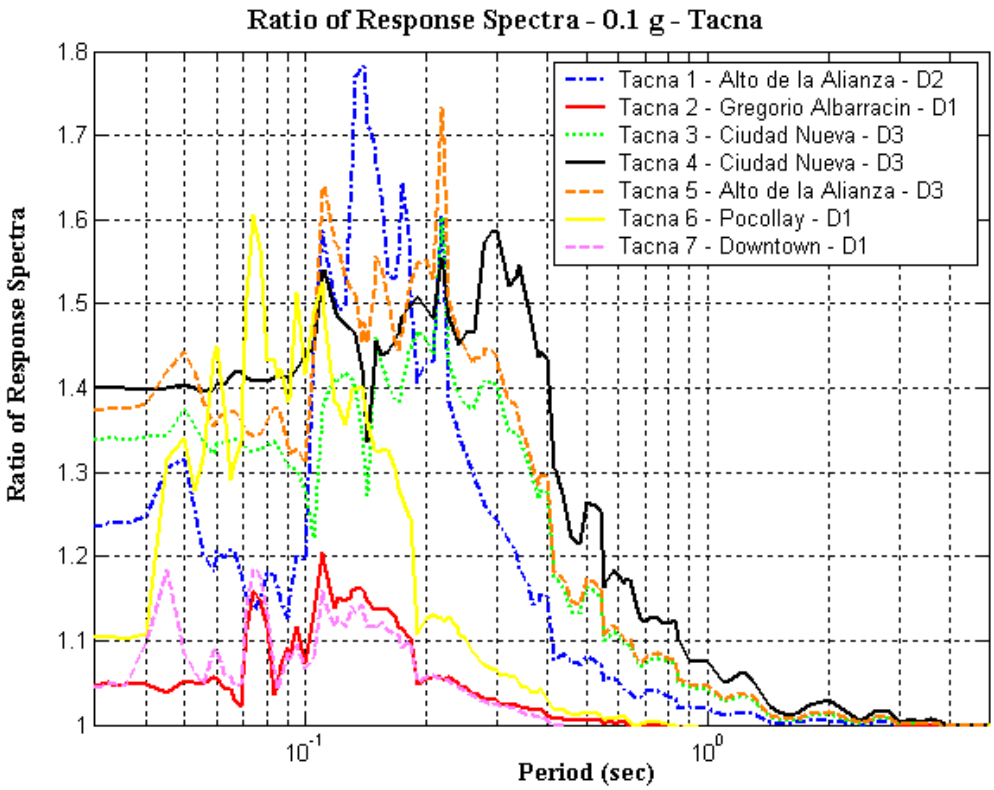

Figure 5.20 Ratio of Response Spectra – Accelerations scaled to 0.1 g. – Tacna city.

Table 5.10 Spectral acceleration at selected periods.

	Spectral Accelerations							
	PGA	**0.05 sec**	**0.1 sec**	**0.2 sec**	**0.3 sec**	**0.5 sec**	**1 sec**	**2 sec**
Tacna 1	0.12	0.13	0.13	0.31	0.30	0.22	0.24	0.08
Tacna 2	0.11	0.11	0.13	0.22	0.25	0.23	0.24	0.05
Tacna 3	0.13	0.14	0.14	0.31	0.34	0.23	0.24	0.04
Tacna 4	0.14	0.14	0.16	0.32	0.38	0.25	0.25	0.04
Tacna 5	0.14	0.15	0.15	0.33	0.34	0.24	0.24	0.04
Tacna 6	0.11	0.14	0.18	0.23	0.26	0.23	0.23	0.05
Tacna 7	0.10	0.11	0.13	0.22	0.25	0.23	0.23	0.08

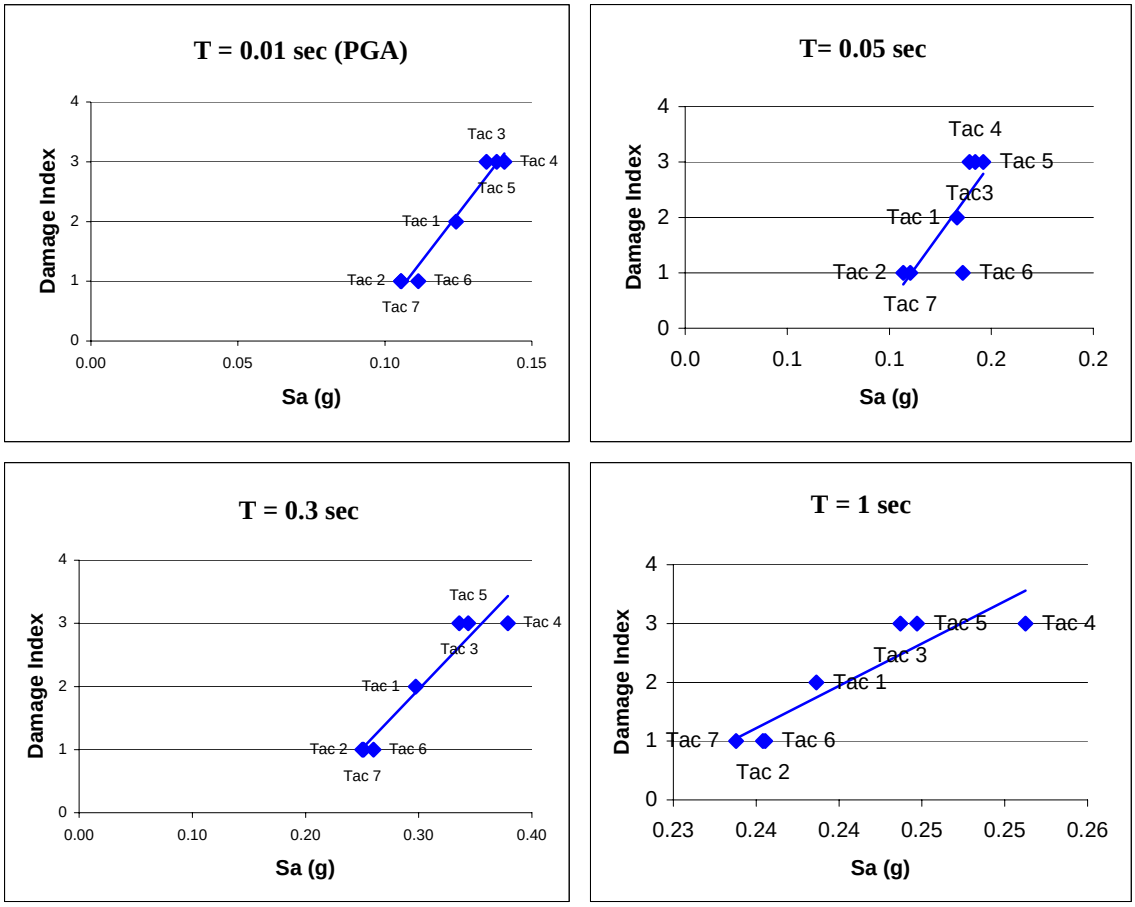

Figure 5.12 Correlation between damage level and spectral accelerations for certain periods.

Figures 5.10 and 5.12 indicate that site amplification, reflected in high ratios of response spectra, correlates well with observed damage. Sites 3,4,5 that are located in "Alto de la Alianza" and "Ciudad Nueva" districts, which are the districts with poorer soil conditions presented greater acceleration values and amplification ratios when compared to the ones obtained for sites 2, 6, and 7. This can be observed at almost all spectral periods, except for periods equal or greater than 2 seconds from which almost not amplification was produced in all cases. A notable exception is Tacna 1, which has high amplification but a damage index of only D2. The spectral amplifications for these sites occur only at low spectral periods. The Pocollay district (Tacna 6) also has low

damage with relatively high spectral amplification at low periods ranging from 0.04 to 0.2 seconds. This may imply that structures in the area were not affected significantly by amplifications in the high frequency region.

As was the case for Moquegua city, it is difficult to suggest general conclusions, however he believes that “Alto de la Alianza” and “Ciudad Nueva” evidenced the influence of site effects on the ground motions and damage levels. This influence is due to the presence of softer soils and, in some cases, the change in topography of those areas.

5.3.3 Conclusions regarding damage in the city of Tacna

The districts of Alto de la Alianza, Ciudad Nueva and Tacna suffered higher level of damages, while at the same time site response analyses indicated the potential for site amplification at these sites. The estimated amplification factors could be used as a guide for the design of future structures in these areas. As it was mentioned before for the city of Moquegua structural factors, such as quality of construction, had also significant effect on damages.

CHAPTER 6

CONCLUSIONS AND RECOMMENDATIONS

6.1 Summary

This study presented an analysis of site response in the 2001 Southern Peru earthquake. Specifically, the influence of site response on the recorded motions and on the damage in the cities of Tacna and Moquegua was studied by means of a comprehensive field investigation and a set of site response analyses. The field investigation included Spectral Analysis of Surface Waves (SASW) and Standard Penetration Tests (SPT), which were performed at different sites in the cities of Moquegua and Tacna. Profiles of shear wave velocity and other relevant soil properties were obtained for each site under study. These profiles were used in a detailed analysis of the ground motions recorded during the 2001 Southern Peru earthquake, including the evaluation of ground motion parameters. Site response analyses were then performed for the ground motion stations using the equivalent linear program SHAKE91. An evaluation of all the parameters that create uncertainty to the site response analysis was carried out using a Montecarlo approach. Different parameters were randomly varied for the different profiles and site response analyses were performed for the new set of profiles. Site response analysis for sites located in the cities of Tacna and Moquegua were also performed. These studies provided evidence of the influence of site effects in the ground motions throughout these cities. Finally, the correlation between damage distribution and the amplification of motion produced by site effects at the different sites was considered and evaluated. Districts with high concentration of damage were shown to be correlated with soil profiles producing higher levels of ground motion amplification.

6.2 Conclusions and recommendations

The main conclusions obtained in the present study are presented below. These conclusions are separated into conclusions regarding the recorded ground motions (Chapter 4) and conclusions regarding the correlation of damage and local soil conditions.

6.2.1 Site effects on recorded ground motions

The comparison of the recorded motions with attenuation relationships for subduction zone environments showed that the ground motion stations of Arica Casa and Arica Costanera presented PGA values significantly higher than those predicted by the attenuation relationships. Moreover, recorded ground motions were larger for these two stations than those recorded at Moquegua, which is significantly closer to the causative fault. This observation initially suggested the presence of site effects.

Ground motion parameters of the recorded motions were compared with predictions of attenuation relationships. Most of the recorded significant duration values were found to be around the mean value predicted by attenuation relationship, however, the significant duration estimated for Moquegua station was under predicted. For the case of Arias Intensity, current attenuation relationships generally underestimated the recorded values. This is not surprising given that the attenuation relationships do not include records from subduction zone earthquakes; however, this observation point to the need of determining similar relationships for this type of earthquakes. For frequency domain parameters, the comparison with attenuation relationships showed an over prediction of the predominant and mean square periods. Moreover, the trends observed in the values of

frequency domain parameters with distance are opposite to the predicted by the attenuation relationships.

The evaluation of the response spectra of the recorded motions showed that some of the stations (Moquegua, Arica Costanera, Arica Casa, Poconchile, and Cuya), presented a bimodal response spectrum, with one peak at short periods and another at longer periods. The longer period peak may reflect the influence of a deep impedance contrast, or possibly source effects. Finally, it was observed a significant dip in spectral accelerations for the three further sites for 2 seconds spectral period.

Site effects were quantified by means of the ratio of response spectra (RRS). Site response analyses using a suite of input motions generated from finite fault simulations (Silva 2004) indicated that the general shape of the RRS is generally independent of input motion while peak amplitudes of RRS (RRS_{max}) vary within a relatively small range. The average coefficient of variation for RRS_{max} is 0.043; this variation was considered to be relatively small compared with the potential range of RRS in soils. Amplifications were generally negligible beyond the natural period of each site.

The influence of the uncertainty in soil parameters that could not be measured in the SASW testing was studied using a Montecarlo simulation approach. Variations in input motion intensity resulted in the expected pattern for site response (a shift of peak response towards higher periods) . However, the variation in the amplitude and value of RRS due to input motion intensity were small compared with the variability due to the variation in input motions. Moreover, in most cases intensity of input motion did not have considerable influence in site response (i.e., on the RRS values). This implies that soil non-linearity is not a controlling parameter in site response estimates. The

randomization of other parameters for which there was uncertainty, such as soil non linearity and the depth to bedrock did not affect significantly the resulting RRS; on the other hand, the V_s of bedrock had an influence on the magnitude of the RRS. In general, RRS values were larger if V_s was allowed to vary from the values estimated from SASW to a value of 1000 m/s. this change did not affect the frequency of the RRS.

Bias was introduced in the analysis by incorporating the randomization of parameters that were not quantified with certainty in SASW testing. The bias was introduced because the randomization was not centered on the deterministic V_s profiles. The most significant bias introduced in the analysis resulted from the randomization of depth to bedrock. The additional depth to bedrock implied lower amplifications at low periods and higher amplifications at long periods. The randomization of the V_s of rock introduced a positive bias at all periods (e.g., higher values of RRS) for all sites but Arica Costanera.

The main conclusion from the present analysis is that local site conditions did play a role in amplifying short period motions. However, it is important to note that the site response analyses presented herein have some important limitations. The input motions may have energy at long periods that comes either from surface waves or from site effects due to deeper soil (or rock) layers at each recording station. This should not have a large effect on the results because the analyses are focused on the effect of the surficial layers. Even if the input motion had extra energy at long periods, the RRS at short periods should not be affected much by this energy. On the other hand, the presence of impedance contrast at a depth beyond that captured by the SASW analyses may

introduce resonances that are not captured by the site response analyses. Amplification at periods longer than the site characteristic period is beyond the capability of the analysis.

Values of RRS obtained in the site response analysis compare well with site amplification factors proposed Rodriguez-Marek et al. (2001). This supports the contention that site amplification for UBC sites currently include levels of non-linearity that are markedly large.

6.2.2 Correlation of site effects with observed damage

The site response analysis of sites located in the critical areas indicated some correlation between site effects and observed damage in the cities of Tacna and Moquegua. Additionally, construction quality and materials played a significant role in the observed damage levels. It was observed that adobe-built houses performance during the earthquake was poor, also some specific areas in both cities presented unexpected damage levels. However, since construction quality was assumed to be consistent throughout both cities, the observed correlation between damage distribution and site effects is considered valid.

Moquegua City

Larger spectral acceleration values for most spectral periods were obtained in site response analyses for sites located in San Francisco district, which is the district that presented higher damage levels. Also for most spectral periods, higher values of spectral acceleration produced correspond to higher levels of observed earthquake damage. This tendency was more evident for T = 1 second. The exceptions to this trend and the limitations implicit in the determination of damage levles are discussed in Chpater 5. In addition, it was evident that one-dimensional site response alone predicted significant

difference in site amplification in a hillside in the San Francisco district in Moquegua where damage was concentrated on the hillside slopes. Previous observations attributing topographic effects to the damages observed may have to be reviewed.

Tacna City

Site amplification, reflected in high ratios of response spectra, correlated well with observed damage in the city of Tacna. Sites located in the "Alto de la Alianza" and "Ciudad Nueva" districts experienced high damage levels during the earthquake and presented greater amplification ratios when compared to the other sites in the city. This correlation could be observed at almost all spectral periods, except for periods equal or greater than 2 seconds from which almost not amplification was produced in all cases. The spectral amplifications for these sites occur only at low spectral periods. The Pocollay district also had low damage with relatively high spectral amplification at low periods. This may imply that structures in the area were not affected significantly by amplifications for very high frequencies (f > 10Hz).

Frequency content may also have influenced damage distributions. Sites located in "Alto de la Alianza" and "Ciudad Nueva presented greater spectral acceleration values when compared to the ones obtained at other sites, with the highest amplification in a period band from T=0.1 to T=0.3. On the other hand, amplification at other sites occured in a period band between T=0.04 to T=0.1 sec. These results show a notorious influence of soils in the performance of buildings for the different districts.

6.3 Recommendations for future study

As it is usually the case with research work, several topics where further study is needed were identified at the conclusion of this research. These topics are:

- Attenuation relationships for Duration, Arias Intensity, and frequency domain ground motion parameters should be developed for subduction zone environments.
- Damage in adobe construction correlated well with damage in other types of structures for the cities of Tacna and Moquegua. This indicates that such structures could also be used as indicators of ground motion intensity. Such practice was usually not recommended suggesting that the high vulnerability of adobe structures to damage renders them inappropriate for evaluating site response.

In addition, the conclusions presented in the study regarding site amplification effects in the cities of Tacna and Moquegua could be strengthened by incorporating a montecarlo simulation approach similar to that used in Chapter 4. Moreover, the Montecarlo analysis incorporated only ad-hoc measures of uncertainty for soil parameters. Further study is needed to properly quantify these uncertainties.

REFERENCES

Abou-matar, H., and Goble, G. G.(1997). “SPT Dynamic Analysis and Measurements.” Journal of Geotechnical and Geo-environmental Engineering , 1997/921.

Abrahamson, N.A., and Shedlock, K.M. (1997). “Overview (of modern attenuation relationships).” Seism. Res. Letters, 68(1), 9-23.

Abrahamson, N.A., and Silva, W.J. (1997). “Empirical response spectral attenuation relations for shallow crustal earthquakes.” Seism. Res. Letters, 68(1), 94-127.

Ashford, S.A., Sitar, N., Lysmer, J., and Deng, N. (1997). “Topographic Effects on the Seismic Response of Steep Slopes.” Bull. Seism. Soc. Am., 87, 701-709.

Arias, A. (1970). “A measure of earthquake intensity.” in Seismic Design for Nuclear Power Plants, R.J. Hansen, ed., MIT Press, Cambridge, MA, 438-483.

Atkinson, G.M., and Boore, D.M. (2003). “Empirical Ground-Motion Relations for Subduction-Zone Earthquakes and Their Application to Cascadia and Other Regions." Bull. Seism. Soc. Am. 93(4) 1703-1729.

Atkinson, G.M., and Silva, W.J. (1997). “An empirical study of earthquake source spectra for California earthquakes.” Bull. Seism. Soc. Am. 87, 97-113.

Bard P.Y., and Gariel, J.C. (1986). “ The seismic response of two-dimensional sedimentary deposits with large vertical velocity gradients.” Bull. Seism. Soc. Am 76, 343-366.

Bard, P.Y. (1999) “ Microtremor measurements: A tool for site effect estimation?.” The Effects of surface geology on seismic motion, Irikura, Kudo, Okada & Sasatani (ed.), Rotterdam, ISBN 90 5809030 2.

Bard, P.Y. (1995). “Effects of surface geology on ground motion: recent results and remaining issues.” Proc. 10th European Conference on Earthquake Engineering, Duma (ed.), Rotterdam,305-323.

Bardet, J.P., Ichii, K., and Lin, C.H. (2000) “A Computer Program for Equivalent-linear Earthquake site Response Analyses of Layered Soil Deposits.” University of Southern California, Department of Civil Engineering.

Boatwright, J., and Seekins, L. C. (1997). "Response Spectra from the 1989 Loma Prieta, California, Earthquake Regressed for Site Amplification, Attenuation, and Directivity." U.S. Geological Survey, MS 977, Menlo Park, CA.

Bolt, B.A. (1969). “Duration of strong motion.” Proc. 4th World Conf. Earthquake Engrg.,Santiago, Chile, 1304-1315.

Boore, D. M., Harmsen S. C., and Harding, S. T. (1981).”Wave scattering from a step chance in surface topography.” Bull. Seism. Soc. Am, 71, 117-125.

Boore, D. M., Joyner, W. B., and Fumal, T. E. (1997). "Equations for Estimating Horizontal Response Spectra and Peak Acceleration from Western North American Earthquakes: A Summary of Recent Work." Seismological Research Letters, Vol. 68(1), pp. 128-153Borcherdt, R. D. (1994). "Estimates of Site-Dependent Response Spectra for Design (Methodology and Justification)." Earthquake Spectra, Vol. 10(4), pp. 617-653.

Borcherdt, R. D. (1994). "Estimates of Site-Dependent Response Spectra for Design (Methodology and Justification)." Earthquake Spectra, Vol. 10(4), pp. 617-653.

Borcherdt, R.D., and Glassmoyer, G. (1994). “Influences of local geology on strong and weak ground motions recorded in the San Francisco Bay region and their implications for site-specific building-code provisions.” The Loma Prieta, California Earthquake of October 17, 198—-Strong Ground Motion, U. S. Geological Survey Professional Paper 1551-A, A77-A108

Borcherdt, R.D. (1996). “Preliminary amplification estimates inferred from strong ground motion recordings of the Northridge earthquake of January 17, 1994.” Proc., Int. Workshop on Site Response Subjected to Strong Ground Motion, Vol. 1, Port and Harbor Research Institute, Yokosuka, Japan.

Borcherdt, R. D. (2002). “Empirical evidence for acceleration-dependent amplification factors.” Bull. Seism. Soc. Am., 92, 761–782.

Borcherdt, R. D. (2002). "Empirical Evidence for Site Coefficients in Building Code Provisions." Earthquake Spectra, 18(2), 189-217.

Boroschek, R., Soto, P., Leon, R. (2001) “Registros en el norte de Chile, terremoto del sur de Peru, 23 de Junio de 2001 Mw=8.4.” Universidad de Chile, Informe RENADIC 01 / 04.

Bouckovalas G.D., Gazetas G., and Papadimitriou A.G. (1995) “Geotechnical aspects of the 1995 Aegion (Greece) earthquake.” National Technical University of Athens, Greece.

Bouckovalas G.D., and Kouretzis G.P. (2001) “Review of soil and topographic effects in the September 7, 1999 Athens (Greece) earthquake.” Proceedings: Fourth international conference on recent advances in geotechnical earthquake engineering and soil dynamics and symposium in honor of professor William Finn. San Diego, California.

Bouckovalas G.D., and Papadimitriou A.G. (2004) “Numerical evaluation of slope topography effects on seismic ground motion.” SDEE/ICEGE.

Bray, J.D., Seed, R.B., Cluff, L.S., and Seed, H.B. (1994) “Earthquake fault rupture propagation through soil.” J. Geotech. Engrg., ASCE, 120(3), 543-561.

Camara Peruana de la Construccion (CAPECO), (1997). “ Normas Basicas de Diseño Sismo-Resistente.” Lima, Peru.

Chang, S.W., Bray, J.D., and Seed, R.B. (1996). “Engineering implications of ground motions from the Northridge earthquake.” Bull. Seism. Soc. Am., 86, S270-S288.

CISMID, (2001). “Record of the June 23, 2001, Ocona earthquake (Ms 8.1): Moquegua station.” Centro Peruano Japones de Investigaciones Sismicas y Mitigacion de Desastres. National Engineering University, Civil Engineering Department.

Coburn, A., and Spence, R. (1992). Earthquake Protection. West Sussex, England John Wiley & Sons.

Coduto D.P. (2001). Foundation Design Principles and Practices, 2nd Ed., Upper Saddle River, New Jersey.

Cornell, C.A. (1968). “Engineering seismic risk analysis.” Bull. Seism. Soc. Am., 58, 1583-1606.

Cotrado-Flores, D., Sina-Calderon, Y.M. (1994). “Microzonificacion sismica de la ciudad de Tacna.” Thesis. Universidad privada de Tacna. Facultad de Ingenieria Civil.

Crouse, C.B., and McGuire, J. W. (1996). "Site response studies for purpose of revising NEHRP seismic provisions." Earthquake Spectra, 12, 407-439.

Darendeli B.M. (2001). Development of a new family of normalized modulus reduction and material damping curves. Doctoral dissertation, University of Texas at Austin.

Dobry, R., Borcherdt, R.D., Crouse, C.B., Idriss, I.M., Joyner, W.B., Martin, G.R., Power, M.S., Rinne, E.E., and Seed, R.B. (2000). "New site coefficients and site classification system used in recent building seismic code provisions." Earthquake Spectra, 16(1), 41-67.

Dobry, R., and Idriss, I.M. (1978). "Duration characteristics of horizontal components of strong motion earthquake records." Bull. Seism. Soc. Am., 68(5), 1487 – 1520.

Dobry, R., Martin, G.M., Parra, E., and Bhattacharyya, A. (1994). "Development of site-dependent ratios of elastic response spectra (RRS) and site categories for building seismic codes." Proceedings of the NCEER/SEAOC/BSSC workshop on site response during earthquakes and seismic code provisions, University of Southern California, Los Angeles, November 18-20.

Dobry, R., Ramos, R., and Power, M.S. (1997). "Site Factors and Site Categories in Seismic Codes: A Perspective." In Proceedings of the FHWA/NCEER Workshop on the National Representation of Seismic Ground Motion for New and Existing Highway Facilities, Technical Report NCEER-97-0010. Friedland, I. M., Power, M. S., and Mayes, R. L., Eds.

Electrical Power Research Institute, EPRI (1993). "Guidelines for determining design basis ground motions. Volume 1: Method and guidelines for estimating earthquake ground motion in eastern North America." Rpt. No. EPRI TR-102293, Palo Alto, CA.

Fernandez, E., Aguero, C., Ccallo, F., Heras, H., Carpio, J., Jullca, A. (2001). "Intensidades Macrosismicas de las ciudades de Arequipa, Moquegua y Tacna", CNDG.

Field, E.H., and Jacob, K.H. (1995). "A comparison and test of various site-response estimation techniques, including three that are not reference-site dependent." Bull. Seism. Soc. Am., 85, 1127-1143.

Finn, W. D. L. (1991) "Geotechnical aspects of microzonation." Proceedings, 4th Int. Conference On Seismic Zonation; Vol. 4, 199-259.

Frankel, A., Mueller, C. S. (2000). “USGS National Seismic Hazard Maps.” Earthquake Spectra 16(1): 1-19.

Gazetas, G., Kallou P. V., and Psarropoulos P. N. (2002). “Topography and soil effects in the M (sub s) 5.9 Pharnita (Athens) earthquake; the case of Adames.” Kluwer Academy Publishers, Dordrechet, Netherlands., 27 (1,2) 133-169.

Graves, R.W., Pitarka, A., and Somerville, P.G. (1998). “Ground motion amplification in the Santa Monica area: effects of shallow basin edge structure.” Bull. Seism. Soc. Am., 88, 1224-1242.

Hall, J.F. (1995). “Northridge Earthquake Reconnaissance Report.” Vol. 1 Supplement C to volume 11.

Hardin, B.O. (1978). "The nature of stress-strain behavior of soils." Earthquake Engineering and Soil Dynamics, ASCE, 1, 3-90.

Imai, T., and Tonouchi, K. (1982). "Correlation of N-value with S-wave velocity and shear modulus." Proceedings 2nd European Symposium on Penetration Testing, Amsterdam, 57-72.

Idriss, I. M. (1985). "Evaluating seismic risk in engineering practice." Proceedings of the 11th International Conference of Soil Mechanics and Foundation Engineering, San Francisco, CA, Vol. 1, pp. 255-320.

Idriss, I.M. (1990). “Response of soft soil sites during earthquakes.” Proc. H. Bolton SeedMemorial Symposium, J.M. Duncan (ed.), Vol. 2, 273-290.

Idriss, I.M. (1991). “Procedures for selecting earthquake ground motions at rock sites.” Report to U.S. Department of Commerce, revised 1993.

Idriss, I.M., and Sun, J.I. (1992). “SHAKE91: A computer program for conducting equivalentlinear seismic response analyses of horizontally layered soil deposits.” Center for Geotech. Modeling, Univ. of California, Davis.

Jacob K. H., Gariel, J. C., Armbruster, J., Hough, S., Friberg, P., Tuttle, M. (1990). “Site specific ground motion estimates from New York City.” Earthquake Engineering Research Institute, Oakland, CA, USA., 4 (1), 587-596.

Joyner, W.B., Warrick, R.E., and Fumal, T.E. (1981). “The effect of Quaternary alluvium on strong ground motion in the Coyote Lake, California earthquake of 1979.” Bull. Seism. Soc. Am., 71, 1333-1349.

Joyner, W.B., and Boore, D.M. (1994). “Errata: Method for regression analysis of strong motion data.” Bull. Seism. Soc. Am., 84, 955-956.

Konagai, K., Meguro, K., Koseki, J., Ohi, K., Sato, H., Koshimura, J., Estrada, M., Johansson, M., Mayorca, P., Guzman, R., Kimura. T. (2001).“Provisional Report of the June 23, 2001 Atico Earthquake, Peru”.

Kosaka-Masuno, M., Gonzales-Zenteno, E., Arias-Barahona, H., Minaya-Lizarraga, A., Faran-Bazan, E., Ticona-Paucara, J. (2001). “Seismic Hazard Evaluation in the city of Moquegua.” Convenio UNSA-INDECI. Proyect PER 98/018 PNUD-INDECI, San Agustin de Arequipa National University, Arequipa, Peru.

Kramer, S.L. (1996). Geotechnical Earthquake Engineering, Prentice Hall, Upper Saddle River, NJ.

Lanzo, G., and Vucetic, M. (1999). "Effect of soil plasticity on damping ratio at small cyclic strains." Soils and Foundations, 39(4) 131-141.

Leyendecker, E. V., Hunt, J. R. (2000). “Development of maximum considered earthquake ground motion maps.” Earthquake Spectra 16(1): 21-40.

Liao, S.C., Whitman, R.V. (1986). “Overburden correction factors for SPT in sand.” Journal of Geotechnical Engineering, 112 (3), 373-377.

Martin, P.P., and Seed, H. B. (1982). “One dimensional dynamic ground response analyses.” Journal of Geotechnical Engineering Division, ASCE, 108(7), 935-952.

Martin, G.M., editor (1994). Proceedings of the NCEER/SEAOC/BSSC Workshop on Site Response During Earthquakes and Seismic Code Revisions, University of Southern California.

Mohraz, B. (1976). "Earthquake response spectra for different geologic conditions.” Bull. Seism. Soc. Am., 66, 915-935.

Ocola, L. (1979). " Peru." Department of Energy, Mines and Resources Ottawa, ON, Canada., 4 (3), 189-190.

Okawa, I., Iiba, M., Midorikawa, M., Koyama, S., Mura, K. (2001). " Soil amplification factor for seismic design of buildings." Wind and seismic effects proceedings of the 32nd joint meeting of the U.S. – Japan Cooperative Program in Natural Resources, NIST Special Publication. 963; pp. 195-201.

Park, K. (2004). Shear wave velocity profiling at sites affected by the 2001 southern Peru Earthquake. Master thesis, Utah State University.

Pacific Earthquake Engineering Database (PEER) <http://peer.berkeley.edu/smcat> (March. 15, 2004)

Paredes-Chacon, C. (2001). "Estudio Mapa de Peligros de la ciudad de Tacna." CONVENIO UNJBG – INDECI – PNUD PER 98/018.

Pedersen, H.A., Le Brun, B., Hatzfeld, D., Campillo, M., and Bard, P.Y. (1994). "Ground motion amplification across ridges." Bull. Seism. Soc. Am., 84, 1786-1800.

Rathje, E.M., Abrahamson, N.A., and Bray, J.D. (1998). "Simplified frequency content estimates of earthquake ground motions." Journal of Geotechnical and Geoenvironmental Engineering, ASCE, 124(1), 150-159.

Rathje, E.M., Stokoe, K.H.II., Rosenblad, B. (2003). "Strong Motion Station Characterization and site effects during the 1999 earthquakes in Turkey." Earthquake Spectra, Volume 19, No3, pages 653-675.

Repetto, P., Arango, I., and Seed, H.B., (1980). "Influence of site characteristics on building damage during the October 3, 1974 Lima-Peru Earthquake". Report No UCB/EERC-80/41 September 1980, University of California at Berkeley.

Rodriguez-Marek, A., Bray, J.D., and Abrahamson, N. (2001). "An Empirical Geotechnical Seismic Site Response Procedure." Earthquake Spectra, 17(1), p. 68-88.

Rodriguez-Marek A., and Edwards, C. (2003). "2001 Peruvian Earthquake Reconnaissance Report." Earthquake Spectra, V.19A.

Rosset, P., De la Puente, A., Chouinard, L., Mitchell, D., and Adams, J., “Site effect assessment at small scales in urban areas: a tool for preparedness and mitigation.” Macdonald Eng. Building, 817 Sherbrooke Street West, Montreal, Quebec, H3A2K6. e-mail:rossetph@hotmail.com.

Salas, L. (2002). “Zonificacion geotecnica sismica de la ciudad de Moquegua.” Universidad Privada de Tacna.

Schnabel, P.B., Lysmer, J., and Seed, H.B. (1972). SHAKE: A computer program for earthquake response analysis of horizontally layered sites, Rpt. No. EERC 72/12, Earthquake Engineering Research Center, Univ. of California, Berkeley.

Seed, H.B., Idriss, I.M., and Kiefer, F.W. (1969). "Characteristics of rock motions during earthquakes." Journal of the Soil Mechanics and Foundation Division, ASCE, 95(SM5) 1199-1218.

Seed, H.B., and Idriss, I.M. (1969). “ The influence of soil conditions on ground motions during earthquakes.” Journal of the soil mechanics and foundation engineering division, ASCE, No. 94,93-137.

Seed, H.B., and Idriss, I.M. (1982). Ground Motions and Soil Liquefaction During Earthquakes, Earthquake Engineering Research Institute, Berkeley, California, 134 pp.

Seed, H.B., Ugas, C., and Lysmer, J. (1976). “Site-dependant spectra for earthquake resistant design.” Bull. Seism. Soc. Am., 66, 221-243.

Seed, H.B., Wong, R.T., Idriss, I.M., and Tokimatsu, K. (1986). “Moduli and damping factors for dynamic analyses of cohesionless soils.” J. Geotech. Engrg., ASCE, 112 (11), 1016-1032.

Seed, H. B., and Idriss, I. M. (1970). "Soil moduli and damping factors for dynamic response analyses." Univ. of California, Berkeley, EERC report No. EERC 70-10 (reproduced in H. B. Seed, Vol. 1, Selected papers 1956-1987, BiTech Publishers, Vancouver, B. C., 1990).

Seed, R.B., Chang, S.W., Bray, J.D. (1994). “Ground motions and local site effects.” Report - Earthquake Engineering Research Center, College of Engineering, University of California, Berkeley. Pages 19-69. 1994.

Silva, W.J., Abrahamson, N., Toro, G., and Costantino, C. (1997). Description and validation of the stochastic ground motion model, Report to Brookhaven National Laboratory, Associated Universities, Inc., Upton, NY.

Silva, W.J., Li, S., Darragh, R., and Gregor, N. (1999). Surface geology based strong motion amplification factors for the San Francisco Bay and Los Angeles areas, Report to Pacific Earthquake Engineering Research Center.

Silva, W.J. (2004). Personal communication.

Stepp, J.C., and Wong, I. (2001). “Probabilistic seismic hazard analyses for ground motions and fault displacement at Yucca Mountain, Nevada.” Earthquake Spectra 17(1): 113-149.

Stewart, J.P., Chiou, S.J., Bray, J.D., Somerville, P.G., Graves, R.W., and Abrahamson, N.A. (2001). "Ground motion evaluation procedures for performance based design." Rpt. No. PEER-2001/09, Pacific Earthquake Engineering Research Center, University of California, Berkeley, 229 pgs.

Stewart, J.P., and Baturay, M.B. (2001). “Uncertainties and residuals in ground motion estimates at soil sites.” Proc. 4th Int. Conf. Recent Advances in Geotech. Eqk. Engrg. Soil Dyn., San Diego, CA. Paper 3.14.

Stewart, J.P., Liu, A.H., and Choi, Y. (2003). "Amplification Factors for Spectral Acceleration in Tectonically Active Regions." Bull. Seism. Soc. Am., Vol 93(1), 332-352.

Stewart, J.P., and Sholtis, S.E. (2004). "Case study of strong ground motion variations across cut slope." Proc. 11th Int. Conf. Soil Dyn. Earthquake Engrg. & 3rd Int. Conf. Earthquake Geotech. Engrg., D. Doolin, A. Kammerer, T. Nogami, R.B. Seed, and I. Towhata (ed.), Berkeley, CA, Vol. 1, 917-922.

Stewart, J.P., and Baturay M.B. (2003). “Uncertainty and bias in ground motion estimates from ground response analyses.” Bull. Seism. Soc. Am., Vol 93, No5.

Stokoe, K.H., Wright, S.G., Bay, J.A., and Roesset, J.M. (2000). “Characterization of Geotechnical Sites by SASW method.” University of Texas at Austin.

Stokoe, K.H., Bay, J.A., Redpath, B., Diehl, J.G., Steller, R.A., Wong, I., Thomas, P., Luebber, M. (1995). “Comparison of Vs profiles from three seismic methods at Yucca Mountain.” University of Texas at Austin.

Sun, J.I., Golesorkhi, R., and Seed, H.B. (1988). "Dynamic Moduli and Damping Ratios for Cohesive Soils." Report No. UCB/EERC-88/15, Earthquake Engineering Research Center, College of Engineering, University of California, Berkeley, California.

Travasarou, T., Bray, J.D., and Abrahamson N.A. (2003). “Empirical attenuation relationship for Arias Intensity.” Earthquake Engineering and Structural Dynamics. 32(7), 1133-1155.

Trifunac, M.D. (1973). “Scattering of SH waves by a semi cylindrical canyon.” Earthquake Engrg. Struct. Dyn., 1(3), 267-281.

United States Geological Survey (USGS) Database (2003) <http://www.usgs.gov>

UBC, Building Seismic Safety Council (BSSC), (1994), “Edition NEHRP Recommended Provisions for Seismic Regulations for New Buildings.” Federal Emergency Management Agency.

UBC, Building Seismic Safety Council (BSSC), (1997), “Edition NEHRP Recommended Provisions for Seismic Regulations for New Buildings.” Federal Emergency Management Agency.

Vucetic, M., and Dobry, R. (1991). “Effect of soil plasticity on cyclic response.” Journal of Geotechnical Engineering, ASCE 117(1): 89-107.

Wells, D.L., and Coppersmith, K.J. (1994). “New empirical relationships among magnitude, rupture length, rupture width, rupture area, and surface displacement.” Bull. Seism. Soc. Am., 84(4): 974-1002.

Wong, H.L., and Trifunac, M.D. (1974). “Scattering of plane SH waves by a semi-elliptical canyon.” Earthquake Engineering Struct. Dyn., 3(2), 157-169.

Youd, L.T., Bardet, J.P., Bray, J.D., (1999). “Kocaeli, Turkey, Earthquake Reconnaissance Report.” Supplement A to volume 16. December 2000.

Youngs, R.R., Silva, W.J. (1997). “Strong ground motion attenuation relationships for subduction zone earthquakes.” Seismological Research Letters 1997(1): 58-73.

Blank Page

Blank Page

APPENDIX A

FIELD TESTING RESULTS

Testing results

Arica sites

The city of Arica, in Chile, is located 19 km south of the border between Chile and Peru. SASW testing was performed at three out of six strong motion stations that recorded the 2001 Peruvian earthquake. Testing was also performed at three other strong motion station sites that did not record the ground motion.

Cerro La Cruz

The testing site is located on a large unpaved vacant lot, one block southwest from the school named Cerro La Cruz, which has a strong motion instrument.

The latitude and longitude coordinates on the testing site are 18.49469° south and 70.31217° west, respectively. A plan view of the site is shown in Figure A.1. A photograph of the testing site is exposed in Figure A.2. The shear wave velocity profile at the site is presented in Figure A.3. Tabulated values of shear wave velocity and assumed layer properties used in forward modeling are presented in Table A.1. This site is underlain by fairly uniform material with a shear wave velocity of about 1100 m/s. Average shear wave velocity in the upper 30 m, V_{S30}, at this site is 1132 m/s and the site is classified as site class S_B, from the Uniform Building Code (UBC).

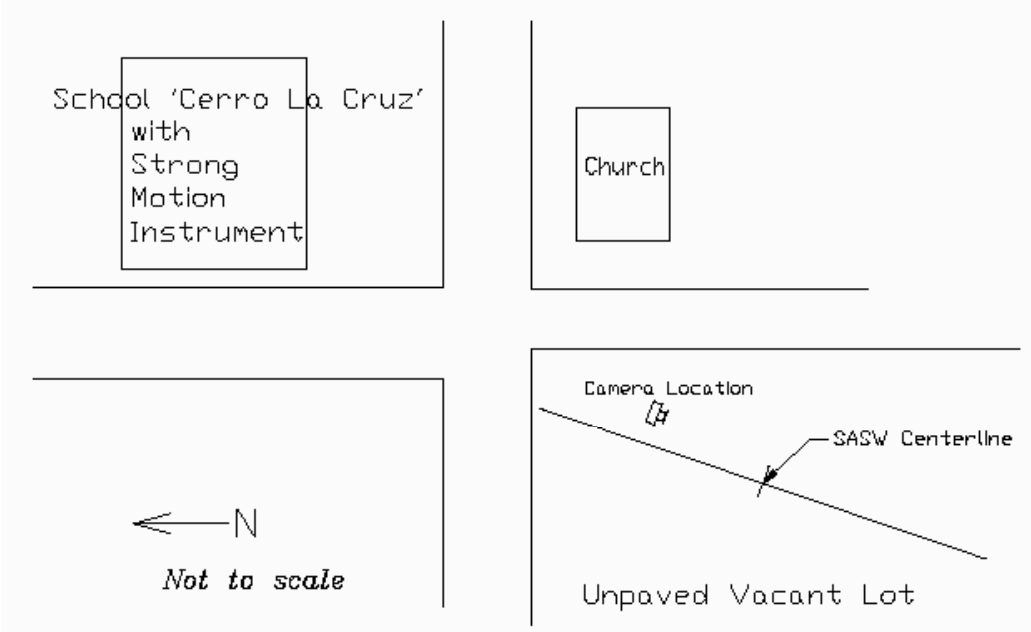

Figure A.1 A plan view of SASW testing site located on block southwest from the school "Cerro La Cruz school site"

Figure A.1 Photograph of SASW testing at site of Cerro La Cruz

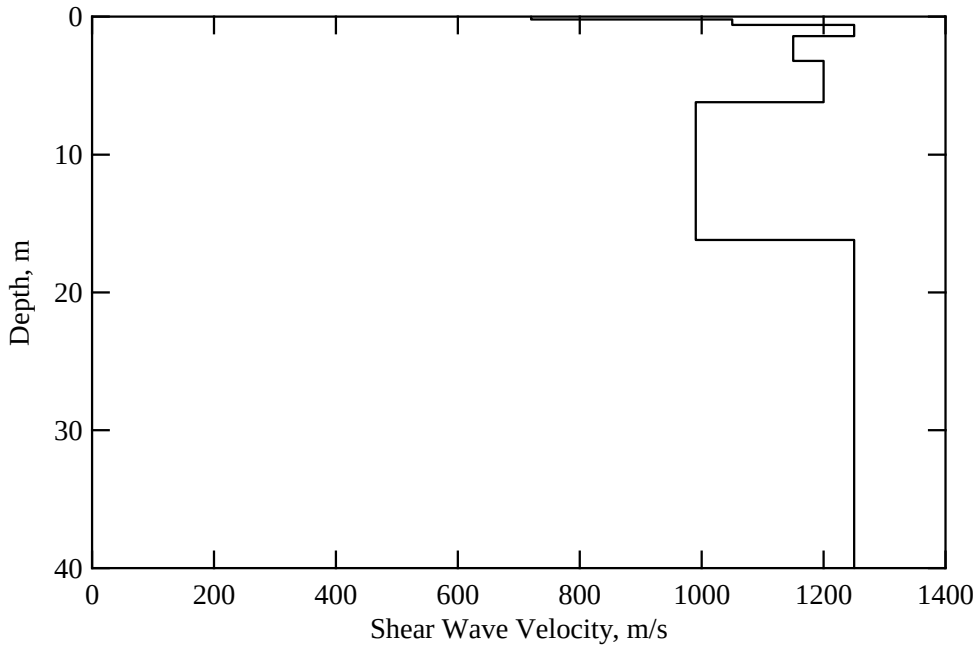

Figure A.3 Shear wave velocity profile determined from forward modeling at Cerro La Cruz site

Table A.1 Tabulated Values of Measured and Assumed Layer Properties at Cerro La Cruz Site

Depth to Top Layer, m	Layer Thickness, m	Shear Wave Velocity, m/s	P-wave Velocity, m/s	Poisson's Ratio	Mass Density g/cc
0.0	0.2	720	1347	0.3	2.10
0.2	0.4	1050	1964	0.3	2.25
0.6	0.8	1250	2339	0.3	2.25
1.4	1.8	1150	2152	0.3	2.25
3.2	3.0	1200	2339	0.3	2.25
6.2	10.0	990	1852	0.3	2.10
16.2	23.8	1250	2339	0.3	2.25

Juan Noe Greviani Hospital

The testing site is located on the small and unpaved parking lot of Juan Noe Greviani Hospital, and has a strong motion instrument. The latitude and longitude coordinates on the testing site are 18.49469° south and 70.31417° west, respectively. A

plan view of the site is shown in Figure A.4. A photograph of this site is presented in Figure A.5.

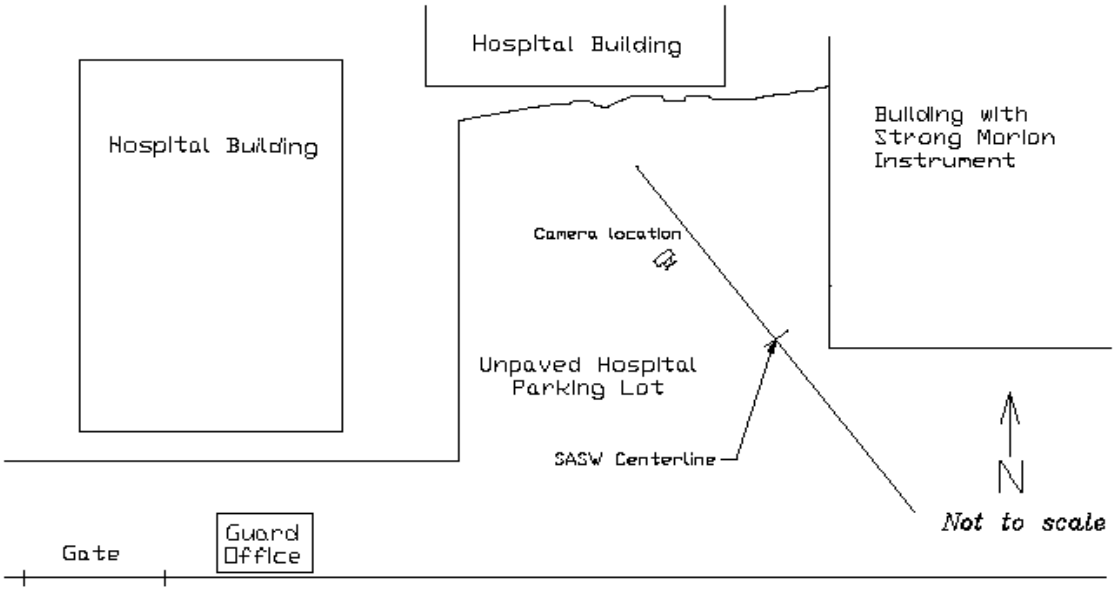

Figure A.4 A plan view of SASW testing site located in the Juan Noe Greviani hospital parking lot.

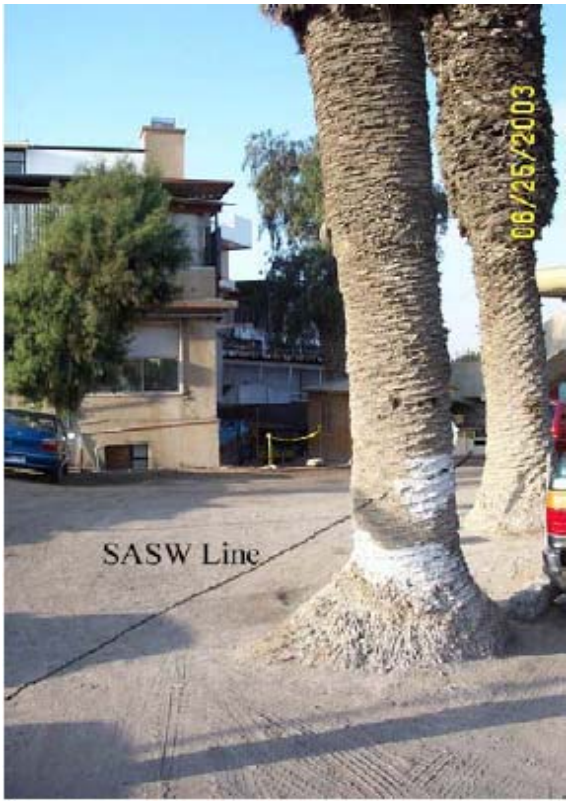

Figure A.5 Photograph of SASW testing site of Juan Noe Greviani Hospital

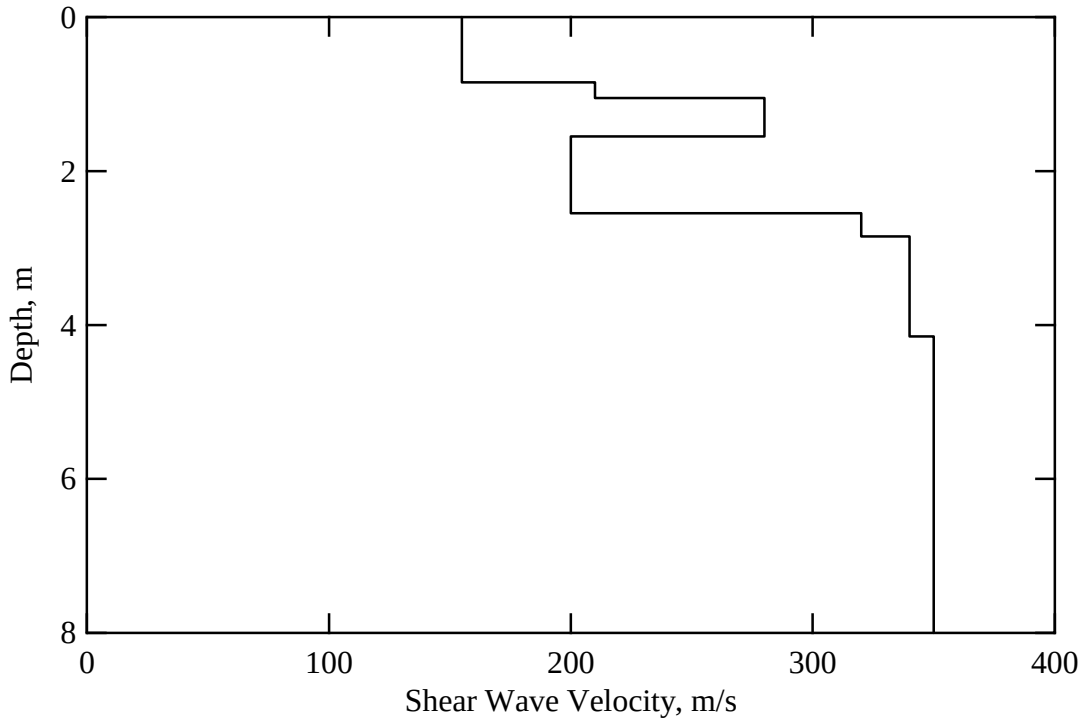

Figure A.6 Shear wave velocity profile determined from forward modeling at Juan Noe Greviani Hospital site

Table A.2 Tabulated Values of Measured and Assumed Layer Properties at Juan Noe Greviani Hospital site.

Depth to Top Layer, m	Layer Thickness, m	Shear Wave Velocity, m/s	P-wave Velocity, m/s	Poisson's Ratio	Mass Density g/cc
0.00	0.85	155	290	0.3	1.8
0.85	0.20	210	393	0.3	1.8
1.05	0.50	280	524	0.3	1.8
1.55	1.00	200	374	0.3	1.8
2.55	0.30	320	599	0.3	1.8
2.85	1.30	340	636	0.3	1.8
4.15	3.85	350	655	0.3	1.8

The shear wave velocity profile at the site is detailed in Figure A.6. Tabulated values of shear wave velocity and assumed layer properties used in forward modeling are presented in Table A.2. Here, since testing was performed in very small and busy hospital parking lot, the resolution of this site (around 8 m deep) is not deep enough due to the

short wavelength. Average shear wave velocity in the upper 30 m, V_{S30}, at this site was not calculated because of the low resolution of the profile.

Arica Costanera

The testing site is located on the parking lot of the University of Tarapaca whose soil lab has a strong motion instrument. The latitude and longitude coordinates on the testing site are 18.47382° south and 70.31342° west, respectively. A plan view of the site is shown in Figure A.7. A photograph of this site with the soil lab in the university is exposed in Figure A.8. The shear wave velocity profile at the site is presented in Figure A.9. Tabulated values of shear wave velocity and assumed layer properties used in forward modeling are presented in Table A.3. This site apparently presents a thin soft layer close to the surface, stiff materials from the depth of around 36 m, and thick and fairly uniform materials between those two layers. V_{S30}, at this site is 389 m/s and this site is classified as a site class S_C from uniform building code.

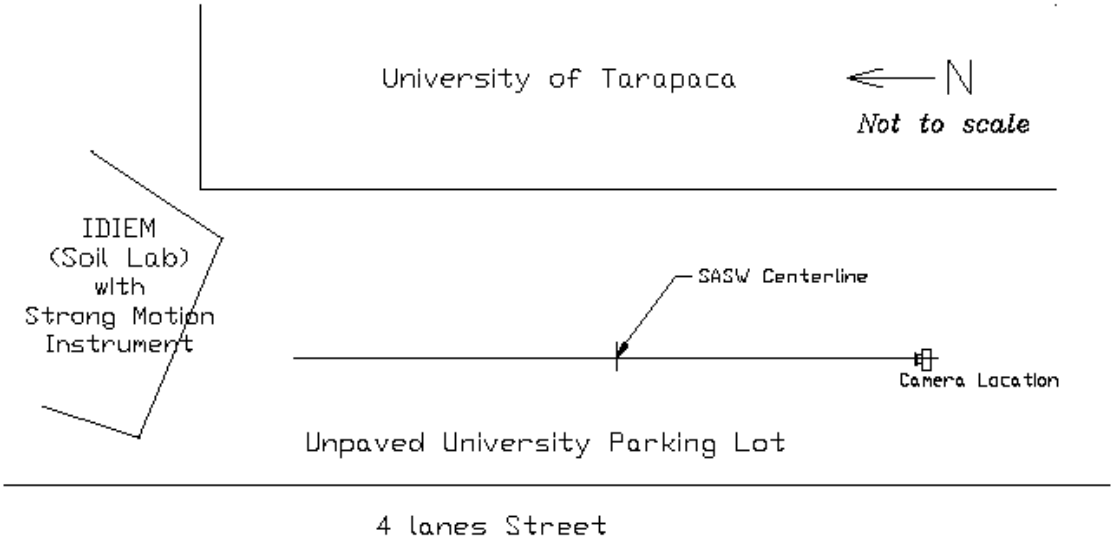

Figure A.7 A plan view of SASW testing site of Arica Costanera, located in the University of Tarapaca.

Figure A.8 Photograph of SASW testing at site of Arica Costanera 500

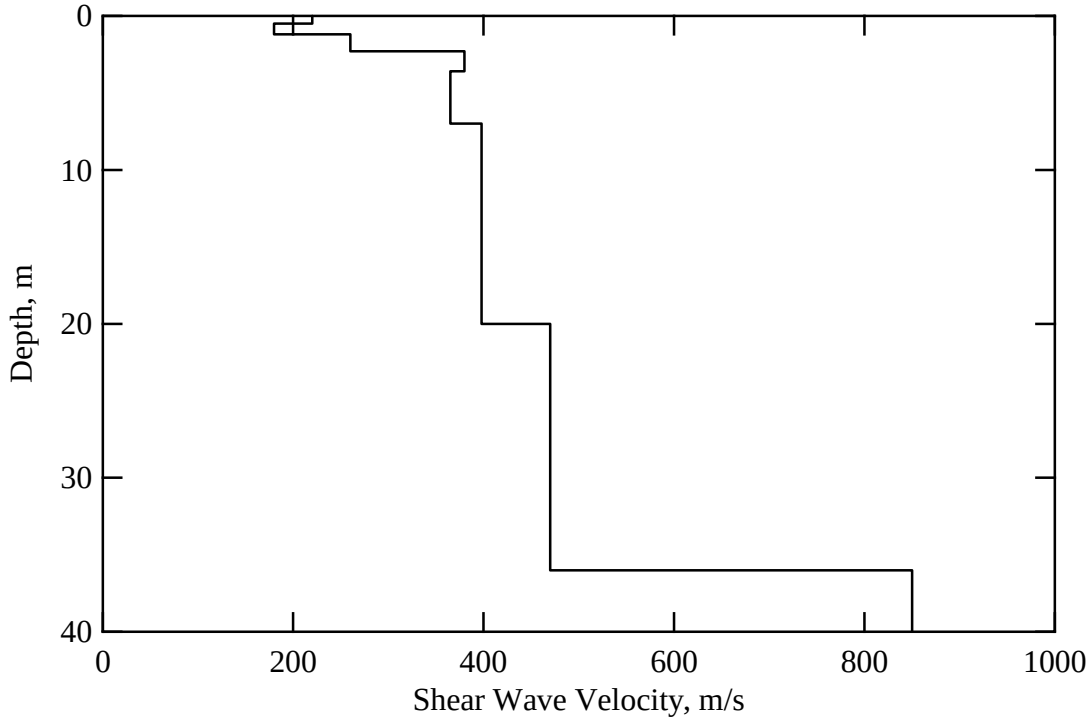

Figure A.9 Shear wave velocity profile determined from forward modeling at Arica Costanera site.

Table A.3 Tabulated Values of Measured and Assumed Layer Properties at Arica Costanera Site

Depth to Top Layer, m	Layer Thickness, m	Shear Wave Velocity, m/s	P-wave Velocity, m/s	Poisson's Ratio	Mass Density g/cc
0.0	0.5	220	412	0.3	1.80
0.5	0.7	180	337	0.3	1.80
1.2	1.1	260	486	0.3	1.80
2.3	1.3	380	711	0.3	1.80
3.6	3.4	365	683	0.3	1.80
7.0	13.0	398	745	0.3	1.80
20.0	16.0	470	879	0.3	1.95
36.0	4.0	850	1590	0.3	2.10

Arica Casa

The testing site is located on the local public parking lot near the Arica Casa site, which is a regional cemetery. The latitude and longitude of the testing site are 18.48158° south and 70.30853° west, respectively. A strong motion instrument is in a one-story brick building next to the testing site. A plan view of the site is presented in Figure A.10.

The shear wave velocity profile at the site is shown in Figure A.11. Tabulated values of shear wave velocity and assumed layer properties used in forward modeling are presented in Table A.5. Average shear wave velocity in the upper 25 m at this site is 406 m/s.

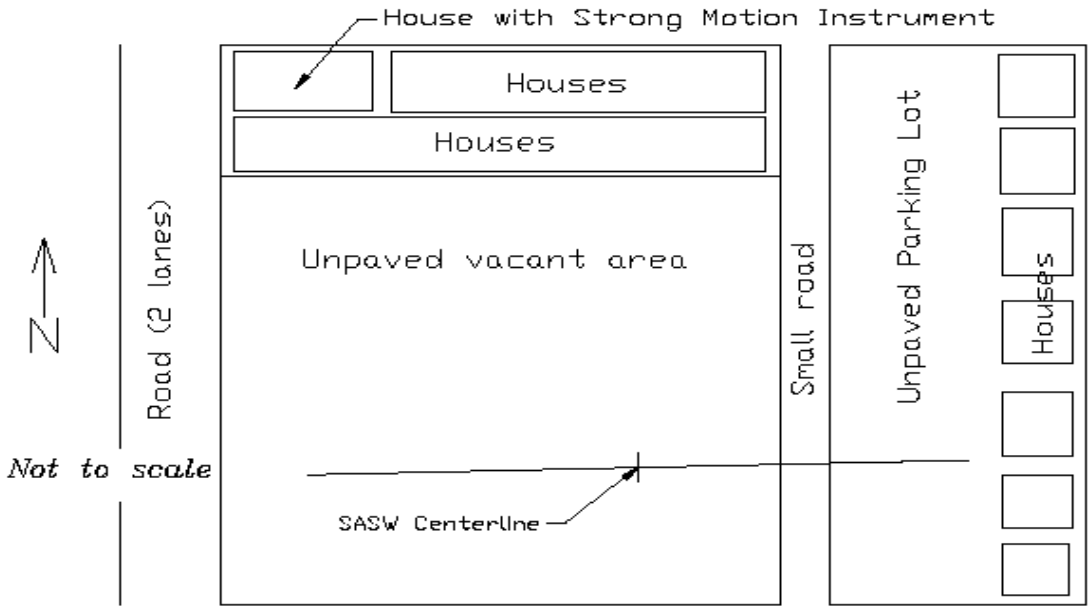

Figure A.10 A plan view of SASW testing site of Arica Casa 600

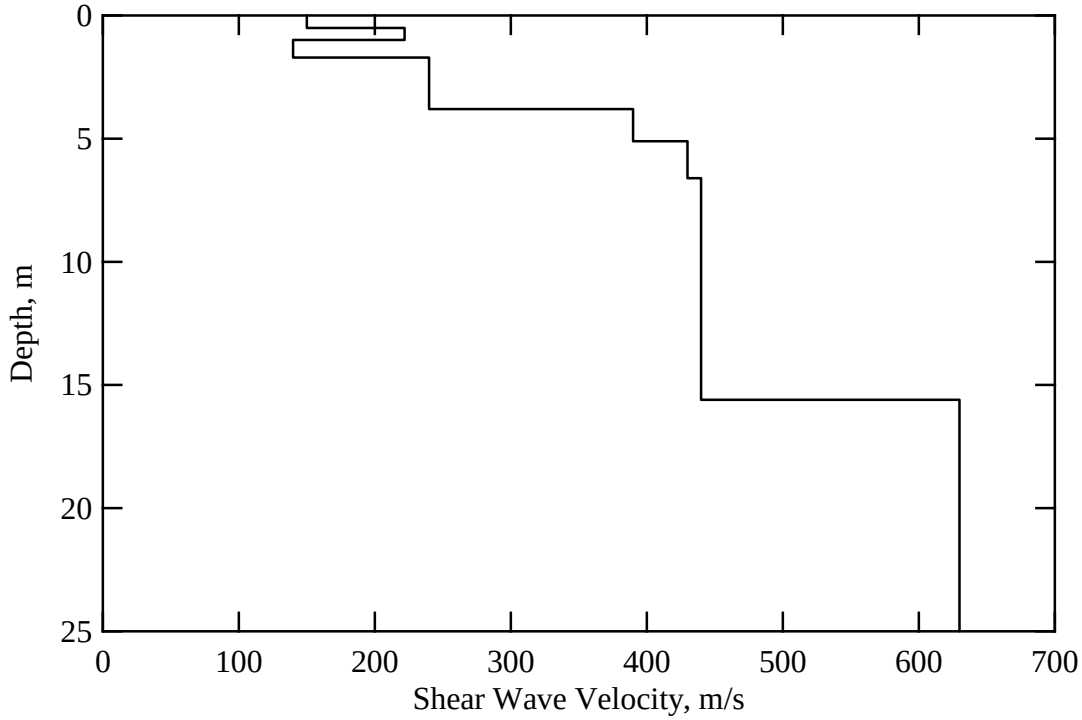

Figure A.11 Shear wave velocity profile determined from forward modeling at Arica Casa site

Table A.4 Tabulated Values of Measured and Assumed Layer Properties at Arica Casa Site

Depth to Top Layer, m	Layer Thickness, m	Shear Wave Velocity, m/s	P-wave Velocity, m/s	Poisson's Ratio	Mass Density g/cc
0.0	0.50	150	281	0.3	1.80
0.5	0.50	222	415	0.3	1.80
1.0	0.70	140	262	0.3	1.80
1.7	2.10	240	449	0.3	1.80
3.8	1.30	390	730	0.3	1.80
5.1	1.50	430	805	0.3	1.95
6.6	9.00	440	823	0.3	1.95
15.6	9.40	630	1179	0.3	1.95

Poconchile

The testing site is located up on a sandy hill located in the small village of Poconchile. The site coordinates are 18.45619° south and 70.06689° west, respectively. The strong motion instrument was placed inside the police station. This site is located in a very arid desert area in the northern part of Chile. One old adobe church next to the police station completely collapsed, and big old adobe blocks were collecting to reconstruct the church in same place. A plan view of the site is shown in Figure A.12. A photograph of this site is exposed in Figure A.13. The shear wave velocity profile at the site is presented in Figure A.14. Tabulated values of shear wave velocity and assumed layer properties used in forward modeling are presented in Table A.5. Average shear wave velocity in the upper 30 m, V_{S30}, at this site is 511 m/s and this site is classified into site class S_C from uniform building code.

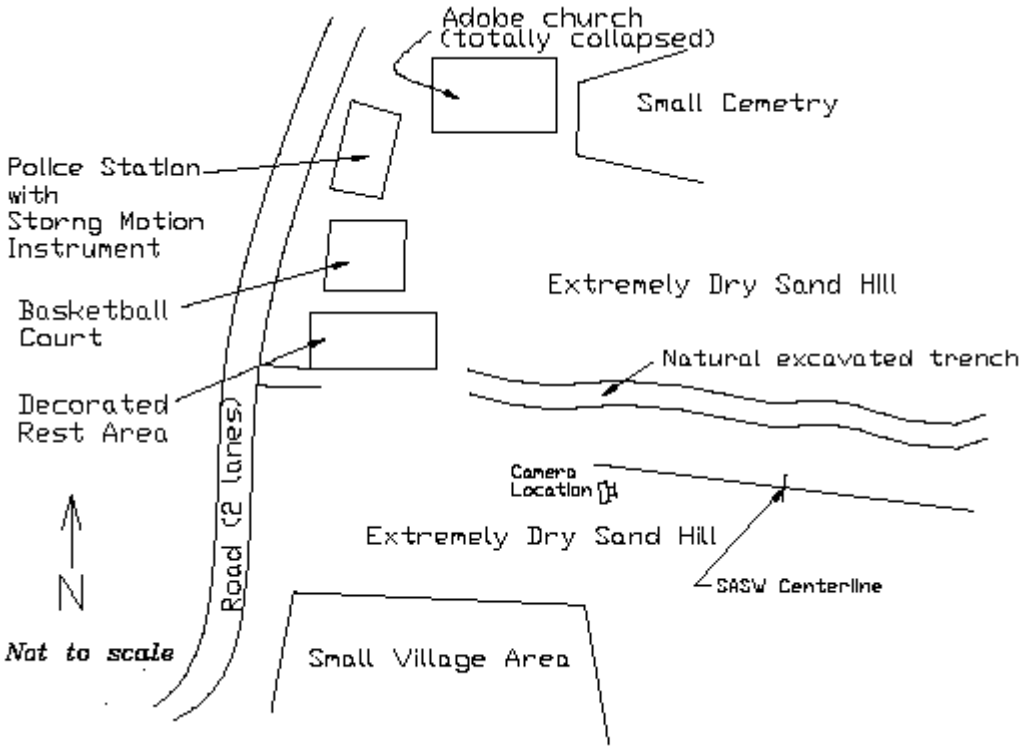

Figure A.12 Plan view of SASW testing site of Poconchile, located close to the border between Peru and Chile.

Figure A.13 Photograph of SASW testing at site of Poconchile

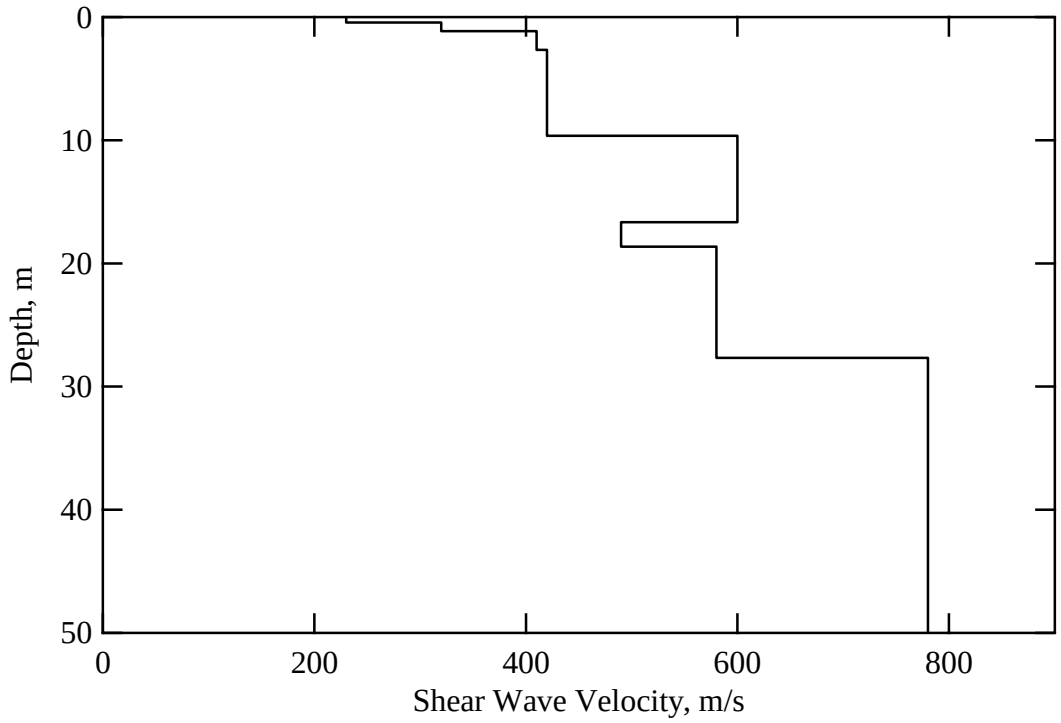

Figure A.14 Shear wave velocity profile determined from forward modeling at Poconchile site

Table A.5 Tabulated Values of Measured and Assumed Layer Properties at Poconchile Site

Depth to Top Layer, m	Layer Thickness, m	Shear Wave Velocity, m/s	P-wave Velocity, m/s	Poisson's Ratio	Mass Density g/cc
0.00	0.45	230	430	0.3	1.80
0.45	0.70	320	599	0.3	1.80
1.15	1.50	410	767	0.3	1.95
2.65	7.00	420	786	0.3	1.95
9.65	7.00	600	1123	0.3	1.95
16.65	2.00	490	917	0.3	1.95
18.65	9.00	580	1085	0.3	1.95
27.65	22.35	780	1459	0.3	2.10

Chacalluta-Chilean immigration office

The testing site is located on the vacant secured lot in the area known as Chacalluta where the Chilean immigration office on the border between Chile and Peru is

placed. The coordinates of the testing site are 18.31767° south and 70.31553° west. The strong motion instrument is located inside the immigration office. Damage due to the earthquake could not be found at the time of testing. A plan view of the site is shown in Figure A.15. A photograph of this site is exposed 63 in Figure A.16. Figure A.17 presents the shear wave velocity profile at the site. Tabulated values of shear wave velocity and assumed layer properties used in forward modeling are presented in Table A.6. Average shear wave velocity in the upper 30 m, V_{S30}, at this site is 287 m/s and this site is classified into site class S_D from uniform building code.

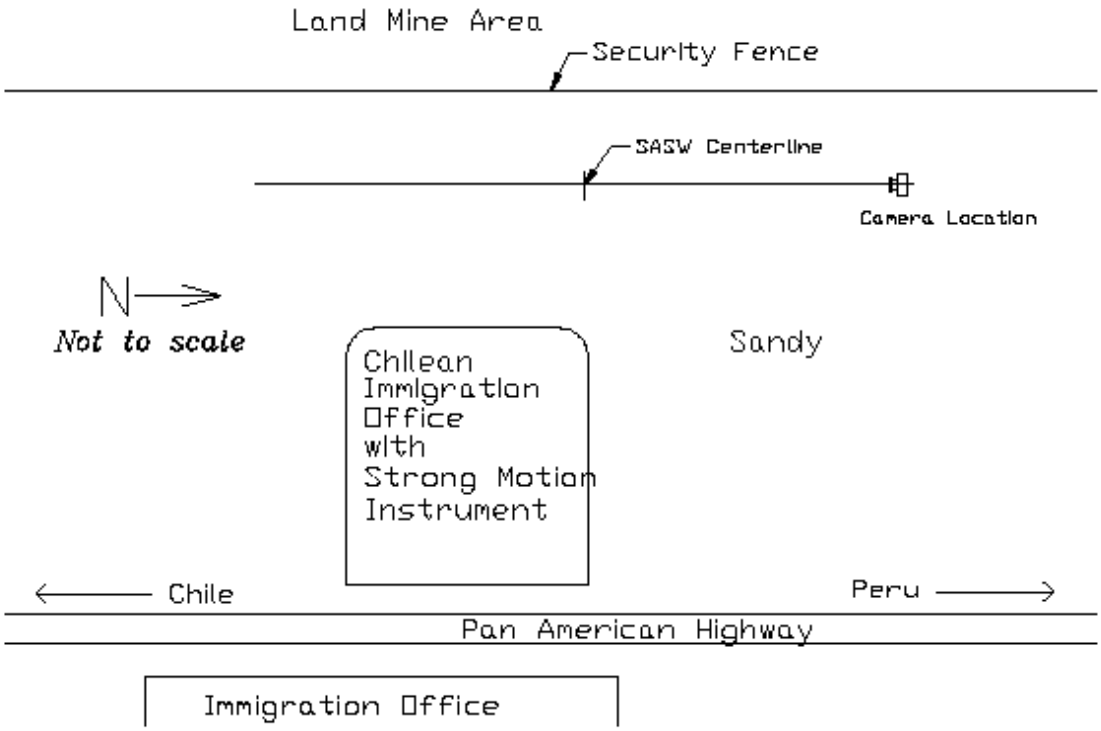

Figure A.15 A plan view of SASW testing site of Chacalluta-Chilean Immigration Office

Figure A.16 Photograph of SASW testing at site of Chacalluta-Chilean Immigration Office

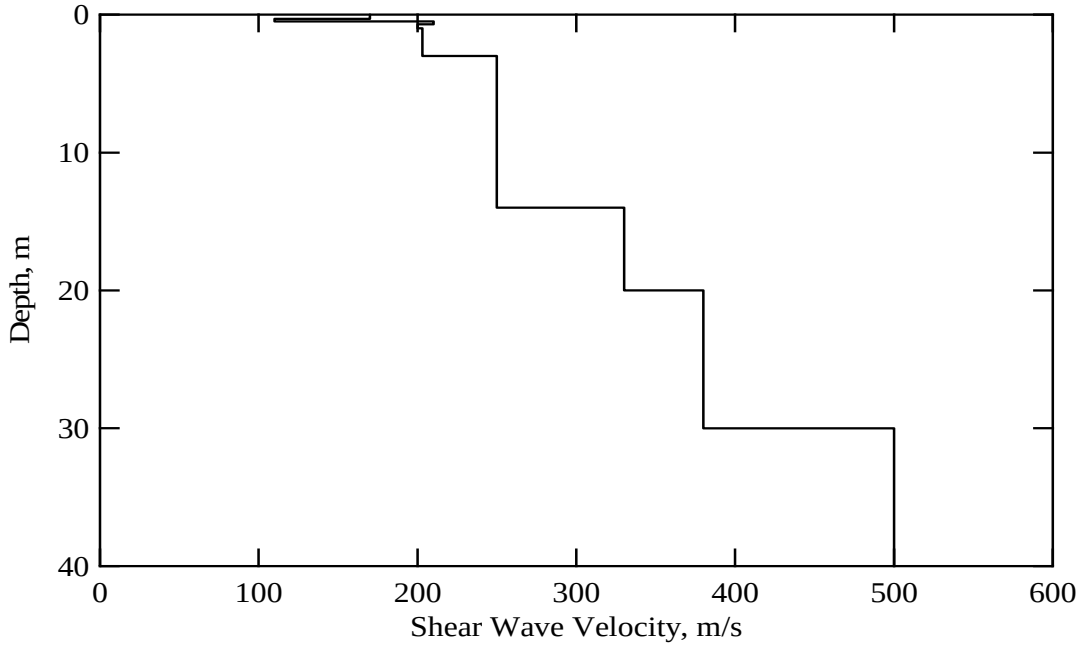

Figure A.17 Shear wave velocity profile determined from forward modeling at Chacalluta- Chilean immigration office site

Table A.6 Tabulated Values of Measured and Assumed Layer Properties at Chacalluta-Chilean Immigration Office Site

Depth to Top Layer, m	Layer Thickness, m	Shear Wave Velocity, m/s	P-wave Velocity, m/s	Poisson's Ratio	Mass Density g/cc
0.0	0.3	170	318	0.3	1.80
0.3	0.2	110	206	0.3	1.80
0.5	0.2	210	393	0.3	1.80
0.7	0.3	200	393	0.3	1.80
1.0	2.0	203	380	0.3	1.80
3.0	11.0	250	468	0.3	1.80
14.0	6.0	330	617	0.3	1.80
20.0	10.0	380	711	0.3	1.80
30.0	10.0	500	935	0.3	1.95

Table A.7 Average Shear Wave Velocities in the Upper 30 m (or 25 m) with UBS Site Classification in Arica Sites

Site	**Cerro La Cruz**	**Juan Noe Greviani Hospital[b]**	**Arica Costanera**	**Arica Casa**	**Poconchile**	**Chacalluta – Chilean Immigration Office**
V_{S30}[a]	1132 m/s	-	389 m/s	406 m/s [c]	511 m/s	287 m/s
UBC class	S_B	-	S_C	-	S_C	S_D

[a] Average shear wave velocity in the upper 30 m.
[b] V_{S30} was not calculated because this site only resolution down to 8 m.
[c] This site has the average shear wave velocity from the upper 25 m.

Tacna Sites

The city of Tacna is located at the southern end of Peru, near the border with Chile, approximately 38 km northeast of the Pacific coastline on an arid strip of land bounded by the steep mountain chain called The Andes. The city is located about 135 km from the rupture zone of the earthquake. This city is an extremely arid area with an annual average precipitation of 20 mm. The predominant geologic deposit, which is referred to as "conglomerate," is a Quaternary alluvium consisting mainly of cobbles and boulders (EERI 2003).

SASW testing was performed at seven sites in four different districts in the city of Tacna. Average shear wave velocity profiles on the Alto de la Alianza and the Ciudad Nueva districts could be similar. This is because, according to the reconnaissance report, these districts are on the same volcanic tuffs and silty sands formed from weathering of tuffs or air fall volcanic ash and damage patterns in these two districts were similar, although they have varying degrees of weathering (EERI 2003).

Association "San Pedro"

The testing site is located on Association "San Pedro" in the Alto de la Alianza district. The latitude and longitude coordinates on the testing site are 17.99986° south and 70.25997° west, respectively. This site is up on the northern hill with sand fill. A plan view of the site is shown in Figure A.18. A photograph of this site is shown in Figure A.19. The shear wave velocity profile at the site is shown in Figure A.20. Tabulated values of shear wave velocity and assumed layer properties used in forward modeling are presented in Table A.8. Average shear wave velocity in the upper 30 m, V_{S30}, at this site is 473 m/s and this site is classified into site class S_C from uniform building code.

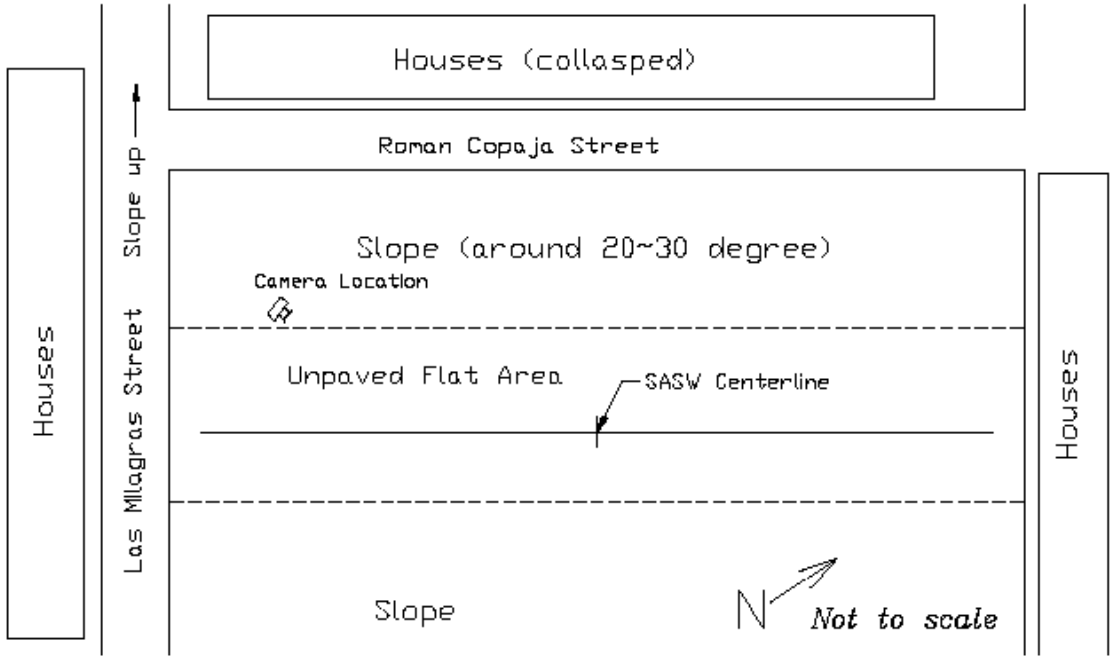

Figure A.18 A plan view of SASW testing site of Association "San Pedro" in Alto de la Alianza district

Figure A.19 Photograph of SASW testing at site of Association "San Pedro" site

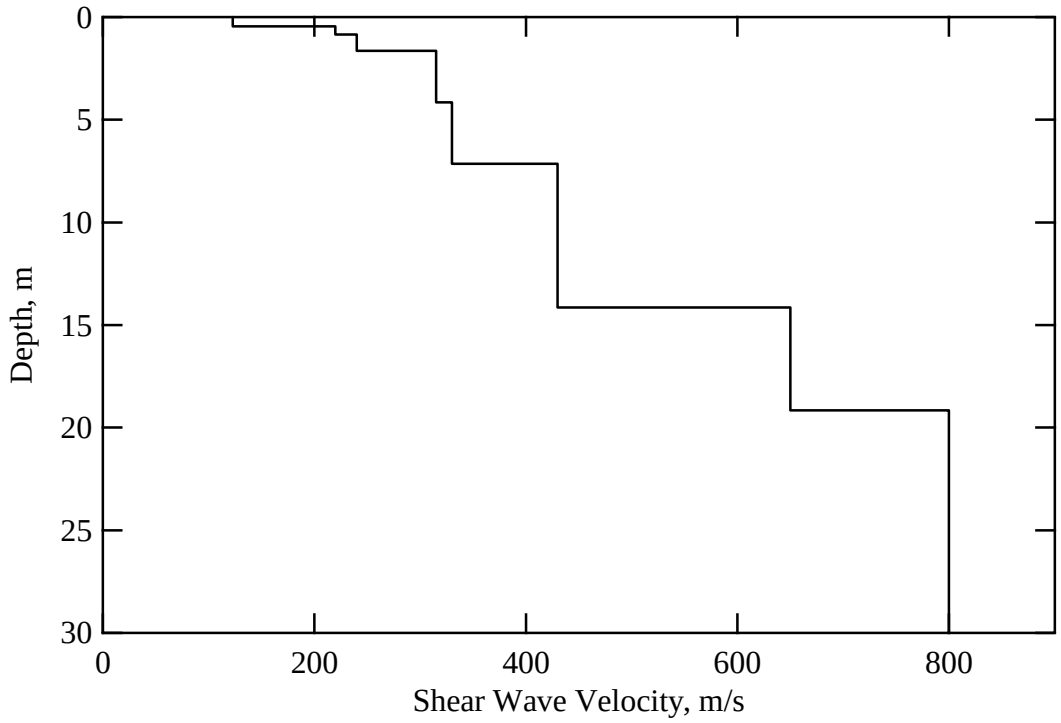

Figure A.20 Shear wave velocity profile determined from forward modeling at Association
"San Pedro" site

Table A.8 Tabulated Values of Measured and Assumed Layer Properties at Association "San Pedro" Site

Depth to Top Layer, m	Layer Thickness, m	Shear Wave Velocity, m/s	P-wave Velocity, m/s	Poisson's Ratio	Mass Density g/cc
0.00	0.45	123	230	0.3	1.80
0.45	0.40	220	412	0.3	1.80
0.85	0.80	240	449	0.3	1.80
1.65	2.50	315	589	0.3	1.80
4.15	3.00	330	655	0.3	1.80
7.15	7.00	430	805	0.3	1.95
14.15	5.00	650	1216	0.3	1.95
19.15	10.85	800	1497	0.3	2.10

Colegio "Enrique Paillardelle"

The testing site is located on the vacant area of the east side of the school named Emrique Paillardelle, which had small earthquake damage. This site is in the Vinani or Cono Sur district where is southern part of the city of Tacna. The latitude and longitude coordinates on the testing site are 18.05993° south and 70.25031° west, respectively. Gravelly soil was found at this site from a shallow test pit of 2.5 m of depth encountered at the site. A plan view of the site is shown in Figure A.21.

A photograph of this site is shown in Figure A.22. The shear wave velocity profile at the site is shown in Figure A.23. Tabulated values of shear wave velocity and assumed layer properties used in forward modeling are presented in Table A.9. Average shear wave velocity in the upper 25 m, V_{S25}, at this site is 670 m/s.

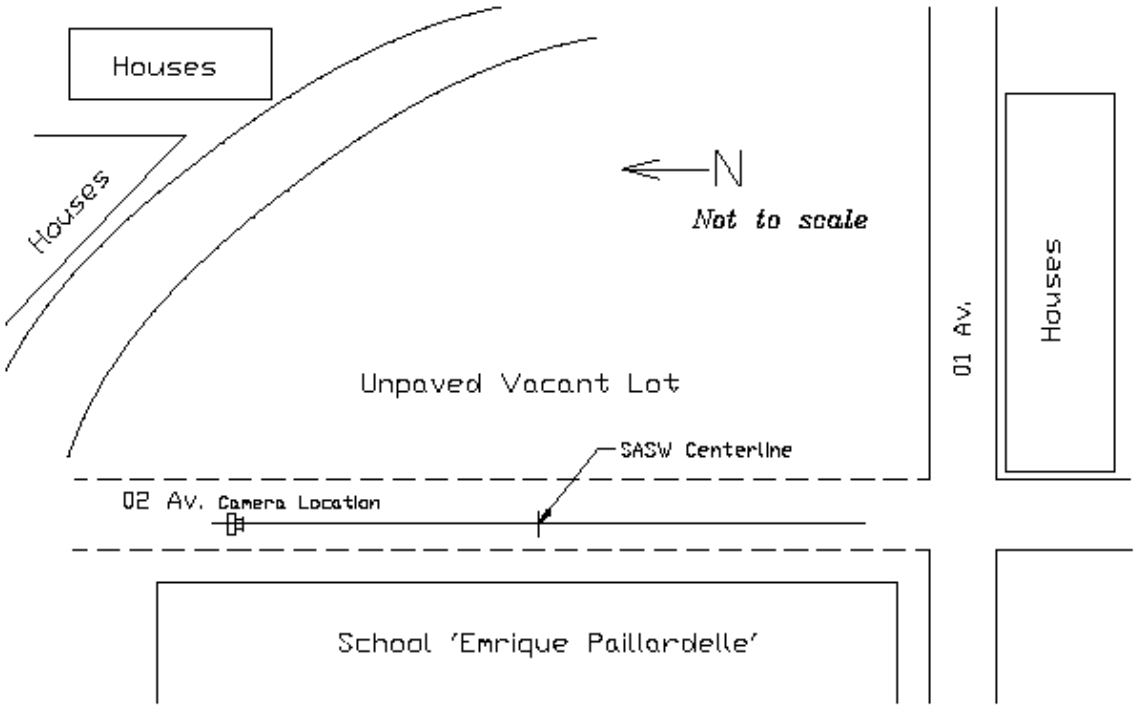

Figure A.21 A plan view of SASW testing site of Colegio "Emrique Paillardelle" in Vinani district

Figure A.22 Photograph of SASW testing at site of Colegio “Emrique Paillardelle” 800

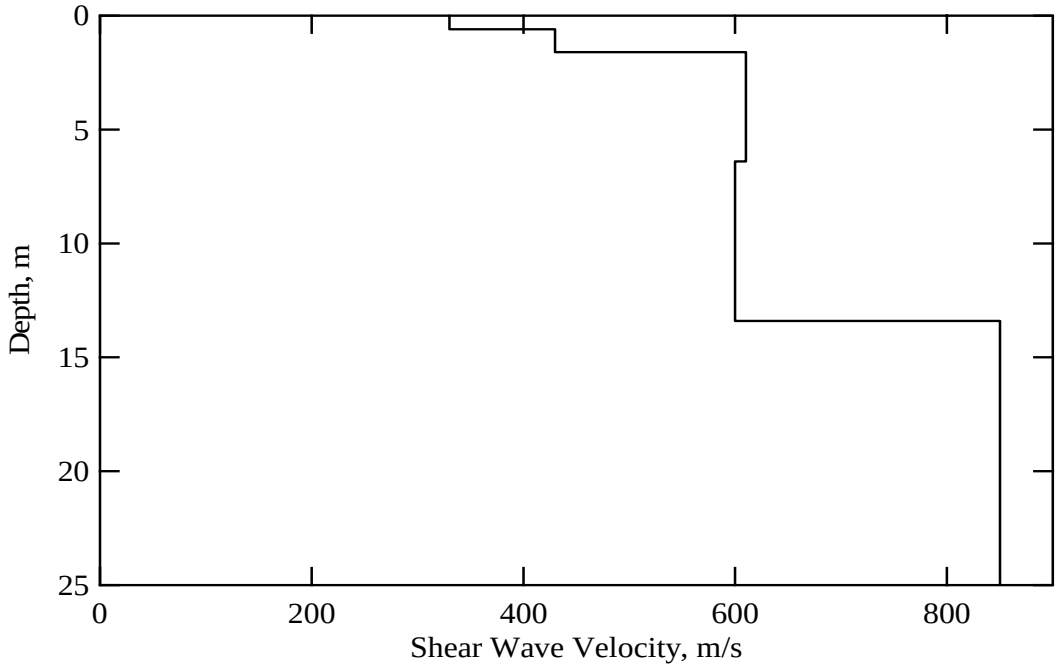

Figure A.23 Shear wave velocity profile determined from forward modeling at Colegio “Emrique Paillardelle” site.

Table A.9 Tabulated Values of Measured and Assumed Layer Properties at Colegio "Emrique Paillardelle" Site

Depth to Top Layer, m	Layer Thickness, m	Shear Wave Velocity, m/s	P-wave Velocity, m/s	Poisson's Ratio	Mass Density g/cc
0.0	0.6	330	617	0.3	1.80
0.6	1.0	430	805	0.3	1.95
1.6	4.8	610	1141	0.3	1.95
6.4	7.0	600	1123	0.3	1.95
13.4	11.6	850	1590	0.3	2.10

Municipal gas station

The testing site is located on the Municipal Gas Station in the Ciudad Nueva district. Its latitude and longitude coordinates are 17.98100° south and 70.23183° west, respectively. Similar to the Association "San Pedro" site, most brick bearing wall houses suffered severe damage from the earthquake. A plan view of the site is shown in Figure A.24. A photograph of this site is shown in Figure A.25. The shear wave velocity profile at the site is shown in Figure A.26. Tabulated values of shear wave velocity and assumed layer properties used in forward modeling are presented in Table A.10. Average shear wave velocity in the upper 30 m, V_{S30}, at this site is 419 m/s and this site is classified into site class S_C from uniform building code.

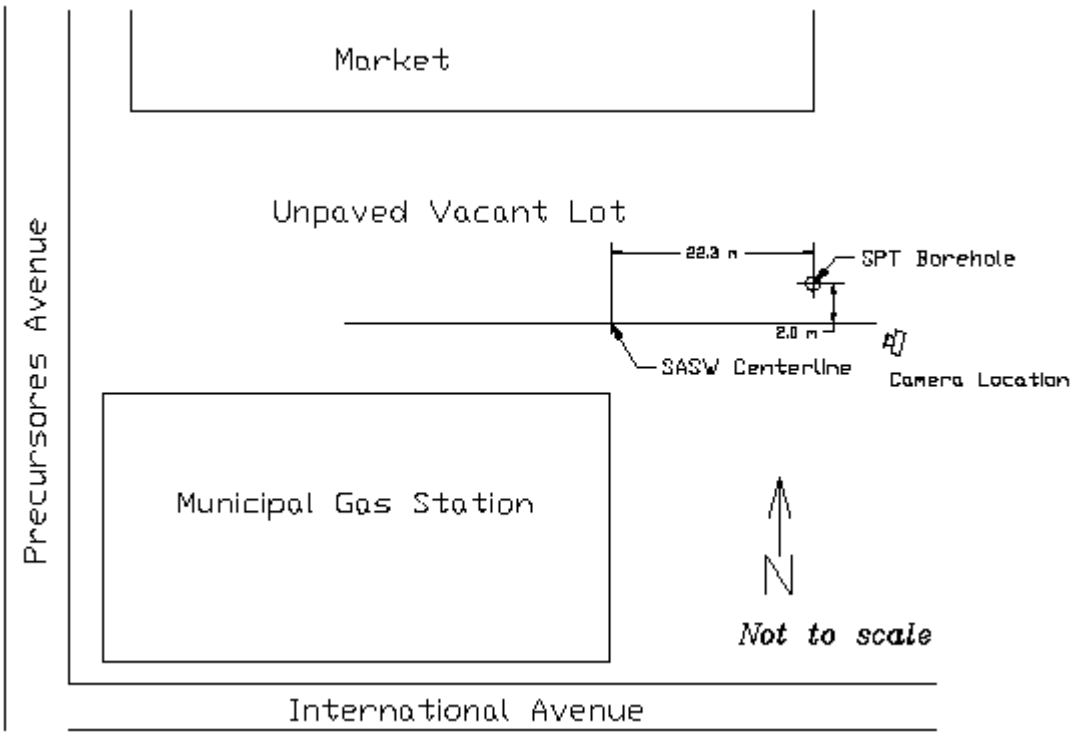

Figure A.24A plan view of SASW testing site of Municipal Gas Station in Ciudad Nueva district

Figure A.25 Photograph of SASW testing at site of Municipal Gas Station

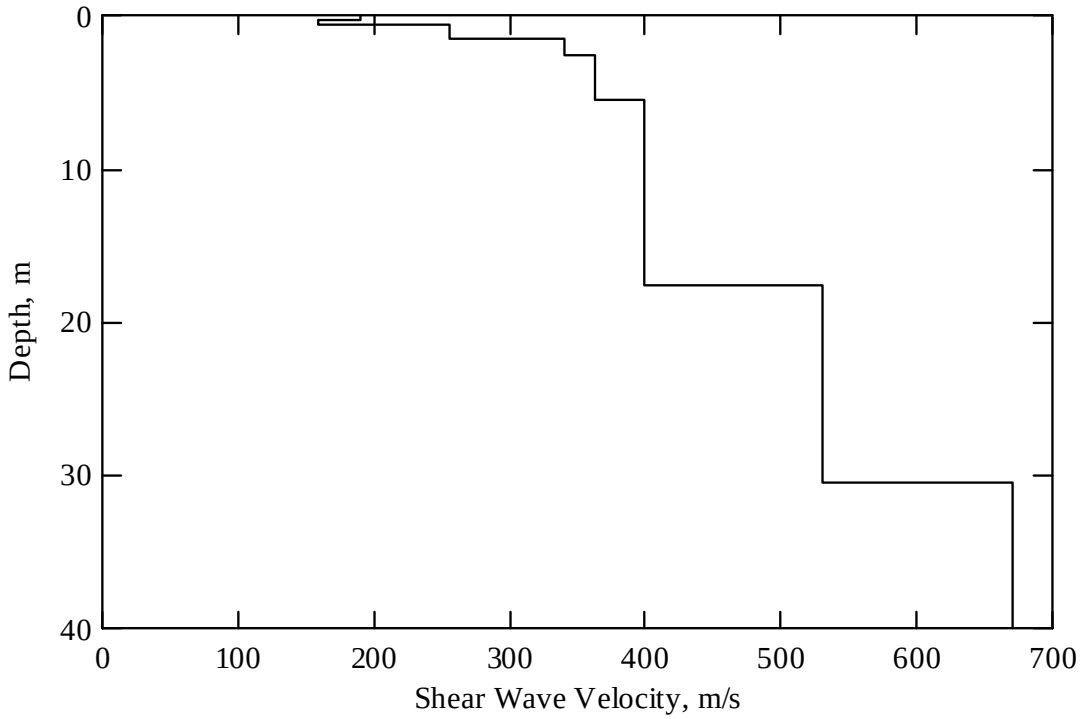

Figure A.26 Shear wave velocity profile determined from forward modeling at Municipal
Gas Station site

Table A.10 Tabulated Values of Measured and Assumed Layer Properties at Municipal Gas Station Site

Depth to Top Layer, m	Layer Thickness, m	Shear Wave Velocity, m/s	P-wave Velocity, m/s	Poisson's Ratio	Mass Density g/cc
0.0	0.2	190	327	0.3	1.80
0.2	0.3	160	299	0.3	1.80
0.5	1.0	255	477	0.3	1.80
1.5	1.0	340	675	0.3	1.80
2.5	3.0	363	721	0.3	1.80
5.5	12.0	400	748	0.3	1.95
17.5	13.0	530	992	0.3	1.95
30.5	9.5	670	1254	0.3	1.95

Standard penetration test

For this site SPT testing was performed, the SPT was rejected at about 9.45 meters; samples were taken and classified following USCS classification system. Table A.11 presents the results obtained, Figure A.27 shows the SPT profile obtained.

Table A.11 SPT results obtained for Tacna Site.

Depth	N	$(N_1)_{60}$	SUCS Classification
1.45	51	53	SM
2.45	44	40	SM
3.45	100	79	SM
4.45	87	70	SM
5.45	105	76	SM
6.45	77	57	SM
7.45	23	16	SM
8.45	72	45	SM
9.45	147	86	SM

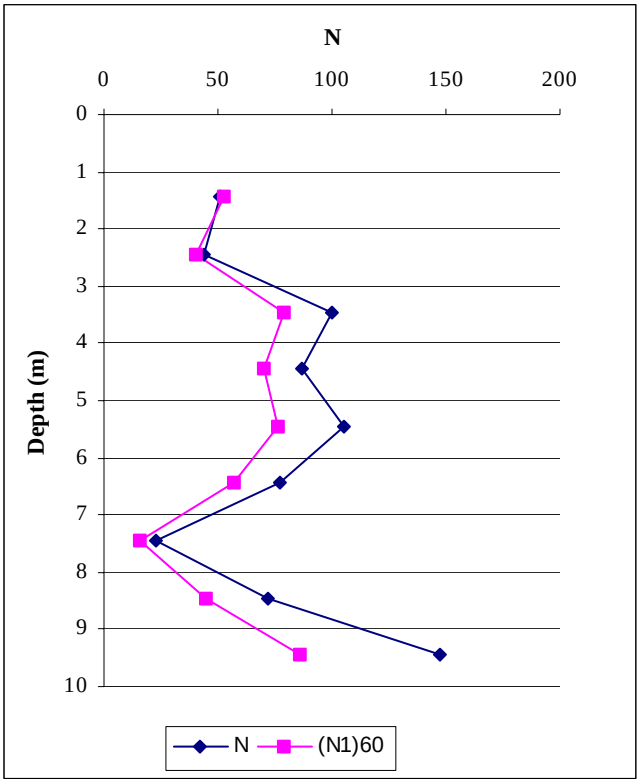

Figure A.27 SPT profile obtained for Tacna Site

La Bombonera Stadium

The testing site is located on the southwest side of the La Bombonera Stadium in the Ciudad Nueva district. The latitude and longitude coordinates on the testing site are 17.98519° south and 70.23869° west, respectively. A plan view of the site is shown in Figure A.28. A photograph of this site is exposed in Figure A.29. The shear wave velocity profile at the site is presented in Figure A.30. Tabulated values of shear wave velocity and assumed layer properties used in forward modeling are presented in Table A.12. Here, a stiffer layer was detected at around 35 m of depth; however, the precise shear wave velocity could not be determined due to scattered dispersion data measured at this site. Average shear wave velocity in the upper 30 m, V_{S30}, at this site is 409 m/s and this site is classified into site class S_C from uniform building code.

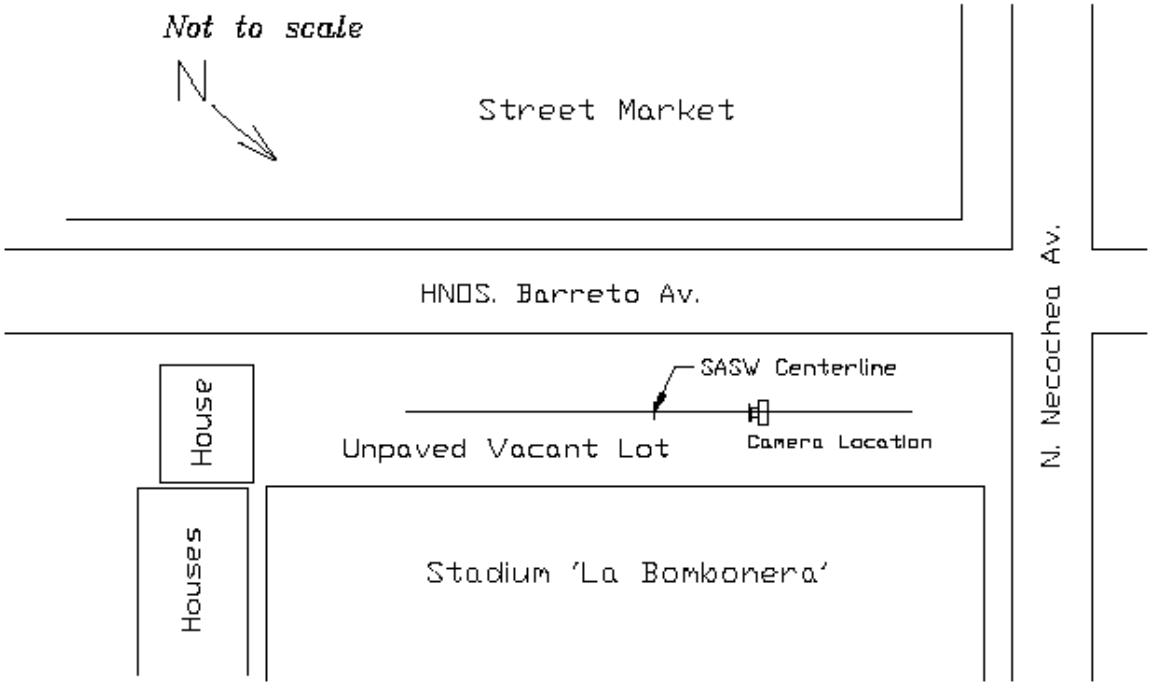

Figure A.28 A plan view of SASW testing site of La Bombonera Stadium in the Ciudad Nueva district

Figure A.29 Photograph of SASW testing at site of La Bombonera Stadium

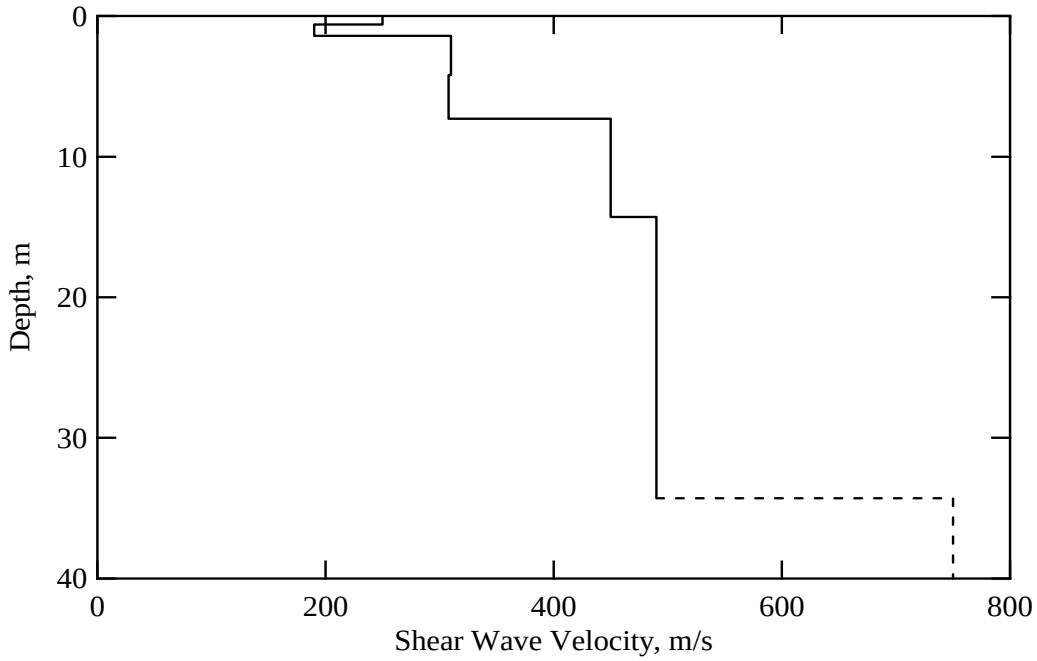

Figure A.30 Shear wave velocity profile determined from forward modeling at La Bombonera Stadium site.

Table A.12 Tabulated Values of Measured and Assumed Layer Properties at La Bombonera Stadium Site

Depth to Top Layer, m	Layer Thickness, m	Shear Wave Velocity, m/s	P-wave Velocity, m/s	Poisson's Ratio	Mass Density g/cc
0.0	0.6	250	468	0.3	1.80
0.6	0.8	190	356	0.3	1.80
1.4	2.8	310	580	0.3	1.80
4.2	3.1	308	576	0.3	1.80
7.3	7.0	450	842	0.3	1.95
14.3	20.0	490	917	0.3	1.95
34.3	5.7	750*	1403	0.3	2.10

* A stiffer layer was detected at this depth; however, the precise shear wave velocity could not be determined.

Soccer field in Alto de la Alianza District

The testing site is located on the vacant area with trees of the southern side of the soccer field in the Alto de la Alianza district. The latitude and longitude coordinates on the testing site are 17.99417° south and 70.24369° west, respectively. A plan view of the site is shown in Figure A.31. A photograph of this site is exposed in Figure A.32. The shear wave velocity profile at the site is presented in Figure A.33. Tabulated values of shear wave velocity and assumed layer properties used in forward modeling are presented in Table A.13. Here again, a stiffer layer was detected at around 35 m of depth; however, the precise shear wave velocity could not be determined due to scattered dispersion data measured at this site. Average shear wave velocity in the upper 30 m, V_{S30}, at this site is 452 m/s and this site is classified into site class S_C from uniform building code.

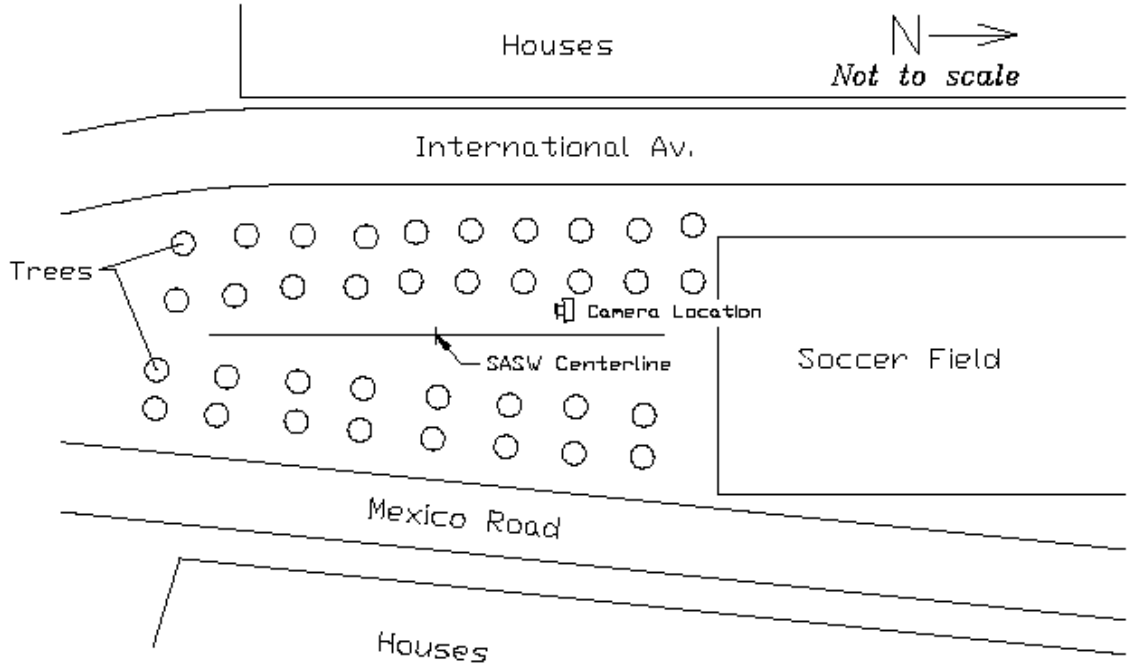

Figure A.31 A plan view of SASW testing site of Soccer Field in Alto de la Alianza district

Figure A.32 Photograph of SASW testing at site of Soccer Field in Alto de la Alianza district

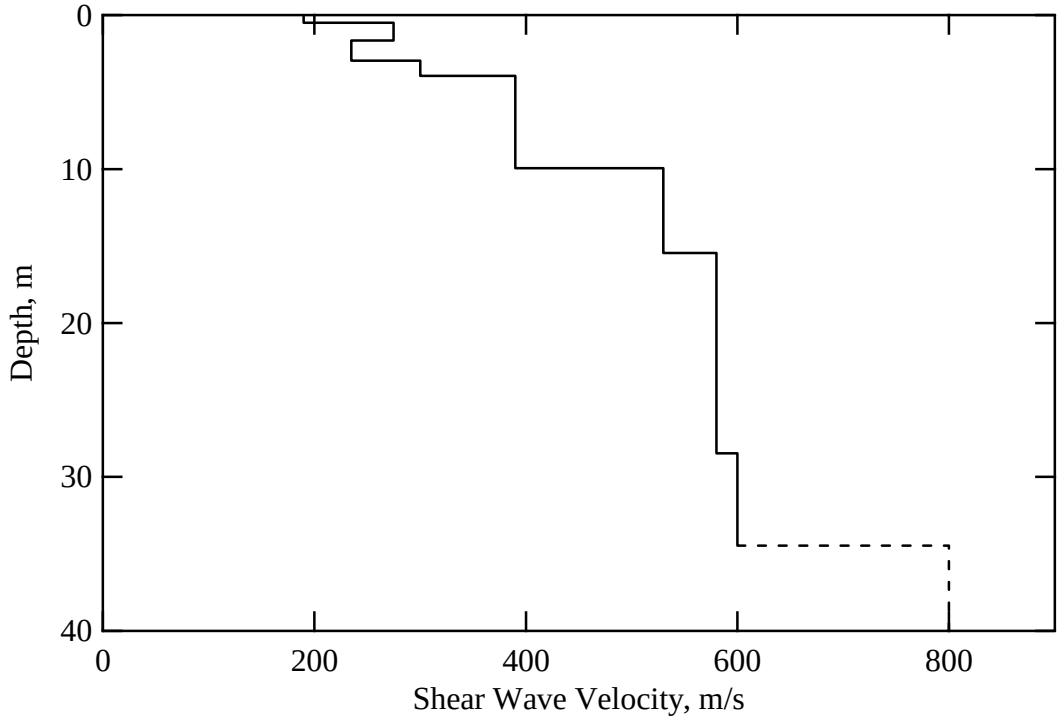

Figure A.33 Shear wave velocity profile determined from forward modeling at Soccer Field site in Alto de la Alianza district

Table A.13 Tabulated Values of Measured and Assumed Layer Properties at Soccer Field Site in Alto de la Alianza District

Depth to Top Layer, m	Layer Thickness, m	Shear Wave Velocity, m/s	P-wave Velocity, m/s	Poisson's Ratio	Mass Density g/cc
0.00	0.50	190	356	0.3	1.80
0.50	1.15	275	515	0.3	1.80
1.65	1.30	235	440	0.3	1.80
2.95	1.00	300	561	0.3	1.80
3.95	6.00	390	730	0.3	1.80
9.95	5.50	530	992	0.3	1.95
15.45	13.00	580	1085	0.3	1.95
28.45	6.00	600	1123	0.3	1.95
34.45	5.55	800*	1497	0.3	2.10

* A stiffer layer was detected at this depth; however, the precise shear wave velocity could not be determined.

Colegio "Hermogenes Arenas Yanez"

The testing site is located at the unpaved vacant lot in the intersection between June 24 road and 200 miles avenue in the Cicoavi district, western end of the City. The school, named Hermogenes Arenas Yanez, which did not suffer much damage from the earthquake, is located on one of the sides of the 200 miles avenue. The latitude and longitude coordinates on the testing site are 18.04136° south and 70.28156° west, respectively. A plan view of the site is shown in Figure A.34. A photograph of this site is exposed in Figure A.35. The shear wave velocity profile at the site is shown in Figure A.36. Tabulated values of shear wave velocity and assumed layer properties used in forward modeling are presented in Table A.14. This site seems to have simply two or three subsurface layers. Average shear wave velocity in the upper 30 m, V_{S30}, at this site is 652 m/s and this site is classified into site class S_C.

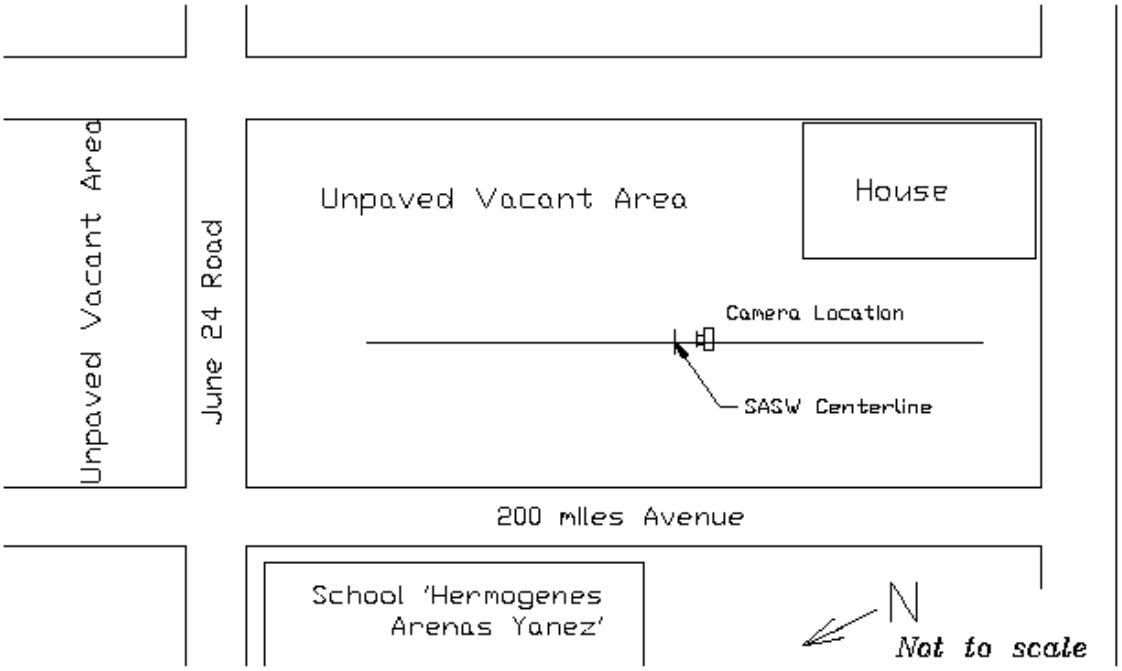

Figure A.34 A plan view of SASW testing site of Colegio "Hermogenes Arenas Yanez" in Cicoavi district

Figure A.35 Photograph of SASW testing at site of Colegio "Hermogenes Arenas Yanez"

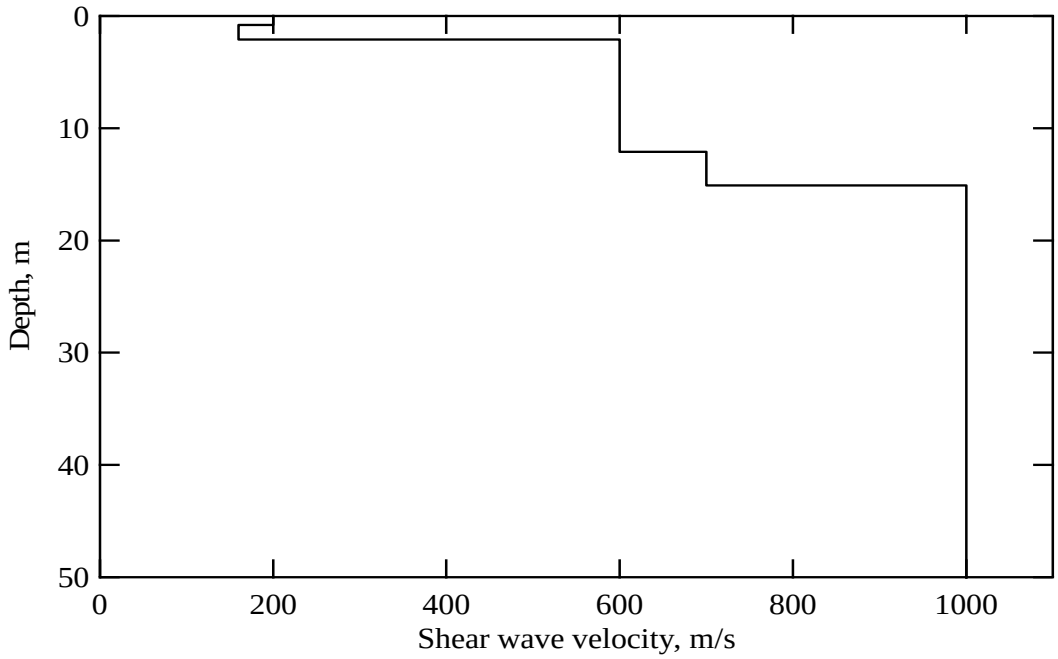

Figure A.36 Shear wave velocity profile determined from forward modeling at Colegio "Hermogenes Arenas Yanez" site

Table A.14 Tabulated Values of Measured and Assumed Layer Properties at Colegio "Hermogenes Arenas Yanez" site

Depth to Top Layer, m	Layer Thickness, m	Shear Wave Velocity, m/s	P-wave Velocity, m/s	Poisson's Ratio	Mass Density g/cc
0.0	0.8	200	374	0.3	1.80
0.8	1.3	160	299	0.3	1.80
2.1	10.0	600	1123	0.3	1.95
12.1	3.0	700	1310	0.3	2.10
15.1	34.9	1000	1871	0.3	2.25

Colegio "Coronel Bolognesi"

The testing site is located on the northern side of the school named Coronel Bolognesi, which is in the downtown Tacna. The latitude and longitude coordinates on the testing site are 18.00436° south and 70.25353° west, respectively. The school was built using reinforced concrete frame with bricks, and suffered moderate damage. It was operating without full recovery at the testing time. A plan view of the site is shown in Figure A.37. A photograph of this site is shown in Figure A.38. The shear wave velocity profile at the site is shown in Figure A.39. Tabulated values of shear wave velocity and assumed layer properties used in forward modeling are presented in Table A.15. Here again, simply two or three subsurface layers were found at this site. Average shear wave velocity in the upper 30 m, V_{S30}, at this site is 615 m/s and this site is classified into site class S_C from uniform building code.

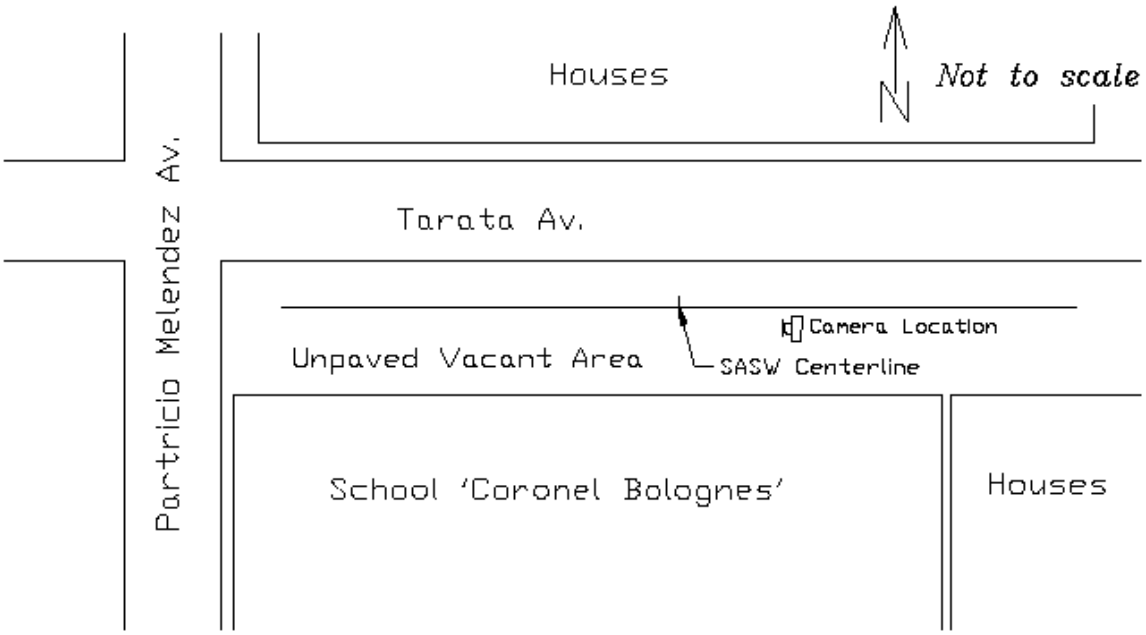

Figure A.37 A plan view of SASW testing site of Colegio "Coronel Bolognesi" in downtown district

Figure A.38 Photograph of SASW testing at site of Colegio "Coronel Bolognesi"

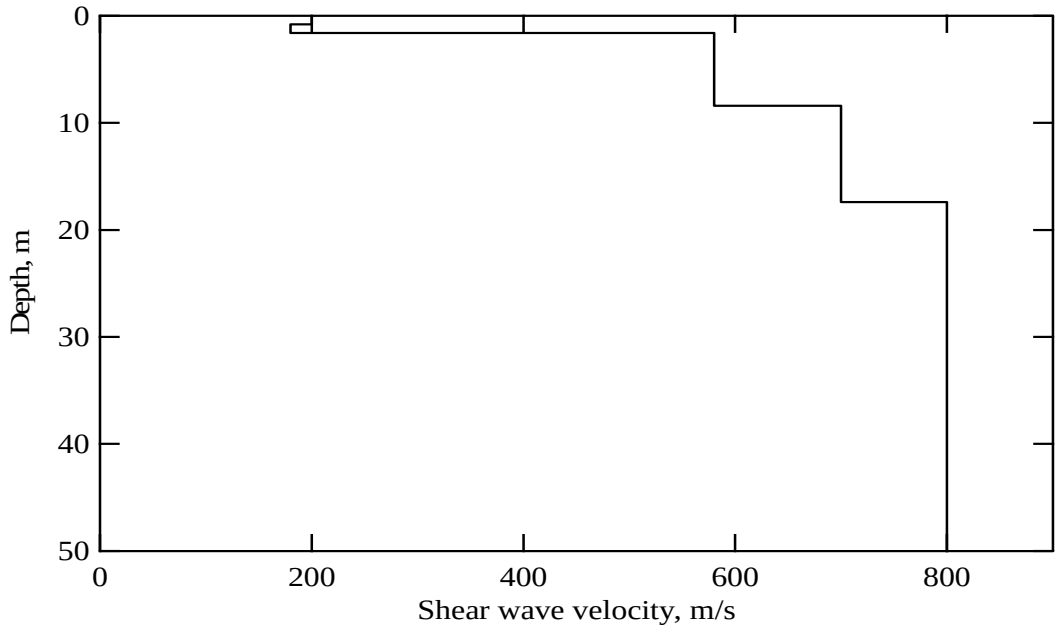

Figure A.39 Shear wave velocity profile determined from forward modeling at Colegio "Coronel Bolognesi" site

Table A.15 Tabulated Values of Measured and Assumed Layer Properties at Colegio "Coronel Bolognesi" site

Depth to Top Layer, m	Layer Thickness, m	Shear Wave Velocity, m/s	P-wave Velocity, m/s	Poisson's Ratio	Mass Density g/cc
0.0	0.8	200	374	0.3	1.80
0.8	0.8	180	337	0.3	1.80
1.6	6.8	580	1085	0.3	1.95
8.4	9.0	700	1310	0.3	2.10
17.4	32.6	800	1497	0.3	2.10

Table A.16 Average Shear Wave Velocity in the Upper 30 m (or 25 m) with UBS Site Classification in Tacna Sites

Site	**Association "San Pedro"**	**Colegio "Enrique Paillardelle"**	**"Municipal" Gas Station**	**La Bombonera Stadium**	**Soccer Field Alto de la Alianza"**	**Colegio "Hermogenes Arenas Yanez"**	**Colegio "Coronel Bolognesi"**
V_{S30} [a]	473 m/s	670 m/s [b]	419 m/s	409 m/s	452 m/s	625 m/s	615 m/s
UBC class	S_C	-	S_C	S_C	S_C	S_C	S_C

[a] Average shear wave velocity in the upper 30 m.

[b] This site has the average shear wave velocity from the upper 25 m.

Moquegua sites

The city of Moquegua is at about 55 km east of the Pacific coast and at an average elevation of 1,400 meters above the sea level. The weather in Moquegua is extremely dry, annual precipitation is on average 15 mm. Quaternary deposits in Moquegua are dominated by alluvial-type deposits, composed mainly of sandy gravels. This city had the largest number of affected buildings in the 23 June 2001 earthquake, and most of the damage was to old adobe construction, which is prevalent in Moquegua (EERI 2003). SASW testing was performed at five sites in Moquegua city.

Calle Nueva

Calle Nueva site is located on the Nueva Street in San Francisco hill, San Francisco district. Its latitude and longitude coordinates are 17.19729° south and 70.94065° west, respectively. The testing was performed on the narrow road with moderately steep slope. A plan view of the site is shown in Figure A.40. A photograph of this site is exposed in Figure A.41. The shear wave velocity profile at the site is presented in Figure A.42. Tabulated values of shear wave velocity and assumed layer properties used in forward modeling are presented in Table A.17. Average shear wave velocity in the upper 30 m, V_{S30}, at this site is 421 m/s and this site is classified into site class S_C from uniform building code.

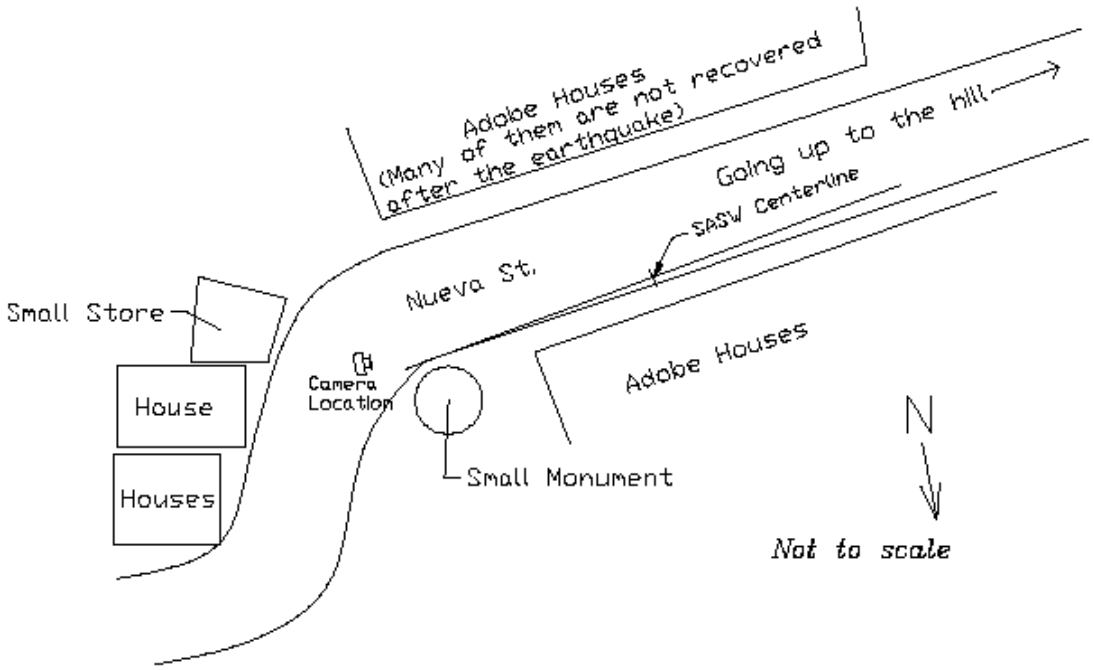

Figure A.40 Plan view of SASW testing at site of Calle Nueva, located on Nueva St. in the southern part of San Francisco hill

Figure A.41 Photograph of SASW testing at site of Calle Nueva

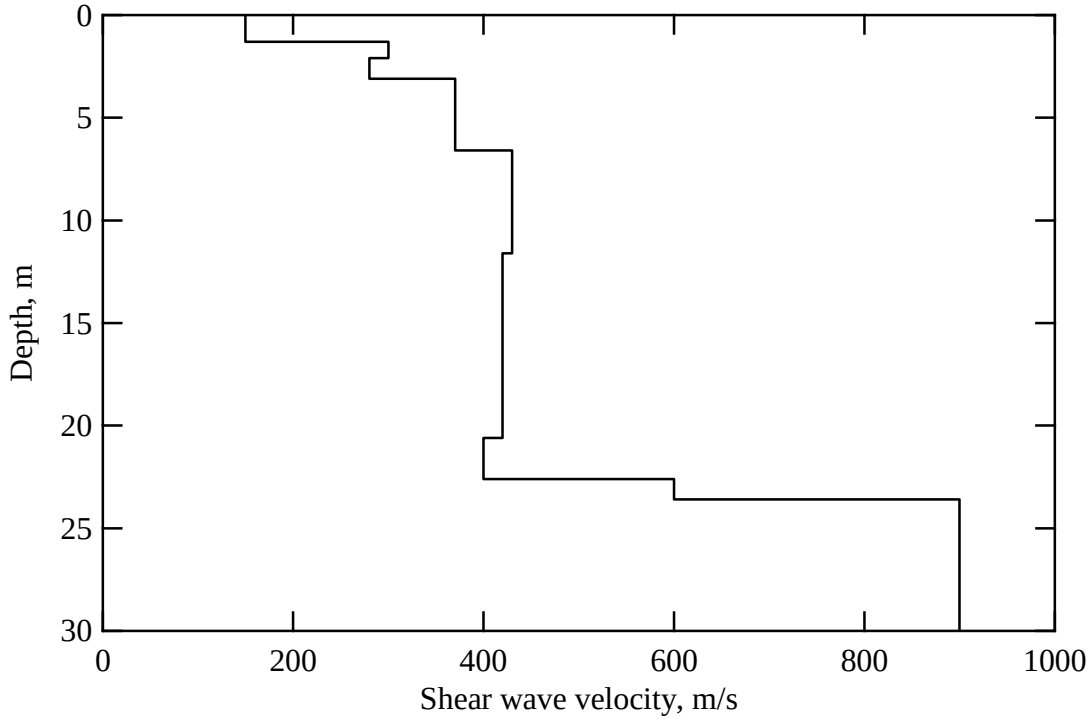

Figure A.42 Shear wave velocity profile determined from forward modeling at Calle Nueva site

Table A.17 Tabulated Values of Measured and Assumed Layer Properties at Calle Nueva Site

Depth to Top Layer, m	Layer Thickness, m	Shear Wave Velocity, m/s	P-wave Velocity, m/s	Poisson's Ratio	Mass Density g/cc
0.0	1.3	150	281	0.3	1.80
1.3	0.8	300	561	0.3	1.80
2.1	1.0	280	524	0.3	1.80
3.1	3.5	370	692	0.3	1.80
6.6	5.0	430	805	0.3	1.95
11.6	9.0	420	786	0.3	1.95
20.6	2.0	400	748	0.3	1.95
22.6	1.0	600	1123	0.3	1.95
23.6	6.4	900	1684	0.3	2.10

Ground motion station

The Ground Motion Station site is located at the Bolivar Avenue and right next to the 25 de Noviembre Stadium. Its latitude and longitude coordinates are 17.18913° south and 70.92921° west, respectively. A plan view of the site is shown in Figure A.43. A photograph of this site is exposed in Figure A.44. Figure A.45 presents the shear wave velocity profile. Tabulated values of shear wave velocity and assumed layer properties used in forward modeling are presented in Table A.18. Average shear wave velocity in the upper 25 m, V_{S25}, at this site is 542 m/s.

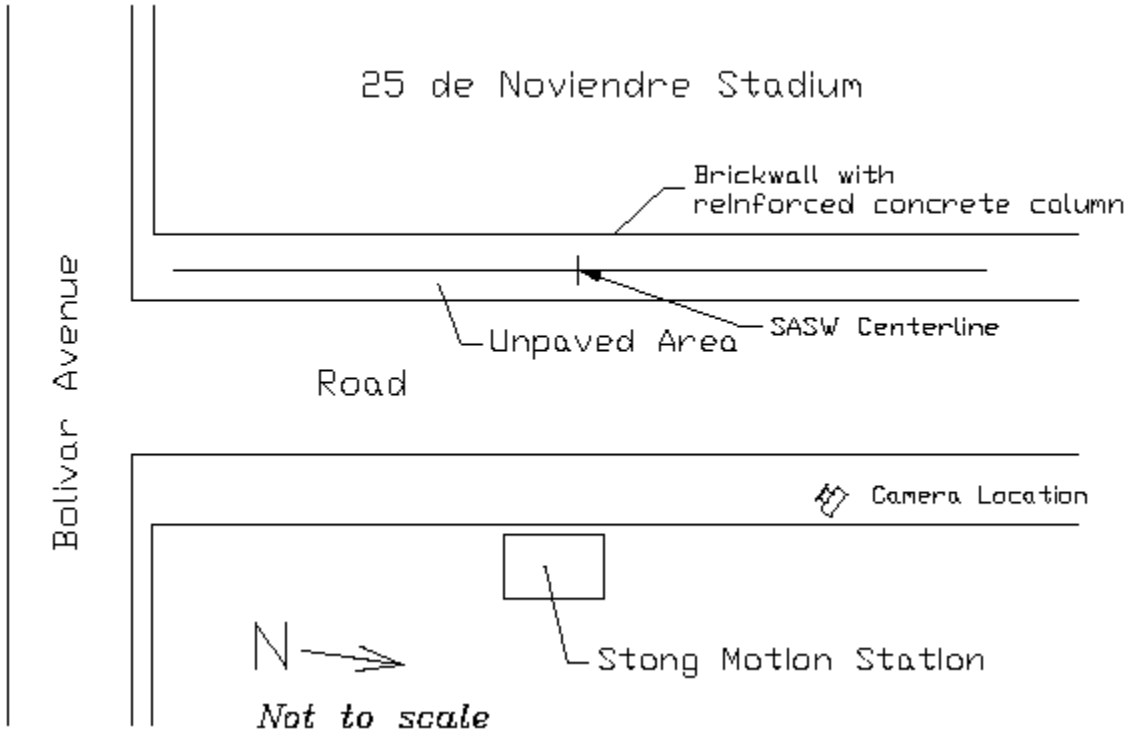

Figure A.43 Plan view of SASW testing at site of Strong Motion Station, located on east side of the "25 de Noviembre" stadium.

Figure A.44 Photograph of SASW testing at site of Strong Motion Station

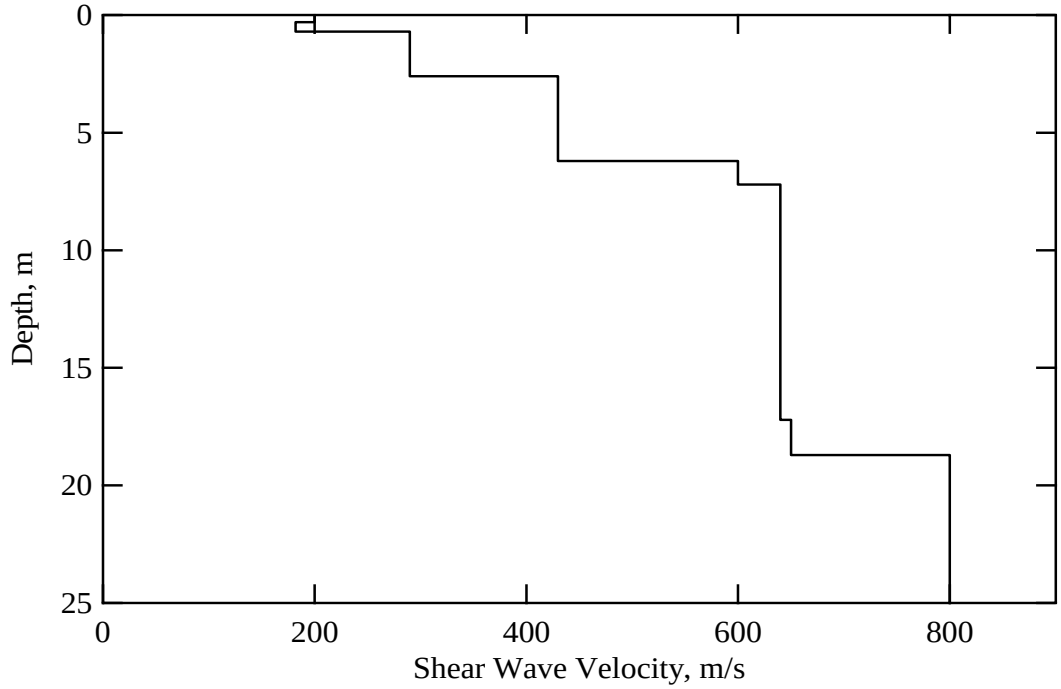

Figure A.45 Shear wave velocity profile determined from forward modeling at Strong Motion Station site.

Depth to Top Layer, m	Layer Thickness, m	Shear Wave Velocity, m/s	P-wave Velocity, m/s	Poisson's Ratio	Mass Density g/cc
0.0	0.3	200	374	0.3	1.80
0.3	0.4	182	341	0.3	1.80
0.7	1.9	290	543	0.3	1.80
2.6	3.6	430	805	0.3	1.95
6.2	1.0	600	1048	0.3	1.95
7.2	10.0	640	1197	0.3	1.95
17.2	1.5	650	1310	0.3	1.95
18.7	6.3	800	1497	0.3	2.10

Table A.18 Tabulated Values of Measured and Assumed Layer Properties at Strong Motion Station Site

“9 de Octubre” Street

This site is located on 9 de Octubre Street in the San Francisco hill, San Francisco district. Its latitude and longitude coordinates are 17.19834° south and 70.39993° west, respectively. A plan view of the site is shown in Figure A.46. Here, testing was performed on asphalt paved-narrow road with steep slope.

A photograph of this site is shown in Figure A.47. The shear wave velocity profile at the site is shown in Figure A.48. Tabulated values of shear wave velocity and assumed layer properties used in forward modeling are presented in Table A.19. Average shear wave velocity in the upper 25 m, V_{S25}, at this site is 567 m/s.

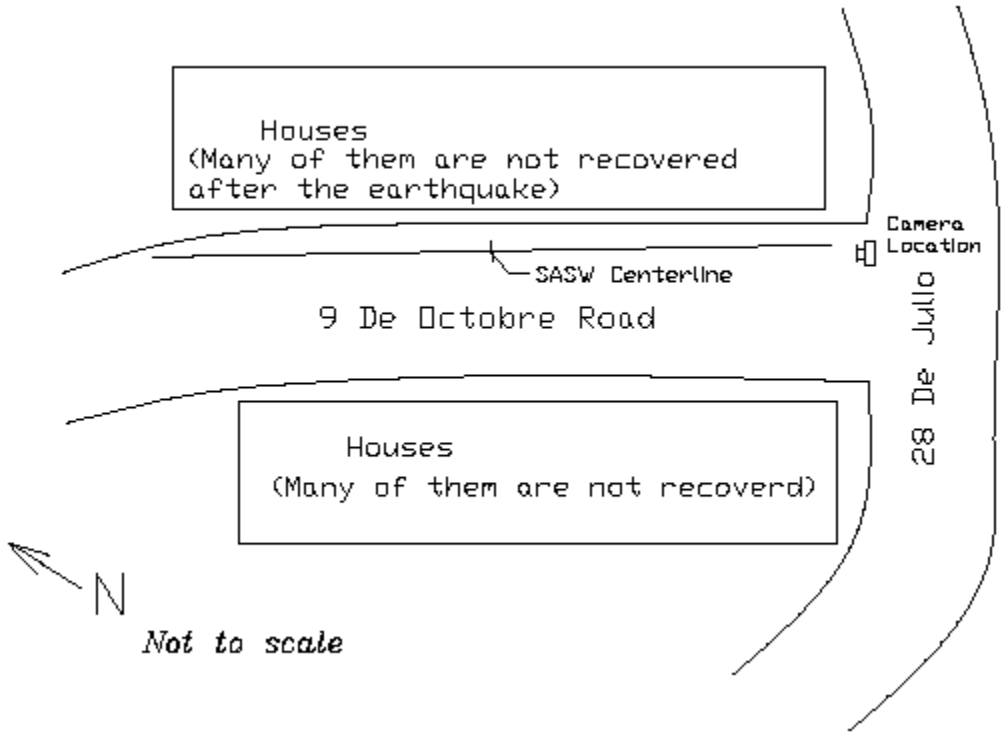

Figure A.46 Plan view of SASW testing at site of 9 de Octubre St., located on 9 de Octubre road in the northern part of San Francisco hill.

Figure A.47 Photograph of SASW testing at site of 9 de Octubre St. 700

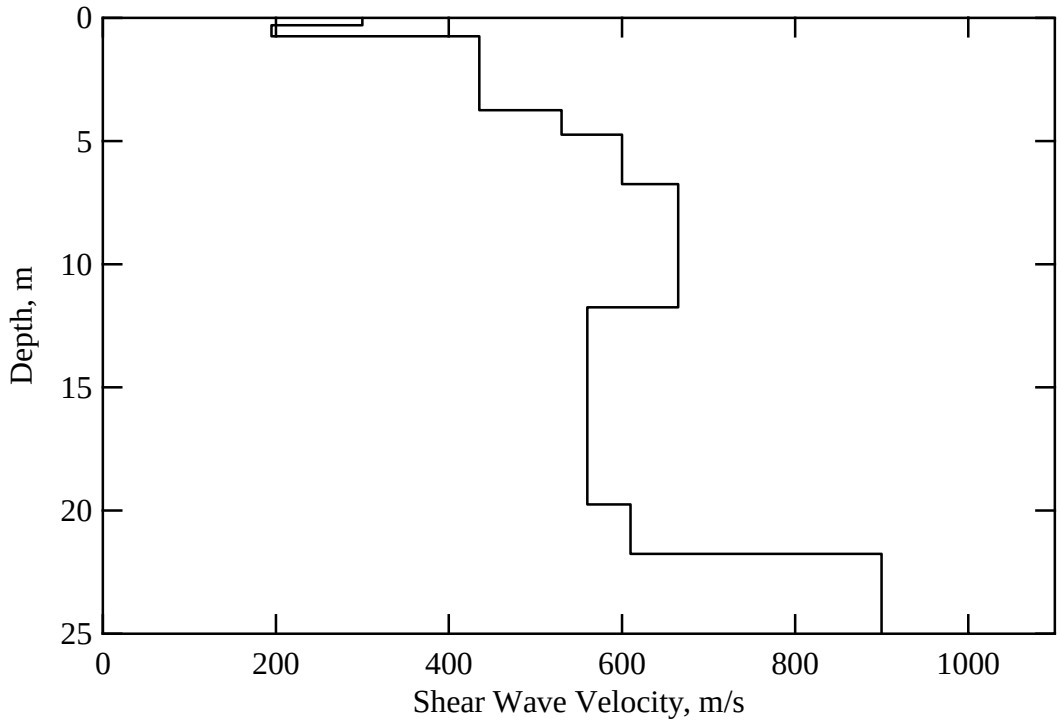

Figure A.48 Shear wave velocity profile determined from forward modeling at 9 de Octubre St. site

Table A.19 Tabulated Values of Measured and Assumed Layer Properties at 9 de Octubre St. Site

Depth to Top Layer, m	Layer Thickness, m	Shear Wave Velocity, m/s	P-wave Velocity, m/s	Poisson's Ratio	Mass Density g/cc
0.00	0.30	300	561	0.3	1.80
0.30	0.45	195	365	0.3	1.80
0.75	3.00	435	814	0.3	1.95
3.75	1.00	530	992	0.3	1.95
4.75	2.00	600	1123	0.3	1.95
6.75	5.00	665	1244	0.3	1.95
11.75	8.00	560	1048	0.3	1.95
19.75	2.00	610	1141	0.3	1.95
21.75	3.25	900	1684	0.3	2.10

San Antonio Hospital

This site is located on right behind the San Antonio Hospital in San Antonio district. The latitude and longitude coordinates on the testing site are 17.21421° south and 70.94712° west, respectively. A plan view of the site is shown in Figure A.49. Here, an outcrop was exposed next to the SASW line. A photograph of this site is shown in Figure A.50. The shear wave velocity profile at the site is shown in Figure A.51. Tabulated values of shear wave velocity and assumed layer properties used in forward modeling are presented in Table A.20. An abrupt velocity increase occurs at around 17 m of depth. However, with this measurement dispersion the SASW can only establish a lower bound for the velocity. The refraction test could be helpful for this kind of SASW problems. The velocity of this layer is at least 1300 m/s. Average shear wave velocity in the upper 25 m, V_{S25}, at this site is 567 m/s.

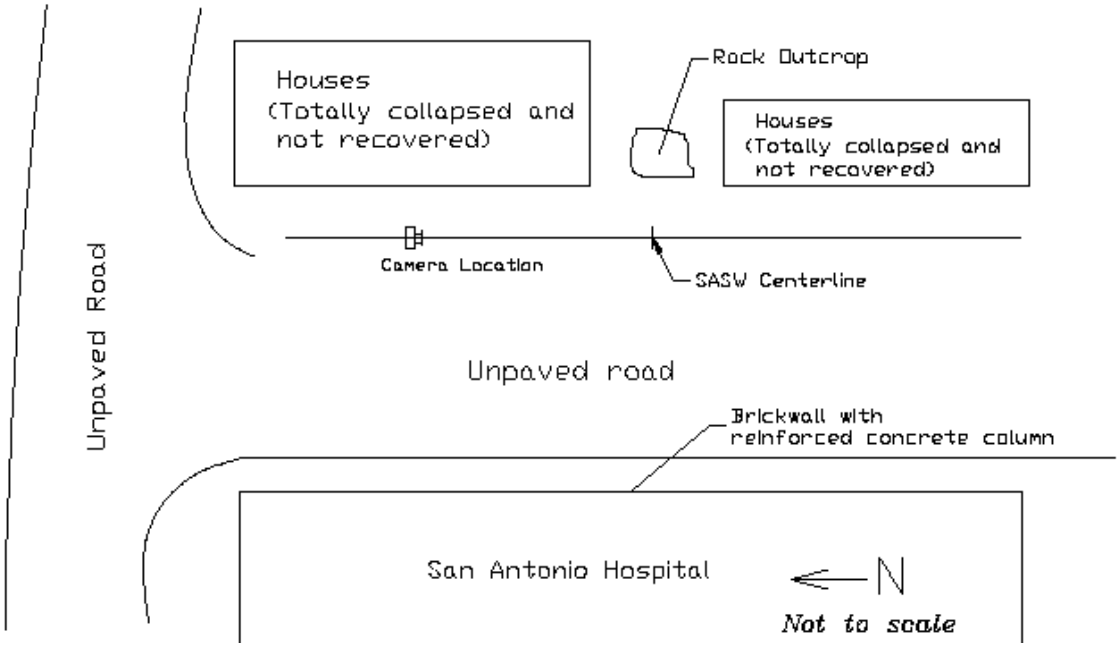

Figure A.49 A plan view of SASW testing at site of San Antonio Hospital, located on the east side of San Antonio hospital

Figure A.50 Photograph of SASW testing at site of San Antonio Hospital 700

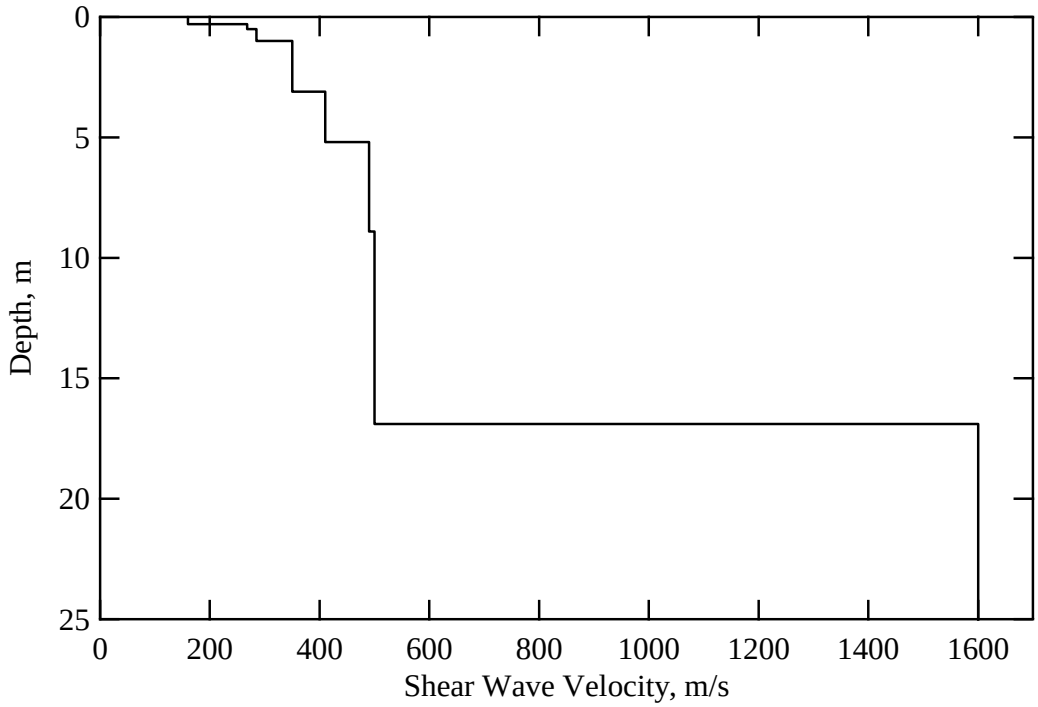

Figure A.51 Shear wave velocity profile determined from forward modeling at San Antonio Hospital site

Table A.20 Tabulated Values of Measured and Assumed Layer Properties at San Antonio Hospital Site

Depth to Top Layer, m	Layer Thickness, m	Shear Wave Velocity, m/s	P-wave Velocity, m/s	Poisson's Ratio	Mass Density, g/cc
0.0	0.3	160	299	0.3	1.80
0.3	0.2	268	501	0.3	1.80
0.5	0.5	285	533	0.3	1.80
1.0	2.1	350	655	0.3	1.80
3.1	2.1	410	767	0.3	1.95
5.2	3.7	490	917	0.3	1.95
8.9	8.0	500	935	0.3	1.95
16.9	8.1	1600*	1871	0.3	2.25

*An abrupt velocity increase occurs at this depth. However, with this measurement dispersion the SASW method can only establish a lower bound for the velocity of the deepest layer. The velocity of this layer is at least 1300 m/s.

474 Lima Street

The testing site is located on the small private parking lot of address of 474 Lima on the Lima Street in the downtown area. The latitude and longitude coordinates on the testing site are 17.19565° south and 70.93625° west, respectively. Since testing was conducted at the small parking lot due to difficulties to find a proper site, insufficient wavelength was generated and only a profile of up to 12 m of depth can be resolved. A plan view of the site is shown in Figure A.52. A photograph of this site is exposed in Figure A.53. The shear wave velocity profile at the site is presented in Figure A.54. Tabulated values of shear wave velocity and assumed layer properties used in forward modeling are presented in Table A.21.

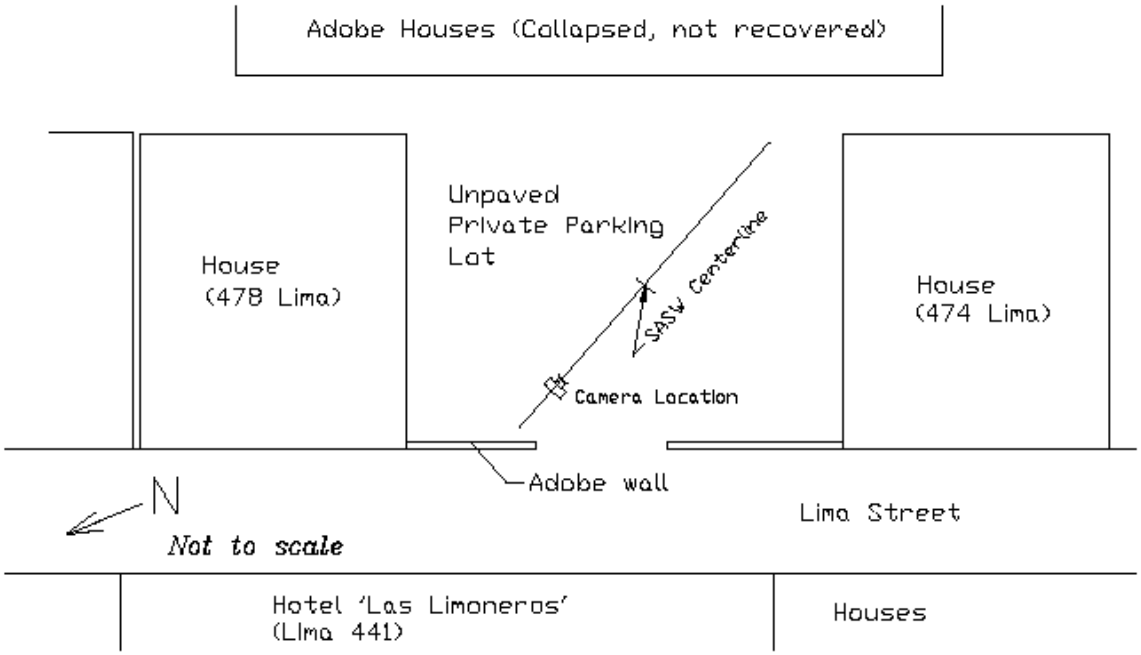

Figure A.52 Plan view of SASW testing at site of 474 Lima St., located on Lima St. in downtown area

Figure A.53 Photograph of SASW testing at site of 474 Lima St. 500

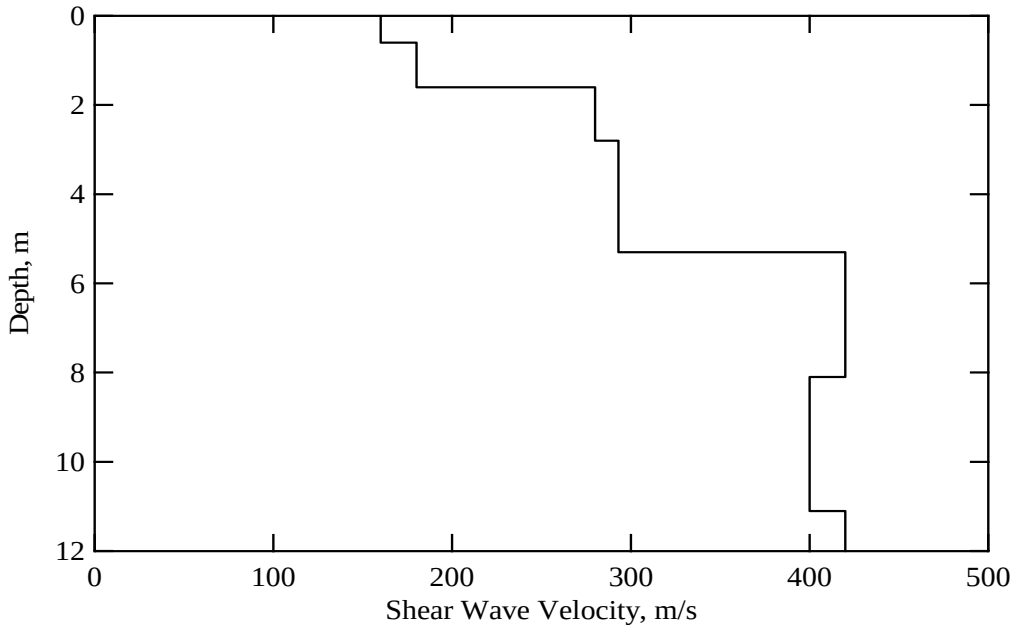

Figure A.54 Shear wave velocity profile determined from forward modeling at 474 Lima St. site

Table A.21 Tabulated Values of Measured and Assumed Layer Properties at 474 Lima St. Site

Depth to Top Layer, m	Layer Thickness, m	Shear Wave Velocity, m/s	P-wave Velocity, m/s	Poisson's Ratio	Mass Density g/cc
0.0	0.6	160	299	0.3	1.80
0.6	1.0	180	337	0.3	1.80
1.6	1.2	280	524	0.3	1.80
2.8	2.5	293	548	0.3	1.80
5.3	2.8	420	786	0.3	1.95
8.1	3.0	400	748	0.3	1.95
11.1	0.9	420	786	0.3	1.95

Table A.22 Average shear wave velocity in the upper 30 m (or 25 m) with UBS site classification at Moquegua Sites.

Site	**Calle Nueva**	**Strong Motion Station**	**"9 de Octubre" Street**	**San Antonio Hospital**	**474 Lima Street [c]**
V_{S30} [a]	421 m/s	542 m/s [b]	567 m/s [b]	567 m/s b	-
UBC class	SC	-	-	-	-

[a] Average shear wave velocity in the upper 30 m.

[b] This site had average shear wave velocity in the upper 25 m.

[c] V_{S30} was not calculated because this site only had depth resolution of 12 m.

Pan American Highway sites

Shintari

Shintari site is located on the landmark of 1238+, which means 1238 km away from Lima, the capital city of Peru, on the Pan-American Highway. The latitude and longitude coordinates on the testing site are 17.79025° south and 70.67208° west, respectively. This embankment was 13 m wide at top, and reached their maximum height of about 10 m with approximately 35 degrees of side slope. The embankment suffered raveling along the side slope, ground deformation, and large vertical and lateral offsets in the pavement, etc. (EERI 2003). A plan view of the Shintari site is shown in Figure A.55. A photograph of this site is exposed in Figure A.56. Figure A.57 presents the shear wave velocity profile at the. Tabulated values of shear wave velocity and assumed layer properties used in forward modeling are presented in Table A.23. Average shear wave velocity in the upper 15 m, V_{S15}, at this site is 405 m/s.

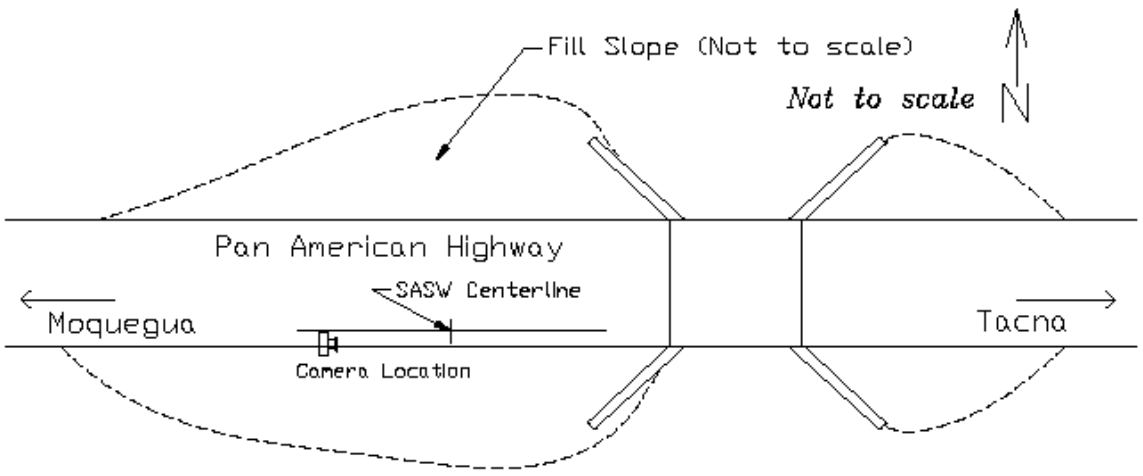

Figure A.55 A plan view of SASW testing at site of Shintari, located on mark point 1238 + along the Pan American highway between Tacna and Moquegua

Figure A.56 Photograph of SASW testing at site of Shintari

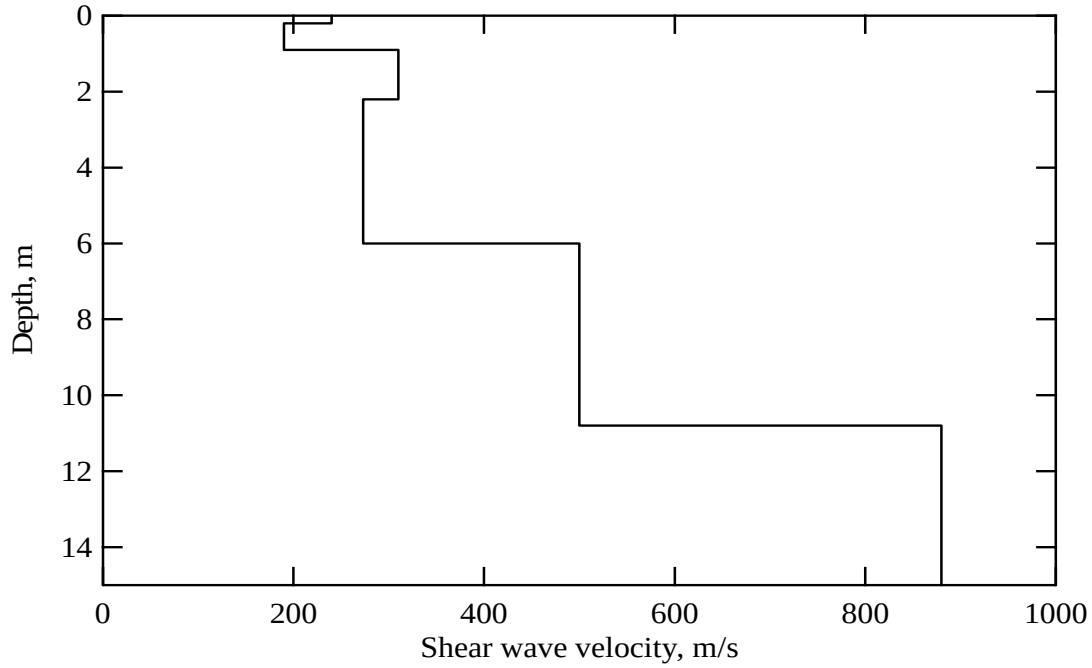

Figure A.57 Shear wave velocity profile determined from forward modeling at Shintari site

Table A.22 Tabulated Values of Measured and Assumed Layer Properties at Shintari Site

Depth to Top Layer, m	Layer Thickness, m	Shear Wave Velocity, m/s	P-wave Velocity, m/s	Poisson's Ratio	Mass Density g/cc
0	0.2	240	449	0.3	1.80
0.2	0.7	190	356	0.3	1.80
0.9	1.3	310	580	0.3	1.80
2.2	3.8	273	511	0.3	1.80
6.0	4.8	500	935	0.3	1.95
10.8	4.2	880	1646	0.3	2.10

Standard penetration test

SPT testing was also performed for this site, the SPT was rejected at about 8.95 meters, and samples were taken and classified following USCS classification system. Table A.23 presents the results obtained, Figure A.58 shows the SPT profile obtained.

Table A.23 SPT results obtained for Shintari Site.

Depth	**N**	**$(N_1)_{60}$**	**SUCS Classification**
0.00			GP-GM
0.50	87	107	GP-GM
0.95	57	64	GP-GM
1.40	32	34	GP-GM
2.30	15	14	SM
3.30	17	14	SM
4.30	20	16	SM
5.30	17	12	SM
6.30	25	19	SM
7.30	28	19	SM
8.30	55	35	SM
8.95	92	55	SM

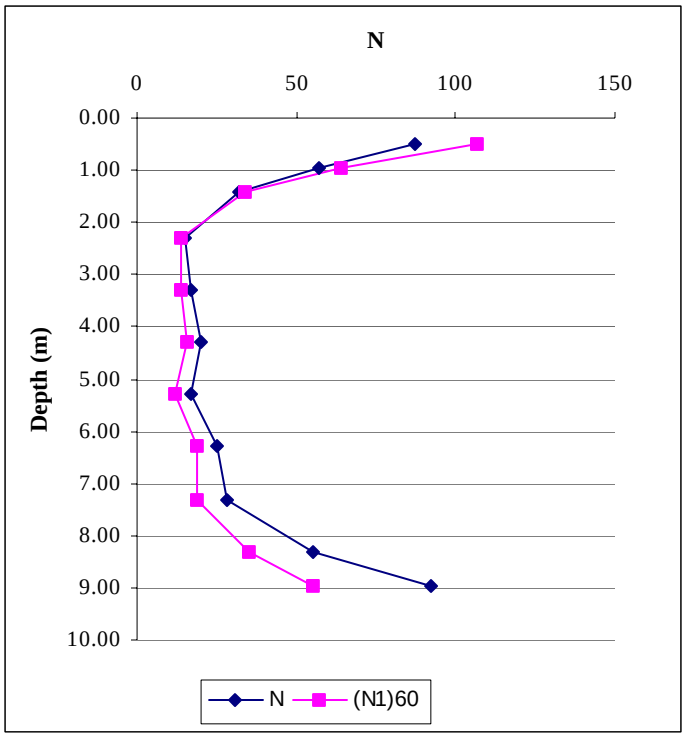

Figure A.58 SPT profile obtained for Shintari Site.

Valley Fill

Valley Fill site is located on the landmark of 1234+, which means 1234 km away from Lima, the capital city of Peru, on the Pan-American Highway. The latitude and longitude coordinate on the testing site are 17.28136° south and 70.71275° west, respectively. This embankment was 70 m long and reached maximum heights of about 30 m with 30 to 40 degrees of side slope. This site also suffered large damage like large ground deformations, consequent damage, and significant settlement of the road surface (EERI 2003). A plan view of Valley Fill site is shown in Figure A.59. A photograph of this site is exposed in Figure A.60. The shear wave velocity profile at the site is presented This embankment was 70 m long and reached maximum heights of about 30 m with 30 to 40 degrees of side slope. This site also suffered large damage like large ground deformations, consequent damage, and significant settlement of the road surface (EERI

2003). in Figure A.61. Tabulated values of shear wave velocity and assumed layer properties used in forward modeling are presented in Table A.23. Average shear wave velocity in the upper 15 m, V_{S15}, at this site is 367 m/s.

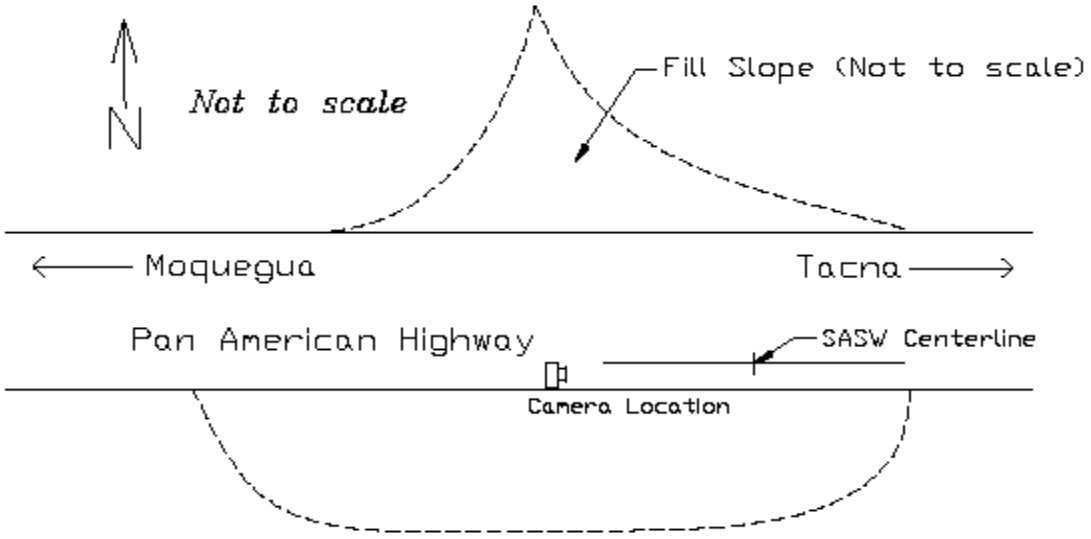

Figure A.59 A plan view of SASW testing at site of Valley Fill, located on mark point 1234 + along the Pan American highway between Tacna and Moquegua

Figure A.60 Photograph of SASW testing at site of Valley Fill

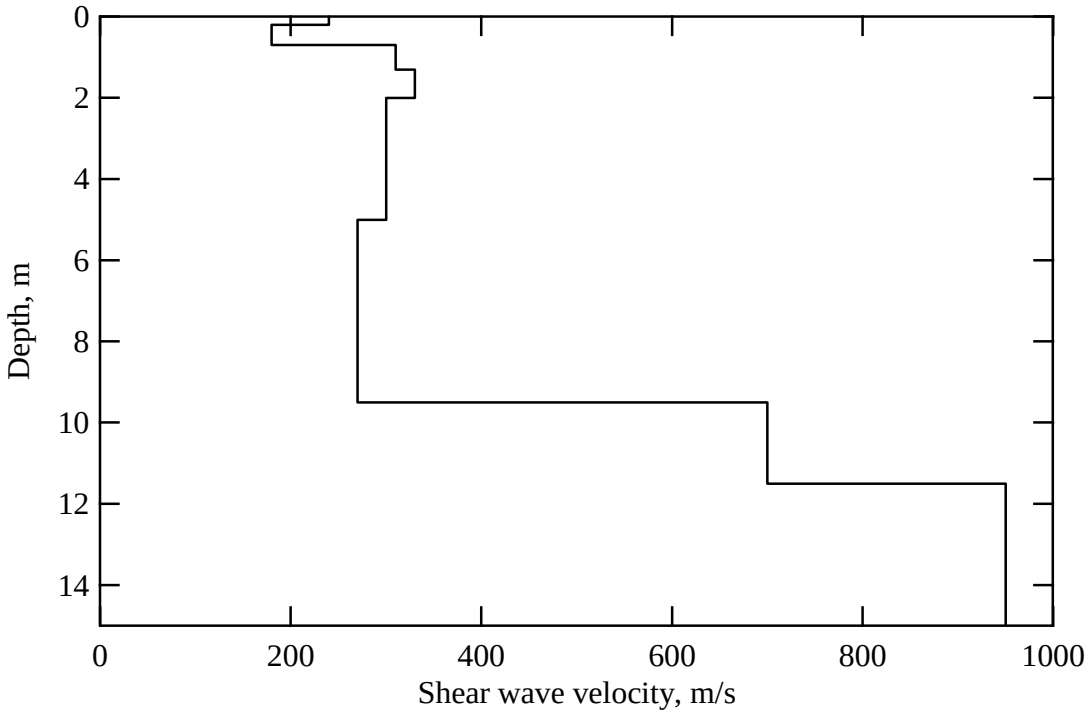

Figure A.61 Shear wave velocity profile determined from forward modeling at Valley Fill site

Table A.24 Tabulated Values of Measured and Assumed Layer Properties at Valley Fill Site

Depth to Top Layer, m	Layer Thickness, m	Shear Wave Velocity, m/s	P-wave Velocity, m/s	Poisson's Ratio	Mass Density g/cc
0.0	0.2	240	449	0.3	1.80
0.2	0.5	180	337	0.3	1.80
0.7	0.6	310	580	0.3	1.80
1.3	0.7	330	617	0.3	1.80
2.0	3.0	300	524	0.3	1.80
5.0	4.5	270	505	0.3	1.80
9.5	2.0	700	1310	0.3	2.10
11.5	3.5	950	1777	0.3	2.10

Standard penetration test

SPT testing was also performed for this site, the SPT was rejected at about 12.3 meters, and samples were taken and classified following USCS classification system. Table A.25 presents the results obtained, Figure A.62 shows the SPT profile obtained.

Table A.25 SPT results obtained for Valley Fill Site.

Depth	N	$(N_1)_{60}$	SUCS Classification
			CL
0.3	85	108	SM
1.3	18	19	SP-SM
3.3	11	9	SP-SM
4.3	16	13	SP-SM
5.3	42	31	SP-SM
6.3	17	13	SP-SM
7.3	14	10	SP-SM
8.3	15	9	SP-SM
9.3	12	7	SP-SM
10.3	21	12	SP-SM
11.3	60	33	SP-SM
12.3	107	55	SP-SM

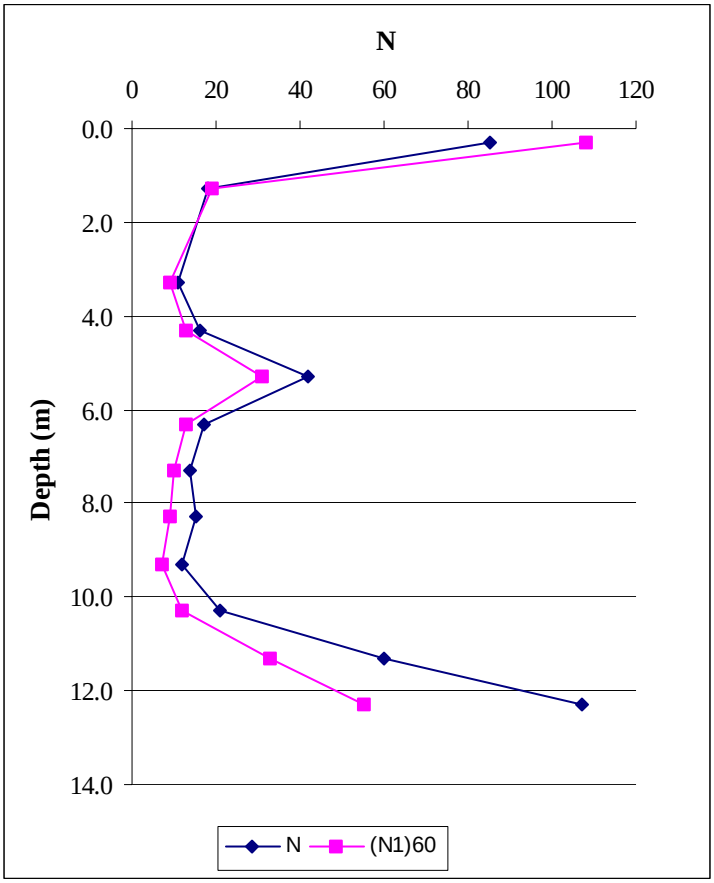

Figure A.62 SPT profile obtained for Valley Fill Site.

Locumba bridge sites

Locumba 1

Locumba 1 is located right next to the Locumba River on the northern side of the gravel levee, under the Locumba Bridge. The latitude and longitude coordinates on the testing site are 17.68739º south and 70.84203º west, respectively.

Here, Locumba bridge and its vicinities suffered severe liquefaction-induced damage during the earthquake such as vertical offsets between the bridge and the adjacent ground, lateral spread on the cornfield, and localized lateral offsets and differential settlement along the south bank, etc. (EERI 2003). A plan view of the Locumba 1 is shown in Figure A.63. A photograph of this site is exposed in Figure A.64. The shear wave velocity profile at the site is presented in Figure A.65. Tabulated values of shear wave velocity and assumed layer properties used in forward modeling are presented in Table A.26. The water table at Locumba 1 is located at the depth of approximately 0.4 m, and remarkably low shear wave velocities were detected near surface.

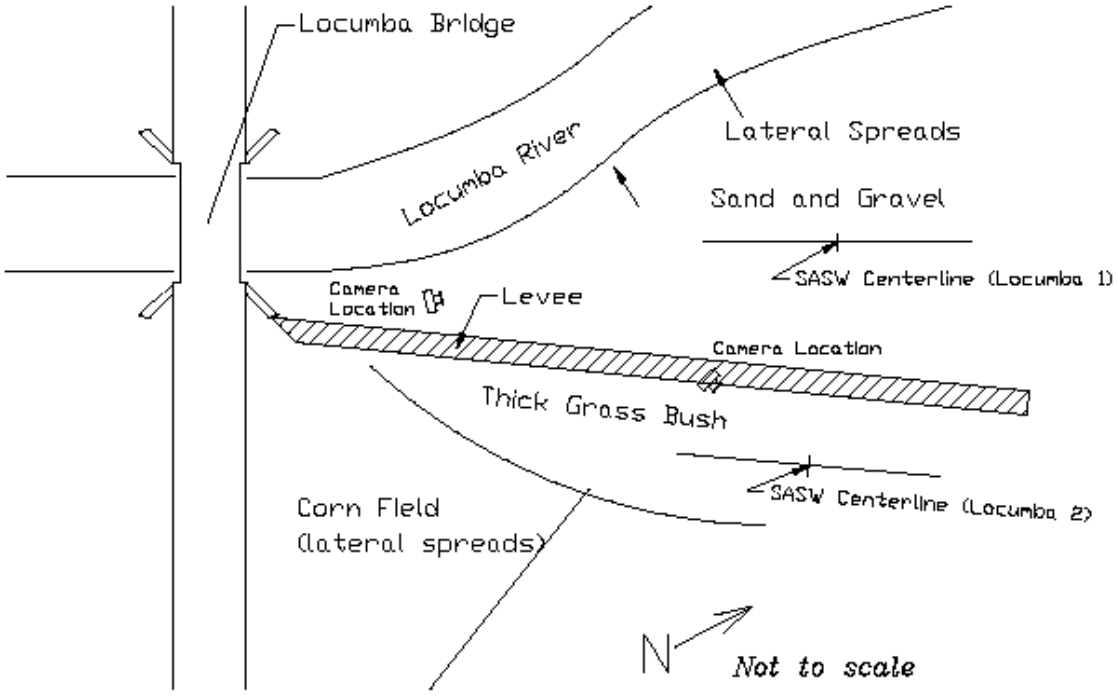

Figure A.63 A plan view of SASW testing lines of Locumba site, located near the Locumba Bridge.

Figure A.64 Photograph of SASW testing at line of Locumba 1

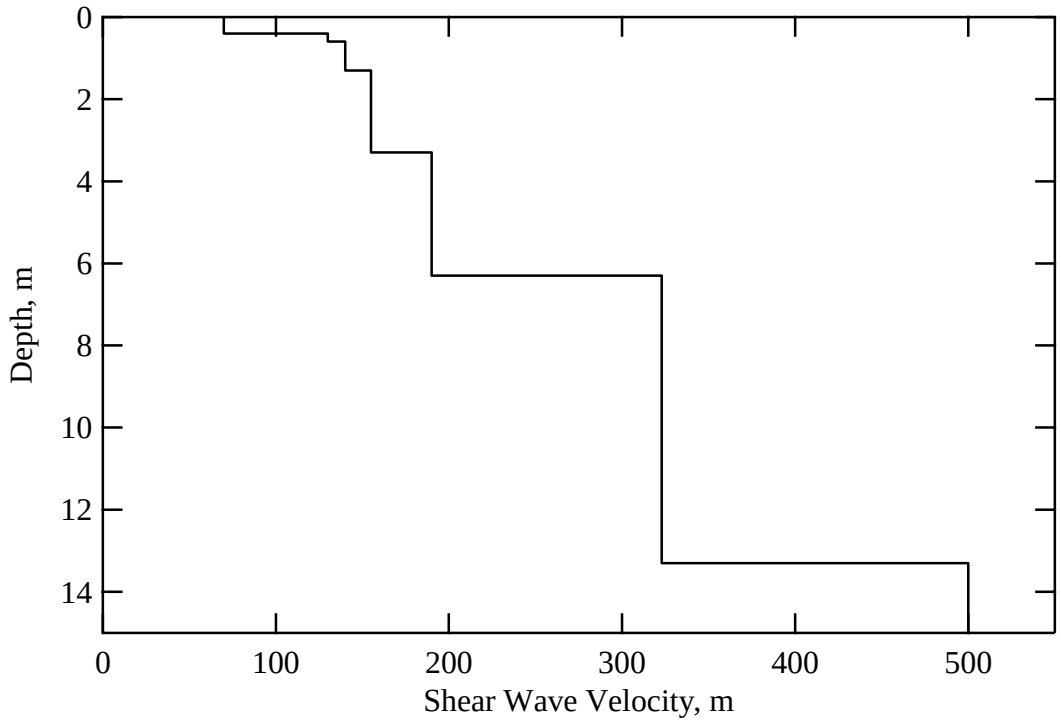

Figure A.65 Shear wave velocity profile determined from forward modeling at Locumba 1

Table A.26 Tabulated Values of Measured and Assumed Layer Properties at Locumba 1

Depth to Top Layer, m	Layer Thickness, m	Shear Wave Velocity, m/s	P-wave Velocity, m/s	Poisson's Ratio	Mass Density, g/cc
0.0	0.4	70	131	0.3	1.8
0.4	0.2	130	1500	0.4962	2.0
0.6	0.7	140	1500	0.4956	2.0
1.3	2.0	155	1500	0.4946	2.0
3.3	3.0	190	1500	0.4918	2.0
6.3	7.0	323	1500	0.4757	2.0
13.3	1.7	500	1500	0.4375	2.0

Standard penetration test

For this site also, SPT testing was performed, the SPT was rejected at about 2.35 meters because of the presence of sandy-gravelly soils, then Peck Cone testing was performed at the same site in order to have an idea of the soil profile. Just 2 samples were taken from the SPT and classified following USCS classification system. Table A.27

presents the results obtained for both SPT and Peck Cone and Figure A.66 shows the SPT and Peck Cone profiles obtained.

Table A.27 SPT results obtained for Locumba 1 Site.

SPT testing - Locumba 1			
Depth	**N**	**$(N_1)_{60}$**	**SUCS Classification**
0[a]			GP
2.35[b]	19	17	SP

[a] Excavation was carried out up to 2 m, groundwater table presence made excavation very difficult.

[b] SPT was rejected here, Peck Cone was used. Calibration of the Peck cone showed that N values of Peck Cone were 2 times the ones of SPT.

Peck Cone testing - Locumba 1	
Depth	**N**
0.3	31
0.6	28
0.9	32
1.2	27
1.5	32
1.8	71
2.1	44
2.4	54
2.7	38
3.0	37
3.3	112
3.6	46
3.9	83
4.2	94

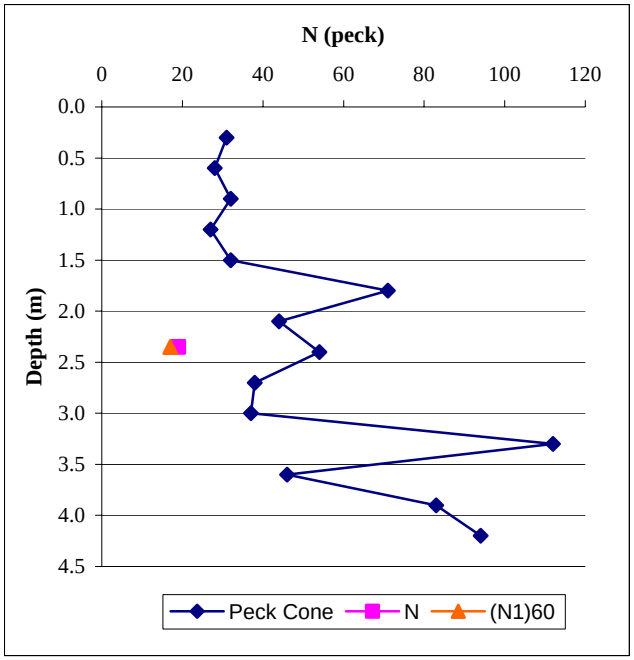

Figure A.66 SPT profile obtained for Locumba 1 Site

3.3.6.2 Locumba 2

Locumba 2 is located on the thick grass bush on the east of the cornfield. The latitude and longitude coordinates on the testing site were missed, but the coordinates may be very close to the one of Locumba 1, 17.68738º south and 70.84203° west, respectively, because these two lines were around 30 m apart from each other. A plan view of the Locumba 2 is shown in Figure A.63. A photograph of this site is exposed in Figure A.67. The shear wave velocity profile at the site is presented in Figure A.68. Tabulated values of shear wave velocity and assumed layer properties used in forward modeling are presented in Table A.28.

The water table at Locumba 2 is located at the depth of approximately 0.7 m, and again extremely low shear wave velocities were detected near surface.

Figure A.67 Photograph of SASW testing at line of Locumba 2

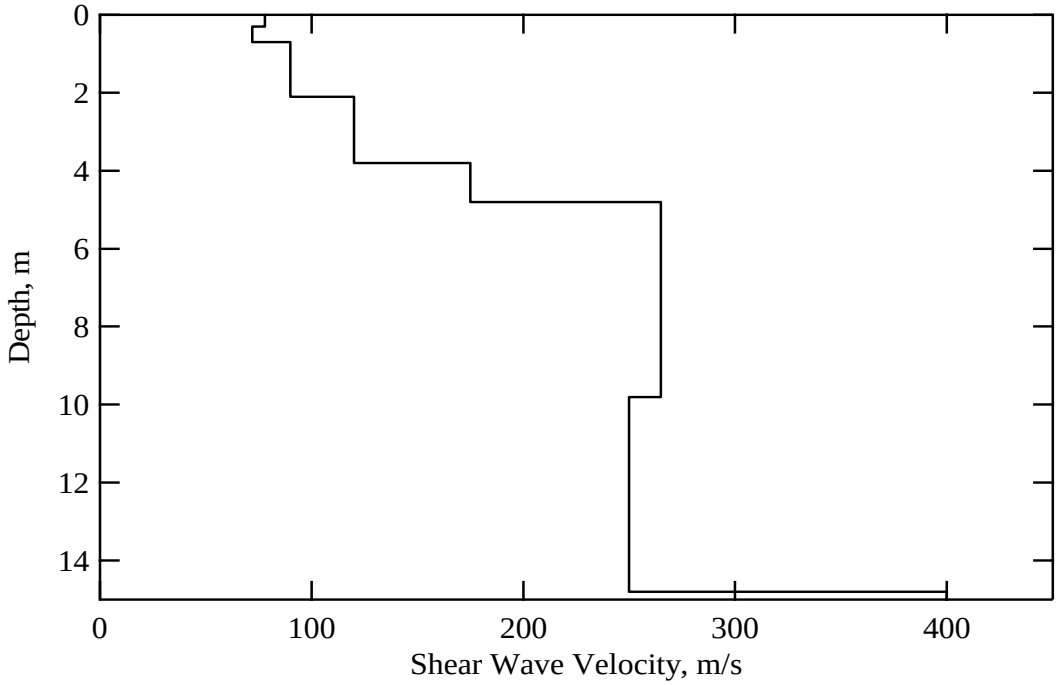

Figure A.68 Shear wave velocity profile determined from forward modeling at Locumba 2

Table A.28 Tabulated Values of Measured and Assumed Layer Properties at Locumba 2

Depth to Top Layer, m	Layer Thickness, m	Shear Wave Velocity, m/s	P-wave Velocity, m/s	Poisson's Ratio	Mass Density, g/cc
0.0	0.3	78	146	0.3	1.8
0.3	0.4	72	135	0.3	1.8
0.7	1.4	90	1500	0.4982	2.0
2.1	1.7	120	1500	0.4968	2.0
3.8	1.0	175	1500	0.4931	2.0
4.8	5.0	265	1500	0.4839	2.0
9.8	5.0	250	1500	0.4857	2.0
14.8	0.2	400	1500	0.4617	2.0

Standard penetration test

For this site again, SPT testing was performed, the SPT was rejected at about 4.0 meters because of the presence of sandy-gravelly soils, it is important to note that the SPT was having problems to penetrate these soils since the depth of 2 m, therefore Peck Cone testing was performed at the same site in order to have an idea of the soil profile. A few samples were taken from the SPT and classified following USCS classification system. Table A.29 presents the results obtained for both STP and Peck Cone and Figure A.69 shows the SPT and Peck Cone profiles obtained.

Table A.29 SPT results obtained for Locumba 2 Site.

SPT testing - Locumba 1			
Depth	**N**	**$(N_1)_{60}$**	**SUCS Classification**
0.00			CL
0.30	4	5	
1.30	6	6	ML
2.30	19	17	SP-SM
2.90	17	14	
3.90	23	17	SP
3.45	[a]		GP
3.95			SP
4.95			
6.45			CL
7.45			SP
8.45			ML
9.45			SP-SM

[a] SPT was rejected here, Peck Cone was used. Calibration of the Peck cone showed that N values of Peck Cone were 2 times the ones of SPT.

Peck Cone testing - Locumba 1	
Depth	**N**
0.3	3
0.6	6
0.9	3
1.2	6
1.5	36
1.8	16
2.1	2
2.4	4
2.7	10
3.0	28
3.3	68
3.6	66
3.9	54
4.2	61
4.5	50

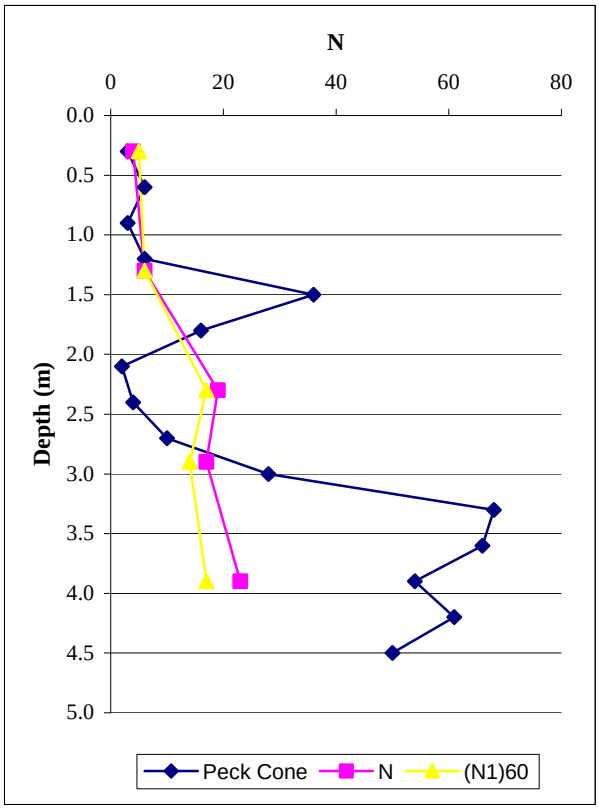

Figure A.69 SPT profile obtained for Locumba 2 Site

APPENDIX B

RESULTS OBTAINED FROM THE

EVALUATION OF THE SPT ANALYZER DATA

Project Name - PJ PERU
Pile Name - PN 1
Description - PD TACNA
Operator Name - OP ER AC

AR	**Area**	7.87	cm^2
LE	**Length below sensors to pile bottom**	3.97	meters
SP	**Specific Weight Density**	77.3	tonnes/meter^3
WS	**Wave Speed**	5123	meters/second
EM	**Elastic Modulus**	206840	tonnes/cm^2

Strain transducers and accelerometers

F3	**F1**	216.45
F4	**F2**	26.40
A3	**A1**	325.00
A4	**A2**	345.00

start	9	10:39:46
stop	46	10:41:57
start	47	11:06:20
stop	99	11:08:50

NOTES

LP	Length of Penetration (penetration depth)
BN	Blow Number
EMX	Maximum Energy
DMX	Maximum Displacement
VMX	Maximum Velocity
FMX	Maximum Force
BMP	Blow Rate
ETR	Energy Transfer Ratio-Rated
EF2	Energy of F^2 (ASTM D4633)
RAT	Length Ratio for SPT (should be between 90 and 120% for a valid test)
CSB	Maximum Toe Stress
JC	Case Damping Constant
WC	Wave Speed Calculated
Wh	Theoretical Potential Energy for the SPT ram
N_{60}	Blow Number Corrected by Energy

Date	Time	LP (m)	BN	EMX (ton-m)	DMX (mm)	VMX (m/sec)	FMX (ton)	BPM (blows/min)	ETR (%)	EF2 (ton-m)	RAT	CSB (Mpa)	jc	WC (m/sec)	N_{60}	Comments
6/29/2003	10:39:46	1	9	0.250	34	3.27	87	0.0	52.6	0.150	1.3	68.40	0	5123	8	
6/29/2003	10:39:54	1	11	0.274	21	3.25	95	0.0	57.7	0.142	1.3	80.20	0	5123	11	
6/29/2003	10:39:57	1	12	0.279	16	3.08	92	0.0	58.7	0.136	1.4	79.50	0	5123	12	
6/29/2003	10:40:01	1	13	0.272	15	2.90	106	0.0	57.3	0.111	1.4	98.80	0	5123	12	
6/29/2003	10:40:04	1	14	0.268	14	3.06	109	20.8	56.5	0.110	1.5	108.40	0	5123	13	
6/29/2003	10:40:07	1	15	0.274	19	3.05	109	19.4	57.7	0.000	0.5	122.40	0	5123	14	
6/29/2003	10:40:10	1	16	0.268	14	3.09	109	19.4	56.5	0.128	1.5	111.10	0	5123	15	
6/29/2003	10:40:13	1	17	0.295	15	3.25	110	19.0	62.1	0.149	1.5	109.90	0	5123	18	
6/29/2003	10:40:16	1	18	0.279	14	3.13	109	0.0	58.8	0.133	1.4	109.20	0	5123	18	
6/29/2003	10:40:20	1	19	0.288	15	3.10	102	0.0	60.7	0.139	1.4	97.00	0	5123	19	
6/29/2003	10:40:23	1	20	0.279	13	3.00	102	0.0	58.8	0.112	1.7	112.20	0	5123	20	
6/29/2003	10:40:33	1	21	0.276	13	3.05	104	0.0	58.1	0.114	1.6	111.90	0	5123	20	
6/29/2003	10:40:36	1	22	0.272	12	3.12	104	0.0	57.3	0.143	1.5	87.20	0	5123	21	
6/29/2003	10:40:40	1	23	0.267	11	3.13	107	0.0	56.2	0.116	1.5	114.30	0	5123	22	
6/29/2003	10:40:44	1	24	0.260	11	3.34	110	0.0	54.7	0.127	1.6	127.40	0	5123	22	
6/29/2003	10:40:48	1	25	0.258	11	2.93	93	0.0	54.3	0.127	1.7	74.10	0	5123	23	
6/29/2003	10:40:51	1	26	0.269	12	3.10	100	0.0	56.6	0.135	1.6	94.80	0	5123	25	
6/29/2003	10:40:54	1	27	0.271	11	3.17	109	0.0	57.2	0.150	1.5	68.20	0	5123	26	
6/29/2003	10:40:57	1	28	0.269	11	3.29	114	19.5	56.8	0.144	1.4	102.10	0	5123	27	
6/29/2003	10:41:01	1	29	0.258	11	3.22	112	0.0	54.4	0.130	1.6	118.60	0	5123	26	
6/29/2003	10:41:04	1	30	0.268	11	3.22	113	0.0	56.5	0.146	1.7	109.70	0	5123	28	
6/29/2003	10:41:08	1	31	0.275	11	3.29	104	0.0	58.0	0.145	1.4	79.10	0	5123	30	
6/29/2003	10:41:12	1	32	0.280	12	3.28	112	0.0	59.0	0.134	1.7	118.90	0	5123	31	
6/29/2003	10:41:15	1	33	0.297	14	3.37	106	19.8	62.6	0.152	1.4	66.90	0	5123	34	
6/29/2003	10:41:18	1	34	0.264	11	3.38	103	0.0	55.6	0.131	1.4	87.40	0	5123	32	
6/29/2003	10:41:21	1	35	0.249	9	3.22	102	19.8	52.4	0.114	1.7	105.90	0	5123	31	
6/29/2003	10:41:24	1	36	0.267	11	3.03	105	19.4	56.2	0.119	1.5	107.80	0	5123	34	
6/29/2003	10:41:27	1	37	0.246	10	3.20	96	19.4	51.9	0.124	1.4	86.80	0	5123	32	
6/29/2003	10:41:31	1	38	0.260	10	3.15	107	0.0	54.9	0.141	1.4	90.90	0	5123	35	
6/29/2003	10:41:34	1	39	0.261	11	2.95	101	19.5	55.0	0.119	1.4	113.10	0	5123	36	
6/29/2003	10:41:36	1	40	0.260	11	2.87	92	21.2	54.8	0.121	1.4	76.70	0	5123	37	
6/29/2003	10:41:39	1	41	0.264	13	3.20	112	22.4	55.7	0.142	1.3	102.80	0	5123	38	
6/29/2003	10:41:42	1	42	0.260	11	2.93	102	20.5	54.7	0.127	1.4	94.40	0	5123	38	
6/29/2003	10:41:49	1	43	0.256	11	2.93	104	0.0	54.0	0.133	1.4	95.30	0	5123	39	
6/29/2003	10:41:52	1	44	0.263	12	3.18	112	20.6	55.5	0.141	1.3	112.10	0	5123	41	
6/29/2003	10:41:54	1	45	0.256	11	3.04	104	21.5	54.0	0.129	1.4	111.80	0	5123	41	
6/29/2003	10:41:57	1	46	0.274	14	3.16	113	22.0	57.8	0.148	1.3	111.40	0	5123	44	
6/29/2003	11:06:20	2	47	0.237	30	3.28	93	0.0	49.9	0.182	1.2	91.10	0	5123	39	
6/29/2003	11:06:24	2	48	0.251	24	3.04	100	0.0	53.0	0.151	1.2	97.20	0	5123	42	
6/29/2003	11:06:27	2	49	0.246	22	2.99	99	0.0	51.9	0.153	1.2	78.30	0	5123	42	
6/29/2003	11:06:30	2	50	0.244	18	3.19	106	21.5	51.3	0.165	1.2	106.00	0	5123	43	
6/29/2003	11:06:33	2	51	0.247	17	3.28	106	0.0	52.0	0.168	1.3	99.90	0	5123	44	
6/29/2003	11:06:36	2	52	0.240	16	3.36	104	20.8	50.5	0.167	1.2	94.60	0	5123	44	
6/29/2003	11:06:40	2	53	0.262	17	3.31	111	0.0	55.2	0.191	1.2	97.80	0	5123	49	
6/29/2003	11:06:43	2	54	0.252	15	3.36	108	19.2	53.2	0.191	1.2	107.40	0	5123	48	
6/29/2003	11:06:46	2	55	0.249	15	3.25	107	19.0	52.5	0.194	1.2	105.20	0	5123	48	
6/29/2003	11:06:49	2	56	0.269	16	3.26	101	0.0	56.6	0.174	1.2	85.70	0	5123	53	
6/29/2003	11:06:53	2	57	0.247	13	3.21	102	0.0	52.0	0.139	1.2	99.10	0	5123	49	
6/29/2003	11:06:56	2	58	0.238	13	3.10	108	20.3	50.1	0.150	1.3	109.40	0	5123	48	
6/29/2003	11:06:59	2	59	0.255	16	3.03	101	19.0	53.8	0.150	1.2	96.20	0	5123	53	
6/29/2003	11:07:02	2	60	0.235	12	3.15	112	19.7	49.6	0.153	1.2	116.40	0	5123	50	
6/29/2003	11:07:04	2	61	0.251	15	3.01	106	20.9	52.9	0.148	1.2	90.60	0	5123	54	
6/29/2003	11:07:07	2	62	0.250	16	3.16	116	21.2	52.6	0.158	1.2	116.00	0	5123	54	
6/29/2003	11:07:11	2	63	0.250	13	3.00	110	0.0	52.7	0.163	1.2	106.90	0	5123	55	
6/29/2003	11:07:14	2	64	0.258	16	3.01	109	0.0	54.3	0.152	1.2	103.30	0	5123	58	
6/29/2003	11:07:17	2	65	0.269	18	2.94	109	20.2	56.8	0.157	1.2	106.00	0	5123	62	
6/29/2003	11:07:20	2	66	0.273	19	3.07	109	22.2	57.4	0.151	1.2	109.80	0	5123	63	
6/29/2003	11:07:23	2	67	0.252	13	2.94	110	0.0	53.1	0.164	1.2	102.90	0	5123	59	
6/29/2003	11:07:26	2	68	0.259	14	3.35	102	21.1	54.5	0.153	1.3	100.80	0	5123	62	
6/29/2003	11:07:29	2	69	0.270	21	2.97	101	0.0	57.0	0.145	1.2	80.50	0	5123	66	
6/29/2003	11:07:33	2	70	0.264	18	2.99	106	0.0	55.7	0.161	1.2	103.40	0	5123	65	
6/29/2003	11:07:36	2	71	0.267	14	3.31	111	19.9	56.3	0.167	1.3	106.70	0	5123	67	
6/29/2003	11:07:38	2	72	0.267	16	3.23	101	21.2	56.3	0.163	1.3	103.20	0	5123	68	
6/29/2003	11:07:41	2	73	0.273	15	3.46	101	19.5	57.5	0.169	1.3	97.70	0	5123	70	
6/29/2003	11:07:44	2	74	0.237	3	3.13	91	21.4	50.0	0.000	0.1	88.70	0	5123	62	
6/29/2003	11:07:47	2	75	0.250	10	3.30	105	21.9	52.7	0.156	1.2	92.60	0	5123	66	
6/29/2003	11:07:49	2	76	0.271	16	3.16	114	23.6	57.1	0.169	1.2	112.80	0	5123	72	
6/29/2003	11:07:52	2	77	0.274	14	3.71	113	23.6	57.8	0.181	1.3	112.20	0	5123	74	
6/29/2003	11:07:54	2	78	0.269	18	3.79	112	23.3	56.7	0.000	0.6	127.30	0	5123	74	
6/29/2003	11:07:57	2	79	0.273	13	3.67	115	23.4	57.5	0.183	1.2	115.20	0	5123	76	
6/29/2003	11:08:00	2	80	0.293	21	3.69	115	20.8	61.8	0.185	1.2	111.20	0	5123	82	
6/29/2003	11:08:02	2	81	0.307	25	3.66	116	23.9	64.7	0.000	0.7	134.00	0	5123	87	
6/29/2003	11:08:05	2	82	0.246	13	3.51	85	23.7	51.8	0.168	1.3	83.20	0	5123	71	
6/29/2003	11:08:08	2	83	0.256	10	3.23	117	0.0	54.0	0.175	1.2	114.30	0	5123	75	
6/29/2003	11:08:10	2	84	0.232	16	3.74	101	25.1	49.0	0.142	1.2	99.80	0	5123	69	
6/29/2003	11:08:13	2	85	0.270	13	3.64	106	24.2	56.9	0.190	1.2	94.60	0	5123	81	
6/29/2003	11:08:15	2	86	0.276	12	3.81	118	23.1	58.1	0.209	1.2	118.30	0	5123	83	
6/29/2003	11:08:18	2	87	0.310	22	3.95	112	22.9	65.4	0.235	1.2	92.20	0	5123	95	
6/29/2003	11:08:20	2	88	0.271	12	3.82	114	23.2	57.2	0.210	1.2	114.60	0	5123	84	
6/29/2003	11:08:24	2	89	0.281	20	3.39	108	0.0	59.3	0.153	1.2	97.20	0	5123	88	
6/29/2003	11:08:29	2	91	0.289	19	3.72	118	22.4	60.8	0.219	1.2	117.00	0	5123	92	

Date	Time	LP (m)	BN	EMX (ton-m)	DMX (mm)	VMX (m/sec)	FMX (ton)	BPM (blows/min)	ETR (%)	EF2 (ton-m)	RAT	CSB (Mpa)	jc	WC (m/sec)	N_{60}	Comments
6/29/2003	11:08:31	2	92	0.264	10	3.73	115	24.1	55.6	0.183	1.2	109.10	0	5123	85	
6/29/2003	11:08:34	2	93	0.280	12	3.66	116	21.1	59.0	0.199	1.2	109.00	0	5123	91	
6/29/2003	11:08:37	2	94	0.276	12	3.87	115	23.0	58.2	0.194	1.2	109.50	0	5123	91	
6/29/2003	11:08:39	2	95	0.284	15	3.61	118	22.5	59.8	0.201	1.3	109.10	0	5123	95	
6/29/2003	11:08:42	2	96	0.279	12	3.87	124	21.9	58.7	0.225	1.2	114.90	0	5123	94	
6/29/2003	11:08:44	2	97	0.289	16	3.79	120	22.5	60.9	0.214	1.2	111.80	0	5123	98	
6/29/2003	11:08:47	2	98	0.287	13	3.90	121	22.4	60.5	0.225	1.2	108.80	0	5123	99	
6/29/2003	11:08:50	2	99	0.292	16	3.84	122	22.4	61.4	0.217	1.2	115.40	0	5123	101	
						Average Energy Ratio =			**56.0**							

Project Name - PJ PERU 2
Pile Name - PN 2
Description - PD ;;
Operator Name - OP JW AC

AR	**Area**	7.87	cm^2
LE	**Length below sensors to pile bottom**	2	meters
SP	**Specific Weight Density**	77.3	tonnes/meter^3
WS	**Wave Speed**	5123	meters/second
EM	**Elastic Modulus**	206840	tonnes/cm^2

Strain transducers and accelerometers

F3	**F1**	216.4
F4	**F2**	216.4
A3	**A1**	325.0
A4	**A2**	345.0

start	3	13:53:59
stop	72	13:57:14
start	75	14:02:51
stop	285	14:10:48
start	288	14:21:15
stop	483	14:29:17
start	492	14:36:16
stop	534	14:41:22

NOTES

LP	Length of Penetration (penetration depth)
BN	Blow Number
EMX	Maximum Energy
DMX	Maximum Displacement
VMX	Maximum Velocity
FMX	Maximum Force
BMP	Blow Rate
ETR	Energy Transfer Ratio-Rated
EF2	Energy of F^2 (ASTM D4633)
RAT	Length Ratio for SPT (should be between 90 and 120% for a valid test)
CSB	Maximum Toe Stress
JC	Case Damping Constant
WC	Wave Speed Calculated
Wh	Theoretical Potential Energy for the SPT ram
N_{60}	Blow Number Corrected by Energy

Date	Time	LP (m)	BN	EMX (ton-m)	DMX (mm)	VMX (m/sec)	FMX (ton)	BPM (blows/min)	ETR (%)	EF2 (ton-m)	RAT	CSB (Mpa)	jc	WC (m/sec)	N_{60}	Comments
6/30/2003	13:53:59	0.9	3	0.257	14	3.20	64	0.0	54.1	0.070	1.7	8.90	0	5123	3	
6/30/2003	13:54:20	0.9	6	0.286	14	3.81	97	0.0	60.2	0.093	1.4	54.10	0	5123	6	
6/30/2003	13:54:27	0.9	9	0.286	13	3.99	90	29.2	60.3	0.095	1.4	48.30	0	5123	9	
6/30/2003	13:54:33	0.9	12	0.293	15	4.04	93	28.7	61.7	0.110	1.4	52.60	0	5123	12	
6/30/2003	13:54:41	0.9	15	0.334	16	4.48	102	29.3	70.4	0.118	1.5	72.90	0	5123	18	
6/30/2003	13:54:47	0.9	18	0.313	16	3.93	83	28.9	66.0	0.110	1.9	53.50	0	5123	20	
6/30/2003	13:54:53	0.9	21	0.306	11	3.92	84	29.5	64.6	0.115	1.9	46.70	0	5123	23	
6/30/2003	13:55:05	0.9	24	0.314	11	4.10	88	29.1	66.2	0.114	1.5	59.00	0	5123	26	
6/30/2003	13:55:12	0.9	27	0.322	21	4.04	94	27.1	67.9	0.121	1.4	27.70	0	5123	31	
6/30/2003	13:55:26	0.9	30	0.348	26	4.24	97	0.0	73.4	0.112	1.7	75.40	0	5123	37	
6/30/2003	13:55:33	0.9	33	0.321	19	3.87	90	27.7	67.7	0.115	1.5	49.80	0	5123	37	
6/30/2003	13:55:40	0.9	36	0.321	16	3.92	93	0.0	67.7	0.108	1.4	54.50	0	5123	41	
6/30/2003	13:55:47	0.9	39	0.333	17	4.20	102	27.7	70.3	0.113	1.4	54.40	0	5123	46	
6/30/2003	13:55:54	0.9	42	0.319	18	3.94	86	25.0	67.3	0.110	1.4	57.20	0	5123	47	
6/30/2003	13:56:01	0.9	45	0.322	18	4.01	92	26.4	67.8	0.000	0.3	84.50	0	5123	51	
6/30/2003	13:56:17	0.9	48	0.312	18	4.35	88	20.4	65.8	0.100	1.7	13.20	0	5123	53	
6/30/2003	13:56:25	0.9	51	0.173	18	3.42	71	0.0	36.5	0.000	0.3	42.30	0	5123	31	
6/30/2003	13:56:30	0.9	54	0.276	15	3.63	89	30.7	58.2	0.088	1.4	39.50	0	5123	52	
6/30/2003	13:56:37	0.9	57	0.316	20	3.75	95	32.0	66.5	0.097	1.4	46.40	0	5123	63	
6/30/2003	13:56:43	0.9	60	0.335	19	3.99	101	30.3	70.5	0.117	1.5	53.30	0	5123	71	
6/30/2003	13:56:56	0.9	63	0.301	17	4.27	78	29.1	63.4	0.093	1.4	316.20	0	5123	67	
6/30/2003	13:57:01	0.9	66	0.357	19	3.94	104	32.0	75.3	0.115	1.5	52.90	0	5123	83	
6/30/2003	13:57:08	0.9	69	0.298	16	3.92	91	30.9	62.8	0.000	0.8	73.80	0	5123	72	
6/30/2003	13:57:14	0.9	72	0.224	11	3.07	78	30.5	47.2	0.069	1.4	53.60	0	5123	57	
6/30/2003	14:02:51	0.9	75	0.267	15	3.56	79	0.0	56.3	0.130	2.6	67.20	0	5123	70	
6/30/2003	14:02:58	0.9	78	0.298	17	3.67	100	25.3	62.8	0.128	2.3	73.60	0	5123	82	
6/30/2003	14:03:05	0.9	81	0.319	21	3.71	93	29.1	67.2	0.119	2.4	67.60	0	5123	91	
6/30/2003	14:03:11	0.9	84	0.328	18	3.85	100	30.8	69.1	0.115	2.3	66.00	0	5123	97	
6/30/2003	14:03:17	0.9	87	0.308	15	3.79	99	28.9	64.9	0.122	2.3	73.20	0	5123	94	
6/30/2003	14:03:23	0.9	90	0.313	24	3.78	98	26.0	65.9	0.112	2.4	82.60	0	5123	99	
6/30/2003	14:03:29	0.9	93	0.308	19	3.89	94	28.1	64.9	0.134	2.3	98.30	0	5123	101	
6/30/2003	14:03:43	0.9	96	0.255	18	3.73	82	28.5	53.8	0.098	2.3	54.90	0	5123	86	
6/30/2003	14:03:49	0.9	99	0.335	22	3.82	93	29.5	70.5	0.000	0.9	101.00	0	5123	116	
6/30/2003	14:03:56	0.9	102	0.331	21	3.67	90	27.5	69.7	0.121	2.3	69.40	0	5123	118	
6/30/2003	14:04:04	0.9	105	0.324	21	4.39	105	0.0	68.2	0.141	2.3	68.80	0	5123	119	
6/30/2003	14:04:10	0.9	108	0.332	21	4.48	108	31.1	69.9	0.149	2.2	64.20	0	5123	126	
6/30/2003	14:04:16	0.9	111	0.323	23	4.42	95	30.7	68.1	0.147	2.4	81.20	0	5123	126	
6/30/2003	14:04:22	0.9	114	0.334	26	3.87	107	30.3	70.5	0.144	2.3	76.30	0	5123	134	
6/30/2003	14:04:28	0.9	117	0.348	24	4.07	106	30.0	73.3	0.137	2.3	72.30	0	5123	143	
6/30/2003	14:04:34	0.9	120	0.337	29	3.93	105	31.2	70.9	0.139	2.3	69.00	0	5123	142	
6/30/2003	14:04:39	0.9	123	0.236	45	3.74	97	31.4	49.8	0.135	2.3	69.70	0	5123	102	
6/30/2003	14:04:47	0.9	126	0.297	40	3.74	92	30.0	62.6	0.140	2.3	85.10	0	5123	131	
6/30/2003	14:04:54	0.9	129	0.353	28	4.21	100	24.2	74.3	0.162	2.3	79.90	0	5123	160	
6/30/2003	14:05:00	0.9	132	0.324	26	4.06	102	31.3	68.2	0.135	2.3	58.00	0	5123	150	
6/30/2003	14:05:05	0.9	135	0.345	14	4.37	107	30.2	72.6	0.140	2.2	67.50	0	5123	163	
6/30/2003	14:05:11	0.9	138	0.343	13	4.07	105	30.4	72.3	0.140	2.2	69.50	0	5123	166	
6/30/2003	14:05:17	0.9	141	0.369	13	4.07	103	30.0	77.8	0.146	2.3	73.00	0	5123	183	
6/30/2003	14:05:23	0.9	144	0.380	12	4.01	102	29.5	80.1	0.155	2.3	97.10	0	5123	192	
6/30/2003	14:05:29	0.9	147	0.351	11	3.97	104	29.9	73.9	0.147	2.3	78.50	0	5123	181	
6/30/2003	14:05:35	0.9	150	0.396	13	4.34	100	30.7	83.5	0.137	2.4	48.10	0	5123	209	
6/30/2003	14:05:41	0.9	153	0.330	12	3.93	92	28.7	69.6	0.131	2.3	72.30	0	5123	177	
6/30/2003	14:05:47	0.9	156	0.359	12	4.03	102	29.3	75.6	0.141	2.3	87.40	0	5123	197	
6/30/2003	14:05:54	0.9	159	0.315	9	4.06	87	20.3	66.4	0.000	0.9	86.60	0	5123	176	
6/30/2003	14:06:00	0.9	162	0.371	11	4.13	106	28.8	78.3	0.147	2.2	70.20	0	5123	211	
6/30/2003	14:06:06	0.9	165	0.364	12	3.81	90	28.4	76.8	0.122	2.3	64.60	0	5123	211	
6/30/2003	14:06:13	0.9	168	0.250	7	3.54	79	27.8	52.8	0.000	0.6	89.50	0	5123	148	
6/30/2003	14:06:19	0.9	171	0.384	12	4.16	106	28.3	80.9	0.153	2.3	77.40	0	5123	231	
6/30/2003	14:06:25	0.9	174	0.358	13	4.26	99	29.5	75.5	0.143	2.3	79.40	0	5123	219	
6/30/2003	14:06:31	0.9	177	0.399	23	4.74	101	30.2	84.1	0.151	2.3	70.10	0	5123	248	
6/30/2003	14:06:36	0.9	180	0.339	22	4.06	100	31.1	71.5	0.142	2.2	88.70	0	5123	215	
6/30/2003	14:06:43	0.9	183	0.333	17	4.22	86	31.1	70.2	0.147	2.3	304.50	0	5123	214	
6/30/2003	14:07:00	0.9	186	0.380	18	4.77	102	27.5	80.1	0.140	2.2	55.90	0	5123	248	
6/30/2003	14:07:07	0.9	189	0.381	15	3.84	105	30.5	80.2	0.126	2.3	54.40	0	5123	253	
6/30/2003	14:07:13	0.9	192	0.389	21	4.33	99	31.6	82.0	0.123	2.3	54.40	0	5123	262	
6/30/2003	14:07:18	0.9	195	0.354	18	4.14	93	31.2	74.6	0.123	2.3	65.60	0	5123	242	
6/30/2003	14:07:24	0.9	198	0.330	19	4.49	96	31.9	69.5	0.144	2.2	81.90	0	5123	229	
6/30/2003	14:07:30	0.9	201	0.401	23	4.54	92	31.9	84.5	0.130	2.2	62.50	0	5123	283	
6/30/2003	14:07:35	0.9	204	0.413	25	4.33	109	31.3	87.0	0.139	2.2	52.90	0	5123	296	
6/30/2003	14:07:41	0.9	207	0.412	28	4.89	108	32.7	86.8	0.135	2.2	53.60	0	5123	299	
6/30/2003	14:07:46	0.9	210	0.386	20	4.42	105	33.4	81.4	0.135	2.2	66.20	0	5123	285	
6/30/2003	14:07:51	0.9	213	0.396	19	4.55	103	34.4	83.4	0.137	2.3	67.50	0	5123	296	
6/30/2003	14:07:56	0.9	216	0.360	17	4.32	100	33.9	75.8	0.145	2.3	137.90	0	5123	273	
6/30/2003	14:08:02	0.9	219	0.404	25	4.67	106	34.1	85.2	0.139	2.2	114.50	0	5123	311	
6/30/2003	14:08:07	0.9	222	0.386	26	3.93	101	36.3	81.3	0.157	2.3	146.10	0	5123	301	
6/30/2003	14:08:12	0.9	225	0.378	27	4.22	105	35.6	79.6	0.138	2.3	127.60	0	5123	299	
6/30/2003	14:08:17	0.9	228	0.406	28	4.58	99	35.0	85.6	0.142	2.3	132.20	0	5123	325	
6/30/2003	14:08:21	0.9	231	0.402	29	4.71	109	36.3	84.7	0.134	2.2	105.10	0	5123	326	

Date	Time	LP (m)	BN	EMX (ton-m)	DMX (mm)	VMX (m/sec)	FMX (ton)	BPM (blows/min)	ETR (%)	EF2 (ton-m)	RAT	CSB (Mpa)	jc	WC (m/sec)	N_{60}	Comments
6/30/2003	14:08:26	0.9	234	0.388	27	4.60	102	36.2	81.7	0.129	2.3	29.70	0	5123	319	
6/30/2003	14:08:32	0.9	237	0.369	26	4.33	106	36.3	77.8	0.138	2.3	48.20	0	5123	307	
6/30/2003	14:08:38	0.9	240	0.379	29	4.03	106	21.2	79.9	0.137	2.3	29.10	0	5123	320	
6/30/2003	14:09:48	0.9	252	0.314	17	3.94	92	31.9	66.1	0.164	2.2	67.90	0	5123	278	
6/30/2003	14:09:55	0.9	255	0.380	17	3.98	105	33.6	80.0	0.132	2.3	130.10	0	5123	340	
6/30/2003	14:10:00	0.9	258	0.414	21	4.52	97	33.4	87.3	0.132	2.3	30.50	0	5123	375	
6/30/2003	14:10:06	0.9	261	0.394	13	4.00	99	33.5	83.0	0.136	2.3	47.20	0	5123	361	
6/30/2003	14:10:11	0.9	264	0.354	10	3.71	105	33.9	74.7	0.141	2.3	65.80	0	5123	329	
6/30/2003	14:10:16	0.9	267	0.361	11	3.94	102	35.4	76.0	0.133	2.3	60.90	0	5123	338	
6/30/2003	14:10:21	0.9	270	0.404	21	4.89	93	36.7	85.2	0.000	0.9	96.00	0	5123	383	
6/30/2003	14:10:27	0.9	273	0.354	14	3.73	90	36.7	74.7	0.000	0.9	100.80	0	5123	340	
6/30/2003	14:10:31	0.9	276	0.371	10	3.34	72	36.4	78.2	0.129	2.6	390.80	0	5123	360	
6/30/2003	14:10:36	0.9	279	0.306	14	3.97	90	35.7	64.4	0.145	2.3	350.00	0	5123	299	
6/30/2003	14:10:43	0.9	282	0.286	10	4.15	87	34.6	60.2	0.145	2.3	71.10	0	5123	283	
6/30/2003	14:10:48	0.9	285	0.308	14	3.56	88	31.1	65.0	0.145	2.3	373.00	0	5123	309	
6/30/2003	14:21:15	0.9	288	0.227	6	2.74	68	0.0	47.8	0.148	3.2	44.90	0	5123	229	
6/30/2003	14:21:21	0.9	291	0.303	19	3.24	70	33.4	63.9	0.000	1	94.40	0	5123	310	
6/30/2003	14:21:26	0.9	294	0.276	12	3.51	99	36.0	58.1	0.000	3.8	101.40	0	5123	285	
6/30/2003	14:21:33	0.9	297	0.299	15	3.97	90	34.5	62.9	0.132	3.2	327.10	0	5123	311	
6/30/2003	14:21:38	0.9	300	0.348	20	4.08	99	32.2	73.4	0.137	3.5	78.90	0	5123	367	
6/30/2003	14:21:44	0.9	303	0.298	16	3.80	83	33.6	62.8	0.156	3.6	296.10	0	5123	317	
6/30/2003	14:21:49	0.9	306	0.343	18	4.14	95	33.6	72.2	0.137	3.2	75.60	0	5123	368	
6/30/2003	14:21:59	0.9	312	0.330	17	3.95	95	36.3	69.5	0.171	3.1	217.00	0	5123	361	
6/30/2003	14:22:08	0.9	318	0.311	18	4.24	95	36.9	65.6	0.151	3.1	96.60	0	5123	348	
6/30/2003	14:22:18	0.9	324	0.289	12	4.22	95	33.1	61.0	0.156	3.1	92.30	0	5123	329	
6/30/2003	14:22:27	0.9	327	0.391	24	4.27	98	34.6	82.4	0.191	3.1	368.70	0	5123	449	
6/30/2003	14:22:33	0.9	330	0.309	13	4.43	91	22.2	65.2	0.165	3.3	274.60	0	5123	359	
6/30/2003	14:22:38	0.9	333	0.303	13	4.13	96	33.7	63.8	0.171	3.3	308.00	0	5123	354	
6/30/2003	14:22:44	0.9	336	0.337	17	4.49	92	35.8	71.0	0.179	3.3	290.40	0	5123	398	
6/30/2003	14:22:48	0.9	339	0.323	14	4.68	89	35.9	68.0	0.177	3.1	232.20	0	5123	384	
6/30/2003	14:22:53	0.9	342	0.282	12	4.41	90	36.4	59.4	0.152	3.2	180.70	0	5123	339	
6/30/2003	14:23:00	0.9	345	0.292	14	4.67	84	34.4	61.5	0.149	3.2	223.70	0	5123	354	
6/30/2003	14:23:05	0.9	348	0.296	15	4.67	92	35.5	62.4	0.159	3.1	165.20	0	5123	362	
6/30/2003	14:23:10	0.9	351	0.300	16	4.53	92	35.4	63.3	0.160	3.1	185.80	0	5123	370	
6/30/2003	14:23:15	0.9	354	0.297	19	4.43	95	35.9	62.6	0.165	3.3	209.40	0	5123	369	
6/30/2003	14:23:20	0.9	357	0.307	19	4.34	98	36.3	64.8	0.173	3.3	226.70	0	5123	386	
6/30/2003	14:23:25	0.9	360	0.284	21	4.30	100	37.0	59.9	0.182	3.2	142.90	0	5123	359	
6/30/2003	14:23:29	0.9	363	0.300	21	4.13	95	36.4	63.2	0.172	3.2	179.90	0	5123	382	
6/30/2003	14:23:34	0.9	366	0.308	22	4.21	99	37.1	64.9	0.169	3.1	174.90	0	5123	396	
6/30/2003	14:23:39	0.9	369	0.307	21	4.02	87	37.0	64.6	0.171	3.1	36.40	0	5123	397	
6/30/2003	14:23:44	0.9	372	0.295	21	3.86	86	36.7	62.2	0.162	3.1	30.90	0	5123	386	
6/30/2003	14:23:49	0.9	375	0.289	19	3.96	91	38.2	60.8	0.175	3.1	43.90	0	5123	380	
6/30/2003	14:23:53	0.9	378	0.263	15	3.81	97	37.7	55.5	0.170	2.9	192.00	0	5123	350	
6/30/2003	14:23:58	0.9	381	0.273	17	3.83	92	36.8	57.6	0.164	3.1	103.50	0	5123	366	
6/30/2003	14:24:03	0.9	384	0.287	15	3.80	91	38.1	60.4	0.172	3.1	49.30	0	5123	387	
6/30/2003	14:24:08	0.9	387	0.290	16	3.98	99	36.5	61.1	0.172	2.9	166.40	0	5123	394	
6/30/2003	14:24:12	0.9	390	0.271	16	3.79	95	37.0	57.1	0.166	3.1	45.40	0	5123	371	
6/30/2003	14:24:17	0.9	393	0.271	13	3.88	98	38.1	57.0	0.173	2.9	114.00	0	5123	373	
6/30/2003	14:24:22	0.9	396	0.289	14	4.05	96	37.2	60.9	0.167	2.9	129.00	0	5123	402	
6/30/2003	14:24:27	0.9	399	0.269	13	3.97	98	36.8	56.8	0.166	2.9	180.00	0	5123	378	
6/30/2003	14:24:31	0.9	402	0.260	10	3.63	87	37.7	54.9	0.160	3.1	2.90	0	5123	368	
6/30/2003	14:24:36	0.9	405	0.294	15	4.02	93	37.7	62.0	0.169	3.1	162.90	0	5123	419	
6/30/2003	14:24:41	0.9	408	0.286	14	4.13	98	38.1	60.3	0.172	3.1	210.00	0	5123	410	
6/30/2003	14:24:46	0.9	411	0.292	12	3.94	94	37.5	61.6	0.155	3.1	248.00	0	5123	422	
6/30/2003	14:24:50	0.9	414	0.273	10	4.13	97	38.0	57.6	0.170	3.1	213.70	0	5123	397	
6/30/2003	14:24:55	0.9	417	0.271	10	4.06	97	37.4	57.2	0.164	3.1	267.90	0	5123	398	
6/30/2003	14:25:00	0.9	420	0.304	14	4.16	97	37.5	64.0	0.159	3.1	196.40	0	5123	448	
6/30/2003	14:25:06	0.9	423	0.280	9	4.15	91	38.4	59.1	0.161	3.3	39.50	0	5123	417	
6/30/2003	14:25:10	0.9	426	0.289	11	3.81	97	37.6	60.8	0.170	3.1	311.50	0	5123	432	
6/30/2003	14:25:28	0.9	429	0.261	11	3.54	97	35.5	55.0	0.201	2.9	0.00	0	5123	393	
6/30/2003	14:25:32	0.9	432	0.274	10	3.82	98	38.3	57.7	0.157	3.5	37.90	0	5123	415	
6/30/2003	14:25:37	0.9	435	0.270	11	3.72	96	39.3	56.8	0.145	3.5	6.00	0	5123	412	
6/30/2003	14:26:00	0.9	444	0.310	13	4.49	94	0.0	65.3	0.178	2.9	92.70	0	5123	483	
6/30/2003	14:26:26	0.9	447	0.244	11	4.16	78	0.0	51.5	0.158	3.3	90.90	0	5123	384	
6/30/2003	14:26:47	0.9	450	0.200	5	2.49	85	0.0	42.1	0.000	0.3	75.80	0	5123	316	
6/30/2003	14:28:35	0.9	471	0.232	11	2.65	89	36.5	48.8	0.151	3.2	64.30	0	5123	383	
6/30/2003	14:28:51	0.9	477	0.259	11	2.66	101	36.6	54.6	0.178	3.1	108.10	0	5123	434	
6/30/2003	14:29:01	0.9	480	0.231	10	2.54	94	0.0	48.6	0.162	3.1	89.00	0	5123	389	
6/30/2003	14:29:17	0.9	483	0.236	11	3.29	92	36.9	49.8	0.171	2.9	3.40	0	5123	401	
6/30/2003	14:36:16	0.9	492	0.235	10	2.84	94	37.1	49.4	0.177	3.8	47.60	0	5123	405	
6/30/2003	14:37:08	0.9	507	0.228	9	3.26	94	0.0	48.1	0.203	3.8	91.50	0	5123	406	
6/30/2003	14:38:31	0.9	519	0.217	8	3.22	87	0.0	45.8	0.000	1.7	75.00	0	5123	396	
6/30/2003	14:38:44	0.9	522	0.236	8	2.85	81	32.2	49.7	0.149	3.8	69.00	0	5123	432	
6/30/2003	14:39:43	0.9	525	0.246	9	3.23	100	29.2	51.8	0.196	3.7	66.30	0	5123	453	
6/30/2003	14:39:51	0.9	528	0.228	8	2.86	94	0.0	48.0	0.166	3.8	0.00	0	5123	422	
6/30/2003	14:40:15	0.9	531	0.228	9	2.84	97	0.0	48.0	0.182	3.7	100.20	0	5123	425	
6/30/2003	14:41:22	0.9	534	0.224	9	2.82	92	0.0	47.2	0.171	3.7	45.20	0	5123	420	
						Average Energy Ratio =			**66.3**							

Project Name - PJ PERU 3
Pile Name - PN 3
Description - PD ;;
Operator Name - OP AC JW

AR	**Area**	7.87	cm^2
LE	**Length below sensors to pile bottom**	8.54	meters
SP	**Specific Weight Density**	77.3	tonnes/meter^3
WS	**Wave Speed**	5123	meters/second
EM	**Elastic Modulus**	206840	tonnes/cm^2

Strain transducers and accelerometers

F3	**F1**	216.4
F4	**F2**	216.4
A3	**A1**	325
A4	**A2**	345

start	1	11:45:22
stop	86	11:50:36
start	91	13:57:51
stop	101	13:58:08
start	10	14:28:00
stop	45	16:21:39
start	50	16:50:12
stop	55	16:50:45

NOTES

LP	Length of Penetration (penetration depth)
BN	Blow Number
EMX	Maximum Energy
DMX	Maximum Displacement
VMX	Maximum Velocity
FMX	Maximum Force
BMP	Blow Rate
ETR	Energy Transfer Ratio-Rated
EF2	Energy of F^2 (ASTM D4633)
RAT	Length Ratio for SPT (should be between 90 and 120% for a valid test)
CSB	Maximum Toe Stress
JC	Case Damping Constant
WC	Wave Speed Calculated
Wh	Theoretical Potential Energy for the SPT ram
N_{60}	Blow Number Corrected by Energy

Date	Time	LP (m)	BN	EMX (ton-m)	DMX (mm)	VMX (m/sec)	FMX (ton)	BPM (blows/min)	ETR (%)	EF2 (ton-m)	RAT	CSB (Mpa)	jc	WC (m/sec)	N_{60}	Comments
7/1/2003	11:45:22	0.2	1	0.245	6	3.32	81	0.0	51.6	0.123	1.5	76.50	0	5123	1	
7/1/2003	11:45:24	0.2	2	0.259	6	3.64	90	30.2	54.6	0.131	1.4	66.10	0	5123	2	
7/1/2003	11:45:26	0.2	3	0.239	6	3.84	88	29.9	50.4	0.125	1.4	29.20	0	5123	3	
7/1/2003	11:45:32	0.2	4	0.237	6	3.42	87	0.0	50.0	0.115	1.6	29.10	0	5123	3	
7/1/2003	11:45:42	0.2	5	0.227	6	3.29	93	0.0	47.9	0.118	1.8	103.30	0	5123	4	
7/1/2003	11:45:46	0.2	6	0.321	2	3.27	81	0.0	67.7	0.106	1.4	38.50	0	5123	7	
7/1/2003	11:46:01	0.2	7	0.253	7	3.69	88	0.0	53.4	0.126	1.4	36.30	0	5123	6	
7/1/2003	11:46:07	0.2	8	0.286	8	3.91	90	0.0	60.4	0.138	1.5	188.10	0	5123	8	
7/1/2003	11:46:09	0.2	9	0.276	8	3.58	76	29.5	58.2	0.117	1.5	181.30	0	5123	9	
7/1/2003	11:46:11	0.2	10	0.267	8	3.37	80	28.3	56.3	0.119	1.5	32.50	0	5123	9	
7/1/2003	11:46:13	0.2	11	0.000	0	0.00	80	29.5	0.0	0.370	19.3	2.40	0	5123	0	
7/1/2003	11:46:15	0.2	12	0.246	6	3.21	81	29.8	51.8	0.120	1.5	40.60	0	5123	10	
7/1/2003	11:46:17	0.2	13	0.236	6	3.32	81	30.6	49.7	0.112	1.5	45.60	0	5123	11	
7/1/2003	11:46:19	0.2	14	0.246	6	3.29	78	30.2	51.8	0.106	1.5	41.80	0	5123	12	
7/1/2003	11:46:47	0.2	15	0.250	6	3.45	79	0.0	52.6	0.112	1.4	44.40	0	5123	13	
7/1/2003	11:46:49	0.2	16	0.233	5	3.32	79	30.9	49.1	0.109	1.4	49.80	0	5123	13	
7/1/2003	11:46:57	0.2	18	0.252	6	2.62	92	0.0	53.2	0.000	1.5	106.00	0	5123	16	
7/1/2003	11:47:07	0.2	22	0.268	5	3.29	25	28.9	56.5	0.003	0.6	74.20	0	5123	21	
7/1/2003	11:47:09	0.2	23	0.262	6	3.39	79	27.1	55.2	0.106	1.5	26.40	0	5123	21	
7/1/2003	11:47:20	0.2	24	0.224	6	2.81	93	0.0	47.2	0.000	1.3	59.30	0	5123	19	
7/1/2003	11:47:22	0.2	25	0.237	5	2.99	84	32.6	50.0	0.446	8.2	35.00	0	5123	21	
7/1/2003	11:47:27	0.2	26	0.231	6	3.66	85	0.0	48.7	0.101	1.5	49.10	0	5123	21	
7/1/2003	11:47:29	0.2	27	0.229	6	2.68	87	29.3	48.3	0.099	1.4	53.30	0	5123	22	
7/1/2003	11:47:31	0.2	28	0.235	6	2.57	87	28.4	49.5	0.000	1.9	94.10	0	5123	23	
7/1/2003	11:47:33	0.2	29	0.000	0	0.00	90	29.2	0.0	0.414	12.9	0.00	0	5123	0	
7/1/2003	11:47:35	0.2	30	0.281	7	3.39	92	28.9	59.1	0.101	1.5	66.40	0	5123	30	
7/1/2003	11:47:37	0.2	31	0.220	6	3.34	74	30.2	46.3	0.091	1.5	32.70	0	5123	24	
7/1/2003	11:47:39	0.2	32	0.220	5	2.72	78	29.4	46.4	0.092	1.5	40.80	0	5123	25	
7/1/2003	11:47:41	0.2	33	0.236	6	2.74	83	30.0	49.7	0.090	1.5	37.80	0	5123	27	
7/1/2003	11:47:43	0.2	34	0.226	6	2.79	80	29.4	47.6	0.091	1.5	58.70	0	5123	27	
7/1/2003	11:47:45	0.2	35	0.225	6	2.62	83	30.3	47.5	0.393	1.6	53.60	0	5123	28	
7/1/2003	11:47:47	0.2	36	0.237	6	2.87	82	29.0	50.0	0.092	1.5	46.00	0	5123	30	
7/1/2003	11:47:56	0.2	37	0.272	12	2.81	77	0.0	57.3	0.090	1.7	43.70	0	5123	35	
7/1/2003	11:47:58	0.2	38	0.244	6	2.66	88	30.9	51.3	0.084	1.5	50.10	0	5123	32	
7/1/2003	11:48:00	0.2	39	0.220	6	2.85	75	30.5	46.3	0.102	1.5	44.50	0	5123	30	
7/1/2003	11:48:06	0.2	40	0.241	6	2.99	78	0.0	50.8	0.000	1	85.00	0	5123	34	
7/1/2003	11:48:08	0.2	41	0.000	0	0.00	89	28.7	0.0	0.428	21.4	1.80	0	5123	0	
7/1/2003	11:48:10	0.2	42	0.235	6	2.94	84	30.0	49.5	0.108	1.4	61.80	0	5123	35	
7/1/2003	11:48:12	0.2	43	0.210	5	2.97	77	29.8	44.2	0.097	1.5	34.80	0	5123	32	
7/1/2003	11:48:14	0.2	44	0.236	6	2.54	85	30.1	49.7	0.000	2.2	91.20	0	5123	36	
7/1/2003	11:48:18	0.2	45	0.234	6	2.91	87	0.0	49.4	0.109	1.5	36.80	0	5123	37	
7/1/2003	11:48:20	0.2	46	0.235	6	2.93	74	28.5	49.6	0.001	1.4	82.50	0	5123	38	
7/1/2003	11:48:36	0.2	47	0.268	6	3.12	83	0.0	56.6	0.112	1.5	56.80	0	5123	44	
7/1/2003	11:48:38	0.2	48	0.239	6	2.68	78	30.5	50.3	0.000	1.3	82.90	0	5123	40	
7/1/2003	11:48:44	0.2	49	0.224	6	2.63	75	0.0	47.2	0.100	1.5	75.90	0	5123	39	
7/1/2003	11:48:46	0.2	50	0.251	6	2.85	81	30.5	52.9	0.001	1.5	100.00	0	5123	44	
7/1/2003	11:48:48	0.2	51	0.257	6	2.97	83	29.8	54.1	0.439	7.8	61.20	0	5123	46	
7/1/2003	11:48:51	0.2	52	0.000	0	0.00	79	0.0	0.0	0.382	13.8	0.10	0	5123	0	
7/1/2003	11:48:53	0.2	53	0.239	6	2.39	77	30.0	50.4	0.091	1.5	56.10	0	5123	45	
7/1/2003	11:49:03	0.2	54	0.252	6	2.82	73	0.0	53.1	0.000	0.3	84.70	0	5123	48	
7/1/2003	11:49:05	0.2	55	0.000	0	0.00	74	32.6	0.0	0.415	14.1	2.50	0	5123	0	
7/1/2003	11:49:07	0.2	56	0.000	0	0.00	79	32.5	0.0	0.347	12.9	0.00	0	5123	0	
7/1/2003	11:49:17	0.2	57	0.272	6	3.08	72	0.0	57.4	0.382	8.4	126.80	0	5123	55	
7/1/2003	11:49:19	0.2	58	0.282	7	3.08	86	35.3	59.5	0.121	1.5	61.90	0	5123	58	
7/1/2003	11:49:20	0.2	59	0.252	7	3.06	69	37.3	53.1	0.000	1.2	81.10	0	5123	52	
7/1/2003	11:49:23	0.2	60	0.249	6	3.27	80	0.0	52.5	0.340	8.6	45.50	0	5123	53	
7/1/2003	11:49:25	0.2	61	0.276	6	3.24	81	35.7	58.1	0.001	1.5	80.50	0	5123	59	
7/1/2003	11:49:30	0.2	62	0.253	6	3.43	96	0.0	53.3	0.127	1.5	60.10	0	5123	55	
7/1/2003	11:49:33	0.2	63	0.253	7	4.04	96	0.0	53.3	0.130	1.5	34.00	0	5123	56	
7/1/2003	11:49:35	0.2	64	0.249	7	3.70	92	36.6	52.6	0.120	1.5	29.10	0	5123	56	
7/1/2003	11:49:44	0.2	65	0.278	7	3.95	93	0.0	58.6	0.128	1.4	36.80	0	5123	63	
7/1/2003	11:49:46	0.2	66	0.252	6	2.85	85	31.3	53.2	0.123	1.5	45.90	0	5123	59	
7/1/2003	11:49:48	0.2	67	0.254	7	3.08	80	30.9	53.6	0.118	1.5	48.40	0	5123	60	
7/1/2003	11:49:50	0.2	68	0.269	7	3.18	92	30.3	56.6	0.000	1	87.70	0	5123	64	
7/1/2003	11:49:52	0.2	69	0.261	7	3.26	95	29.8	55.1	0.127	1.4	59.30	0	5123	63	
7/1/2003	11:49:54	0.2	70	0.254	7	3.02	76	29.2	53.6	0.111	1.5	53.10	0	5123	63	
7/1/2003	11:50:04	0.2	71	0.254	7	2.88	81	0.0	53.4	0.099	1.6	29.80	0	5123	63	
7/1/2003	11:50:06	0.2	72	0.277	7	2.99	83	30.8	58.3	0.104	1.5	48.30	0	5123	70	
7/1/2003	11:50:08	0.2	73	0.289	8	3.18	85	32.0	60.9	0.107	1.5	44.00	0	5123	74	
7/1/2003	11:50:10	0.2	74	0.261	7	2.78	77	32.2	55.1	0.000	1.3	78.60	0	5123	68	
7/1/2003	11:50:12	0.2	75	0.292	11	3.17	88	32.7	61.6	0.108	1.5	40.50	0	5123	77	
7/1/2003	11:50:13	0.2	76	0.000	0	0.00	83	32.1	0.0	0.333	14.1	0.00	0	5123	0	
7/1/2003	11:50:15	0.2	77	0.260	7	2.90	85	30.9	54.9	0.108	1.6	46.30	0	5123	70	
7/1/2003	11:50:17	0.2	78	0.270	7	2.97	79	30.8	56.9	0.393	9.7	34.80	0	5123	74	
7/1/2003	11:50:21	0.2	79	0.267	7	2.87	82	0.0	56.2	0.105	1.8	31.40	0	5123	74	
7/1/2003	11:50:23	0.2	80	0.258	7	2.81	70	31.3	54.4	0.000	3.5	83.10	0	5123	73	
7/1/2003	11:50:25	0.2	81	0.273	7	3.18	70	31.7	57.6	0.001	3.6	95.40	0	5123	78	

Date	Time	LP (m)	BN	EMX (ton-m)	DMX (mm)	VMX (m/sec)	FMX (ton)	BPM (blows/min)	ETR (%)	EF2 (ton-m)	RAT	CSB (Mpa)	jc	WC (m/sec)	N_{60}	Comments
7/1/2003	11:50:27	0.2	82	0.255	7	2.93	69	31.4	53.8	0.000	4.5	77.00	0	5123	74	
7/1/2003	11:50:28	0.2	83	0.254	7	2.79	72	32.9	53.6	0.363	9.6	38.50	0	5123	74	
7/1/2003	11:50:30	0.2	84	0.272	7	3.08	82	32.7	57.4	0.102	1.5	26.90	0	5123	80	
7/1/2003	11:50:34	0.2	85	0.297	7	3.55	93	0.0	62.5	0.000	3.4	93.40	0	5123	89	
7/1/2003	11:50:36	0.2	86	0.267	6	2.96	77	31.7	56.3	0.112	1.5	44.20	0	5123	81	
7/1/2003	13:57:51	2	91	0.228	17	4.19	87	36.6	48.0	0.157	1.2	13.90	0	5123	73	
7/1/2003	13:57:59	2	96	0.245	21	4.46	93	35.8	51.7	0.162	1.2	23.00	0	5123	83	
7/1/2003	13:58:08	2	101	0.235	23	4.42	87	34.2	49.5	0.155	1.2	20.20	0	5123	83	
7/1/2003	14:28:00	2.9	10	0.236	16	4.55	85	0.0	49.8	0.156	1.2	24.70	0	5123	8	
7/1/2003	16:21:39	6	45	0.000	8	3.09	0	0.0	0.0	0.000	0.1	67.80	0	5123	0	
7/1/2003	16:50:12	7	50	0.242	15	3.06	98	32.7	51.0	0.197	1.1	50.00	0	5123	43	
7/1/2003	16:50:45	7	55	0.000	18	3.24	0	0.0	0.0	0.000	0.2	43.50	0	5123	0	
						Average Energy Ratio =			**53.1**							

Project Name - PJ PERU 3
Pile Name - PN 3
Description - PD ;;
Operator Name - OP JW AC

AR	**Area**	7.87 cm^2
LE	**Length below sensors to pile bottom**	2.44 meters
SP	**Specific Weight Density**	77.3 tonnes/meter^3
WS	**Wave Speed**	5123 meters/second
EM	**Elastic Modulus**	206840 tonnes/cm^2

Strain transducers and accelerometers

F3	**F1**	216.4
F4	**F2**	216.4
A3	**A1**	325
A4	**A2**	345

start	1	11:45:22
stop	86	11:50:36
start	91	13:57:51
stop	101	13:58:08
start	10	14:28:00
stop	15	14:28:16
start	20	14:52:06
stop	35	14:52:47
start	40	15:57:24
stop	45	16:21:39
start	50	16:50:12
stop	60	16:51:06

NOTES

LP	Length of Penetration (penetration depth)
BN	Blow Number
EMX	Maximum Energy
DMX	Maximum Displacement
VMX	Maximum Velocity
FMX	Maximum Force
BMP	Blow Rate
ETR	Energy Transfer Ratio-Rated
EF2	Energy of F^2 (ASTM D4633)
RAT	Length Ratio for SPT (should be between 90 and 120% for a valid test)
CSB	Maximum Toe Stress
JC	Case Damping Constant
WC	Wave Speed Calculated
Wh	Theoretical Potential Energy for the SPT ram
N_{60}	Blow Number Corrected by Energy

Date	Time	LP (m)	BN	EMX (ton-m)	DMX (mm)	VMX (m/sec)	FMX (ton)	BPM (blows/min)	ETR (%)	EF2 (ton-m)	RAT	CSB (Mpa)	jc	WC (m/sec)	N_{60}	Comments
7/1/2003	11:45:22	0.2	1	0.245	6	3.32	81	0.0	51.6	0.123	1.5	76.50	0	5123	1	
7/1/2003	11:45:24	0.2	2	0.259	6	3.64	90	30.2	54.6	0.131	1.4	66.10	0	5123	2	
7/1/2003	11:45:26	0.2	3	0.239	6	3.84	88	29.9	50.4	0.125	1.4	29.20	0	5123	3	
7/1/2003	11:45:32	0.2	4	0.237	6	3.42	87	0.0	50.0	0.115	1.6	29.10	0	5123	3	
7/1/2003	11:45:42	0.2	5	0.227	6	3.29	93	0.0	47.9	0.118	1.8	103.30	0	5123	4	
7/1/2003	11:45:46	0.2	6	0.321	2	3.27	81	0.0	67.7	0.106	1.4	38.50	0	5123	7	
7/1/2003	11:46:01	0.2	7	0.253	7	3.69	88	0.0	53.4	0.126	1.4	36.30	0	5123	6	
7/1/2003	11:46:07	0.2	8	0.286	8	3.91	90	0.0	60.4	0.138	1.5	188.10	0	5123	8	
7/1/2003	11:46:09	0.2	9	0.276	8	3.58	76	29.5	58.2	0.117	1.5	181.30	0	5123	9	
7/1/2003	11:46:11	0.2	10	0.267	8	3.37	80	28.3	56.3	0.119	1.5	32.50	0	5123	9	
7/1/2003	11:46:13	0.2	11	0.000	0	0.00	80	29.5	0.0	0.370	19.3	2.40	0	5123	0	
7/1/2003	11:46:15	0.2	12	0.246	6	3.21	81	29.8	51.8	0.120	1.5	40.60	0	5123	10	
7/1/2003	11:46:17	0.2	13	0.236	6	3.32	81	30.6	49.7	0.112	1.5	45.60	0	5123	11	
7/1/2003	11:46:19	0.2	14	0.246	6	3.29	78	30.2	51.8	0.106	1.5	41.80	0	5123	12	
7/1/2003	11:46:47	0.2	15	0.250	6	3.45	79	0.0	52.6	0.112	1.4	44.40	0	5123	13	
7/1/2003	11:46:49	0.2	16	0.233	5	3.32	79	30.9	49.1	0.109	1.4	49.80	0	5123	13	
7/1/2003	11:46:51	0.2	17	0.000	5	2.38	0	28.9	0.0	0.000	0.4	79.80	0	5123	0	
7/1/2003	11:46:57	0.2	18	0.252	6	2.62	92	0.0	53.2	0.000	1.5	106.00	0	5123	16	
7/1/2003	11:47:07	0.2	22	0.268	5	3.29	25	28.9	56.5	0.003	0.6	74.20	0	5123	21	
7/1/2003	11:47:09	0.2	23	0.262	6	3.39	79	27.1	55.2	0.106	1.5	26.40	0	5123	21	
7/1/2003	11:47:20	0.2	24	0.224	6	2.81	93	0.0	47.2	0.000	1.3	59.30	0	5123	19	
7/1/2003	11:47:22	0.2	25	0.237	5	2.99	84	32.6	50.0	0.446	8.2	35.00	0	5123	21	
7/1/2003	11:47:27	0.2	26	0.231	6	3.66	85	0.0	48.7	0.101	1.5	49.10	0	5123	21	
7/1/2003	11:47:31	0.2	28	0.235	6	2.57	87	28.4	49.5	0.000	1.9	94.10	0	5123	23	
7/1/2003	11:47:33	0.2	29	0.000	0	0.00	90	29.2	0.0	0.414	12.9	0.00	0	5123	0	
7/1/2003	11:47:35	0.2	30	0.281	7	3.39	92	28.9	59.1	0.101	1.5	66.40	0	5123	30	
7/1/2003	11:47:39	0.2	32	0.220	5	2.72	78	29.4	46.4	0.092	1.5	40.80	0	5123	25	
7/1/2003	11:47:41	0.2	33	0.236	6	2.74	83	30.0	49.7	0.090	1.5	37.80	0	5123	27	
7/1/2003	11:47:43	0.2	34	0.226	6	2.79	80	29.4	47.6	0.091	1.5	58.70	0	5123	27	
7/1/2003	11:47:45	0.2	35	0.225	6	2.62	83	30.3	47.5	0.393	1.6	53.60	0	5123	28	
7/1/2003	11:47:47	0.2	36	0.237	6	2.87	82	29.0	50.0	0.092	1.5	46.00	0	5123	30	
7/1/2003	11:47:56	0.2	37	0.272	12	2.81	77	0.0	57.3	0.090	1.7	43.70	0	5123	35	
7/1/2003	11:47:58	0.2	38	0.244	6	2.66	88	30.9	51.3	0.084	1.5	50.10	0	5123	32	
7/1/2003	11:48:00	0.2	39	0.220	6	2.85	75	30.5	46.3	0.102	1.5	44.50	0	5123	30	
7/1/2003	11:48:06	0.2	40	0.241	6	2.99	78	0.0	50.8	0.000	1	85.00	0	5123	34	
7/1/2003	11:48:08	0.2	41	0.000	0	0.00	89	28.7	0.0	0.428	21.4	1.80	0	5123	0	
7/1/2003	11:48:10	0.2	42	0.235	6	2.94	84	30.0	49.5	0.108	1.4	61.80	0	5123	35	
7/1/2003	11:48:12	0.2	43	0.210	5	2.97	77	29.8	44.2	0.097	1.5	34.80	0	5123	32	
7/1/2003	11:48:14	0.2	44	0.236	6	2.54	85	30.1	49.7	0.000	2.2	91.20	0	5123	36	
7/1/2003	11:48:18	0.2	45	0.234	6	2.91	87	0.0	49.4	0.109	1.5	36.80	0	5123	37	
7/1/2003	11:48:20	0.2	46	0.235	6	2.93	74	28.5	49.6	0.001	1.4	82.50	0	5123	38	
7/1/2003	11:48:36	0.2	47	0.268	6	3.12	83	0.0	56.6	0.112	1.5	56.80	0	5123	44	
7/1/2003	11:48:38	0.2	48	0.239	6	2.68	78	30.5	50.3	0.000	1.3	82.90	0	5123	40	
7/1/2003	11:48:44	0.2	49	0.224	6	2.63	75	0.0	47.2	0.100	1.5	75.90	0	5123	39	
7/1/2003	11:48:46	0.2	50	0.251	6	2.85	81	30.5	52.9	0.001	1.5	100.00	0	5123	44	
7/1/2003	11:48:48	0.2	51	0.257	6	2.97	83	29.8	54.1	0.439	7.8	61.20	0	5123	46	
7/1/2003	11:48:51	0.2	52	0.000	0	0.00	79	0.0	0.0	0.382	13.8	0.10	0	5123	0	
7/1/2003	11:48:53	0.2	53	0.239	6	2.39	77	30.0	50.4	0.091	1.5	56.10	0	5123	45	
7/1/2003	11:49:03	0.2	54	0.252	6	2.82	73	0.0	53.1	0.000	0.3	84.70	0	5123	48	
7/1/2003	11:49:05	0.2	55	0.000	0	0.00	74	32.6	0.0	0.415	14.1	2.50	0	5123	0	
7/1/2003	11:49:07	0.2	56	0.000	0	0.00	79	32.5	0.0	0.347	12.9	0.00	0	5123	0	
7/1/2003	11:49:17	0.2	57	0.272	6	3.08	72	0.0	57.4	0.382	8.4	126.80	0	5123	55	
7/1/2003	11:49:19	0.2	58	0.282	7	3.08	86	35.3	59.5	0.121	1.5	61.90	0	5123	58	
7/1/2003	11:49:20	0.2	59	0.252	7	3.06	69	37.3	53.1	0.000	1.2	81.10	0	5123	52	
7/1/2003	11:49:23	0.2	60	0.249	6	3.27	80	0.0	52.5	0.340	8.6	45.50	0	5123	53	
7/1/2003	11:49:25	0.2	61	0.276	6	3.24	81	35.7	58.1	0.001	1.5	80.50	0	5123	59	
7/1/2003	11:49:30	0.2	62	0.253	6	3.43	96	0.0	53.3	0.127	1.5	60.10	0	5123	55	
7/1/2003	11:49:33	0.2	63	0.253	7	4.04	96	0.0	53.3	0.130	1.5	34.00	0	5123	56	
7/1/2003	11:49:35	0.2	64	0.249	7	3.70	92	36.6	52.6	0.120	1.5	29.10	0	5123	56	
7/1/2003	11:49:44	0.2	65	0.278	7	3.95	93	0.0	58.6	0.128	1.4	36.80	0	5123	63	
7/1/2003	11:49:46	0.2	66	0.252	6	2.85	85	31.3	53.2	0.123	1.5	45.90	0	5123	59	
7/1/2003	11:49:48	0.2	67	0.254	7	3.08	80	30.9	53.6	0.118	1.5	48.40	0	5123	60	
7/1/2003	11:49:50	0.2	68	0.269	7	3.18	92	30.3	56.6	0.000	1	87.70	0	5123	64	
7/1/2003	11:49:52	0.2	69	0.261	7	3.26	95	29.8	55.1	0.127	1.4	59.30	0	5123	63	
7/1/2003	11:49:54	0.2	70	0.254	7	3.02	76	29.2	53.6	0.111	1.5	53.10	0	5123	63	
7/1/2003	11:50:04	0.2	71	0.254	7	2.88	81	0.0	53.4	0.099	1.6	29.80	0	5123	63	
7/1/2003	11:50:06	0.2	72	0.277	7	2.99	83	30.8	58.3	0.104	1.5	48.30	0	5123	70	
7/1/2003	11:50:08	0.2	73	0.289	8	3.18	85	32.0	60.9	0.107	1.5	44.00	0	5123	74	
7/1/2003	11:50:10	0.2	74	0.261	7	2.78	77	32.2	55.1	0.000	1.3	78.60	0	5123	68	
7/1/2003	11:50:12	0.2	75	0.292	11	3.17	88	32.7	61.6	0.108	1.5	40.50	0	5123	77	

Date	Time	LP (m)	BN	EMX (ton-m)	DMX (mm)	VMX (m/sec)	FMX (ton)	BPM (blows/min)	ETR (%)	EF2 (ton-m)	RAT	CSB (Mpa)	jc	WC (m/sec)	N_{60}	Comments
7/1/2003	11:50:13	0.2	76	0.000	0	0.00	83	32.1	0.0	0.333	14.1	0.00	0	5123	0	
7/1/2003	11:50:15	0.2	77	0.260	7	2.90	85	30.9	54.9	0.108	1.6	46.30	0	5123	70	
7/1/2003	11:50:17	0.2	78	0.270	7	2.97	79	30.8	56.9	0.393	9.7	34.80	0	5123	74	
7/1/2003	11:50:21	0.2	79	0.267	7	2.87	82	0.0	56.2	0.105	1.8	31.40	0	5123	74	
7/1/2003	11:50:23	0.2	80	0.258	7	2.81	70	31.3	54.4	0.000	3.5	83.10	0	5123	73	
7/1/2003	11:50:25	0.2	81	0.273	7	3.18	70	31.7	57.6	0.001	3.6	95.40	0	5123	78	
7/1/2003	11:50:27	0.2	82	0.255	7	2.93	69	31.4	53.8	0.000	4.5	77.00	0	5123	74	
7/1/2003	11:50:28	0.2	83	0.254	7	2.79	72	32.9	53.6	0.363	9.6	38.50	0	5123	74	
7/1/2003	11:50:30	0.2	84	0.272	7	3.08	82	32.7	57.4	0.102	1.5	26.90	0	5123	80	
7/1/2003	11:50:34	0.2	85	0.297	7	3.55	93	0.0	62.5	0.000	3.4	93.40	0	5123	89	
7/1/2003	11:50:36	0.2	86	0.267	6	2.96	77	31.7	56.3	0.112	1.5	44.20	0	5123	81	
7/1/2003	13:57:51	2	91	0.228	17	4.19	87	36.6	48.0	0.157	1.2	13.90	0	5123	73	
7/1/2003	13:57:59	2	96	0.245	21	4.46	93	35.8	51.7	0.162	1.2	23.00	0	5123	83	
7/1/2003	13:58:08	2	101	0.235	23	4.42	87	34.2	49.5	0.155	1.2	20.20	0	5123	83	
7/1/2003	14:28:00	2.9	10	0.236	16	4.55	85	0.0	49.8	0.156	1.2	24.70	0	5123	8	
7/1/2003	14:28:16	2.9	15	0.000	0	0.00	90	0.0	0.0	0.301	11.4	12.50	0	5123	0	
7/1/2003	14:52:06	2.9	20	0.219	25	3.51	87	19.8	46.2	0.166	1.7	72.10	0	5123	15	
7/1/2003	14:52:15	2.9	25	0.269	29	3.52	91	33.7	56.7	0.195	1.6	63.80	0	5123	24	
7/1/2003	14:52:35	2.9	30	0.230	18	4.46	96	0.0	48.6	0.193	1.7	68.60	0	5123	24	
7/1/2003	14:52:47	2.9	35	0.206	20	3.89	81	36.0	43.5	0.166	1.7	20.50	0	5123	25	
7/1/2003	15:57:24	5	40	0.274	23	3.91	100	0.0	57.8	0.211	1.2	63.90	0	5123	39	
7/1/2003	16:21:39	6	45	0.000	0	0.00	85	0.0	0.0	0.255	5.3	3.40	0	5123	0	
7/1/2003	16:50:12	7	50	0.242	15	3.06	98	32.7	51.0	0.197	1.1	50.00	0	5123	43	
7/1/2003	16:50:45	7	55	0.273	18	3.24	93	0.0	57.5	0.206	1.1	53.00	0	5123	53	
7/1/2003	16:51:06	7	60	0.288	20	3.69	96	32.3	60.6	0.223	1.2	20.70	0	5123	61	
						Average Energy Ratio =			**53.2**							

Project Name - PJ PERU 3.1
Pile Name - PN 3
Description - PD HW 1(8M);;
Operator Name - OP AC JW

AR	**Area**	7.87	cm^2
LE	**Length below sensors to pile bottom**	9.97	meters
SP	**Specific Weight Density**	77.3	tonnes/meter^3
WS	**Wave Speed**	5123	meters/second
EM	**Elastic Modulus**	206840	tonnes/cm^2

Strain transducers and accelerometers

F3	**F1**	216.4
F4	**F2**	216.4
A3	**A1**	325
A4	**A2**	345

start	5	10:00:17
stop	50	10:03:43
start	55	10:47:44
stop	130	10:51:46

NOTES

LP	Length of Penetration (penetration depth)
BN	Blow Number
EMX	Maximum Energy
DMX	Maximum Displacement
VMX	Maximum Velocity
FMX	Maximum Force
BMP	Blow Rate
ETR	Energy Transfer Ratio-Rated
EF2	Energy of F^2 (ASTM D4633)
RAT	Length Ratio for SPT (should be between 90 and 120% for a valid test)
CSB	Maximum Toe Stress
JC	Case Damping Constant
WC	Wave Speed Calculated
Wh	Theoretical Potential Energy for the SPT ram
N_{60}	Blow Number Corrected by Energy

Date	Time	LP (m)	BN	EMX (ton-m)	DMX (mm)	VMX (m/sec)	FMX (ton)	BPM (blows/min)	ETR (%)	EF2 (ton-m)	RAT	CSB (Mpa)	jc	WC (m/sec)	N_{60}	Comments
7/2/2003	10:00:17	8	5	0.251	21	2.96	84	0.0	52.9	0.199	1.1	33.40	0	5123	4	
7/2/2003	10:00:34	8	10	0.250	13	3.11	90	25.8	52.7	0.203	1.2	61.30	0	5123	9	
7/2/2003	10:00:52	8	15	0.251	13	3.15	94	0.0	52.8	0.218	1.2	72.90	0	5123	13	
7/2/2003	10:01:25	8	20	0.264	10	3.51	97	0.0	55.6	0.242	1.2	57.80	0	5123	19	
7/2/2003	10:01:37	8	25	0.260	10	3.36	94	26.8	54.8	0.231	1.1	43.80	0	5123	23	
7/2/2003	10:02:06	8	30	0.277	10	3.20	97	31.4	58.3	0.260	1.1	49.40	0	5123	29	
7/2/2003	10:02:15	8	35	0.274	17	3.40	87	30.8	57.7	0.229	1.1	32.10	0	5123	34	
7/2/2003	10:02:32	8	40	0.277	12	3.61	96	0.0	58.3	0.243	1.2	61.10	0	5123	39	
7/2/2003	10:03:31	8	45	0.271	9	3.55	98	31.2	57.0	0.248	1.1	45.20	0	5123	43	
7/2/2003	10:03:43	8	50	0.276	13	3.46	98	34.8	58.2	0.250	1.1	53.30	0	5123	49	
7/2/2003	10:47:44	8	55	0.260	11	3.14	69	0.0	54.8	0.232	1.3	72.20	0	5123	50	
7/2/2003	10:47:53	8	60	0.278	17	3.57	93	29.7	58.5	0.227	1.2	83.50	0	5123	59	
7/2/2003	10:48:08	8	65	0.258	10	3.48	87	0.0	54.4	0.221	1.2	62.90	0	5123	59	
7/2/2003	10:48:17	8	70	0.249	10	3.32	84	29.7	52.5	0.217	1.2	72.70	0	5123	61	
7/2/2003	10:48:29	8	75	0.279	11	3.85	96	29.0	58.9	0.226	1.2	79.60	0	5123	74	
7/2/2003	10:48:39	8	80	0.239	9	3.14	89	28.6	50.4	0.211	1.2	84.40	0	5123	67	
7/2/2003	10:48:55	8	85	0.269	10	3.33	88	0.0	56.7	0.224	1.2	67.40	0	5123	80	
7/2/2003	10:49:13	8	90	0.237	9	2.94	82	30.6	50.0	0.200	1.2	68.20	0	5123	75	
7/2/2003	10:49:22	8	95	0.277	9	3.40	92	30.1	58.4	0.233	1.2	87.80	0	5123	92	
7/2/2003	10:49:34	8	100	0.253	9	3.51	90	29.4	53.3	0.210	1.2	85.40	0	5123	89	
7/2/2003	10:49:46	8	105	0.287	10	3.70	91	0.0	60.5	0.230	1.2	67.00	0	5123	106	
7/2/2003	10:50:43	8	115	0.273	8	3.64	92	0.0	57.5	0.235	1.3	78.90	0	5123	110	
7/2/2003	10:50:54	8	120	0.327	24	3.78	88	0.0	69.0	0.222	1.3	48.20	0	5123	138	
7/2/2003	10:51:46	8	130	0.311	8	2.82	79	0.0	65.5	0.000	0.3	107.40	0	5123	142	
						Average Energy Ratio =			**56.6**							

Project Name - PJ PERU 3.1
Pile Name - PN 3
Description - PD HW 1(8M);;
Operator Name - OP AC JW

AR	**Area**	7.87	cm^2
LE	**Length below sensors to pile bottom**	9.97	meters
SP	**Specific Weight Density**	77.3	tonnes/meter^3
WS	**Wave Speed**	5123	meters/second
EM	**Elastic Modulus**	206840	tonnes/cm^2

Strain transducers and accelerometers

F3	**F1**	216.4
F4	**F2**	216.4
A3	**A1**	325
A4	**A2**	345

start	5	10:00:17
stop	50	10:03:43
start	55	10:47:44
stop	130	10:51:46

NOTES

LP	Length of Penetration (penetration depth)
BN	Blow Number
EMX	Maximum Energy
DMX	Maximum Displacement
VMX	Maximum Velocity
FMX	Maximum Force
BMP	Blow Rate
ETR	Energy Transfer Ratio-Rated
EF2	Energy of F^2 (ASTM D4633)
RAT	Length Ratio for SPT (should be between 90 and 120% for a valid test)
CSB	Maximum Toe Stress
JC	Case Damping Constant
WC	Wave Speed Calculated
Wh	Theoretical Potential Energy for the SPT ram
N_{60}	Blow Number Corrected by Energy

Date	Time	LP (m)	BN	EMX (ton-m)	DMX (mm)	VMX (m/sec)	FMX (ton)	BPM (blows/min)	ETR (%)	EF2 (ton-m)	RAT	CSB (Mpa)	jc	WC (m/sec)	N_{60}	Comments
7/2/2003	10:00:17	8	5	0.251	21	2.96	84	0.0	52.9	0.199	1.1	33.40	0	5123	4	
7/2/2003	10:00:34	8	10	0.250	13	3.11	90	25.8	52.7	0.203	1.2	61.30	0	5123	9	
7/2/2003	10:00:52	8	15	0.251	13	3.15	94	0.0	52.8	0.218	1.2	72.90	0	5123	13	
7/2/2003	10:01:25	8	20	0.264	10	3.51	97	0.0	55.6	0.242	1.2	57.80	0	5123	19	
7/2/2003	10:01:37	8	25	0.260	10	3.36	94	26.8	54.8	0.231	1.1	43.80	0	5123	23	
7/2/2003	10:02:06	8	30	0.277	10	3.20	97	31.4	58.3	0.260	1.1	49.40	0	5123	29	
7/2/2003	10:02:15	8	35	0.274	17	3.40	87	30.8	57.7	0.229	1.1	32.10	0	5123	34	
7/2/2003	10:02:32	8	40	0.277	12	3.61	96	0.0	58.3	0.243	1.2	61.10	0	5123	39	
7/2/2003	10:03:31	8	45	0.271	9	3.55	98	31.2	57.0	0.248	1.1	45.20	0	5123	43	
7/2/2003	10:03:43	8	50	0.276	13	3.46	98	34.8	58.2	0.250	1.1	53.30	0	5123	49	
7/2/2003	10:47:44	8	55	0.260	11	3.14	69	0.0	54.8	0.232	1.3	72.20	0	5123	50	
7/2/2003	10:47:53	8	60	0.278	17	3.57	93	29.7	58.5	0.227	1.2	83.50	0	5123	59	
7/2/2003	10:48:08	8	65	0.258	10	3.48	87	0.0	54.4	0.221	1.2	62.90	0	5123	59	
7/2/2003	10:48:17	8	70	0.249	10	3.32	84	29.7	52.5	0.217	1.2	72.70	0	5123	61	
7/2/2003	10:48:29	8	75	0.279	11	3.85	96	29.0	58.9	0.226	1.2	79.60	0	5123	74	
7/2/2003	10:48:39	8	80	0.239	9	3.14	89	28.6	50.4	0.211	1.2	84.40	0	5123	67	
7/2/2003	10:48:55	8	85	0.269	10	3.33	88	0.0	56.7	0.224	1.2	67.40	0	5123	80	
7/2/2003	10:49:13	8	90	0.237	9	2.94	82	30.6	50.0	0.200	1.2	68.20	0	5123	75	
7/2/2003	10:49:22	8	95	0.277	9	3.40	92	30.1	58.4	0.233	1.2	87.80	0	5123	92	
7/2/2003	10:49:34	8	100	0.253	9	3.51	90	29.4	53.3	0.210	1.2	85.40	0	5123	89	
7/2/2003	10:49:46	8	105	0.287	10	3.70	91	0.0	60.5	0.230	1.2	67.00	0	5123	106	
7/2/2003	10:49:59	8	110	0.000	0	0.00	92	28.9	0.0	0.340	5.2	0.60	0	5123	0	
7/2/2003	10:50:43	8	115	0.273	8	3.64	92	0.0	57.5	0.235	1.3	78.90	0	5123	110	
7/2/2003	10:50:54	8	120	0.327	24	3.78	88	0.0	69.0	0.222	1.3	48.20	0	5123	138	
7/2/2003	10:51:46	8	130	0.311	8	2.82	79	0.0	65.5	0.000	0.3	107.40	0	5123	142	
						Average Energy Ratio =			**56.6**							

Project Name - PJ PERU 4
Pile Name - PN 4
Description - PD HW 2;;
Operator Name - OP AC ER

AR	**Area**	7.87	cm^2
LE	**Length below sensors to pile bottom**	2.44	meters
SP	**Specific Weight Density**	77.3	tonnes/meter^3
WS	**Wave Speed**	5123	meters/second
EM	**Elastic Modulus**	206840	tonnes/cm^2

Strain transducers and accelerometers

F3	**F1**	216.4
F4	**F2**	216.4
A3	**A1**	325
A4	**A2**	345

start	5	16:06:42
stop	80	16:09:43
start	85	16:34:28
stop	90	16:34:49
start	95	17:14:06
stop	115	17:15:09

NOTES

LP	Length of Penetration (penetration depth)
BN	Blow Number
EMX	Maximum Energy
DMX	Maximum Displacement
VMX	Maximum Velocity
FMX	Maximum Force
BMP	Blow Rate
ETR	Energy Transfer Ratio-Rated
EF2	Energy of F^2 (ASTM D4633)
RAT	Length Ratio for SPT (should be between 90 and 120% for a valid test)
CSB	Maximum Toe Stress
JC	Case Damping Constant
WC	Wave Speed Calculated
Wh	Theoretical Potential Energy for the SPT ram
N_{60}	Blow Number Corrected by Energy

Date	Time	LP (m)	BN	EMX (ton-m)	DMX (mm)	VMX (m/sec)	FMX (ton)	BPM (blows/min)	ETR (%)	EF2 (ton-m)	RAT	CSB (Mpa)	jc	WC (m/sec)	N_{60}	Comments
7/2/2003	16:06:42	0	5	0.251	8	4.31	82	32.1	52.8	0.280	9.1	61.50	0	5123	4	
7/2/2003	16:07:05	0	10	0.317	9	4.46	92	31.7	66.8	0.132	1.6	35.80	0	5123	11	
7/2/2003	16:07:24	0	15	0.295	11	4.12	89	0.0	62.2	0.401	10.2	60.60	0	5123	16	
7/2/2003	16:07:33	0	20	0.337	27	4.10	92	31.7	71.1	0.428	8.7	78.60	0	5123	24	
7/2/2003	16:07:42	0	25	0.284	7	4.31	90	33.7	59.8	0.423	1.6	65.10	0	5123	25	
7/2/2003	16:07:51	0	30	0.263	6	3.95	92	32.6	55.4	0.116	1.6	55.20	0	5123	28	
7/2/2003	16:08:04	0	35	0.265	13	4.40	90	0.0	55.7	0.107	1.6	45.40	0	5123	32	
7/2/2003	16:08:15	0	40	0.297	16	4.13	94	32.1	62.5	0.373	7.9	69.40	0	5123	42	
7/2/2003	16:08:24	0	45	0.301	13	4.55	91	32.8	63.4	0.387	9.6	57.00	0	5123	48	
7/2/2003	16:08:38	0	50	0.302	14	4.82	87	0.0	63.6	0.112	1.5	16.40	0	5123	53	
7/2/2003	16:08:47	0	55	0.300	17	4.70	96	34.6	63.3	0.119	1.5	0.00	0	5123	58	
7/2/2003	16:08:55	0	60	0.319	10	4.47	99	34.8	67.3	0.125	1.6	59.40	0	5123	67	
7/2/2003	16:09:25	0	75	0.298	7	4.22	97	35.2	62.8	0.378	9.2	60.40	0	5123	79	
7/2/2003	16:09:43	0	80	0.318	13	4.59	96	0.0	67.0	0.121	1.5	40.30	0	5123	89	
7/2/2003	16:34:28	1	85	0.193	23	4.28	89	0.0	40.6	0.133	1.5	9.40	0	5123	58	
7/2/2003	16:34:49	1	90	0.292	21	4.31	96	28.7	61.5	0.118	1.4	7.90	0	5123	92	
7/2/2003	17:14:06	2	95	0.347	37	4.95	89	0.0	73.0	0.173	1.3	22.60	0	5123	116	
7/2/2003	17:14:20	2	100	0.330	19	4.50	95	31.7	69.5	0.178	1.3	54.80	0	5123	116	
7/2/2003	17:14:34	2	105	0.348	34	4.31	91	33.1	73.4	0.153	1.5	16.50	0	5123	128	
7/2/2003	17:14:49	2	110	0.325	23	4.61	89	0.0	68.4	0.166	1.4	39.30	0	5123	125	
7/2/2003	17:15:09	2	115	0.350	41	4.91	91	31.8	73.7	0.165	1.3	23.00	0	5123	141	
						Average Energy Ratio =			**63.5**							

Project Name - PJ PERU 4
Pile Name - PN 4
Description - PD ;;
Operator Name - OP AC ER

AR	**Area**	7.87	cm^2
LE	**Length below sensors to pile bottom**	2.44	meters
SP	**Specific Weight Density**	77.3	tonnes/meter^3
WS	**Wave Speed**	5123	meters/second
EM	**Elastic Modulus**	206840	tonnes/cm^2

Strain transducers and accelerometers

F3	**F1**	216.4
F4	**F2**	216.4
A3	**A1**	325
A4	**A2**	345

start	5	16:06:42
stop	80	16:09:43
start	85	16:34:28
stop	90	16:34:49
start	100	17:14:20
stop	110	17:14:49

NOTES

LP	Length of Penetration (penetration depth)
BN	Blow Number
EMX	Maximum Energy
DMX	Maximum Displacement
VMX	Maximum Velocity
FMX	Maximum Force
BMP	Blow Rate
ETR	Energy Transfer Ratio-Rated
EF2	Energy of F^2 (ASTM D4633)
RAT	Length Ratio for SPT (should be between 90 and 120% for a valid test)
CSB	Maximum Toe Stress
JC	Case Damping Constant
WC	Wave Speed Calculated
Wh	Theoretical Potential Energy for the SPT ram
N_{60}	Blow Number Corrected by Energy

Date	Time	LP (m)	BN	EMX (ton-m)	DMX (mm)	VMX (m/sec)	FMX (ton)	BPM (blows/min)	ETR (%)	EF2 (ton-m)	RAT	CSB (Mpa)	jc	WC (m/sec)	N_{60}	Comments
7/2/2003	16:06:42	0	5	0.253	7	4.03	82	32.1	53.3	0.280	9.1	71.00	0	5123	4	
7/2/2003	16:07:05	0	10	0.325	9	4.15	92	31.7	68.6	0.132	1.6	85.30	0	5123	11	
7/2/2003	16:07:24	0	15	0.300	11	3.86	89	0.0	63.2	0.401	10.2	60.30	0	5123	16	
7/2/2003	16:07:42	0	25	0.290	7	4.06	90	33.7	61.1	0.423	1.6	73.80	0	5123	25	
7/2/2003	16:07:51	0	30	0.271	6	3.94	92	32.6	57.2	0.116	1.6	61.10	0	5123	29	
7/2/2003	16:08:04	0	35	0.272	13	4.19	90	0.0	57.3	0.107	1.6	62.50	0	5123	33	
7/2/2003	16:08:15	0	40	0.305	15	3.83	94	32.1	64.2	0.373	7.9	71.20	0	5123	43	
7/2/2003	16:08:24	0	45	0.305	13	4.28	91	32.8	64.2	0.387	9.6	65.20	0	5123	48	
7/2/2003	16:08:38	0	50	0.312	14	4.28	87	0.0	65.7	0.112	1.6	58.10	0	5123	55	
7/2/2003	16:08:47	0	55	0.315	17	4.27	96	34.6	66.4	0.119	1.5	45.50	0	5123	61	
7/2/2003	16:08:55	0	60	0.327	10	4.18	99	34.8	68.9	0.125	1.6	57.40	0	5123	69	
7/2/2003	16:09:08	0	65	0.000	0	0.00	97	36.0	0.0	0.392	17.1	0.60	0	5123	0	
7/2/2003	16:09:17	0	70	0.000	0	0.00	80	34.8	0.0	0.405	16.6	1.00	0	5123	0	
7/2/2003	16:09:25	0	75	0.306	7	4.10	97	35.2	64.6	0.378	9.2	81.40	0	5123	81	
7/2/2003	16:09:43	0	80	0.330	14	4.10	96	0.0	69.6	0.121	1.6	69.00	0	5123	93	
7/2/2003	16:34:28	1	85	0.202	23	4.00	89	0.0	42.7	0.133	1.5	17.10	0	5123	60	
7/2/2003	16:34:49	1	90	0.302	21	3.78	96	28.7	63.5	0.118	1.5	10.40	0	5123	95	
7/2/2003	17:14:20	2	100	0.337	19	4.08	95	31.7	71.0	0.178	1.3	34.40	0	5123	118	
7/2/2003	17:14:49	2	110	0.336	24	4.10	89	0.0	70.8	0.166	1.4	64.00	0	5123	130	
								Average Energy Ratio =	**63.1**							

Project Name - PJ PERU 4.1
Pile Name - PN 4
Description - PD HW 2;;
Operator Name - OP AC ER

AR	**Area**	7.87	cm^2
LE	**Length below sensors to pile bottom**	6.05	meters
SP	**Specific Weight Density**	77.3	tonnes/meter^3
WS	**Wave Speed**	5123	meters/second
EM	**Elastic Modulus**	206840	tonnes/cm^2

Strain transducers and accelerometers

F3	**F1**	216.4
F4	**F2**	216.4
A3	**A1**	325
A4	**A2**	345

start	5	10:23:32
stop	45	10:44:36
start	50	11:41:06
stop	60	12:28:24
start	65	12:49:47
stop	75	12:50:16
start	80	13:12:46
stop	85	13:13:14
start	90	14:19:28
stop	95	14:20:00
start	105	14:35:52
stop	115	14:36:54
start	120	15:14:55
stop	195	15:18:13

NOTES

LP	Length of Penetration (penetration depth)
BN	Blow Number
EMX	Maximum Energy
DMX	Maximum Displacement
VMX	Maximum Velocity
FMX	Maximum Force
BMP	Blow Rate
ETR	Energy Transfer Ratio-Rated
EF2	Energy of F^2 (ASTM D4633)
RAT	Length Ratio for SPT (should be between 90 and 120% for a valid test)
CSB	Maximum Toe Stress
JC	Case Damping Constant
WC	Wave Speed Calculated
Wh	Theoretical Potential Energy for the SPT ram
N_{60}	Blow Number Corrected by Energy

Date	Time	LP (m)	BN	EMX (ton-m)	DMX (mm)	VMX (m/sec)	FMX (ton)	BPM (blows/min)	ETR (%)	EF2 (ton-m)	RAT	CSB (Mpa)	jc	WC (m/sec)	N_{60}	Comments
7/3/2003	10:23:32	4	5	0.000	0	0.00	91	0.0	0.0	0.271	7.1	16.20	0	5123	0	
7/3/2003	10:43:29	5	15	0.325	28	4.01	97	34.9	68.5	0.238	1.2	85.80	0	5123	17	
7/3/2003	10:43:40	5	20	0.334	10	4.09	109	0.0	70.4	0.250	1.2	90.80	0	5123	23	
7/3/2003	10:43:50	5	25	0.341	25	4.44	108	29.9	71.9	0.247	1.2	88.40	0	5123	30	
7/3/2003	10:43:59	5	30	0.338	29	4.30	111	31.6	71.2	0.233	1.3	86.80	0	5123	36	
7/3/2003	10:44:09	5	35	0.335	19	3.97	97	30.9	70.6	0.238	1.2	76.50	0	5123	41	
7/3/2003	10:44:24	5	40	0.321	27	4.07	106	34.0	67.6	0.221	1.3	96.90	0	5123	45	
7/3/2003	10:44:36	5	45	0.328	29	3.78	100	33.8	69.2	0.226	1.2	90.30	0	5123	52	
7/3/2003	11:41:06	6	50	0.289	15	4.33	97	0.0	60.9	0.235	1.2	99.50	0	5123	51	
7/3/2003	12:27:59	7	55	0.302	31	4.09	98	0.0	63.6	0.261	1.3	104.50	0	5123	58	
7/3/2003	12:28:24	7	60	0.326	27	3.98	92	32.4	68.7	0.272	1.2	87.90	0	5123	69	
7/3/2003	12:49:47	8	65	0.281	29	4.10	99	30.6	59.2	0.255	1.1	84.80	0	5123	64	
7/3/2003	12:50:01	8	70	0.285	23	3.55	105	31.6	60.0	0.260	1.1	105.90	0	5123	70	
7/3/2003	12:50:16	8	75	0.290	25	3.58	106	32.0	61.0	0.268	1.1	105.60	0	5123	76	
7/3/2003	13:12:46	9	80	0.000	0	0.00	90	0.0	0.0	0.342	2.5	11.40	0	5123	0	
7/3/2003	13:13:14	9	85	0.298	40	4.86	102	35.6	62.8	0.278	1.1	29.20	0	5123	89	
7/3/2003	14:19:28	10	90	0.000	0	0.00	109	30.5	0.0	0.293	2.9	18.00	0	5123	0	
7/3/2003	14:20:00	10	95	0.000	0	0.00	97	31.2	0.0	0.289	3.4	12.30	0	5123	0	
7/3/2003	14:35:52	11	105	0.000	0	0.00	95	0.0	0.0	0.401	2.6	15.30	0	5123	0	
7/3/2003	14:36:25	11	110	0.337	18	3.67	98	0.0	71.0	0.302	1.1	33.70	0	5123	130	
7/3/2003	14:36:54	11	115	0.000	0	0.00	99	0.0	0.0	0.348	2.9	20.30	0	5123	0	
7/3/2003	15:14:55	12	120	0.253	8	3.37	94	0.0	53.3	0.233	1.1	71.10	0	5123	107	
7/3/2003	15:15:13	12	125	0.334	19	3.98	93	0.0	70.4	0.285	1.1	77.10	0	5123	147	
7/3/2003	15:15:27	12	130	0.323	17	4.12	86	35.7	68.0	0.253	1.1	78.20	0	5123	147	
7/3/2003	15:15:36	12	135	0.331	27	3.89	84	36.1	69.7	0.247	1	73.20	0	5123	157	
7/3/2003	15:15:44	12	140	0.329	28	3.63	86	36.0	69.3	0.254	1.1	43.60	0	5123	162	
7/3/2003	15:15:52	12	145	0.348	28	4.06	93	33.9	73.3	0.260	1.1	88.90	0	5123	177	
7/3/2003	15:16:22	12	150	0.341	25	3.76	87	0.0	71.9	0.277	1.1	69.80	0	5123	180	
7/3/2003	15:16:39	12	155	0.334	9	4.21	97	37.9	70.4	0.278	1.2	77.60	0	5123	182	
7/3/2003	15:16:48	12	160	0.293	8	3.66	95	40.7	61.7	0.260	1.1	79.60	0	5123	165	
7/3/2003	15:16:59	12	165	0.297	7	4.06	85	40.5	62.6	0.268	1.1	68.00	0	5123	172	
7/3/2003	15:17:10	12	170	0.000	0	0.00	91	20.3	0.0	0.419	2.2	3.50	0	5123	0	
7/3/2003	15:17:23	12	175	0.321	16	4.22	96	40.2	67.7	0.255	1.1	56.40	0	5123	197	
7/3/2003	15:17:33	12	180	0.293	19	4.34	97	39.6	61.7	0.262	1.1	74.00	0	5123	185	
7/3/2003	15:17:42	12	185	0.311	8	3.60	94	19.5	65.6	0.257	1.1	78.30	0	5123	202	
7/3/2003	15:18:13	12	195	0.341	11	4.42	79	0.0	71.9	0.260	1.1	113.50	0	5123	234	
						Average Energy Ratio =			**66.7**							

Project Name - PJ PERU 4.1
Pile Name - PN 4
Description - PD HW 2;;
Operator Name - OP AC ER

AR	**Area**	7.87	cm^2
LE	**Length below sensors to pile bottom**	13.07	meters
SP	**Specific Weight Density**	77.3	tonnes/meter^3
WS	**Wave Speed**	5123	meters/second
EM	**Elastic Modulus**	206840	tonnes/cm^2

Strain transducers and accelerometers

F3	**F1**	216.4
F4	**F2**	216.4
A3	**A1**	325
A4	**A2**	345

start	5	10:23:32
stop	45	10:44:36
start	50	11:41:06
stop	60	12:28:24
start	65	12:49:47
stop	75	12:50:16
start	80	13:12:46
stop	95	14:20:00
start	110	14:36:25
stop	195	15:18:13

NOTES

LP	Length of Penetration (penetration depth)
BN	Blow Number
EMX	Maximum Energy
DMX	Maximum Displacement
VMX	Maximum Velocity
FMX	Maximum Force
BMP	Blow Rate
ETR	Energy Transfer Ratio-Rated
EF2	Energy of F^2 (ASTM D4633)
RAT	Length Ratio for SPT (should be between 90 and 120% for a valid test)
CSB	Maximum Toe Stress
JC	Case Damping Constant
WC	Wave Speed Calculated
Wh	Theoretical Potential Energy for the SPT ram
N_{60}	Blow Number Corrected by Energy

Date	Time	LP (m)	BN	EMX (ton-m)	DMX (mm)	VMX (m/sec)	FMX (ton)	BPM (blows/min)	ETR (%)	EF2 (ton-m)	RAT	CSB (Mpa)	jc	WC (m/sec)	N_{60}	Comments
7/3/2003	10:23:32	4	5	0.000	0	0.00	91	0.0	0.0	0.271	7.1	16.20	0	5123	0	
7/3/2003	10:43:29	5	15	0.325	28	4.01	97	34.9	68.5	0.238	1.2	85.80	0	5123	17	
7/3/2003	10:43:40	5	20	0.334	10	4.09	109	0.0	70.4	0.250	1.2	90.80	0	5123	23	
7/3/2003	10:44:09	5	35	0.335	19	3.97	97	30.9	70.6	0.238	1.2	76.50	0	5123	41	
7/3/2003	10:44:24	5	40	0.321	27	4.07	106	34.0	67.6	0.221	1.3	96.90	0	5123	45	
7/3/2003	10:44:36	5	45	0.328	29	3.78	100	33.8	69.2	0.226	1.2	90.30	0	5123	52	
7/3/2003	11:41:06	6	50	0.289	15	4.33	97	0.0	60.9	0.235	1.2	99.50	0	5123	51	
7/3/2003	12:27:59	7	55	0.302	31	4.09	98	0.0	63.6	0.261	1.3	104.50	0	5123	58	
7/3/2003	12:28:24	7	60	0.326	27	3.98	92	32.4	68.7	0.272	1.2	87.90	0	5123	69	
7/3/2003	12:49:47	8	65	0.281	29	4.10	99	30.6	59.2	0.255	1.1	84.80	0	5123	64	
7/3/2003	12:50:01	8	70	0.285	23	3.55	105	31.6	60.0	0.260	1.1	105.90	0	5123	70	
7/3/2003	12:50:16	8	75	0.290	25	3.58	106	32.0	61.0	0.268	1.1	105.60	0	5123	76	
7/3/2003	13:12:46	9	80	0.353	51	4.36	90	0.0	74.4	0.295	1.1	62.50	0	5123	99	
7/3/2003	14:20:00	10	95	0.000	0	0.00	97	31.2	0.0	0.289	3.4	12.30	0	5123	0	
7/3/2003	14:36:25	11	110	0.337	18	3.67	98	0.0	71.0	0.302	1.1	33.70	0	5123	130	
7/3/2003	15:14:55	12	120	0.253	8	3.37	94	0.0	53.3	0.233	1.1	71.10	0	5123	107	
7/3/2003	15:15:13	12	125	0.334	19	3.98	93	0.0	70.4	0.285	1.1	77.10	0	5123	147	
7/3/2003	15:15:27	12	130	0.323	17	4.12	86	35.7	68.0	0.253	1.1	78.20	0	5123	147	
7/3/2003	15:15:36	12	135	0.331	27	3.89	84	36.1	69.7	0.247	1	73.20	0	5123	157	
7/3/2003	15:15:44	12	140	0.329	28	3.63	86	36.0	69.3	0.254	1.1	43.60	0	5123	162	
7/3/2003	15:15:52	12	145	0.348	28	4.06	93	33.9	73.3	0.260	1.1	88.90	0	5123	177	
7/3/2003	15:16:22	12	150	0.341	25	3.76	87	0.0	71.9	0.277	1.1	69.80	0	5123	180	
7/3/2003	15:16:39	12	155	0.334	9	4.21	97	37.9	70.4	0.278	1.2	77.60	0	5123	182	
7/3/2003	15:16:48	12	160	0.293	8	3.66	95	40.7	61.7	0.260	1.1	79.60	0	5123	165	
7/3/2003	15:16:59	12	165	0.297	7	4.06	85	40.5	62.6	0.268	1.1	68.00	0	5123	172	
7/3/2003	15:17:10	12	170	0.000	0	0.00	91	20.3	0.0	0.419	2.2	3.50	0	5123	0	
7/3/2003	15:17:23	12	175	0.321	16	4.22	96	40.2	67.7	0.255	1.1	56.40	0	5123	197	
7/3/2003	15:17:33	12	180	0.293	19	4.34	97	39.6	61.7	0.262	1.1	74.00	0	5123	185	
7/3/2003	15:17:42	12	185	0.311	8	3.60	94	19.5	65.6	0.257	1.1	78.30	0	5123	202	
7/3/2003	15:18:13	12	195	0.341	11	4.42	79	0.0	71.9	0.260	1.1	113.50	0	5123	234	
								Average Energy Ratio =	**66.76**							

APPENDIX C

COMPUTER CODE TO OBTAIN MODULUS

DEGRADATION AND DAMPING CURVES

The following code was developed using the programming language MATLAB. The purpose of the code is to randomly create modulus degradation and damping curves following the criteria suggested by Darendeli (2000).

```
%function [Strain,Modulus,Damping] = curves1(PI,SIGo)
%usage:  [Strain,Modulus,Damping] = curves1(PI,SIGo)
% Returns:
% Strain = array that contains the strains calculated and used to plot the
% curves.
% Modulus = array that contains the modulus reduction values calculated to plot the
 curves.
% Damping = array that contains the damping ratios calculated and used to
% plot the curves.
% Calculation of reference strain,curvature coefficient,small strain
% material damping ratio and the scaling coefficient.
X=normrnd(0,1,1,nsim);
j=[0.0001,0.0003,0.0005,0.0007,0.0010,0.0020,0.0040,0.0060,0.0080,0.0100,0.0200,0.04
 00,0.0600,0.0800,0.1000,0.2000,0.4000,0.6000,0.8000,1.0000];
SIGo=[0.57522 2.01331 4.88939];    %should be in ATM
Modulus10=zeros(length(j),length(X)*length(SIGo));
Damping10=zeros(length(j),length(X)*length(SIGo));
Dampingmean=zeros(length(j),length(SIGo));
Modulusmean=zeros(length(j),length(SIGo));
PI=0;
OCR=4;
frq=10;
N=10;
nn=1;   %counter for curve number
for m=1:length (SIGo)
   phi1=0.0352;
   phi2=0.0010;
```

```
phi3=0.3246;
phi4=0.3483;
phi5=0.9190;
phi6=0.8005;
phi7=0.0129;
phi8=-0.1069;
phi9=-0.2889;
phi10=0.2919;
phi11=0.6329;
phi12=-0.0057;
phi13=-4.23;
phi14=3.62;
phi15=-5.00;
phi16=-0.25;
phi17=5.62;
phi18=2.78;
% jr = reference strain.
% PI = plastic index.
% OCR = overconsolidation ratio.
% SIGo = initial effective stress.
% a= curvature coefficient.
% Dmin= small strain material damping ratio.
% b= scaling coefficient.
% frq=loading frequency.
% N=number of loading cycles.
for u=1:length(X)
   x=(X(1,u));
   jr=(phi1+phi2*PI*OCR^phi3)*SIGo(m)^phi4;
   a= phi5;
   Dmin=(phi6+phi7*PI*OCR^phi8)*(SIGo(m))^phi9*(1+phi10*log(frq));
   b= phi11+phi12*log(N);
```

```
% GGmax=normalized shear modulus (G/Gmax)
% j=shearing strain.
% Dadjusted=scaled and capped material damping ratio (percent)
GGmax=zeros(20,1);
Dadjusted=zeros(20,1);
StdDamp=zeros(20,1);
StdMod=zeros(20,1);
StdDamp1=zeros(20,1);
StdMod1=zeros(20,1);
i=1;
for n=1:length(j)
   GGmax(i,1)=1/(1+(j(n)/jr)^a);
   c1=-1.1143*a^2+1.8618*a+0.2523;
   c2=0.0805*a^2-0.0710*a-0.0095;
   c3=-0.0005*a^2+0.0002*a+0.0003;
   Dmasinga1=(100/pi)*(4*((j(n)-jr*log((j(n)+jr)/jr))/(((j(n))^2/(j(n)+jr))))-2);
   Dmasing=c1*Dmasinga1+c2*Dmasinga1^2+c3*Dmasinga1^3; %(%)
   Dadjusted(i,1)=b*(GGmax(i,1))^0.1*Dmasing+Dmin;
   StandDamp(i,1)=exp(phi15)+exp(phi16)*sqrt(Dadjusted(i,1));
  StandMod(i,1)=exp(phi13)+sqrt((0.25/exp(phi14))-((GGmax(i,1)-
  0.5)^2/exp(phi14)));
    StdDamp(i,1)=Dadjusted(i,1)+x*StandDamp(i,1);      %%%%%
   StdMod(i,1)=GGmax(i,1)-x*StandMod(i,1);           %%%%%
   if(StdMod(i,1) < 0.01)
   StdMod(i,1)=0.01;
   end
   if(StdDamp(i,1) < 0.05)
      StdDamp(i,1) = 0.05;
   end
   i=i+1;
end
```

```
        Damping(:,nn)=StdDamp(:,1);
        Modulus(:,nn)=StdMod(:,1);
        jref(nn)=jr;
        nn=nn+1;
        end  %for each nsim
        Dampingmean(:,m) = Dadjusted(:,1);
        Modulusmean(:,m) = GGmax(:,1);
end  %for SIGo
Strain=j;
save STATION0 Strain Damping Modulus Dampingmean Modulusmean
%FOR PLOTTING
figure(1);clf
figure(2);clf
for i=1:nsim
   figure(1);
   subplot(3,1,1),semilogx(j,Modulus(:,i));hold on;
   subplot(3,1,2),semilogx(j,Modulus(:,nsim+i),'r');hold on
   subplot(3,1,3),semilogx(j,Modulus(:,nsim*2+i),'k');hold on
   figure(2);
   subplot(3,1,1),semilogx(j,Damping(:,i));hold on;
   subplot(3,1,2),semilogx(j,Damping(:,nsim+i),'r');hold on
   subplot(3,1,3),semilogx(j,Damping(:,nsim*2+i),'k');hold on
end
figure(1);
subplot(3,1,1),semilogx(j,Modulusmean(:,1),'y','linewidth',2);
subplot(3,1,2),semilogx(j,Modulusmean(:,2),'y','linewidth',2);
subplot(3,1,3),semilogx(j,Modulusmean(:,3),'y','linewidth',2);
figure(2);
subplot(3,1,1),semilogx(j,Dampingmean(:,1),'y','linewidth',2);
subplot(3,1,2),semilogx(j,Dampingmean(:,2),'y','linewidth',2);
subplot(3,1,3),semilogx(j,Dampingmean(:,3),'y','linewidth',2);
```

APPENDIX D

SITE RESPONSE ANALYSIS PROCEDURE

The present appendix intends to summarize the process followed for site response analysis with an example. The ground motion station at Moquegua city is used as illustration.

First the outcrop acceleration time histories provided by Dr. Walter Silva for the Moquegua Ground Motion Station Site were averaged and the average was scaled to different levels, Figure D.1 presents the average acceleration time history scaled to 03 g. Then the response spectrum was calculated and it is presented in Figure D.2.

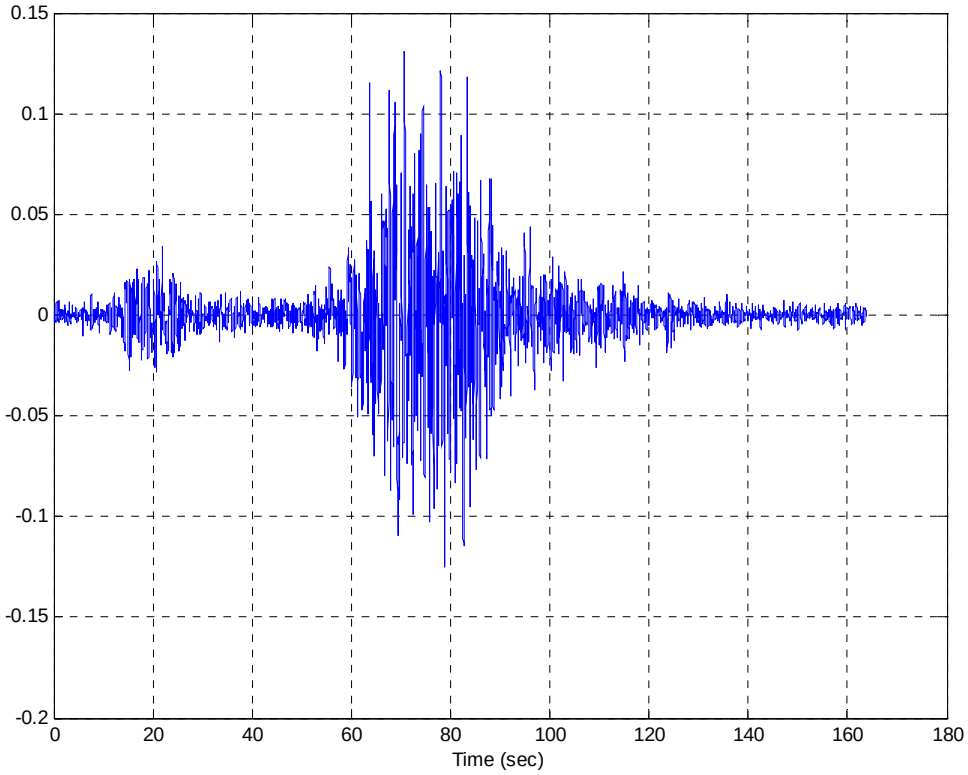

Figure D.1 Average Acceleration Time History.

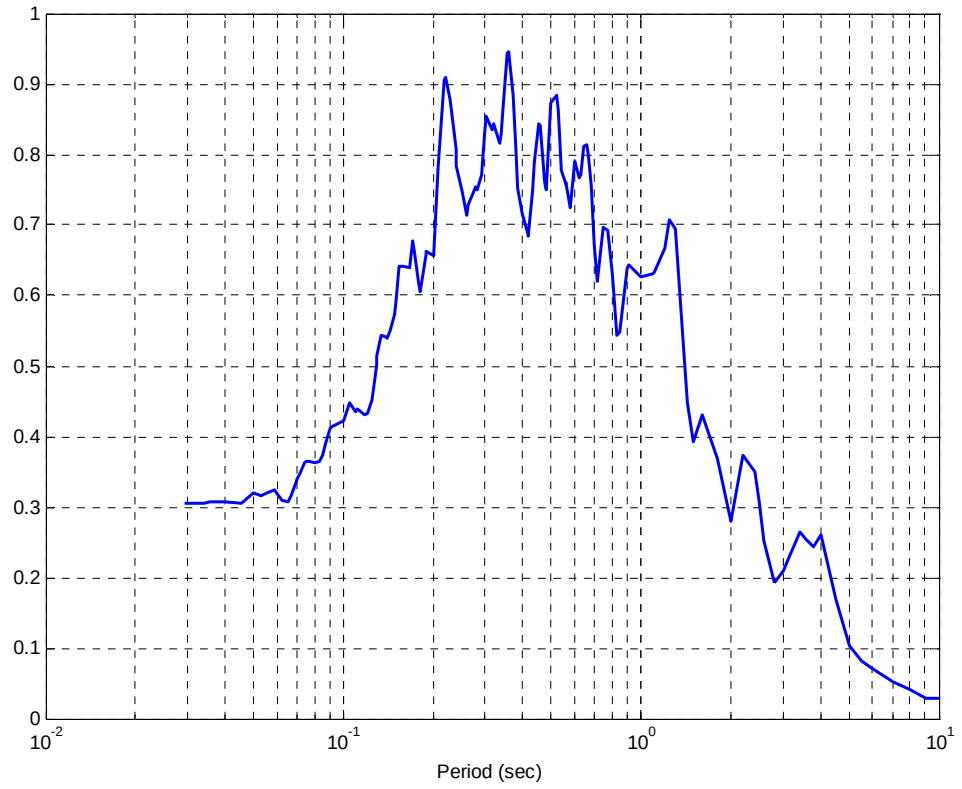

Figure D.2 Response Spectra of the Input Ground Motion.

After the Response Spectra was found the ground motion was applied to a soil profile obtained at the Ground Motion Station (Figure D.3) using the equivalent linear analysis of the program SHAKeE 91 (the input file used is presented at the end of the present appendix as Table D.1) and the acceleration time history at the ground surface was obtained (Figure D.4), then the response spectra was calculated and plotted (Figure D.5).

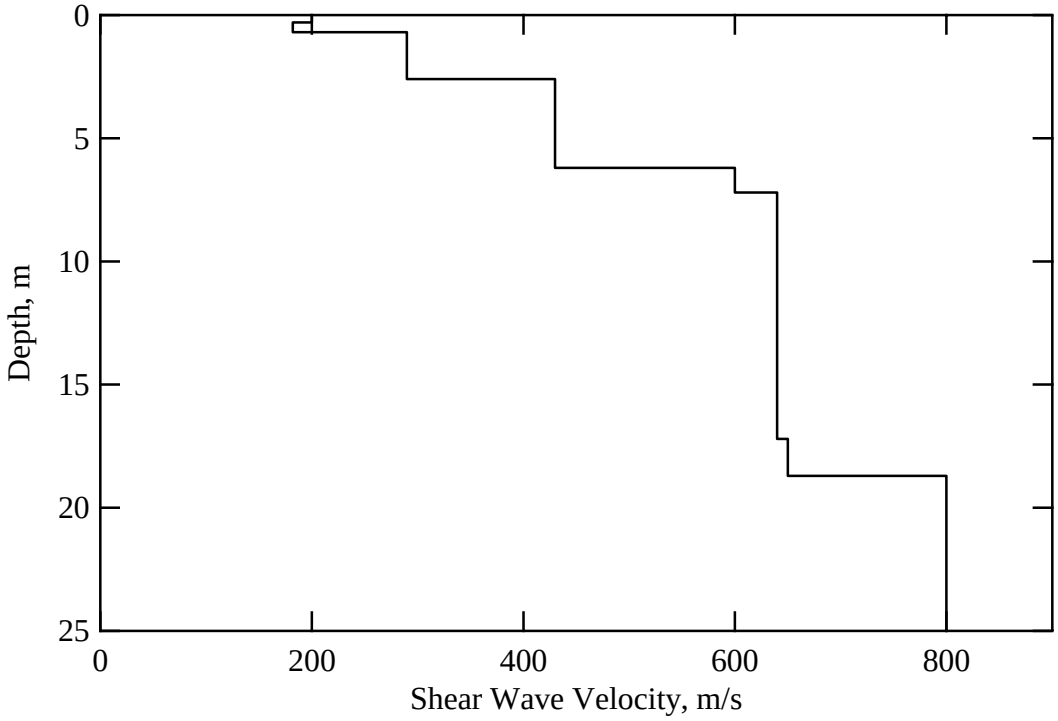

Figure D.3 Input Shear Wave Velocity Profile.

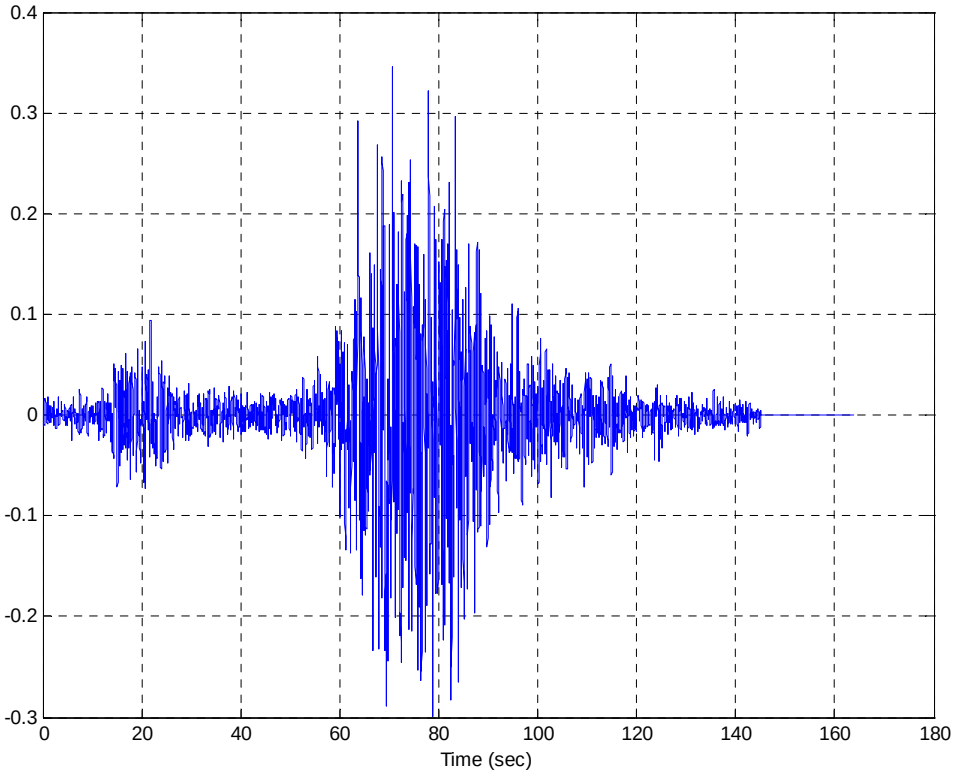

Figure D.4 Output Acceleration Time History.

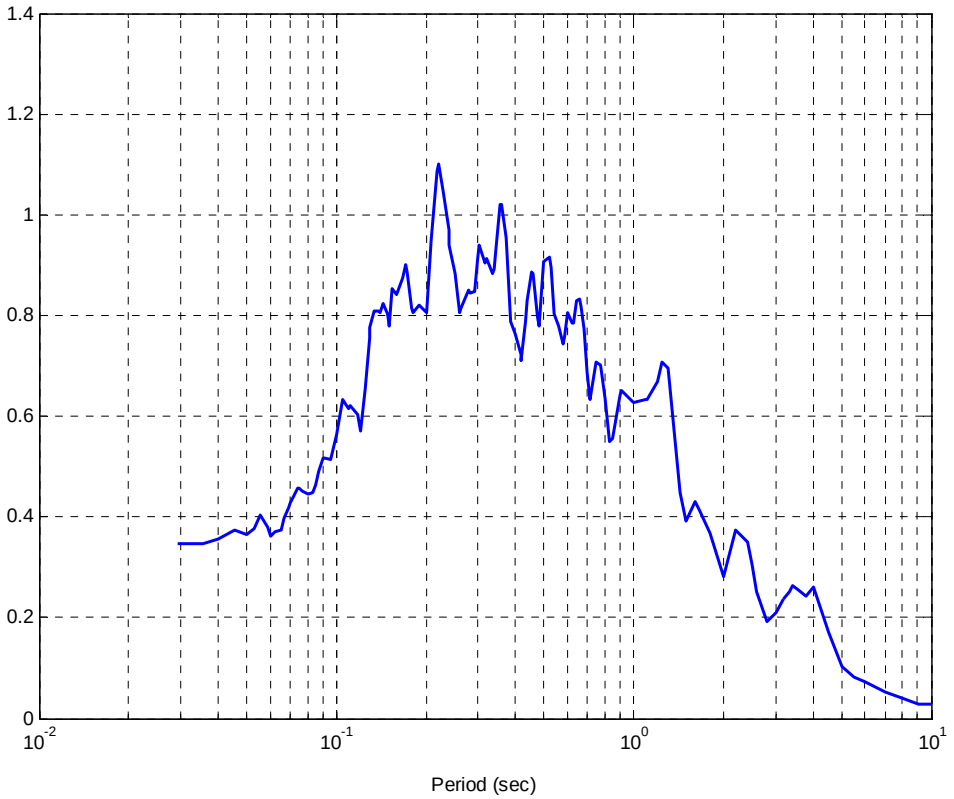

Figure D.5 Response Spectra of the Output Ground Motion.

Some additional results were obtained and analyzed such as the variation of strain and stress through depth (Figure D.6a and D.6b), the maximum acceleration variation through depth (Figure D.7) as well as the final shear wave velocity profile (Figure D.8).

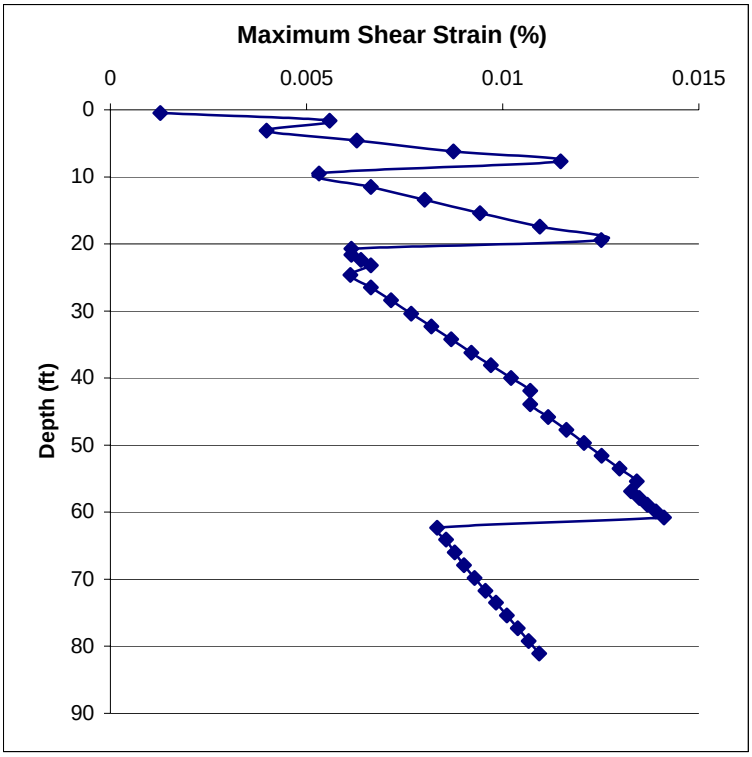

Figure D.6a Maximum Shear Strain.

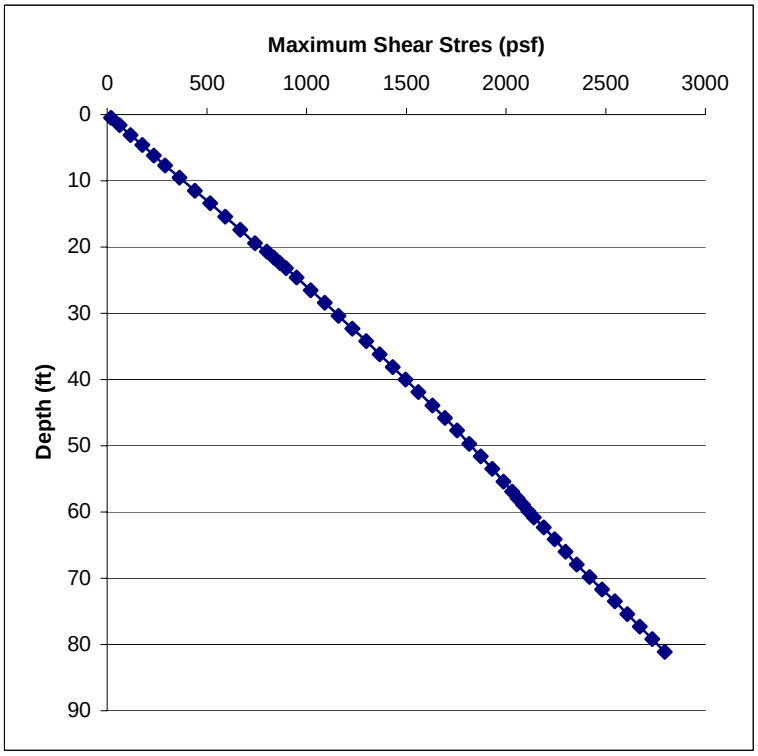

Figure D.6b Maximum Shear Stress.

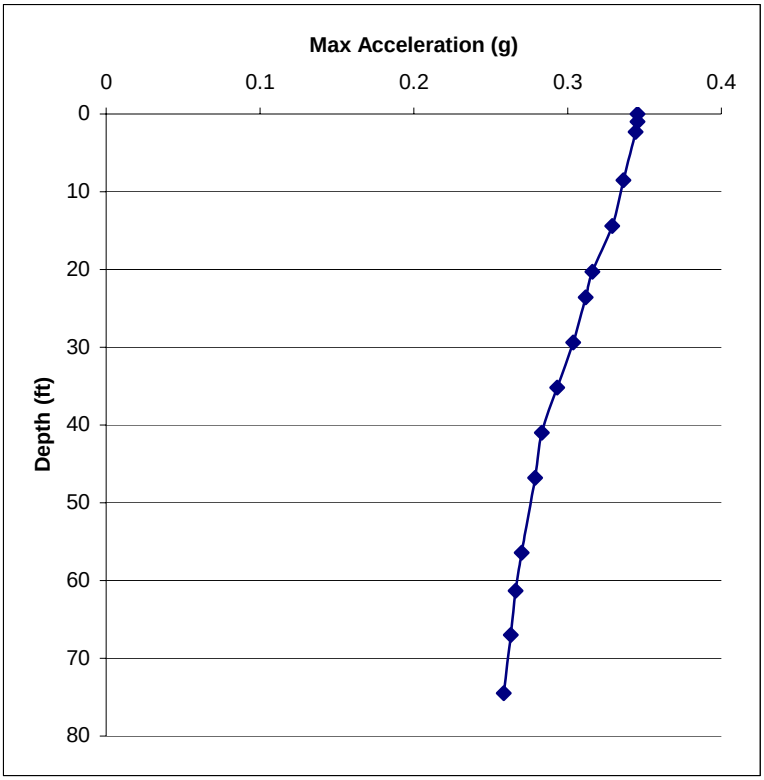

Figure D.7 Maximum Acceleration.

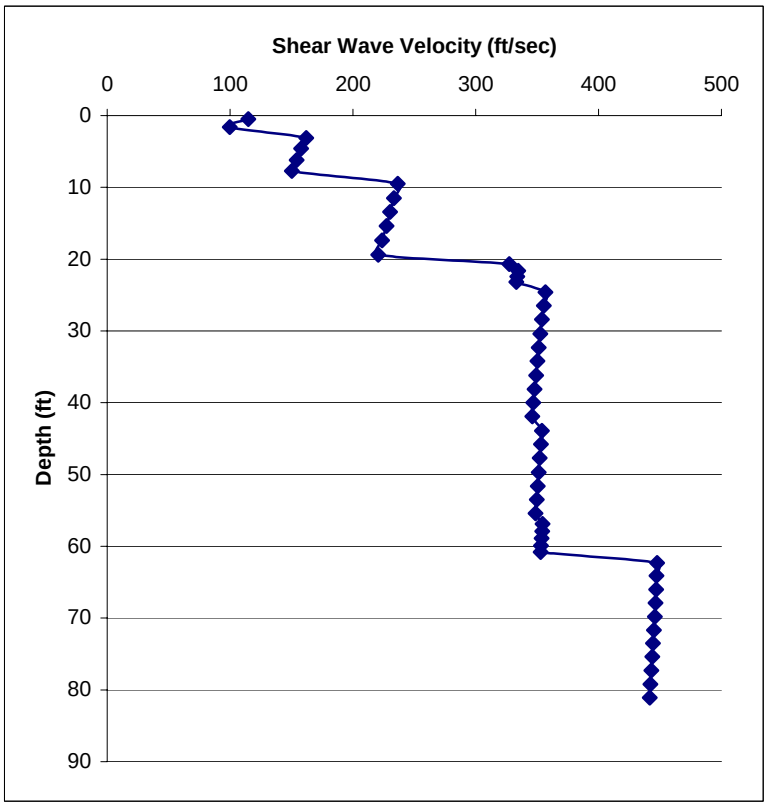

Figure D.8 Final Shear Wave Velocity Profile.

It is important to indicate that the Modulus degradation and Damping Ratio curves used in the analysis are the ones proposed by EERI (1993) that

are depth dependent curves. The curves used are presented in Figure D.9a and D.9b respectively.

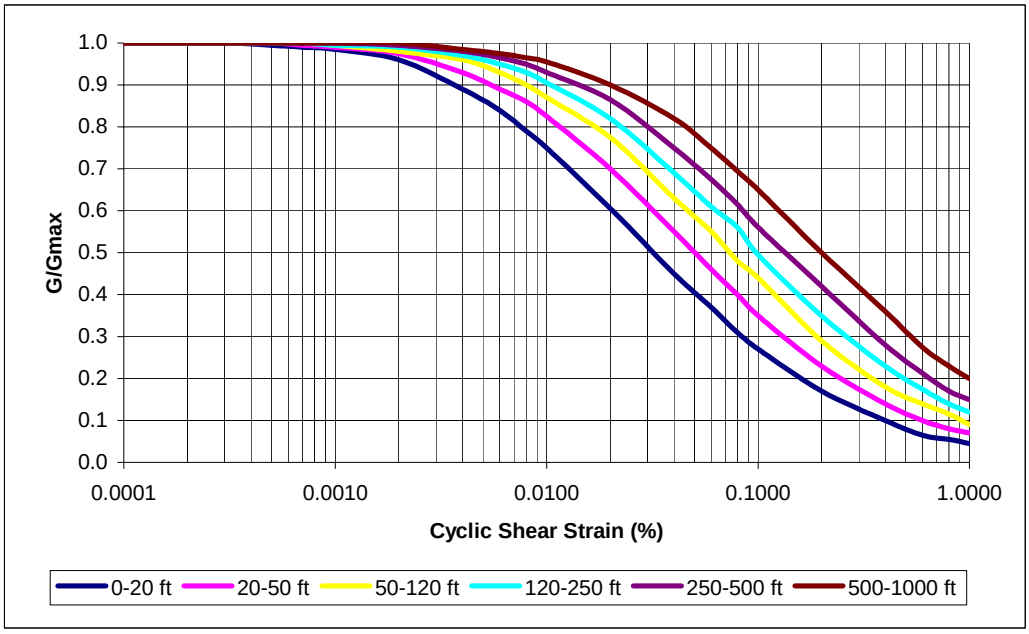

Figure D.9a Modulus Degradation Curves

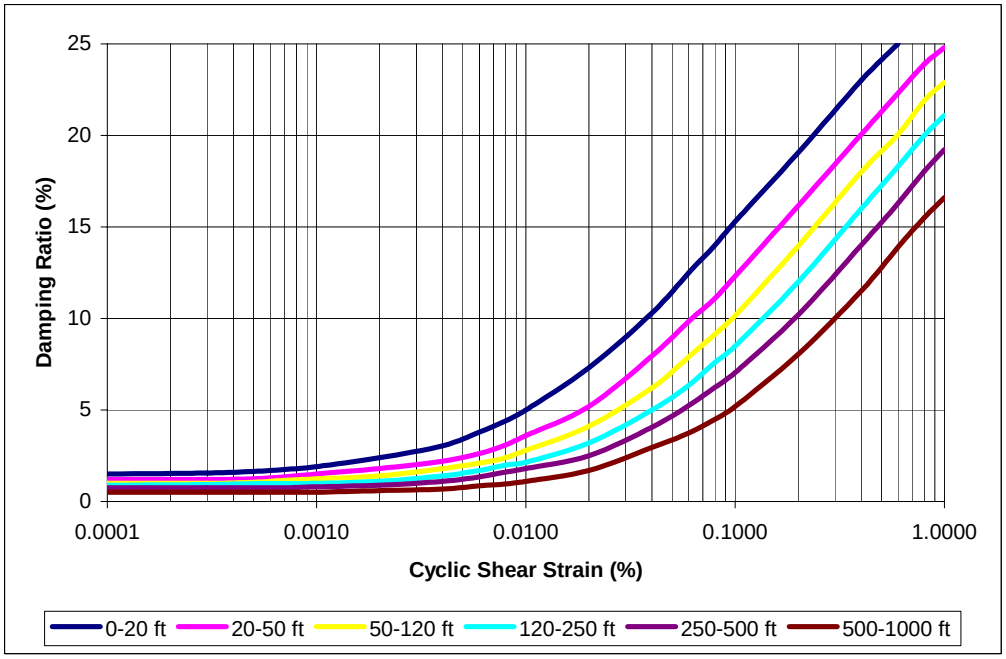

Figure D.9b Damping Ratio Curves

Table D.1 Input file used in Shake

option 1 - dynamic soil properties
1
6
20 #1 MODULUS EPRI CURVES 0-20 ft
0.0001 0.0003 0.0005 0.0007 0.0010 0.0020 0.0040 0.0060
0.0080 0.0100 0.0200 0.0400 0.0600 0.0800 0.1000 0.2000
0.4000 0.6000 0.8000 1.0000
1.000 1.000 0.995 0.990 0.985 0.960 0.890 0.840
0.790 0.750 0.605 0.450 0.370 0.310 0.270 0.170
0.100 0.065 0.055 0.045
18 DAMPING EPRI CURVES 0-20 ft
0.0001 0.0003 0.0005 0.0007 0.0010 0.0020 0.0040 0.0060
0.0080 0.0100 0.0200 0.0400 0.0600 0.0800 0.1000 0.2000
0.4000 0.6000
1.500 1.550 1.650 1.750 1.900 2.400 3.050 3.800
4.400 5.000 7.300 10.300 12.500 14.000 15.300 19.050
23.000 25.000
20 #2 MODULUS EPRI CURVES 20-50 ft
0.0001 0.0003 0.0005 0.0007 0.0010 0.0020 0.0040 0.0060
0.0080 0.0100 0.0200 0.0400 0.0600 0.0800 0.1000 0.2000
0.4000 0.6000 0.8000 1.0000
1.000 1.000 1.000 0.995 0.990 0.975 0.930 0.890
0.860 0.825 0.700 0.550 0.460 0.400 0.350 0.230
0.140 0.100 0.080 0.070
20 DAMPING EPRI CURVES 20-50 ft
0.0001 0.0003 0.0005 0.0007 0.0010 0.0020 0.0040 0.0060
0.0080 0.0100 0.0200 0.0400 0.0600 0.0800 0.1000 0.2000
0.4000 0.6000 0.8000 1.0000
1.200 1.200 1.250 1.350 1.500 1.800 2.200 2.620
3.100 3.600 5.200 7.950 9.850 11.100 12.300 16.150
20.050 22.300 23.900 24.800
20 #3 MODULUS EPRI CURVES 50-120 ft
0.0001 0.0003 0.0005 0.0007 0.0010 0.0020 0.0040 0.0060
0.0080 0.0100 0.0200 0.0400 0.0600 0.0800 0.1000 0.2000
0.4000 0.6000 0.8000 1.0000
1.000 1.000 1.000 1.000 0.995 0.980 0.960 0.930
0.900 0.870 0.775 0.630 0.550 0.480 0.440 0.290
0.180 0.140 0.115 0.090
20 DAMPING EPRI CURVES 50-120 ft
0.0001 0.0003 0.0005 0.0007 0.0010 0.0020 0.0040 0.0060
0.0080 0.0100 0.0200 0.0400 0.0600 0.0800 0.1000 0.2000
0.4000 0.6000 0.8000 1.0000
1.000 1.000 1.050 1.150 1.250 1.400 1.800 2.100
2.400 2.800 4.100 6.200 7.900 9.150 10.150 13.950
18.000 20.050 21.900 22.900
20 #4 MODULUS EPRI CURVES 120-250 ft
0.0001 0.0003 0.0005 0.0007 0.0010 0.0020 0.0040 0.0060
0.0080 0.0100 0.0200 0.0400 0.0600 0.0800 0.1000 0.2000
0.4000 0.6000 0.8000 1.0000
1.000 1.000 1.000 1.000 0.995 0.990 0.970 0.950
0.930 0.905 0.820 0.690 0.610 0.560 0.495 0.350
0.230 0.175 0.140 0.120

20 DAMPING EPRI CURVES 120-250 ft
0.0001 0.0003 0.0005 0.0007 0.0010 0.0020 0.0040 0.0060
0.0080 0.0100 0.0200 0.0400 0.0600 0.0800 0.1000 0.2000
0.4000 0.6000 0.8000 1.0000
0.900 0.930 0.975 0.985 1.000 1.100 1.400 1.700
2.000 2.150 3.200 5.000 6.350 7.600 8.500 12.000
16.000 18.300 20.000 21.100
20 #5 MODULUS EPRI CURVES 250-500 ft
0.0001 0.0003 0.0005 0.0007 0.0010 0.0020 0.0040 0.0060
0.0080 0.0100 0.0200 0.0400 0.0600 0.0800 0.1000 0.2000
0.4000 0.6000 0.8000 1.0000
1.000 1.000 1.000 1.000 1.000 0.995 0.980 0.960
0.950 0.930 0.865 0.750 0.675 0.615 0.560 0.420
0.280 0.213 0.170 0.150
20 DAMPING EPRI CURVES 250-500 ft
0.0001 0.0003 0.0005 0.0007 0.0010 0.0020 0.0040 0.0060
0.0080 0.0100 0.0200 0.0400 0.0600 0.0800 0.1000 0.2000
0.4000 0.6000 0.8000 1.0000
0.750 0.750 0.750 0.750 0.800 0.900 1.100 1.350
1.600 1.800 2.500 4.050 5.240 6.250 7.050 10.200
14.000 16.300 18.050 19.230
20 #6 MODULUS EPRI CURVES 500-1000 ft
0.0001 0.0003 0.0005 0.0007 0.0010 0.0020 0.0040 0.0060
0.0080 0.0100 0.0200 0.0400 0.0600 0.0800 0.1000 0.2000
0.4000 0.6000 0.8000 1.0000
1.000 1.000 1.000 1.000 1.000 1.000 0.985 0.975
0.965 0.955 0.900 0.820 0.750 0.695 0.650 0.500
0.360 0.275 0.230 0.200
20 1. DAMPING EPRI CURVES 500-1000 ft
0.0001 0.0003 0.0005 0.0007 0.0010 0.0020 0.0040 0.0060
0.0080 0.0100 0.0200 0.0400 0.0600 0.0800 0.1000 0.2000
0.4000 0.6000 0.8000 1.0000
0.500 0.500 0.500 0.500 0.500 0.600 0.690 0.850
0.960 1.100 1.700 2.950 3.740 4.500 5.200 8.050
11.500 13.900 15.500 16.600
3 1 2 3
Option 2 - Soil Profile
2
1 50 Moquegua GMS 80' deposit
1 1 0.984 0.05 0.1124 656
2 1 1.312 0.05 0.1124 596.96
3 1 1.558 0.05 0.1124 951.2
4 1 1.558 0.05 0.1124 951.2
5 1 1.558 0.05 0.1124 951.2
6 1 1.558 0.05 0.1124 951.2
7 1 1.968 0.05 0.1218 1410.4
8 1 1.968 0.05 0.1218 1410.4
9 1 1.968 0.05 0.1218 1410.4
10 1 1.968 0.05 0.1218 1410.4
11 1 1.968 0.05 0.1218 1410.4
12 1 1.968 0.05 0.1218 1410.4
13 1 0.820 0.05 0.1218 1968
14 2 0.820 0.05 0.1218 1968
15 2 0.820 0.05 0.1218 1968
16 2 0.820 0.05 0.1218 1968
17 2 1.929 0.05 0.1218 2099.2

18 2 1.929 0.05 0.1218 2099.2
19 2 1.929 0.05 0.1218 2099.2
20 2 1.929 0.05 0.1218 2099.2
21 2 1.929 0.05 0.1218 2099.2
22 2 1.929 0.05 0.1218 2099.2
23 2 1.929 0.05 0.1218 2099.2
24 2 1.929 0.05 0.1218 2099.2
25 2 1.929 0.05 0.1218 2099.2
26 2 1.929 0.05 0.1218 2099.2
27 3 1.929 0.05 0.1218 2099.2
28 3 1.929 0.05 0.1218 2099.2
29 3 1.929 0.05 0.1218 2099.2
30 3 1.929 0.05 0.1218 2099.2
31 3 1.929 0.05 0.1218 2099.2
32 3 1.929 0.05 0.1218 2099.2
33 3 1.929 0.05 0.1218 2099.2
34 3 0.984 0.05 0.1218 2132
35 3 0.984 0.05 0.1218 2132
36 3 0.984 0.05 0.1218 2132
37 3 0.984 0.05 0.1218 2132
38 3 0.984 0.05 0.1218 2132
39 3 1.879 0.05 0.1311 2624
40 3 1.879 0.05 0.1311 2624
41 3 1.879 0.05 0.1311 2624
42 3 1.879 0.05 0.1311 2624
43 3 1.879 0.05 0.1311 2624
44 3 1.879 0.05 0.1311 2624
45 3 1.879 0.05 0.1311 2624
46 3 1.879 0.05 0.1311 2624
47 3 1.879 0.05 0.1311 2624
48 3 1.879 0.05 0.1311 2624
49 3 1.879 0.05 0.1311 2624
50 3 0.05 0.1311 2624

Option 3 - Input (Object) Motion

3

1450016384 0.01 xxxx.xx (8F9.6)

0.3 25.0 2 8

Option 4 sublayer for input motion

4

50 0

Option 5 Number of iterations

5

1 9 0.65

Option 6 Computation of Accelerations

6

1 2 3 7 10 13 17 20 23 26 29 34 39 42 46

0 1 1 1 1 1 1 1 1 1 1 1 1 1 1

1 0 0 0 0 0 0 0 0 0 0 0 0 0 0

Option 9 Response Spectrum

9

1 0

1 0 32.2

0.05

execution will stop when program encounters 0

0